

**Sedimentological, Ichnological, and Architectural
Characteristics of Geobodies in a Fluvial to Estuary
Setting: the McMurray Formation in the Christina
River area, NE Alberta, Canada**

by
Qi Chen

A thesis submitted in partial fulfillment of the requirements for the degree of
Doctor of Philosophy

Department of Earth and Atmospheric Sciences
University of Alberta

© Qi Chen, 2023

Abstract

The Lower Cretaceous McMurray Formation is the primary host of the crude bitumen reserves in the Athabasca Oils Sand Region. The regionally extensive meander belts associated with estuary point bars have been recognized as the primary reservoir facies in the McMurray Formation. It is widely accepted that dune sands of the cross-bedded sandstone (CB) and point bar heterolithic stratified sandstone and mudstone bedsets (IHS) are the two main facies constituents in the estuary meander belts. Previous studies on the McMurray Formation have emphasized subsurface datasets, which apply regional scale stratigraphic relationships and facies characteristics. These studies commonly generalize the interpretation of the two major facies as a continuous point bar succession: CB represents thalweg-associated sand dunes or the lower part of estuary point bars, and IHS represents the middle to the upper part of the point bars. A detailed investigation of variable geobodies in different parts of a fluvial-estuary setting is generally lacking in the McMurray Formation.

This project provides variable solutions to fill the gap in the above questions. In addition to conventional facies analyses through core and outcrop logging of the McMurray Formation, bedding orientational characteristics of geobodies are analyzed using photogrammetric 3D models of the studied outcrops. The objects of this dissertation are: 1) establish a local stratigraphic framework that can be compared to regional stratigraphy of the McMurray Formation; 2) establish a correlation between lithofacies and dipmeter tadpole log characteristics of estuary point bars; 3) integrate sedimentological, ichnological, and bedding orientational characteristics of depositional units to produce solutions of paleoenvironment reconstruction; and 4) investigate architectural stacking pattern of geobodies in fluvial to estuary settings.

The key results of this dissertation are: 1) the established local stratigraphic framework reveals estuary channel fill developed from progradation of inner estuary channels during regression, and the internal stacking pattern of point bars can be resolved through the interpretation of dipmeter tadpole plots; 2) the CB facies of sand dunes is not always associated with estuarine channel thalweg or lower point bars, middle estuary sand dunes have been efficiently differentiated from point bars from their forward-accretion bedding configuration; 3) four types of deposits are identified in the McMurray Formation progressing from fluvial to the estuary (fluvial deposits, tidally influenced fluvial deposits, inner estuary point bars, and middle estuary compound dunes) through detailed comparison in the sedimentological,

ichnological, and architectural characteristics of geobodies. The recognition and investigation of variable geobodies of the McMurray Formation are crucial for establishing stratigraphic models and paleogeographic reconstructions in sedimentologically complex fluvial to estuary settings.

Acknowledgements

Seven years ago, I was a master's student taking a course-based master program in Integrated Petroleum Geoscience (IPG). At that time, I was unsure whether I would pursue a career path in industry after graduation. I still remember the day I did a field course at the McMurray Formation outcrop in Fort McMurray. The trip was led by Murray Gingras, and he nicely asked me at the outcrop whether I am willing to do a thesis-based graduate program after graduation. I was so grateful for taking this opportunity and joined the Ichnology Research Group in 2015 Fall. Throughout my time as a graduate student, I have had the chance to create memories with so many wonderful people in the group that allowed me to grow as not only a geologist, but also an easygoing, open-minded person. At the beginning of this dissertation, I would like to take this opportunity to thank the following people:

First of all, I am endlessly thankful for my supervisor Murray Gingras seeing my potential, trusting my ability, and providing the opportunity to upgrade to a PhD program after a year of study. I am always impressed the amount of work load you have to deal with throughout your work life. No matter how busy you are, you are always available for us. Under your supervision, I have been encouraged to share my idea, and make my own interpretations (even the ones that does not make sense). For methods or techniques that we are not specialized in, you always coordinate meetings or discussions with specialized experts so that I can get correct understanding of knowledge. Thank you for the opportunities you offered me throughout the years: participating Imperial Barrel Award competition, teaching lab courses as TA, logging cores at core labs, joining conferences to present my work, and travelling to Bay of Fundy. The most important help I got is very detailed guidance for my academic writing that has always be the biggest issue for a second language speaker of English. I truly feel that I can never achieve what I have throughout my grad school experience without your help.

Secondly, I would like to thank the coauthors of my papers for publication: Prof. James MacEachern, Dr. Mike Ranger, and Derek Hayes. I really appreciate your constructive feedbacks for my paper, which boost my paper's quality to meet publication standard. Thank you, Dr. Mike Ranger, for validating my bedding orientational data, and provide meaningful discussion on my depositional models. Dr. James MacEachern is thanked for sharing his many years experience in the McMurray Formation. Derek Hayes is thanked for providing his valuable opinion on his Crooked Rapids outcrop model. Mr. Howard Brekke,

Dr. Milovan Fustic, and Dr. Grant Wach for their review of my published article. Mr. Howard Brekke is specially thanked for his criticism on my dipmeter data interpretation, which deepens my understanding of the principle and limitation of the dipmeter tool.

Thirdly, I would like to thank past and current members of Ichnology Research Group during the time of this project: Scott Botterill, Carolyn Furlong, Eric Timmer, Derek Hayes, Brette Marris, Maya LaGrange Rao, Calla Knudson, Skye Lybbert, Scott Melnyk, Chenyang Feng, Chundi Shan, Maria Rodriguez, Arzu Acikelli, Sara Biddle, Jiahui Gao, Daniel Shaw, Waqar Ahmad, Alina Schchepetkina. We have shared many times of work, discussion, happiness, and frustrations together. Thanks Derek, and Eric for guiding me through my outcrop modeling and well correlation work. Thanks Scott Botterill, Scott Melnyk, and Derek Hayes for proofreading my paper manuscript. Thank you, my office mates throughout the years: Brette Harris, Maya LaGrange Rao, and Zhe Zhang for chatting whenever I need a break throughout a day.

Thanks, my dearest family members: my parents Gongyang Chen, Xuemei Wang, my husband Ruiyang Zhou, and my lovely dog Coca for your endless love, support, and encouragement you have provided me throughout my life and this academic journey. I am grateful to have the world's best family that is always there for me.

Finally, I would like to thank the funding companies of the McMurray Geology Consortium: BP, Cenovus Energy, Husky Energy, CNOOC International, and Woodside Energy Ltd for their generous support. Cenovus Energy is specially thanked for sharing their dipmeter data in their area.

Table of Contents

Abstract	ii
Acknowledgements	iv
Table of Contents	vi
List of tables	x
List of figures	xii
Statement of Contribution	xvii
Chapter 1 :Introduction	1
General overview	1
Geological background overview in the study area	2
Study area and dataset	3
Project motivation and objects	5
Chapter 2 : Facies Distribution and Stratigraphic Architecture of the Lower Cretaceous McMurray Formation, North of Christina River region, Alberta, Canada	8
Introduction	8
Geological setting	9
Study area and methodology	11
Facies associations	13
<i>FA1: Fluvially dominated inner estuarine channel</i>	25
<i>FA2: Tidally Influenced Estuary Channels</i>	26
<i>FA3: Inner estuarine abandoned channel</i>	28
<i>FA4: Wave-influenced delta associated with brackish-water embayment</i>	30
<i>FA5: Storm-influenced to sheltered brackish-water embayment</i>	33
<i>FA6: Lower shoreface to offshore</i>	36
Characteristics of the bounding surfaces	39
<i>Allogenic Flooding Surfaces</i>	42
<i>Autogenic Flooding Surfaces</i>	43

Discussion	43
<i>Stratigraphy and paleogeographic reconstructions of the estuary channels</i>	43
<i>Stratigraphic architecture of the McMurray Formation in the Christina River region</i>	48
Conclusion	52
Chapter 3 : Integrating Facies Analysis with Dipmeter Data to Characterize Point Bars of the Lower Cretaceous McMurray Formation, Christina River, AB, Canada	53
Introduction	53
Geological background	54
Study area and methodology	57
Data acquisition and processing	60
<i>Tadpole plot reclassification</i>	61
Results and interpretation	64
<i>Facies Association 1</i>	64
<i>Facies Association 2</i>	88
<i>Comparing core and dipmeter characteristics of sedimentary facies</i>	95
Discussion	96
<i>Estuarine point bar geometry</i>	96
<i>McMurray Formation depositional model</i>	101
Conclusion	104
Chapter 4 : Recognizing Genetically Related Depositional Packages Using 3D Photogrammetric Outcrop Models in a Fluvially Dominated, Tidally Influenced Meander-Belt Succession.	106
Introduction	106
Geological Background	108
<i>Depositional setting of the McMurray Formation</i>	108
<i>Controversy of the McMurray Formation depositional environment</i>	110
Study area	111
Methods	112
<i>Photogrammetry</i>	112
<i>Bedding orientation calculation</i>	114
<i>Bedding measurement error control</i>	115
<i>Tadpole log calibration</i>	116
Observations and interpretation	118

<i>Lower Christina River Section</i>	118
<i>Upper Christina River Section</i>	126
<i>Depositional Environment Interpretation</i>	137
Discussion.....	137
<i>Depositional environments and processes in a tide-dominated estuary</i>	137
<i>Stratigraphic implications</i>	142
<i>Identification of genetically related depositional packages of point bar deposit in dipmeter tadpole data</i>	143
Architectural model of point bars at Christina River outcrop.....	146
<i>Single point bar model</i>	149
<i>Stacked estuary point bar model</i>	153
Contribution to the McMurray conundrum.....	154
Conclusion	154
Chapter 5 : Variable Geobody Architecture of Fluvial to Estuary Deposits: Case Studies from the McMurray Formation.....	156
Introduction	156
Geological background.....	158
Study area.....	159
Methodology and data analysis	162
<i>Photogrammetric 3D outcrop model</i>	162
<i>Bedding orientation data collection</i>	163
<i>Facies and Facies Associations Classification</i>	165
Results and Interpretation.....	166
<i>Fluvial point bars</i>	166
<i>Tidally influenced fluvial deposits</i>	178
<i>Inner estuary point bars and compound dune complex</i>	188
Discussion.....	201
<i>Fluvial deposits Sedimentology and Architectural Synthesis</i>	205
<i>Tidally influenced fluvial deposits Sedimentology and Architectural Synthesis</i>	206
<i>Inner estuary IHS Sedimentology and Architectural Synthesis</i>	206
<i>Estuary Compound Dunes Sedimentology and Architectural Synthesis</i>	207
Conclusion	208
Chapter 6 : Summary and Conclusion.....	210
Thesis summary	210

Stratigraphic framework.....	210
Integration of facies and dipmeter tadpole data	211
Large point-bar architecture.....	212
Variable geobody architecture along fluvial to estuary settings.....	213
Recommendation for future work.....	214
Conclusions.....	214
References	216
Appendix A.....	229
Core logs from the Christina River region	229

List of tables

Table 2.1 McMurray Formation facies grouped by lithological characteristics.	18
Table 2.2 Facies associations and their facies components.	23
Table 2.3 Facies associations (FA) and facies occurrences of the McMurray Formation in study area. ...	24
Table 3.1 Facies association and their constituent lithofacies in the north of Christina River region.	64
Table 3.2 Core and dipmeter tadpole characteristics of facies F1a mud-breccia dominated sandstone... 65	65
Table 3.3 Core and dipmeter tadpole characteristics of facies F1b massive to cross-stratified sandstone.	68
Table 3.4 Core and dipmeter tadpole characteristics of facies F2a sandstone-dominated IHS.	72
Table 3.5 Core and dipmeter tadpole characteristics of facies F2b mudstone-dominated IHS	77
Table 3.6 Core and dipmeter tadpole characteristics of facies F2c massive to laminated mudstone.	81
Table 3.7 Core and dipmeter tadpole characteristics of facies F2d lenticular to wavy bedded mudstone and sandstone.	85
Table 3.8 Core and dipmeter tadpole characteristics of facies F3a bioturbated to lenticular bedded mudstone and sandstone.	88
Table 3.9 Core and dipmeter tadpole characteristics of facies F3b heterolithic coarsening upward mudstone and sandstone.	91
Table 4.1 Summary of the measured beddings and surfaces of the sedimentary packages identified from the lower and upper Christina River outcrop sections.	131
Table 5.1 Rotation axis information used to restore orientational data to original condition at time of deposition.	165
Table 5.2 Bedding orientation characteristics of the cross-bedded sandstone and IHS facies at Daphne Island outcrop.	169
Table 5.3 Bedding orientation characteristics of the cross-bedded sandstone and IHS facies at Crooked Rapids outcrop.	175
Table 5.4 Bedding orientation characteristics of the cross-bedded sandstone and IHS facies at Hangingstone #1 outcrop.	181
Table 5.5 Bedding orientation characteristics of the cross-bedded sandstone and IHS facies at Hangingstone #2 outcrop.	186

Table 5.6 Bedding orientation characteristics of the cross-bedded sandstone and IHS facies at Christina River outcrop 192

Table 5.7 Bedding orientation characteristics of the cross-bedded sandstone and IHS facies at Amphitheatre outcrop 198

List of figures

Figure 1.1 (A) Paleogeographic reconstruction of the Early Cretaceous Western Canada Sedimentary Basin (WCSB). (B) Schematic stratigraphic column of the McMurray Formation in this thesis.	3
Figure 1.2 Basemap showing study areas location of each chapter in this thesis.	5
Figure 2.1 Stratigraphic models proposed for the McMurray Formation.	9
Figure 2.2 (A) Paleogeographic reconstruction of the Early Cretaceous Western Canada Sedimentary Basin (WCSB) (B) Isopach map of the McMurray Formation overlain by bitumen thickness map in the region (modified from Broughton, 2013).	11
Figure 2.3 Study area and data availability	13
Figure 2.4 Sandstone facies.	15
Figure 2.5 Inclined Heterolithic Stratification (IHS) consisting of sandstone/mudstone.	17
Figure 2.6 Mudstone facies.	18
Figure 2.7 Core photos of FA1 (fluvially dominated inner estuarine channel) and overlying FA3 (mixed tidal flat).	26
Figure 2.8 Core photos of FA2 tidally influenced estuary channel and associated point bars	28
Figure 2.9 Core photos of FA3 mixed tidal flat and abandoned channel.	30
Figure 2.10 Variable core expressions of FA4 wave-influenced delta associated with a brackish-water embayment in well 10-21-090-07W4, well 03-35-089-06W4, and well 09-06-089-06W4.	33
Figure 2.11 Variable core expressions of FA5 brackish-water embayment and FA6 shoreface to offshore in well 03-28-089-06W4, well 10-20-090-07W4, and well 13-11-089-06W4.	35
Figure 2.12 Core photos of a rare FA6 succession showing shoreface to offshore observed in the Wabiskaw Member.	37
Figure 2.13 Details of the bounding surfaces observed in the cores in the study area	40
Figure 2.14 Relative sea-level curve and schematic diagram of the evolutionary history of two depositional models.	45
Figure 2.15 West-to-East stratigraphic cross-section illustrating facies and estuarine channel architecture.	50
Figure 2.16 Schematic diagram showing the proposed stratigraphic architecture of the McMurray Formation in the Christina River region.	51

Figure 3.1 (A) Chronostratigraphy of the Athabasca Oil Sands deposit (modified from Wightman and Pemberton, 1997); (B) High-resolution stratigraphic model for the McMurray Formation; (C) Detailed lithostratigraphic/allostratigraphic relationships in the study area.....	56
Figure 3.2 (A) Paleogeographic reconstruction of the Early Cretaceous Western Canada Sedimentary Basin (WCSB); (B) Paleogeographic reconstruction of Alberta in the Lower Cretaceous showing stratigraphic thickness of the McMurray-Wabiskaw interval.	58
Figure 3.3 Basemap of study area showing wells with petrophysical data, dipmeter logs and logged cores used in this study.	59
Figure 3.4 A sample dipmeter log interpretation from the study area.	62
Figure 3.5 Mud breccia-dominated sandstone – Facies 1a: core and wireline perspectives.	67
Figure 3.6 Massive to cross-stratified sandstone - Facies F1b: core and wireline perspectives.	70
Figure 3.7 Facies F2a of Facies Association 1: core and wireline perspectives.	75
Figure 3.8 Facies F2b of Facies Association 1: core and wireline perspectives.	79
Figure 3.9 Facies F2c of Facies Association 1: core and wireline perspectives.....	84
Figure 3.10 Lenticular to wavy bedded mudstone and sandstone - Facies F2d: core and wireline perspectives.	87
Figure 3.11 Core photos of Facies F3a and F3b of Facies Association 2.	90
Figure 3.12 Core examples of Facies 3 of Facies Association 2.	94
Figure 3.13 Interpreted north-south cross section with classified tadpole plots.	99
Figure 3.14 Interpreted west-east cross section with classified tadpole plots.	100
Figure 3.15 Relative sea-level curve and schematic diagram depicting the evolutionary history and the resulting stratigraphic configuration during the deposition of Allomember C and Allomember B2.	103
Figure 4.1 (A) Paleogeographic reconstruction of the Early Cretaceous Western Canada Sedimentary Basin (WCSB); (B) Stratigraphy of the Athabasca Oil Sands deposit near the study area.....	108
Figure 4.2 Stratigraphic framework representation near the Christina River region.....	111
Figure 4.3 (A) relative location of Amphitheatre, Steepbank and Christina River outcrops; (B) Christina River outcrop satellite image showing the lower and upper section along the cutbank.	112
Figure 4.4 Schematic workflow for generating the 3D photogrammetric outcrop model to characterize McMurray Formation deposits at the Christina River outcrops.	113
Figure 4.5 Schematic diagram showing marker placement along a measured surface..	114

Figure 4.6 Sample subsurface dipmeter tadpole data that have been used to calibrate <i>Pseudo</i> -dipmeter tadpole logs of the outcrop in this study.....	117
Figure 4.7 Outcrop photo of the cross-bedded sandstone in the lower Christina River section with interpreted cross-beds (yellow lines) and cross-set boundaries (blue lines).	119
Figure 4.8 Detailed outcrop photos of the cross-bedded sandstone in the lower Christina River Outcrop section.	120
Figure 4.9 Rose and poles-to-bedding diagrams of the cross-bedded sandstone facies at Christina River Outcrop section.	122
Figure 4.10 Interpreted photomosaics of the lower Christina River outcrop section generated using Metashape 1.7.	124
Figure 4.11 Photomosaic of the lower Christina River outcrop section showing interpreted cross-set boundaries and accretionary surfaces.	125
Figure 4.12 Upper McMurray Formation outcrop overview showing the locations of <i>pseudo</i> -dipmeter tadpole logs.....	127
Figure 4.13 Close-up photos of contacts between the different depositional units.....	128
Figure 4.14 Synthesized rose diagrams and poles-to-bedding diagrams of the cross-bedded sandstone packages and LASs in IHS packages at upper Christina River outcrop section.	130
Figure 4.15 Interpreted photogrammetric outcrop model of the upper Christina River section with <i>pseudo</i> -dipmeter tadpole plots.....	134
Figure 4.16 Schematic diagram of tide-dominated estuary setting.....	139
Figure 4.17 The morphological and architectural characteristics of (A) tide-influenced fluvial channel point bars and (B) tidal compound dunes.....	141
Figure 4.18 Sample dipmeter log 1 shows that the cross-bedded sandstone is potentially genetically associated with overlying IHS facies.....	145
Figure 4.19 (A) Photogrammetric 3D model of the Christina River outcrop; (B) a representative strip log of the measured succession which consists of stacked IHS units that overlies a thick CB unit.	148
Figure 4.20 Depositional model for genetic package 1 that is below WTNRS.	149
Figure 4.21 Schematic diagram of two depositional model scenarios that can explain the succession above WTNRS (IHS1, CB2, IHS2, and IHS3). A) Depositional model scenario 1: Genetically related lateral accretion sets (LASs) in a single meander belt. B) Depositional model scenario 2: Genetically unrelated estuary point bars model.....	150

Figure 5.1 Schematic stratigraphic column of the McMurray Formation as seen at measured outcrops of this study.	157
Figure 5.2 A) Location map of the measured outcrops in relation to Fort McMurray, Alberta, Canada. B) Satellite image of the Daphne Island outcrop; C) Satellite image of the Crooked Rapids outcrop; D) Satellite image of the Hangingstone #1 and #2 outcrops; E) Satellite image of the Christina River outcrop; F) Satellite image of the Amphitheatre outcrop.....	161
Figure 5.3 Schematic workflow of the 3D photogrammetry method used to characterize bar forms of the McMurray Formation at measured outcrops in this study.....	163
Figure 5.4 Detailed photos of common sedimentary and ichnological features identified at Daphne Island outcrop section.....	166
Figure 5.5 A) Photogrammetric 3D model of the Daphne Island outcrop. B) An interpreted zoom in section of the Daphne Island outcrop.	170
Figure 5.6 Detailed photos of common sedimentary and ichnological features identified at Crooked Rapids outcrop section.....	172
Figure 5.7 A) Photogrammetric 3D model of the south end of Crooked Rapids outcrop. B) An interpreted zoom in section of the Crooked Rapids outcrop; C) representative strip log of the north end of the interpreted section in B), showing fluvial point bar deposit overlies fluvial channel sand dunes.....	176
Figure 5.8 Detailed photos of common sedimentary and ichnological features identified at Hangingstone #1 and #2 outcrops.	179
Figure 5.9 A) Photogrammetric 3D model of the Hangingstone #1 outcrop; B) representative strip log of the interpreted section showing deposition of stacked two point bars in inner estuary setting.	182
Figure 5.10 A) Photogrammetric 3D model of the Hangingstone #2 outcrop. B) An interpreted zoom in section of the Hangingstone #2 outcrop. C) representative strip log of the interpreted section in B), showing lateral accretionary deposit of point bar overlies inner estuary channel sand dunes.	187
Figure 5.11 Detailed photos of common sedimentary and ichnological features identified at Christina River outcrop.....	190
Figure 5.12 A) Photogrammetric 3D model of the Christina River outcrop; B) representative strip log of the interpreted section with proposed depositional models.	193
Figure 5.13 Detailed photos of common sedimentary and ichnological features identified at Amphitheatre outcrops.....	197
Figure 5.14 A) Photogrammetric 3D model of the Amphitheatre outcrop. B) An interpreted zoom in section of the Amphitheatre outcrop. C) representative strip log of the interpreted section in B), showing lateral accretionary deposit of point bar overlies middle/outer estuary channel compound dunes.	199

Figure 5.15 The internal architectural difference between bar forms. 202

Figure 5.16 A schematic diagram showing subenvironments of an estuary..... 203

Figure 5.17 Geobody architectural interpretation of each outcrop in this study. **A)** Representative strip logs of studied outcrops. **B)** Rose plots of master bedding planes and cross beds in CB sandstone units of studied outcrops. **C)** Rose plots of master bedding planes of IHS units of studied outcrops. 204

Statement of Contribution

This thesis is original work composed by me, Qi Chen. I confirm the work submitted is my own, with the assistances of my supervisor, Murray K. Gingras. Chapters within this thesis have either been published within peer-reviewed journals or been submitted for publication. In each chapter, the contributions from researchers are stated explicitly below.

Chapter 2 will be submitted for publication as Qi Chen, Scott Botterill, and Murray K. Gingras. “Facies distribution and stratigraphic architecture of valley-fill deposits within the Cretaceous McMurray, North of Christina River region, NE Alberta, Canada”. I completed the core description and well-to-well subsurface correlation in the study area, generated figures and tables, and composed the manuscript. Scott Botterill and Murray K. Gingras proofread and edited the manuscript, and provided comments on the facies interpretation.

Chapter 3 of this thesis has been published in the *Marine and Petroleum Geology* as Qi Chen, Alina Shchepetkina, Scott Melnyk, and Murray K. Gingras, “Integrated facies analysis with dipmeter data to characterize point bars of the Lower Cretaceous McMurray Formation, Christina River, AB, Canada”. I completed the core description, interpreted dipmeter tadpole logs, established well-to-well subsurface correlation, generated figures and tables, and composed the manuscript. Alina Shchepetkina, Scott Melnyk and Murray K. Gingras proofread and edited the manuscript. Reviewers of this paper Howard Brekke, Milovan Fustic, Grant Watch provided guidance and valuable comments. In particular, Howard Brekke kindly offered insights of dipmeter tadpole data interpretation discussion.

Chapter 4 of this thesis has been published in the *Sedimentary Geology* for publication as Qi Chen, Jeffrey L. Kavanaugh, Michael J. Ranger, James MacEachern, and Murray K. Gingras, “Using 3D photogrammetric outcrop model to recognize genetically related depositional packages in the Lower Cretaceous McMurray Formation at Christina River Outcrop, NE Alberta, Canada”. I generated the 3D photogrammetric outcrop model, acquired orientational data of sedimentary surfaces, interpreted the data, generated figures and tables, and composed the manuscript. J.L. Kavanaugh wrote the Python script to convert points coordinates into strikes and dips of planes. Michael J. Ranger and Murray K. Gingras assisted with collecting drone photos at the Christina River outcrops. Michael J. Ranger, James

MacEachern, and Murray K. Gingras proofread the manuscript, and provided comments on the data interpretation.

Chapter 5 of this thesis will be submitted for publication as Qi Chen, Michael J. Ranger, Derek Hayes, James MacEachern and Murray K. Gingras, "Variable geobody architecture of a fluvial to estuary deposits: case studies from the Lower Cretaceous McMurray Formation". I generated 3D photogrammetric outcrop models of studied outcrops, acquired orientational data of sedimentary surfaces, interpreted data, generated figures and tables, and composed the manuscript. J.L. Kavanaugh wrote the Python script to convert points coordinates into strikes and dips of planes. Michael J. Ranger, Derek Hayes, James MacEachern and Murray K. Gingras proofread the manuscript, and provide valuable comments on the interpretation of data.

Chapter 1 (introduction) and Chapter 6 (conclusion) are my own work.

Chapter 1 :Introduction

GENERAL OVERVIEW

The Lower Cretaceous McMurray Formation is located in the Athabasca Oil Sand Region, which hosts covers over 42000km² (AER, 2022). Despite its enormous scale and economic value, there is still a lack of consensus among researchers regarding the stratigraphic framework for the McMurray Formation. Previous research has remarked upon the difficulties in establishing a regional stratigraphic framework for the McMurray Formation largely due to the pronounced valley incisions and complex cross-cutting relations of amalgamated fluvio-tidal channel belts. Local and regional studies of the Athabasca Oils Sand deposit focusing on the stratigraphic framework of the McMurray Formation have led to the recognition of three depositional models: 1) a very large fluvial system (e.g., Mossop and Flach, 1983; Flach and Mossop, 1985; Keith et al., 1988; Muwais and Smith, 1990; Blum and Jennings, 2016; Durkin et al., 2017); 2) a transgression-dominated incised valley fill (e.g., Wightman and Pemberton, 1997; AEUB, 2003; Hein and Langenberg, 2003; Hein and Cotterill, 2006; Hein et al., 2013; Barton, 2016); and 3) normal regression-dominated fluvio-estuarine channel belt model of a deltaic system (e.g., Carrigy, 1971; Château et al., 2019; Château et al., 2020; Rinke-Hardekopf et al., 2022). The most widely used stratigraphic framework for well-log and core-based correlation studies comply with the transgression-dominated incised valley fill model. This model subdivides the McMurray Formation into a series of stacked progradational parasequences that are largely eroded through successive channel incision during major base-level drops. Recently, an increasing number of studies have recognized that channel-fill deposits of the McMurray Formation are not entirely transgressive, but are more consistent with contemporaneous channel meander belts that results from basinward progradation of trunk fluvio-estuarine channel system in a regressive shoreline (Baniak and Kingsmith, 2018; Château et al., 2020). In this dissertation, particular focus is placed on finding evidence supporting the presence of regressive channel-fill deposits. The chapters in this dissertation showcase my most important findings in the study area using a variety of analytical methods, e.g., well-log and core logging analysis, dipmeter tadpoles' interpretation, and photogrammetric outcrop modeling analysis. Furthermore, integrated studies using

combination of different analytical methods (mentioned above) provide an opportunity to differentiate origins of various geobodies in the McMurray Formation.

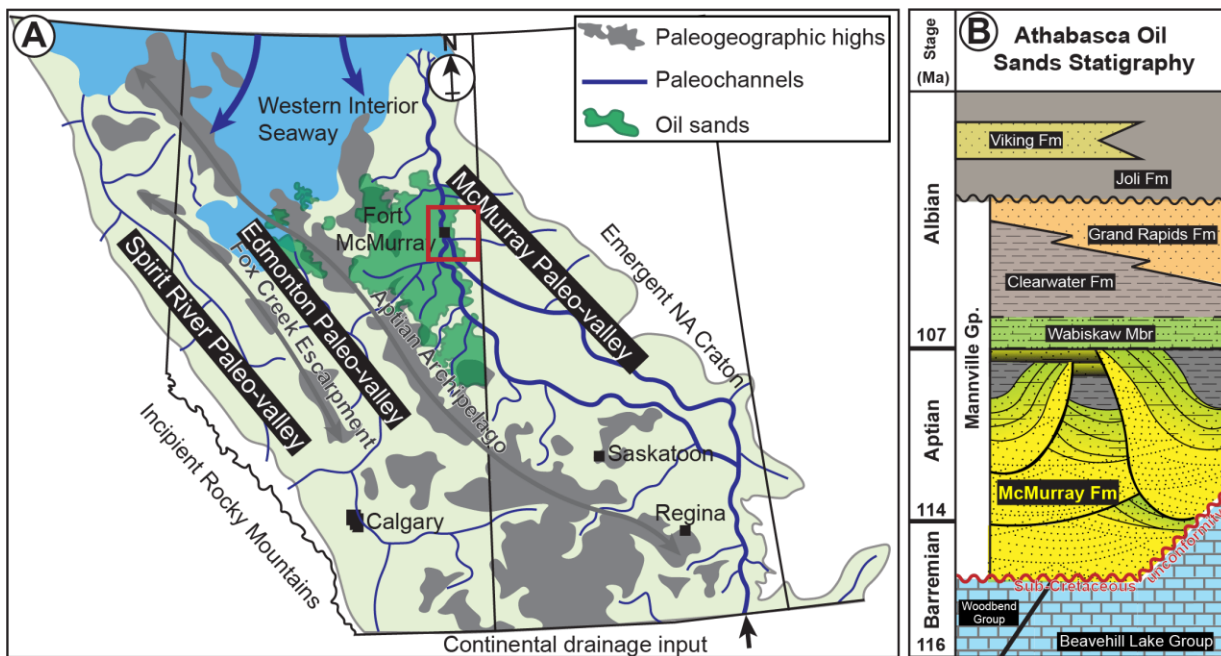
GEOLOGICAL BACKGROUND OVERVIEW IN THE STUDY AREA

In the Athabasca Oil Sands region, the McMurray Formation unconformably overlies a major Sub-Cretaceous Unconformity, which truncates Devonian strata in the foothills and lower Paleozoic strata at the eastern margin of the western Canadian sedimentary basin (Hayes et al., 1994). The paleotopography of the sub-Cretaceous unconformity was influenced by underlying salt dissolution of Devonian Prairie Evaporite Formation (Christopher, 1974; Wightman and Pemberton, 1997; Broughton, 2014), which complicates the interpretation of pre-, syn- and post-depositional tectonism. The orogenesis created paleotopography on the Sub-Cretaceous Unconformity is characterized by three northwest-southeast trending paleovalleys (from west to east in Fig. 1.1A): Spirit River Paleovalley, Edmonton Paleovalley, and McMurray Paleovalley (also named as Assiniboia Paleovalley) (Christopher, 1974). The McMurray Formation was deposited during the long-term southward transgression of Boreal Sea. An informal subdivision of the McMurray Formation into Lower, Middle, and Upper intervals was proposed based on the evolution of depositional systems from fluvial, estuarine, and coastal plain to marginal marine environments during the transgression (Carrigy, 1959; Flach and Mossop, 1985; Hein et al., 2006). Due to the large extent of the McMurray Formation and its stratigraphic complexity, the volume of data is divided among researchers at the Simon Fraser University, University of Calgary, and University of Alberta. A McMurray Geology Consortium (MGC) was formed and divided the Athabasca Oils Sand deposit into 9 regions. Eighteen graduate students from the three universities were assigned with detailed core logging, facies analysis and interpretation, and other relevant objects. The well-to-well correlation focuses on the assigned “Central B” region. In addition to this core- and petrophysical logs-based dataset (“Central B”), outcrops in nearby area are also investigated in this study, and the region including all types of data is referred as Christina River region in this dissertation.

Within the project area, the major structural controls on sedimentation of the McMurray Formation includes a west-flanking Paleozoic carbonate high (Fig. 1.1A), and the longitudinal regional subsidence

caused by underlying salt dissolution of Devonian Prairie Evaporite Formation (Wightman et al., 1995; Hein et al., 2013). McMurray Formation sand is mainly sourced from the south and southeast from Saskatchewan, western Manitoba, northern Montana, and North Dakota, while minor westerly sources from the rising Cordillera contributed sediment to the Wabiskaw Member (Hein et al., 2013). The McMurray Formation deposited in the Christina River region represents sedimentary successions in the eastmost McMurray Paleovalley (Fig. 1.1A).

Figure 1.1 (A) Paleogeographic reconstruction of the Early Cretaceous Western Canada Sedimentary Basin (WCSB), including the location of the ancient meander-belt deposit of the study (modified from Durkin et al., 2017). The study area of this thesis is indicated by the red square in the diagram; **(B)** Schematic stratigraphic column of the McMurray Formation in this thesis. The lower Cretaceous McMurray Formation unconformably overlies the Woodbend Group and Beavehill Lake Group of the upper Devonian Waterways Formation.



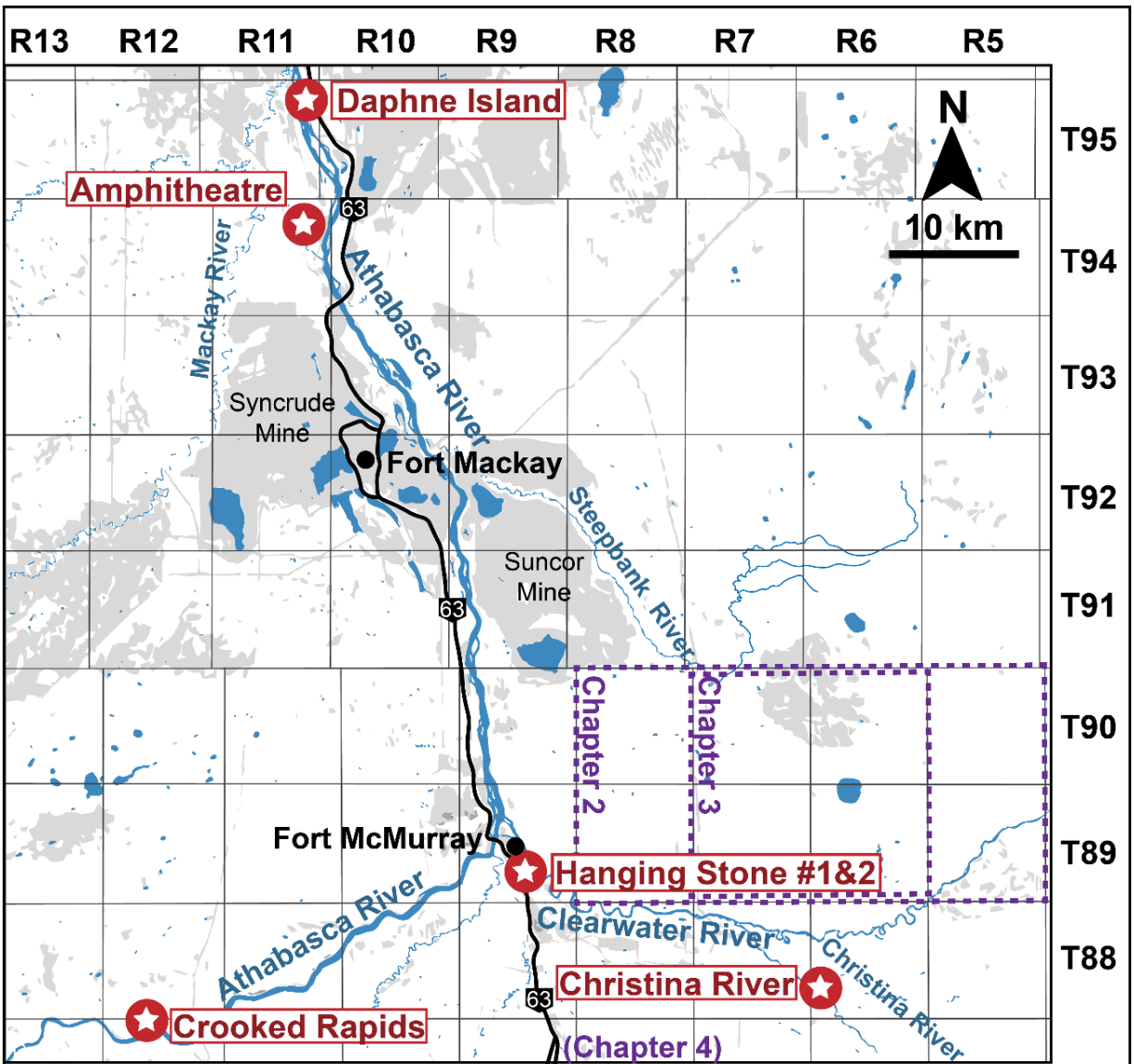
STUDY AREA AND DATASET

This thesis investigates the subsurface and outcrop dataset of the McMurray Formation available in the research area. This dataset includes cores and petrophysical data in area extends between Ranges 5-8W4M and Township 89-90, and variable outcrops along the Athabasca River and its tributaries (Fig. 1.2).

A total of 67 subsurface drill cores were logged for a facies analysis, and stratigraphic correlations between wells were generated using petrophysical well logs from GeoScout database. 161 wells in R5-8 and T89-90 with petrophysical logs were used to determine a local stratigraphic framework in the studied area.

A subset of dense dipmeter log dataset in R6-7 and T89-90 was used in combination of logged cores in the area to conduct an integrated facies analysis characterizing a high-resolution point bar stacking pattern and architecture of the McMurray Formation. Christina River outcrop located one township (approximately 10km) south of the facies analysis area provides a great opportunity to display the stratigraphic architecture of point bars studied using subsurface data. A relatively new outcrop photogrammetric method is adopted at the Christina River outcrop to produce high-resolution georeferenced three-dimensional outcrop models. This method allows fast acquisition of bedding plane orientational data for any surfaces that can be virtually traced across the outcrop. The bedding characteristics of each depositional units are used to recognize genetically related depositional packages and propose depositional model of the estuary meander belts during the McMurray time. Similar outcrop analytical method is used at other McMurray outcrops (Amphitheatre, Hanging Stone #1 and #1, Crooked Rapids, and Daphne Island outcrops) to explore variable geobody architecture of a fluvial to estuary deposit. The results contribute to the refinement of estuary model around the world.

Figure 1.2 Basemap showing study areas location of each chapter in this thesis.



Chapter 5: synthesizing all outcrops labeled with ★

PROJECT MOTIVATION AND OBJECTS

To understand the stratigraphy and depositional environment of the McMurray Formation interval in the Central B area. A stratigraphic correlation and lithofacies analyses are established at the initial stage of this project using core logging and well-to-well correlation in the study area, which form the main content of Chapter 2 (See Fig. 1.2 for study area of this chapter). The majority of the McMurray Formation interval

in the study area is point-bar deposits associated with tidally influenced meander belts (e.g., Mossop, 1980; Crerar and Arnott, 2007; Hubbard et al., 2011; Musial et al., 2012; Baniak and Kingsmith, 2018). Following the work of the Alberta Energy and Utilities Board (2003), channels associated with different stratigraphic units are identified by identifying coarsening-upward allomembers in the Upper McMurray interval. This study established a stratigraphic framework and channel distribution across the area, and two different depositional models are proposed to explain the resulting stratigraphic configuration.

The history of research on the McMurray Formation is complex, many studies have been conducted to resolve the stratigraphic architecture and lithofacies distribution. Among these studies, core- and petrophysical logs-based studies reveal that the McMurray Formation interval is dominated by tidally influenced channel and point bar deposits without delineating the point bar stacking patterns. Internal architectural characteristics of the channel deposits can only be established at local scale using seismic or high-resolution microresistivity data. However, these data are much more expensive, and are much less regionally accessible. Among variable types of data available in the McMurray Formation interval, core and dipmeter log datasets are the two most cost-effective, and regionally available datasets. If a correlation between sedimentary facies and dipmeter tadpole characteristics can be established, then dipmeter tadpole data can contribute to 1) the refinement of core- and well log-based stratigraphic correlation; and 2) the delineation of genetically related point bar successions. This idea inspired the Chapter 3, which integrates dipmeter tadpole patterns, sedimentological and ichnological characteristics from wells available in T89-90, R6-7 (Fig. 1.2).

After investigating core and well logs, the Christina River outcrop located besides the study area of Chapter 2 provides a great opportunity to verify the internal architecture established using core- and well log-based data. Chapter 4 developed a study inspired by work from Hayes et al. (2017) at Steepbank and Amphitheatre Outcrops. *Pseudo*-dipmeter tadpole logs are generated at Christina River Outcrop using bedding orientational data collected from photogrammetric 3D model, which can be interpreted in the same way as the conventional tadpole plots. The results of this study provide a detailed view of facies architecture in a fluviotidal estuary setting, and feasible solutions to the challenge of assigning genetic units in large point-bar architectures in the sedimentary record.

Since the Christina River outcrop reveals variable depositional units, rather than purely estuary point bar deposit, Chapter 5 took a step further to evaluate the well-known outcrops of the McMurray Formation in the NE of the Athabasca Oil Sand region. Photogrammetric models are created for 6 outcrop (see locations in Fig. 1.2). A series of depositional units are identified and interpreted to represent specific depositional environments along a fluvial to estuary depositional setting. The results reveal that the fluvio-estuarine channel-fill deposit of the McMurray Formation is not entirely transgressive.

In summary, this project has the following objectives: 1) establishing stratigraphic framework and channel distribution within each stratigraphic units; 2) investigating lithofacies and dipmeter tadpole characteristics of facies within the meander belt associated point bars, which can be used as analog to guide future refinement of core-based facies analysis using dipmeter tadpole logs in other channelized estuary deposits; 3) providing variable solutions in recognizing genetically related depositional units in fluvio-estuarine settings using 3D photogrammetric outcrop models; and 4) identifying variable geobody architectures in a fluvial to estuary deposit of the McMurray Formation.

Chapter 2 : Facies Distribution and Stratigraphic Architecture of the Lower Cretaceous McMurray Formation, North of Christina River region, Alberta, Canada

INTRODUCTION

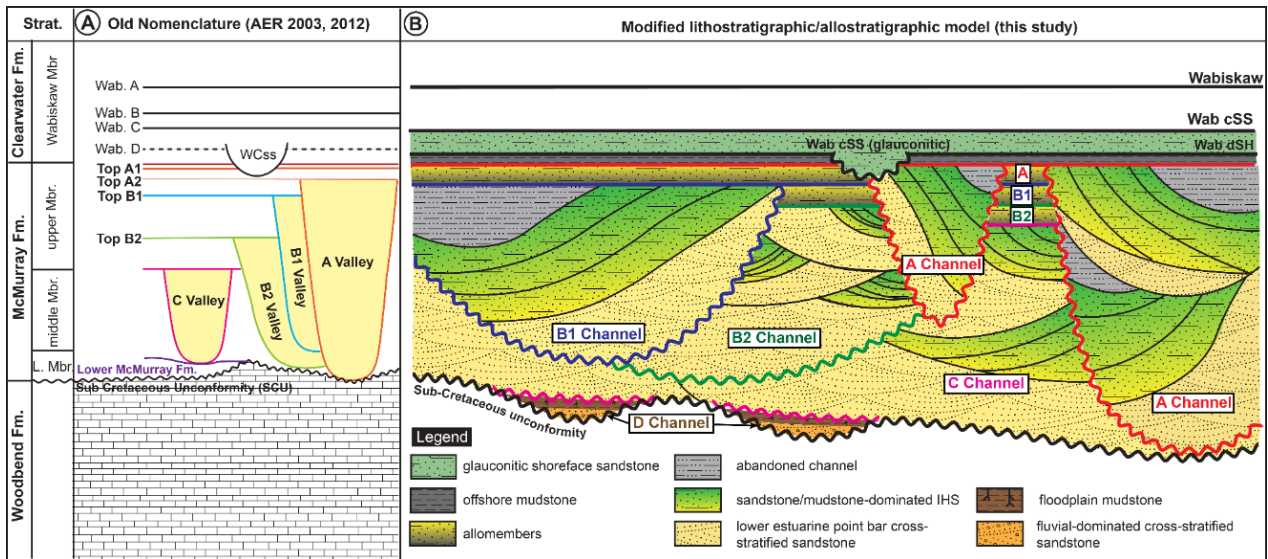
The Lower Cretaceous McMurray Formation is the key reservoir that hosts the Athabasca Oil Sands in the northeast part of the Alberta Foreland Basin. Many studies have been conducted over the past 5 decades attempting to resolve the stratigraphic architecture and lithological heterogeneity of McMurray Formation strata by incorporating core logging, outcrop observations, petrophysical data analysis, and local 3D seismic data imaging. The stratigraphy of Athabasca Wabiskaw-McMurray interval has been investigated by numerous researchers, and various stratigraphic framework models have been proposed and debated (e.g., Nelson and Glaister, 1978; Mossop and Flach, 1983; AEUB, 2003; Mathison, 2004; Hein *et al.*, 2006; Nardin *et al.*, 2010; Barton *et al.*, 2017; Château *et al.*, 2019; Château *et al.*, 2020; Peng *et al.*, 2022; Rinke-Hardekopf *et al.*, 2022). These different McMurray Formation stratigraphic models infer repeated stacking of transgressive-regressive cycles, as well as complex cross-cutting of various types of estuarine point-bars generated by high-sinuosity fluvial and estuarine channels.

A regionally applicable stratigraphic nomenclature is extremely difficult to apply to the Athabasca Wabiskaw-McMurray interval. The regional stratigraphy of the Wabiskaw-McMurray Formation was first considered by the Alberta Energy and Utilities Board in 2003 (AEUB, 2003). To unify the stratigraphy of the McMurray Formation and make it consistent with other stratigraphic models, the McMurray Geology Consortium (MGC) amended that framework. Regional stratigraphic correlations in the southwest, southeast and northeast quadrant of the Athabasca Oil Sand region have been discussed in detail by previous researchers from the MGC (Hagstrom, 2019; Château *et al.*, 2020; Peng *et al.*, 2022); Rinke-Hardekopf *et al.*, 2022. The stratigraphic framework of strata near the Christina River area has not been framed in the regional context.

The challenges of establishing stratigraphic framework in the Christina River area are owing to: 1) the general lack of clear coarsening-upward parasequences that are characteristically assigned to the upper

McMurray Formation; and 2) the pronounced deep incision and complex cross-cutting relations of fluvio-tidal channel belts result in extensive removal of mudstone directly overlying regional flooding surfaces that marks the tops of stratigraphic units. This research attempts to solve the local stratigraphic architecture that can be framed in the regional framework through facies analysis, well-to-well correlations, and paleogeographic reconstruction of the McMurray Formation. Feasible depositional models are discussed to explain the resulting stratigraphic architecture observed in this study, which contributes to the understanding of paleogeographic reconstruction of fluvial to marginal marine settings.

Figure 2.1 Stratigraphic models proposed for the McMurray Formation. **(A)** Lithostratigraphic and allostratigraphic model developed by the Alberta Energy and Utilities Board (2003, now Alberta Energy Regulator). **(B)** Lithostratigraphic and allostratigraphic model established in this study based on the MGC nomenclature. Note the basal erosional contact of channels are autogenic erosional surfaces, which do not serve as boundary of allostratigraphic units in this study.



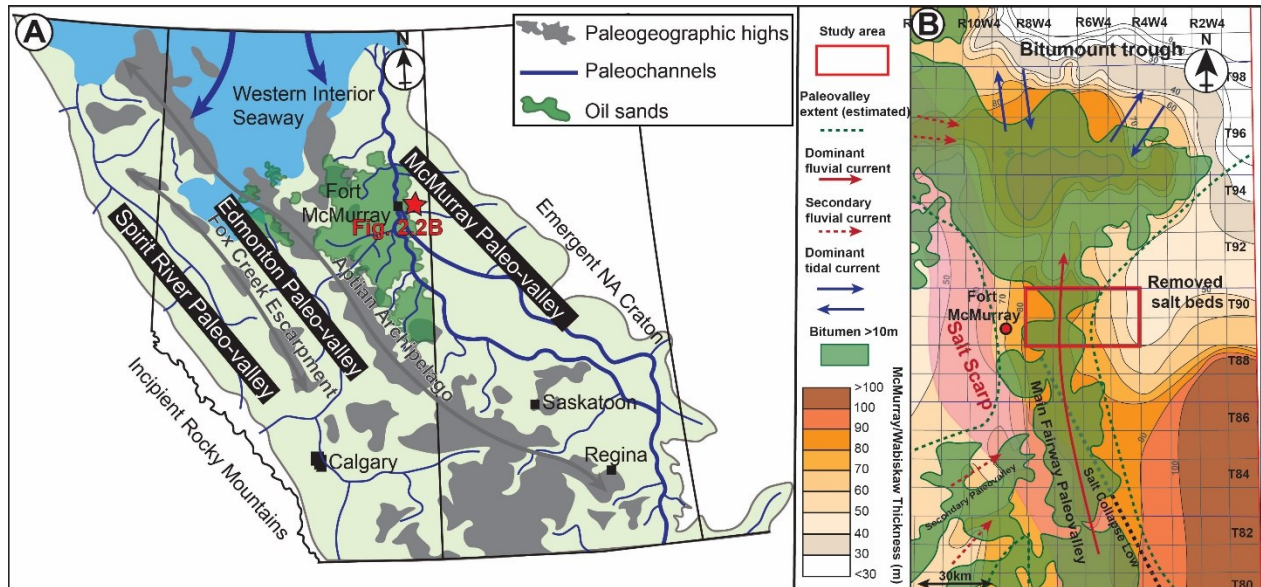
GEOLOGICAL SETTING

In the Athabasca Oil Sands Region, the McMurray Formation unconformably overlies the regionally extensive Sub-Cretaceous Unconformity, which truncates Devonian strata in the foothills and lower Paleozoic strata towards the eastern margin of the Western Canada Sedimentary Basin (Hayes et al., 1994). The paleotopography of the Sub-Cretaceous Unconformity was influenced by salt dissolution of the underlying Devonian Prairie Evaporite Formation (Christopher, 1974; Wightman and Pemberton, 1997; Broughton, 2014), which complicates the interpretation of pre-, syn- and post-depositional tectonism. The Sub-Cretaceous Unconformity, as a result of the formation of the Main McMurray Valley,

marks the base of a northwest-southeast trending sediment transport fairway (Wightman et al., 1995; Hein et al., 2013). The McMurray Formation was deposited during the long-term southward transgression of the Boreal Sea. Informal subdivision of the McMurray Formation into lower, middle, and upper members is based on the evolution of depositional systems from fluvial, estuarine, and coastal plain to marginal marine environments during this transgression (Carrigy, 1959; Flach and Mossop, 1985; Hein and Cotterill, 2006). The McMurray Formation is overlain by the Wabiskaw Member of the Clearwater Formation (Hein *et al.*, 2013). A schematic stratigraphy of the Athabasca Oil Sands deposit is shown in Fig. 2.1.

The study area is located in the easternmost McMurray main fairway paleovalley. The major structural controls on sedimentation of the McMurray Formation include a west-flanking Paleozoic carbonate high, and longitudinal regional subsidence caused by salt dissolution of underlying Devonian Prairie Evaporite Formation (Christopher, 1974; Broughton, 2016). McMurray Formation sand is mainly sourced from the south and southeast, derived from Saskatchewan, western Manitoba, northern Montana, and North Dakota, while minor westerly sources from the rising Cordillera contributed sediment to the Wabiskaw Member (Hein et al., 2013), as indicated in Fig. 2.2A and B.

Figure 2.2 (A) Paleogeographic reconstruction of the Early Cretaceous Western Canada Sedimentary Basin (WCSB), including the location of the ancient meander-belts deposit of the study (modified from Durkin *et al.*, 2017). **(B)** Isopach map of the McMurray Formation overlain by bitumen thickness map in the region (modified from Broughton, 2013). Structural elements (including Bitumount Trough, Salt Scarp and removed salt beds), extent of paleovalleys and fluvial/tide paleocurrent directions are modified from the combined work of Broughton (2013), Hein *et al.*, (2013) and Martinus *et al.*, (2015).

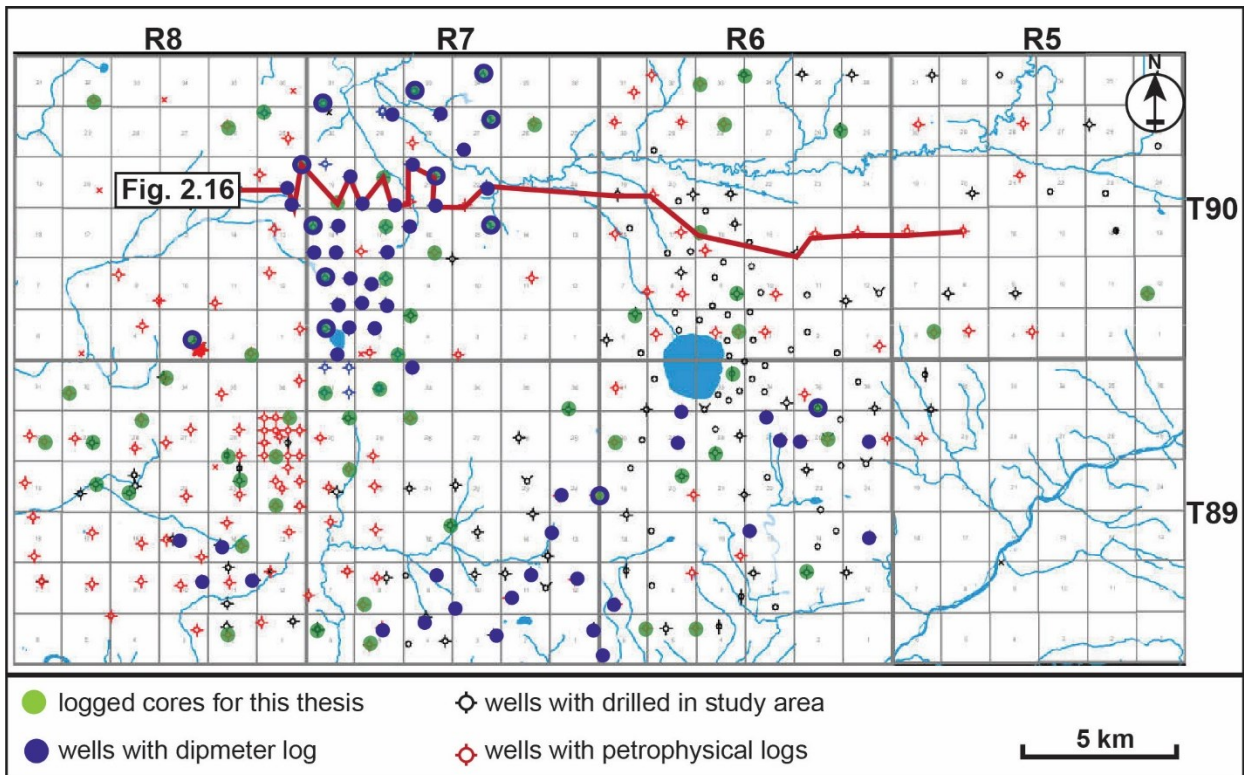


STUDY AREA AND METHODOLOGY

The project area is located approximately 30 kilometres east of Fort McMurray and extends between Townships 89-90 and Ranges 5-8 W4M (Fig. 2.3). This study area is named by MGC as the south of Central-B region. Within the study area there is no outcrop exposure. The McMurray Formation exists within the subsurface between 80-230 metres true vertical depth, and ranges from 60-90 metres in thickness, depending on whether the deposition occurred within paleovalleys or structural highs. The data set consists of 161 wells containing petrophysical logs, of which 89 have cores available. Fifty-three wells include dipmeter logs but are restricted to T90 R7W4 and near the border with T90 R8W4 and T89 R7W4. Among the dipmeter log dataset, Cenovus donated information from 18 wells located in the T89 R6-8W4. Due to the complexity of stacking patterns in fluvial/estuarine point-bars, dipmeter data are crucial for identifying the genetic relationships between point bars.

Sixty-seven cores were logged in detail, focusing on characteristics such as lithology, grain-size, sedimentary structures, accessories features, ichnofossils and bioturbation intensities (BI), and bitumen saturation (Table 2.1). Observed sedimentological and ichnological characteristics permitted the recognition of individual facies, which were further grouped into distinct facies associations. Dipmeter log data were used to assist in the identification of point-bar deposits. A West-East-oriented stratigraphic cross-section was generated, based on identification of major stratigraphic units, and a representative local stratigraphic framework was established for future study in the area nearby. The identification of stratigraphic units is based on the MGC regional framework (Fig. 2.1B). They are referred as allomembers in this study. Lithostratigraphic surfaces are picked based on changes in lithofacies or facies associations. The identified channel belts are bounded at their bases by autogenic erosion surfaces, and by either an allogenic flooding surface (equivalent to transgressive surface of erosion, TSE) or an autogenic flooding surface (caused by channel avulsion associated with delta lobe switching) on their top. Of particular note, the basal erosional surfaces of these channel belts are exclusively autogenic, which are not used to constrain allostratigraphic units in this study. In Fig. 2.1B, same color of the upper and lower bounding surfaces of a channel belt only indicates that the channels were developed during the deposition of allostratigraphic unit. The criteria used to determine regional *versus* local flooding surfaces are discussed below.

Figure 2.3 Study area and data availability



FACIES ASSOCIATIONS

Fluvial, tidal or oscillatory processes acting on the paleo-shoreline and within the estuarine system controlled the depositional architecture and stacking pattern of McMurray Formation strata. Each depositional process or combination of processes (e.g., fluvially dominated, tidally influenced) within the different stratigraphic successions give rise to the various observed facies associations. The core observations suggest an evolution from basal fluvial/estuarine to marginal marine environments as the Boreal Sea transgressed southward during Early Cretaceous time. Four major groups of facies are differentiated based on lithological composition: Sandstone Facies, Inclined Heterolithic (Sand/Mud) Facies, Interbedded Sand/Mud Facies, and Mudstone Facies. Each facies group is further divided into individual facies, based on fabric and textural properties such as sedimentary structures and ichnofossils. In the McMurray Formation to Wabiskaw Member interval, there are 19 facies identified from core

observations. Detailed descriptions and interpretations of each facies are summarized in Table 2.1.

Corresponding facies characteristics are indicated in Figures 2.3, 2.4, and 2.5.

Six facies associations are identified by combining individual facies, which represent sub-environments of a fluvially dominated through to tidally influenced estuary system (Table 2.2). Vertical stacking patterns, nature of contacts, and characteristic thicknesses of these facies and facies associations are summarized in Table 2.3. The distribution of facies associations is strongly influenced by the paleotopography along the Sub-Cretaceous Unconformity. Boundaries between these facies associations may be erosional or gradational. Erosional contacts commonly coincide with boundaries between systematically stacked point-bars, which can be recognized by abrupt changes in dipmeter measurement orientations (e.g., Brekke and Roenitz, 2021). The gradational contacts between facies associations represent gradual transitions related to changes in flow conditions and sediment supply as transgression continued. FA1 represents fluvially dominated channel deposits of the lower McMurray and occupies paleotopographic lows, unconformably overlying Devonian-aged carbonate successions. Middle McMurray strata are characterized by FA2 (tidally influenced inner estuarine channel and associated point bars) and FA3 (inner estuarine abandoned channel), which show significant tidal modulation on amalgamated inner estuarine point bars. FA3 commonly gradationally overlies FA2, resulting in an upward-fining trend that records the gradual abandonment of an inner estuarine channel. FA4 (wave-influenced delta, associated with brackish-water embayment) and FA5 (storm-influenced brackish-water embayment) overlie FA2 and FA3, and constitutes the upper McMurray. FA6 (lower shoreface to offshore) caps FA4 and FA5, marking the continued basinward shifting of facies expression. Examples showing vertical stacking patterns of facies and facies associations are displayed in Fig. 2.13.

Figure 2.4 Sandstone facies. **a)** Core expression of F1a showing granules and pebbles bearing massive to low-angle cross-bedded sandstone with mudstone rip-up clasts. Well 01-05-090-07W4, depth: 197-198.5m. **b)** Core expression of F1b showing mudstone rip-up clasts. Well 01-05-090-07W4, depth: 169-170.5m. **c)** F1b high- to low-angle cross stratification with grain striping, Well 10-21-090-07W4, depth: 173-174.5m interval. **d)** Bioturbated mudstone laminae in grain-stripped cross-bedded sandstone of F1b. **e)** Coal fragments and granules present in F1b. Well 10-17-090-07W4, depth: 174.8-176.3m. **f)** F1f showing mudstone-clast breccia in sandstone. Well 02-19-090-07W4, depth: 155.52-156.27m. **g)** Core expression of F1d showing unidirectional rippled sandstone. Well 10-15-090-07W4, depth: 137.2-137.88m. **h)** Core expression of F1e showing glauconite-bearing sandstone with *Diplocraterion*. Well 11-06-090-07W4, depth: 136.2-137.7m. **i)** F1e showing marine trace fossils assemblages occur in mixed siltstone and glauconite-bearing sandstone unit. Well 02-16-090-07W4. **j)** F1f shows planar laminated sandstone truncating bioturbated massive sandstone. Well 10-21-090-07W4, depth: 128-129.5m. **k)** F1g showing combined flow rippled sandstone with abundant mudstone laminae and carbonaceous fragments. **l)** F1h showing bioturbated cross-stratified sandstone with common *Rosselia* and *Cylindrichnus*. Abbreviations: LAP – low-angle planar stratification; HAP – high-angle planar stratification, M.B – mud-clast breccia; PsL - Pinstripe lamination; PPB - planar parallel bedding; PL - parallel lamination; LB - lenticular bedding; CuR - current ripple; CfR - combined flow ripple; C.F. - coal fragments, Py - Pyrite nodules; Cy – *Cylindrichnus*; Pl - *Planolites*; Lo - *Lockeia*; Di - *Diplocraterion*; As – *Asterosoma*; Pa - *Palaeophycus*; Sc – *Scolicia*; Th - *Thalassinoides*; Ro - *Rosselia*. (next page)

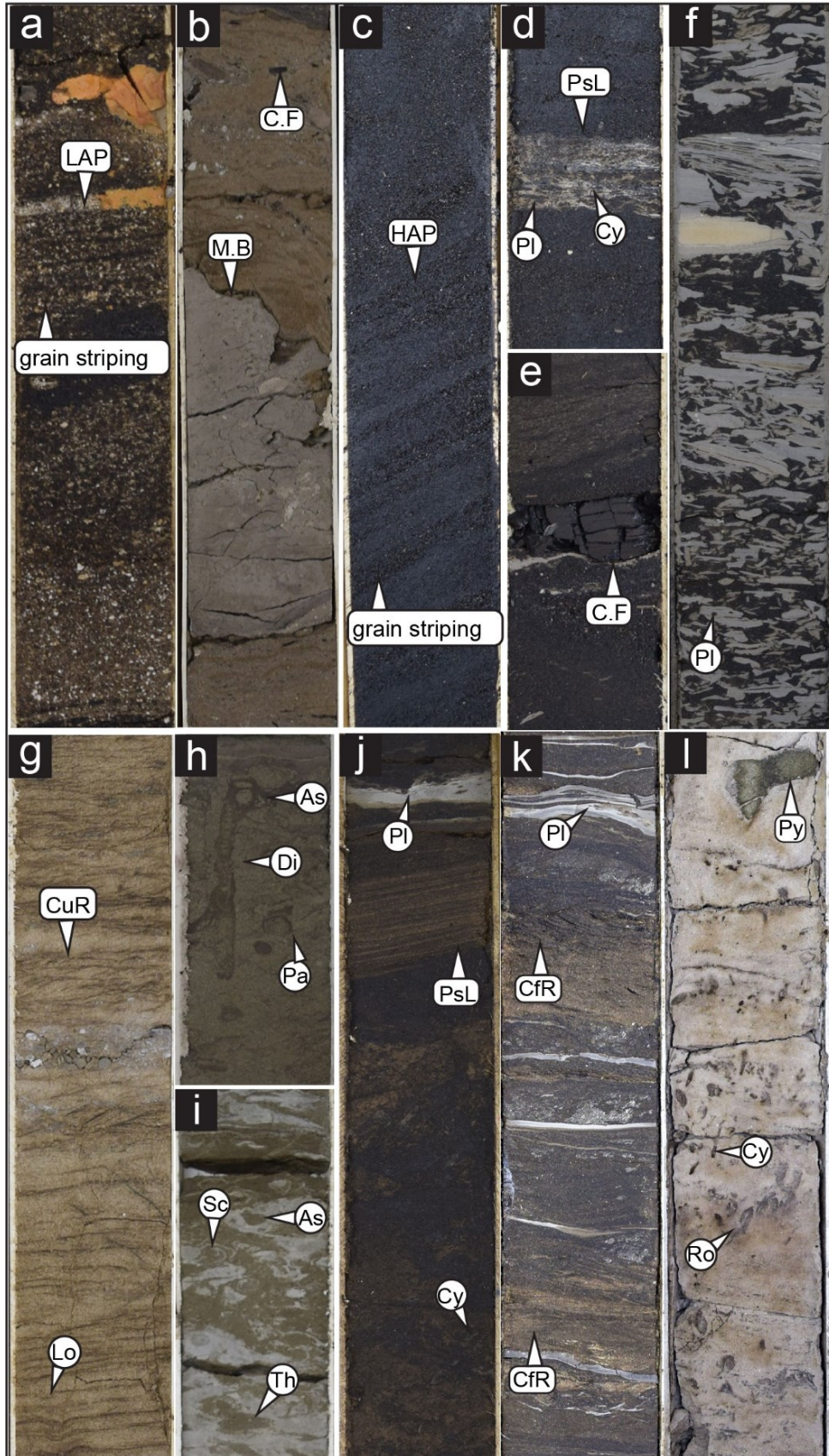


Figure 2.5 Inclined Heterolithic Stratification (IHS) consisting of sandstone/mudstone. Facies and interbedded sandstone/mudstone facies. **a)** Typical core expression of F2a showing homogeneous bioturbation with structureless mud laminae. Well 10-17-090-07W4, depth: 155.3-156.8m. **b)** F2a showing wavy bedded mudstone laminae in sandstone. Well 10-21-090-07W4, depth: 150.1-151.6m. **c)** Typical core expression of F2b showing intense bioturbation with local lenticular bedding. Well 10-21-090-07W4, depth: 156.7-157.6m. **d)** Typical core expression of F3a showing wave- to lenticular-bedded sand/mud. Well 01-05-090-07W4, depth: 184-185.5m. **e)** Core expression of F3b showing moderately burrowed wavy bedded sand and mud. Well 10-21-090-07W4, depth: 132.5-133.6m. **f)** Typical core expression of F3c showing homogeneously bioturbated interbedded sand and mud. Well 10-21-090-07W4, depth: 128-129.5m. Abbreviations: OsR - oscillation ripple; Cy - *Cylindrichnus*; Pl - *Planolites*; Lo - *Lockeia*; Di - *Diplocraterion*; As - *Asterosoma*; Pa - *Palaeophycu*., Sc - *Scolicia*; Gy - *Gyrolithes*; Sk - *Skolithos*; Ar - *Arenicolites*.

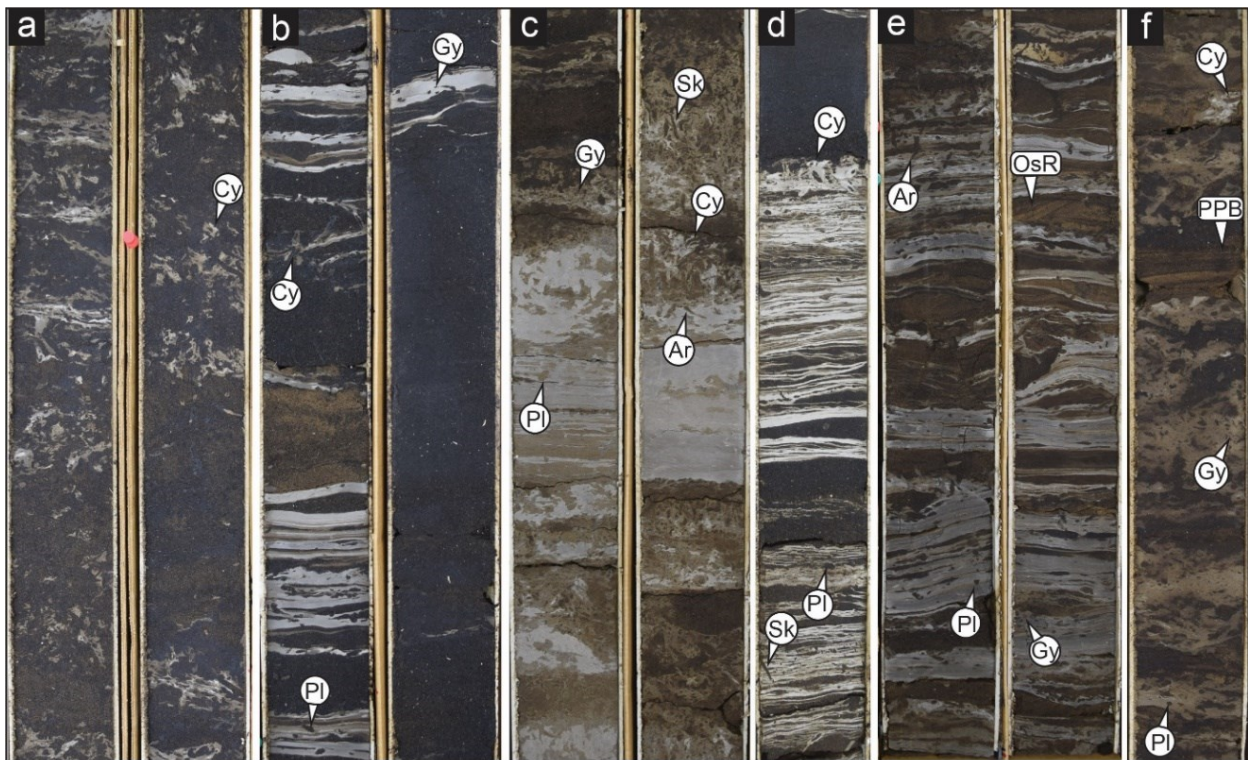


Figure 2.6 Mudstone facies. **a)** Typical core expression of F4a showing homogeneously burrowed mudstone with sandstone laminae. Well: 01-05-090-07W4, depth: 143.95-145.45m. **b)** Typical core expression of F4b showing relatively clean mudstone with minor mud laminae. Well: 05-33-090-07W4, depth: 167.8-169.2m. **c)** Core expression of F4c showing organic-rich mudstone interbeds with sandstone laminae or beds. Well: 10-34-090-07W4, depth: 139-140.6m. **d)** Core expression of F4c showing massive mudstone with intense bioturbation. Well: 10-34-090-07W4, depth: 139-140.6m. **e)** Core expression of F4d showing massive mudstone with BI 0. Well: 10-21-090-07W4, depth: 119-120.5m. Abbreviations: PL - parallel lamination; LB - lenticular bedding; SSD – soft-sediment deformation; Cy – *Cylindrichnus*; PI - *Planolites*; Ar - *Arenicolites*; Sch - *Schaubcylindrichnus*.

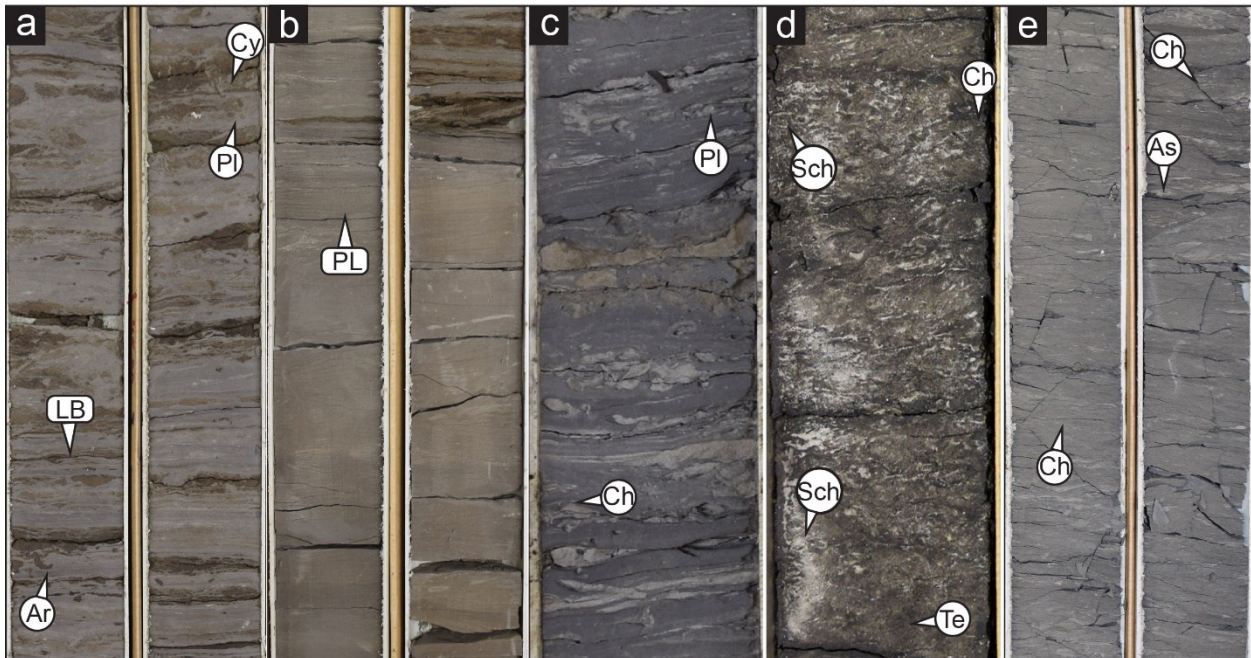






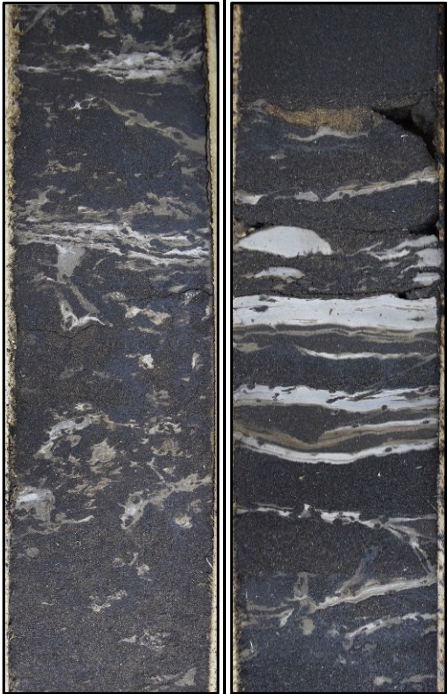







Table 2.1 McMurray Formation facies grouped by lithological characteristics. Abbreviations: Cy - *Cylindrichnus*; PI - *Planolites*; Lo - *Lockeia*; Di – *Diplocraterion*; As – *Asterosoma*; Pa – *Palaeophycus*; Sc - *Scolicia*; Gy – *Gyrolithes*; Sk – *Skolithos*; Ar – *Arenicolites*; Di – *Diplocraterion*; Sc - *Scolicia*; Gy - *Gyrolithes*; Sk - *Skolithos*; Te - *Teichichnus*; Th - *Thalassinoides*; Pa - *Palaeophycus*; Sc - *Scolicia*; Sch - *Schaubcylindrichnus*; Co - *Cosmorhaphie*; Ph - *Phycosiphon*; def. - deformation (next page).

Facies number	sandstone facies F1								
	F1a	F1b	F1c	F1d	F1e	F1f	F1g	F1h	
Facies name	massive to cross-bedded sandstone	massive to planar laminated sandstone	mud-clast breccia bearing massive sandstone	current-rippled sandstone	muddy glauconitic sandstone	bioturbated massive sandstone	current or combined flow rippled sandstone	bioturbated cross-stratified sandstone	
Typical core expression									
Grain size	<ul style="list-style-type: none"> • medium- to coarse-grained sand • pebbles: up to granule 	<ul style="list-style-type: none"> • very fine- to fine-grained sand • clasts: cm-scale diameter 	<ul style="list-style-type: none"> • lower medium- to fine-grained sand 	<ul style="list-style-type: none"> • upper fine-grained sand 	<ul style="list-style-type: none"> • silt to lower upper fine-grained sand 	<ul style="list-style-type: none"> • silt to upper fine-grained sand 	<ul style="list-style-type: none"> • very fine- to lower fine-grained sand 	<ul style="list-style-type: none"> • very fine- to lower fine-grained sand 	
Sedimentary structures	<ul style="list-style-type: none"> • high-angle planar bedding (through cross stratification) • local low-angle planar bedding • massive Ss near erosive base • grain size stripping between medium- and coarse-grained sand 	<ul style="list-style-type: none"> • massive to cross bedded sandstone matrix • local current ripples • Minor climbing ripples • minor tidal bundles in mudstone lamina • local grain size stripping between very fine- and fine-grained sand 	<ul style="list-style-type: none"> • massive matrix 	<ul style="list-style-type: none"> • abundant current ripples or climbing ripples 	<ul style="list-style-type: none"> • structures mottled by bioturbation 	<ul style="list-style-type: none"> • local planar parallel cross stratification , wave ripples • minor wavy bedding 	<ul style="list-style-type: none"> • common current and combined flow ripples • local cross stratification 	<ul style="list-style-type: none"> • low- to high-angle cross stratification • planar parallel stratification 	
Other observation	<ul style="list-style-type: none"> • local mud rip-up clasts • local coal and pyritic coal fragments • granule to granule-size pebbles • local mud and coal laminations 	<ul style="list-style-type: none"> • local to common mudstone breccia • local coal fragments and laminae • common mud laminae 	<ul style="list-style-type: none"> • abundant mudstone rip-up clasts • local coal fragments 	<ul style="list-style-type: none"> • minor granules 	<ul style="list-style-type: none"> • abundant glauconitic sandstone 	<ul style="list-style-type: none"> • local mudstone rip-ups • compressed syneresis cracks 	<ul style="list-style-type: none"> • coal fragments • mudstone laminae 	<ul style="list-style-type: none"> • local pyrite nodules 	
ichnofossils	<ul style="list-style-type: none"> • BI: 0-1 • absent to minor PI confined in mudstone rip-ups/lamina 	<ul style="list-style-type: none"> • BI: 0-1 • absent with minor monospecific Cy in sandstone • ichnofossils confined in mudstone breccia including PI, Ar, and Gy 	<ul style="list-style-type: none"> • BI: 1-4 • Gy and PI in mudstone breccia 	<ul style="list-style-type: none"> • BI: 0-2 • BI increase upward: Cy, Lo, and Gy 	<ul style="list-style-type: none"> • BI: 1-3 • high diversity bioturbation with PI, Sc, Ar, Pa, Cy, Th, and minor Sch. 	<ul style="list-style-type: none"> • BI: 0-4 • common PI, Ar, and Cy. 	<ul style="list-style-type: none"> • BI: 0-1 • PI and Ar 	<ul style="list-style-type: none"> • BI: 0-3 • Common Ro, Cy, and minor Sk 	
Processes	<ul style="list-style-type: none"> • deposition under unidirectional currents • moderate hydrodynamic energy level • periodic fluctuation in flow energy 	<ul style="list-style-type: none"> • deposition under unidirectional currents • moderate hydrodynamic energy level • proximity with tidally influenced environment 	<ul style="list-style-type: none"> • high energy erosive events 	<ul style="list-style-type: none"> • unidirectional deposition • moderate energy 	<ul style="list-style-type: none"> • low physico-chemical stresses • deposition under slow but continuous rates of deposition 	<ul style="list-style-type: none"> • wave current • periodic storm influence 	<ul style="list-style-type: none"> • rapid, incremental sedimentation rate • mixed unidirectional and oscillation currents 	<ul style="list-style-type: none"> • rapid, incremental sedimentation rate 	
Interpretation	2D or 3D migrating dunes at the base of inner estuary channel fill	2D or 3D migrating dunes at the base of inner estuary channel fill	overbank collapsing in estuary channel	upper part of estuary point bar	lower shoreface to proximal offshore	distal delta front or non-deltaic shoreface	tidal bar or distal delta front	lower shoreface	

Facies number	inclined heterolithic sandstone/mudstone facies F2	
	F2a	F2b
Facies description	sporadically burrowed sandstone-dominated IHS.	moderately to highly burrowed mudstone-dominated IHS.
Typical core expression		
Grain size	<ul style="list-style-type: none"> • fine-grained sandstone interbeds with mm- to cm-thick mudstone 	<ul style="list-style-type: none"> • silt to upper fine-grained sand
Sedimentary structures	<ul style="list-style-type: none"> • common parallel to non-parallel wavy bedding near the basal section • flaser bedding in the middle section and upper succession • local current ripples, rarely truncated by mudstone beds 	<ul style="list-style-type: none"> • local wavy bedding and lenticular bedding • massive sandstone/mudstone
Other observations	<ul style="list-style-type: none"> • mudstone laminae are partially destroyed by bioturbation • common mudstone rip-ups • common pinstripe laminae within mudstone beds • minor granules, coal fragments and lamina, mud drapes • local compressed syneresis cracks 	<ul style="list-style-type: none"> • bioturbation partially or completely homogenize the sediment • minor mudstone clasts • rare double mudstone drapes • minor pyritized mudstone section
Ichnofossils	<ul style="list-style-type: none"> • BI: 0-2 • common PI, Gy, and Ar in mud beds • Cy in monospecific abundance, with minor Sk and Th 	<ul style="list-style-type: none"> • BI: 3-5 • common Cy in monospecific abundance • common PI, Gy, Sk, and Ar. • minor As, Pa, and Lo
Processes	<ul style="list-style-type: none"> • salinity-stressed quiescent environment • tidal influence • brackish-water condition • salinity fluctuation • seasonal deposition alternating between freshet-dominated and tide-dominated periods 	<ul style="list-style-type: none"> • tidal influence • seasonal deposition causing shifting of the location of turbidity maximum • reduced influence of freshets • stable brackish-water condition
Interpretation	middle part of the lateral accretion deposit of fluvio-tidal point bars	middle to upper part of the lateral accretion deposit of fluvio-tidal point bars

Facies number	interbedded sandstone/mudstone facies F3			
	F3a	F3b	F3c	F3d
Facies name	lenticular-wavy bedded sandstone interbedded with mudstone	low to moderately bioturbated wavy bedded sandstone and mudstone	homogeneously bioturbated sandstone and mudstone	intensively bioturbated sandstone and mudstone
Typical core expression				
Grain size	• clay to very fine-grained sand	• clay to very fine-grained sand	• clay to very fine-grained sand	• clay to silt or very fine-grained sand
Sedimentary structures	• common wavy and lenticular bedding • local current ripples • local mud drapes	• dominant wavy bedding with minor lenticular bedding • local oscillation ripples • local soft sediment deformation • rare scour surfaces • rare double mud drapes	• common wavy to lenticular bedding • local sharp contact with overlying planar stratified sandstone	• massive to wavy/lenticular bedded sandstone and mudstone
Other observations	• rare soft-sediment deformation	• minor pyritized mudstone section and pyrite nodules • minor mudstone rip-ups • local syneresis cracks	• structures destroyed by bioturbation	• primary structures partially destroyed by bioturbation
Ichnofossils	• BI: 0-2 • common PI, Gy, and Ar, minor Sk and Th • Cy in monospecific abundance	• BI: 1-3 • sporadically distributed PI, and Ar. • minor As, Gy, Di, Te, and Th	• BI: 2-5 • sporadic PI, Ar, and Gy. • minor Cy, Te, and Lo	• BI: 1-3 • monospecific Gy • sporadically distributed PI and Te.
Processes	• salinity-stressed environment • tidal influence • salinity fluctuation • moderate energy level	• brackish-water influence • tidal influence • rapid sedimentation rates with rare erosive events, e.g., storms	• mixed brackish and marine conditions • paralic and quiescent environment with periodic erosive events	• quiescent environment • dominant brackish-water condition • minor marine influence
Interpretation	tidally influenced upper estuary point bar or tidal flat	proximal prodelta or brackish bay margin	storm-influenced embayed shoreface or brackish bay	restricted brackish embayment/interdistributary bay/lagoons






Facies number	mudstone facies F4						
	F4a		F4b	F4c		F4d	F4e
Facies description	low to moderately bioturbated lenticular bedded mudstone		massive to laminated mudstone/silt stone	planar stratified mudstone		massive to fissile mudstone/silt stone	organic-bearing massive mudstone
Typical core expression							
Grain size	• clay to upper very fine-grained sand		• clay to very fine-grained sand	• clay to upper fine-grained sand		• clay to silt	• clay
Sedimentary structures	• common flaser bedding • rare wave ripples		• massive to planar laminated mudstone • local lenticular bedding	• massive to planar laminated mudstone • minor lenticular bedding		• massive mudstone/siltstone	• massive mudstone • often pedogenic
Other observations	• common mud drapes • minor soft sediment deformation		• local pyritized mudstone • minor syneresis cracks	• minor soft-sediment deformation • organic-rich mudstones		• organic rich mudstone fragments common • local pyrite nodules	• local rootlets, pyrite nodules • coal fragments
Ichnofossils	• BI: 1-3 • sporadically distributed Pl, Gy, and Sk • minor Ar, Lo, and Te		• BI: 0-2 • common Pl, rare Te, Ar, Cy and Sk	• BI: 0-5 • common Ch, Pl and As • minor Ph, Sch, Sk, and Ar		• BI: 0-2 • sparse Pl, Co, and As	• BI: 0 • trace fossil absent
Processes	• brackish water condition • quiescent suites • wave and tidal influences • periodic rapid deposition events • more distant geographical location than F3a		• salinity stressed environment • low-energy environment • salinity fluctuation	• mixed marine and brackish water condition • rare high energy event with rapid deposition rates		• stable marine environment • extremely low energy level	• freshwater condition • low energy level • expose to organic materials
Interpretation	intertidal mudflats, distal prodelta, or marginal embayment		abandoned channel deposit	distal prodelta, distal brackish bay, or offshore		offshore embayment	floodplain, overbank, or vegetated tidal flat

Table 2.2 Facies associations and their facies components.

Facies associations		Strat. unit		MGC nomenclature	Including facies																									
					F1a	F1b	F1c	F1d	F1e	F1f	F1g	F1h	F2a	F2b	F3a	F3b	F3c	F3d	F4a	F4b	F4c	F4d	F4e							
FA 6	lower shoreface to offshore	Wabiskaw Member																												
FA 5	storm-influenced brackish embayment	McMurray Formation		middle to upper	A, B1																									
FA 4	wave-influenced delta				B2																									
FA 3	abandoned channel				A, B1, B2, C channels																									
FA 2	tidally influenced inner estuary channel																													
FA 1	fluviially dominated estuary channel			lower	D channel																									
						Major facies						Major facies																		

Table 2.3 Facies associations (FA) and facies occurrences of the McMurray Formation in study area. (i.e., stacking patterns, nature of contacts, characteristic thicknesses, and processes active in settings). Constituent facies in each facies association are listed in ascending order of abundance (dominant facies are highlighted in bold texts).

Facies Association		facies stacking pattern	facies contacts	characteristic thicknesses	processes in setting
FA6	lower shoreface to offshore	<ul style="list-style-type: none"> basal succession is characterized by alternating F3d and F4c the basal succession is overlain by F1e or F1h top of the succession is characterized by thick F4d 	<ul style="list-style-type: none"> FA6 has erosional lower contact with the McMurray Formation succession alternating F3d and F4c have gradational internal contacts F3d and F4c succession has erosional lower contact, and gradational upper contact with F1e or F1h F1e or F1h has upper gradational contact with F4d 	<ul style="list-style-type: none"> FA6: up to ~10m F3d and F4c: 10s of cms to metres F1e or F1h: 10s of cms to a few metres F4d: a few metres to 10s of metres 	<ul style="list-style-type: none"> overall low depositional energy and sedimentation rate with rare storm influence. marine water condition
	Constituent facies: F4d, F3d, F1e , F1h, and F4c				
FA5	storm-influenced brackish embayment	<ul style="list-style-type: none"> entire succession is dominated by alternating F1f, F3c, and F3d thin F4a, and F4c are locally present 	<ul style="list-style-type: none"> FA5 has sharp basal contact with FA2 or FA6, and sharp upper contact with FA6. sharp or gradational internal contact between alternating facies 	<ul style="list-style-type: none"> FA5: 10s of metres to 15m F1f, F3c, and F3d: 10s of cms F4a and F4c: cms to 10s of cms 	<ul style="list-style-type: none"> generally quiescent environment with occasional storm influence brackish-water condition
	Constituent facies: F1f, F3c , F3d, and F4c				
FA4	wave-influenced delta	<ul style="list-style-type: none"> a completely preserved succession is composed of F4a, F3b, and F1g from base to top preservation of a complete succession is rare 	<ul style="list-style-type: none"> FA4 has sharp or erosional basal and upper contacts with FA5 or FA6 F4a has sharp basal contact, and gradational upper contact with F3b F3b has gradational upper contact with F1g 	<ul style="list-style-type: none"> FA4: metres to 12m F4a: 5cm to 3m F3b: 10s of cms to 7m F1g: up to 12m 	<ul style="list-style-type: none"> dominantly flood-induced sedimentation under the influence of wave currents brackish-water condition
	Constituent facies: F4a, F3b , and rare F1g and F1f				
FA3	abandoned channel	<ul style="list-style-type: none"> entire succession is dominated by F4b that locally interbeds with thin F3a or F4a 	<ul style="list-style-type: none"> FA3 has sharp lower contact with FA2, and erosional upper contact with FA2, FA4, FA5, or FA6. Thin F3a and F4a have gradational lower and upper contacts with F4b 	<ul style="list-style-type: none"> FA3: a few metres to 30m F4b: up to 20m local F3a and F4a: 10s of cms to metres 	<ul style="list-style-type: none"> vertical aggradation of sediment during estuarine channel abandonment brackish-water condition
	Constituent facies: F4b , F4a, and F3a				
FA2	tidally influenced inner estuary channel	<ul style="list-style-type: none"> basal succession is characterized by F1b middle succession is dominated by F2a and F2b F1b commonly F1c locally occurs anywhere in FA2 F1d locally preserved on top of succession 	<ul style="list-style-type: none"> FA2 has erosional lower contact with FA1, FA3, or directly overlies Devonian carbonate F1b has erosional basal contact, and gradational upper contact with F2a F2a has gradational lower contact with F1b, and gradational upper contact with F2b F2b has gradational lower contact with F2a, and gradational or sharp upper contact with FA3 	<ul style="list-style-type: none"> FA2: 10s of metres F1b: metres to 10s of metres F2a: metres to 10s of metres F2b: metres to 10s of metres local F1c: 10s of cms to metres local F1d: 10s of cms 	<ul style="list-style-type: none"> fluvial processes with tidal influences brackish-water condition
	Constituent facies: F1b, F2a, F2b , F1c, and F1d				
FA1	fluvially dominated estuary channel	<ul style="list-style-type: none"> entire succession is dominated by F1a F1c locally occurs anywhere in FA1 F1d locally preserved on top of succession 	<ul style="list-style-type: none"> FA1 has erosional basal contact with Devonian carbonate, and sharp contact with overlying FA2 F1a has gradational upper contact with F1d F1c has gradational lower and upper contact with F1a 	<ul style="list-style-type: none"> FA1: locally preserved, up to 17m local F1c: 10s of cms to metres local F1d: up to 8m 	<ul style="list-style-type: none"> fluvial processes freshwater condition
	Constituent facies: F1a , F1b, F1d, and F4e				

FA1: Fluvially dominated inner estuarine channel

Description

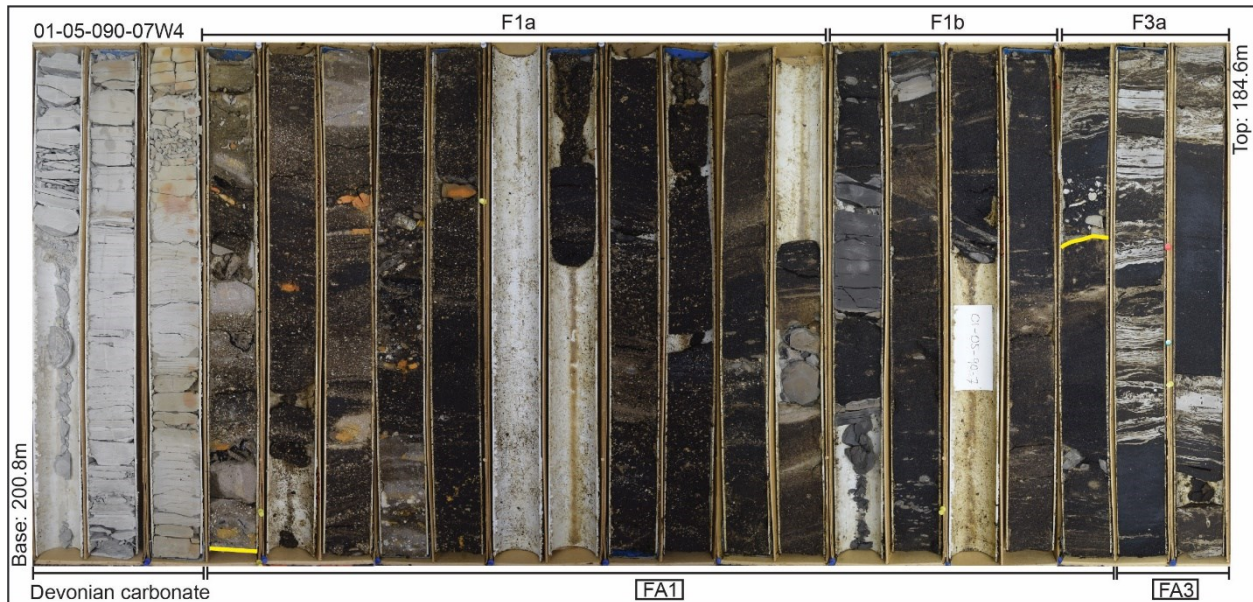
FA1 (F1a, F1b, minor F1d and F4e) (Fig. 2.4 and Fig. 2.7) consists of an erosionally based, fining-upward, sandstone-dominated succession, which is restricted to paleographic lows along the Sub-Cretaceous Unconformity. The top of FA1 is commonly truncated by FA2. In these constituent facies, sedimentary structures are dominated by dune-scale cross-stratified sandstone with subordinate planar parallel lamination and current ripples. The sandstone of F1a and F1b commonly show grain striping and typically contain unburrowed, granule to cobble (cm-10s cm diameter) mud-clast breccia (Fig. 2.4b). The normally graded succession is characterized by an erosional basal contact with granules and pebbles. Rippled sandstone of F1d is locally observed in the upper part of the succession. Mudstone clasts and laminae in these dominant facies also contain localized pyrite nodules, rhythmic lamination, and coal fragments. The organic-bearing massive mudstone F4e is differentiated from other similar facies by its abundant organic debris and rootlets. The facies of FA1 are unburrowed, although diminutive traces of *Planolites* (Fig. 2.4b) are observed rarely in mudstone clasts in the sandstone. The trace fossils bearing mudstone clasts are allochthonous, and do not reflect processes and conditions at the depositional locale.

Interpretation

The fining-upward facies succession records spatial variations in facies that reflect deposition in a fluvially dominated channel. The cross-stratified sandstone of F1a and F1b is interpreted as the migrating dunes in a fluvial channel fill. The mudstone of F4e commonly display pedogenic with rootlets and pyrite nodules, which are indicative of subaerial exposure. Coal fragments and enrichment of organic matters suggest close proximity of plant debris that are commonly found in floodplain or overbank deposits of these fluvial channels. Pebbles of F1a and F1b, unidirectional cross-bedded to massive sandstone near the basal of the succession, as well as the general absence of trace fossils consistently suggest moderate to high energy level in the fluvial channel system. The local presence of mud-clast breccia represents bank collapse resulting from cut bank erosion during high-energy fluvial events. F1d current-ripple

laminated sandstone may occur in the upper portions of the FA1 succession, indicating decreasing energy in the shallower parts of channels.

Figure 2.7 Core photos of FA1 (fluvially dominated inner estuarine channel) and overlying FA3 (mixed tidal flat). Note the erosional contact identified between the two facies associations: well 01-05-090-07W4.



FA2: Tidally Influenced Estuary Channels

Description

FA2 (F1b, F2a, F2b, F1c, and F1d) (Fig. 2.4, Fig. 2.5, and Fig. 2.8) encompasses a fining-upward succession and consists of erosional-based, unidirectional cross-bedded F1b sandstone, overlain by inclined heterolithic stratified (IHS) sandstone and mudstone of F2a and F2b. The FA2 succession is commonly truncated at its top by another FA2 (or rarely FA3) succession. In some cases, ripple-laminated sandstone (F1d) is locally observed near the top of the FA2 succession. This facies association is widely present in the study area and characterizes the majority of deposition within the middle to upper McMurray Formation interval. The majority of cores in the study area show a progressive change upwards from cross-bedded sandstone to IHS facies. Sharp contacts, however, have been observed from a few core examples as well.

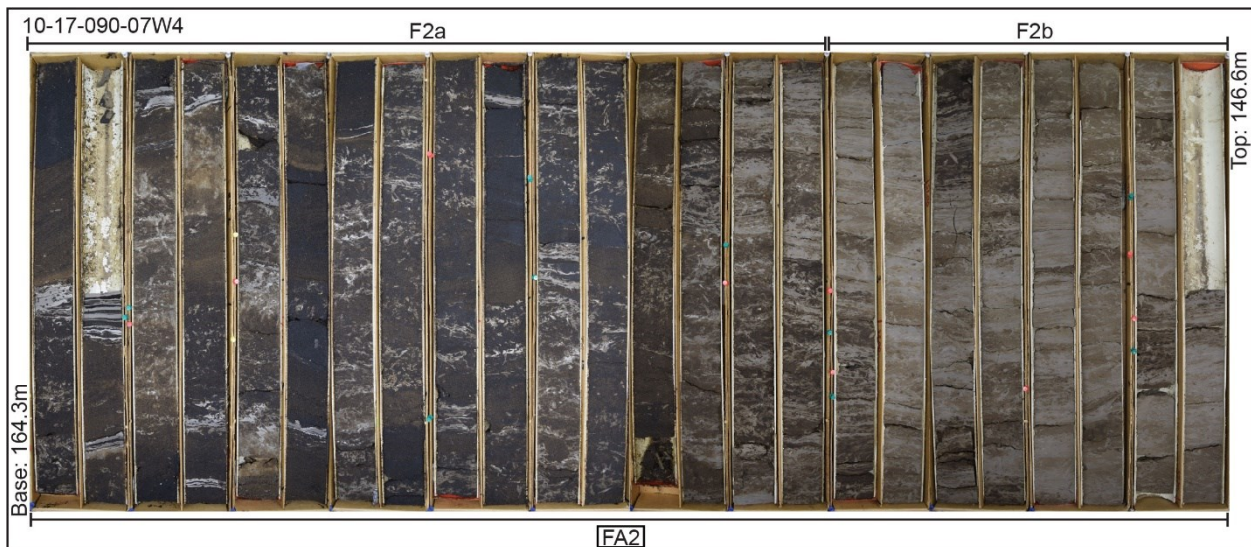
In general, the dominant facies of FA2 displays current-generated primary sedimentary structures, including dune-scale cross-stratification, planar parallel lamination, and current ripples. Wavy to lenticular bedding is locally observed in IHS (F2a and F2b). Mud-clast breccia-bearing sandstone (F1c) is locally preserved in FA2. Unlike the mud-clast breccia observed in FA1, the clasts in F1c are much smaller (millimetre to centimetre scale), are commonly laminated and may contain primary bioturbation (Fig. 2.4f). Ichnologically, the bioturbation intensity of a continuous FA2 succession increases upward from BI 0 to 5. The distribution of trace fossils commonly displays an intermittent pattern and are more dominant in mudstone-rich intervals. The trace-fossil suite comprises the following ichnogenera in descending order of abundance: *Planolites*, *Cylindrichnus*, *Gyrolithes*, *Skolithos*, *Arenicolites*, *Palaeophycus*, *Thalassinoides*, and *Lockeia*. These trace fossils are diminutive and normally occur in low-diversity suites (e.g., 1 to 3 ichnogenera).

Interpretation

The fining-upward FA2 succession records lateral facies changes in amalgamated, tidally influenced inner estuary channel belts. The observed fining-upwards successions are generally interpreted as shoaling point bars. The current-generated sedimentary structures (i.e., dune-scale cross-stratification, current ripples, and planar parallel laminations) observed in the FA2 succession are consistent with large-scale channel thalweg dunes formed on the lower parts of point bars. The common heterolithic stratified facies (F2a and F2b) suggest seasonal fluctuation of depositional energy, which are common facies in tidal influenced successions. Mud-clast breccia of F1f occurs in the middle to upper parts of a continuous succession and is interpreted as the hydraulic erosion and fragmentation of mud beds on the accreting bar surfaces. Where intraformational breccias occur at the bottom of a succession (commonly overlying an erosional contact), they are, instead, interpreted as channel-margin erosion. The ichnological assemblage is characterized by diminutive trace fossils and low diversity, facies-crossing ichnogenera that are consistent with brackish-water conditions (Pemberton et al., 1982; Pemberton et al., 1992; Gingras et al., 1999; Gingras et al., 2016). As such, the combined ichnological and sedimentological observations suggest that FA2 represents the point-bar deposits in a tidally influenced fluvio-estuarine channel.

The commonly truncated top of the succession is due to persistent lateral migration of point bars or shifting of meander belts. Therefore, the preservation of point bars is highly variable, depending on the degree of lateral migration of these channel belts. Complex stacking patterns of the point bars are observed across the study area where multiple channels crosscut each other.

Figure 2.8 Core photos of FA2 tidally influenced estuary channel and associated point bars, showing a continuous fining-upward succession, passing from sandy F2a to muddy F2b. Well 10-17-090-07W4.



FA3: Inner estuarine abandoned channel

Description

FA3 (F4b, F4a, and F3a) (Fig. 2.6 and Fig. 2.9) consists of thick, massive to laminated mudstone/siltstone of F4a and F4b, interbedded with less common lenticular to wavy bedded F3a and centimetre-scale IHS intervals of F2a and F2b. The thickness of this facies association is highly variable but can be up to 30 metres. There are two types of FA3 occurrences observed in cores: 1) anywhere in a stacked point bar succession with erosional top and basal contacts (e.g., Fig. 2.9); and 2) gradationally overlying FA2, forming a continuous fining-upward succession.

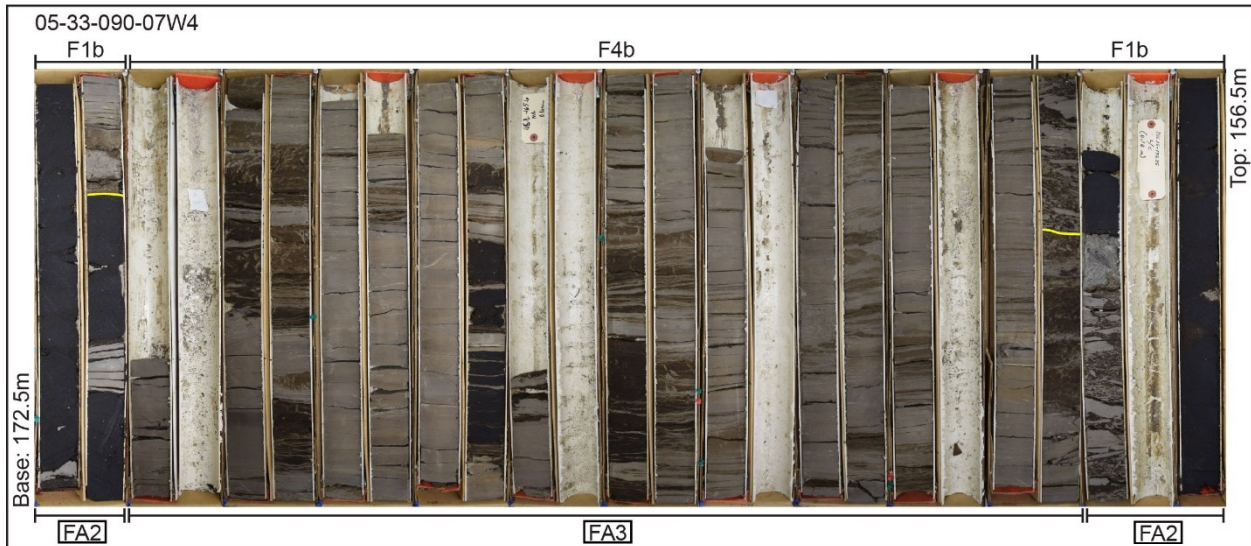
In this mudstone-dominated facies association, primary bedding is preserved in sandstone, including planar parallel lamination and lenticular to wavy bedding. Common sedimentary structures, including oscillation ripple stratification, syneresis cracks, and soft-sediment deformation, also occur within these

composite bedsets. Ichnologically, bioturbation intensities are variable but low throughout the facies association, ranging from BI 0-3. Trace fossil assemblages of FA3 are similar to those of FA2, but tend to display higher diversity and greater bioturbation intensity in sandstone-rich successions. Common ichnogenera observed in FA3 are *Planolites*, *Gyrolithes*, *Skolithos*, *Arenicolites*, *Teichichnus*, and *Cylindrichnus* (in descending order of abundance).

Interpretation

Mudstone-dominated FA3 is interpreted to result from estuary channel abandonment. The top of FA3 is characterized by an erosional contact with other estuarine point-bar deposits (F2a or F2b). The basal contact is locally sharp-based but more commonly gradational with FA2, representing the final abandonment of an estuarine channel point bar. Sandstone-dominated IHS (F2a) is rarely present and are interstratified with the mudstone-rich facies F4a and F4b, which implies periods of current flow through the estuary channel that led to the migration of dune-scale bedforms. The lenticular to wavy bedded F3a and F4a are interpreted to record tidal reworking within the abandoned channel fills. Similar abandoned channel/interchannel facies associations or facies were observed in previous studies by Crerar and Arnott (2007) (their FA3) and Labrecque *et al.* (2011) (their F7). The low-diversity, diminutive, facies-crossing trace fossil assemblage of FA3 is indicative of brackish-water conditions (Pemberton *et al.*, 1982; Pemberton and Wightman, 1992; Gingras *et al.*, 1999; Gingras *et al.*, 2016). As such, combining the occurrences of FA2 with the sedimentological and ichnological characteristics of FA3, this facies association is consistent with the sedimentation within abandoned channels in an inner estuary setting.

Figure 2.9 Core photos of FA3 mixed tidal flat and abandoned channel observed in well 05-33-090-07W4. Note that the abandoned channel is truncated at its top by an overlying channel deposit (erosional contact is marked by a yellow line).



FA4: Wave-influenced delta associated with brackish-water embayment

Description

FA4 (consisting of F4a, F3b, and rare F1g and F1f) (Fig. 2.4, Fig. 2.5, Fig. 2.6, and Fig. 2.10) is characterized by a coarsening-upward succession, and predominantly consists of progressive deposition of lenticular bedded mudstone of F4a, and wavy bedded sandstone and mudstone of F3b, followed by less common current- or combined flow-rippled sandstone of F1g and bioturbated massive sandstone of F1f. This coarsening-upward succession is locally preserved, forming packages that range from 5-10 metres thick. The upper part of the succession is commonly truncated by another cycle FA4 or a succession of FA5 (e.g., Fig. 2.10 and well 10-21-090-07W4 in Fig. 2.13). In these facies, primary sedimentary structures observed in sandstone intervals are both current- and oscillation-generated, including current, oscillation, and combined flow ripple cross-lamination (Fig. 2.4k). Other sedimentary structures, such as local soft-sediment deformation, sour surfaces, double mud drapes, and syneresis cracks, occur within heterolithic composite bedsets that range from lenticular to wavy bedding. FA4 is commonly dominated by heterolithic facies of F4c and F3b (Fig. 2.10A and B), but in rare occurrences, it consists of sandstone facies of F1g (Fig. 2.10C). The ichnological expression of the heterolithic facies

(F4c and F3b) shows a variably increase in bioturbation intensity with BI ranges between 0 to 3. Diversity of ichnogenera increases upward in the succession as the sandstone component increases (Fig. 2.10A and B). Trace fossils are more predominant in mudstone beds. However, in cases where the succession is dominated by rippled sandstone of F1g (Fig. 2.10C), trace fossils are very rare to absent. Millimetre-scale mudstone laminae within this sandstone-dominated succession are commonly associated with soft-sediment deformation and minor *Planolites* and *Teichichnus*. The trace fossils identified in FA4 are generally diminutive in size, and the assemblage encompasses the following ichnogenera, in order of decreasing abundance: *Planolites*, *Arenicolites*, *Gyrolithes*, *Asterosoma*, *Diplocraterion*, *Skolithos*, *Teichichnus*, *Lockeia*, and *Thalassinoides*. The sandstone-dominated facies F1g displays a general lack of bioturbation, with minor *Planolites* and *Arenicolites* observed only in mudstone laminae.

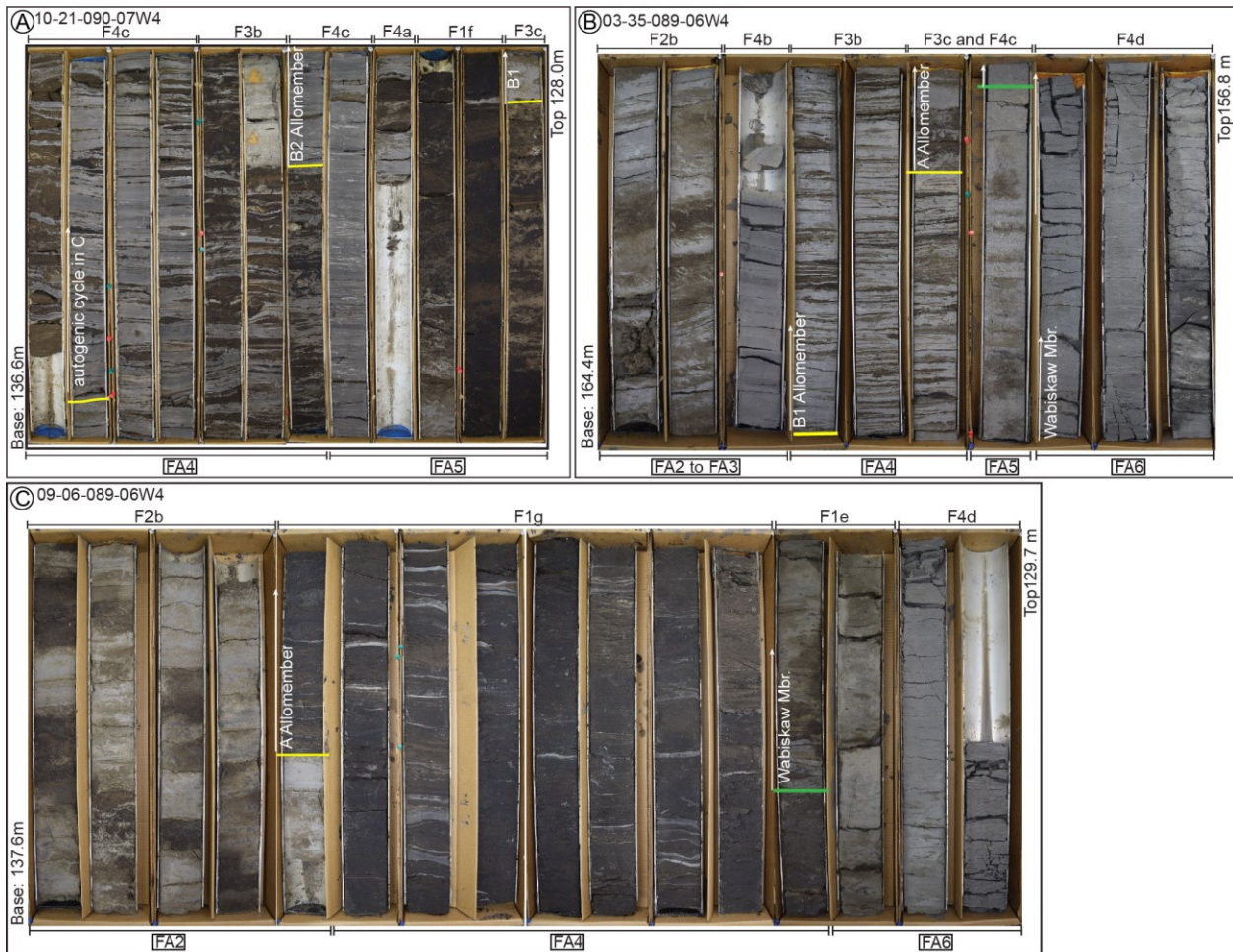
Interpretation

FA4 (F4a, F3b, and rare F1g) is interpreted to represent a wave-influenced deltaic succession that consists of interbedded sandstone and mudstone deposits of distal prodelta or bay-margin deposits (F4a), interbedded sandstone and mudstone (F3b) of the proximal prodelta, and rippled sandstone (F1g) or bioturbated massive sandstone (F1f) of the distal delta front. These facies are stacked vertically, resulting in a coarsening-upward succession that is either equivalent to allomember or to an autogenic cycle (i.e., shingle) within an allomember. The sparse distribution of FA4 may be the result of their preservation as erosional remnants, owing to autogenic lateral migration of estuary channels and incision by stratigraphically younger estuary channels due to allogenic events. Sedimentary structures show that both unidirectional currents and waves interacted with the embayment margin. These are attributed to the joint effect of storm-induced waves and fluvial discharge (e.g., MacEachern *et al.*, 2005; Collins *et al.*, 2017; Lin and Bhattacharya, 2021; MacEachern and Bann, 2023). The multiple lithological expressions (Fig. 2.10 A-C) and their associated ichnological characteristics are the result of temporally and spatially varying fluvial input into the system. The sandstone-dominated expression (i.e., Fig. 2.10C) represents a fluvial-dominated condition, which can be interpreted as deposits of a distributary channel within the distal delta front. Mudstone beds in heterolithic expressions (Fig. 2.10 A-B) are commonly bioturbated, which were deposited under slower deposition that corresponds to base flow conditions of the river. Sandstone

beds were deposited during periods of elevated river sediment influx, and the devoid of bioturbation of these sandstone beds are attributed to elevated physio-chemical stress.

The ichnofossil suite in FA4 comprises diminutive, low-diversity traces that are indicative of persistent brackish-water conditions (Pemberton et al., 1982; Pemberton and Wightman, 1992; Gingras et al., 2016). Comparing with archetypal facies of deltaic settings (i.e., *Phycosiphon* and *Rosselia* Ichnofacies defined by MacEachern and Bann (2020)), the FA4 successions identified in this study shows a marked decrease in diversity and paucity of fully marine elements, which consistently suggests stronger physico-chemical stresses than that of a typical delta. Therefore, we interpret the wave-influenced delta is likely associated with restructured brackish-water embayment that has limited connection to the open sea.

Figure 2.10 Variable core expressions of FA4 wave-influenced delta associated with a brackish-water embayment in well 10-21-090-07W4, well 03-35-089-06W4, and well 09-06-089-06W4. The top of the McMurray formation is marked by a green line that is equivalent to a regional transgressive surface of erosion. **A)** The observed autogenic cycle in stratigraphic unit C coarsens upward from weakly bioturbated, lenticular bedded mudstone and sandstone (F4a) to moderately bioturbated, wavy bedded sandstone and mudstone (F3b). **B)** Allomember B1 characterized by moderately bioturbated, wavy-bedded sandstone and mudstone (F3b). **C)** Allomember A is characterized by current- or combined flow rippled sandstone (F1g).



FA5: Storm-influenced to sheltered brackish-water embayment.

Description

FA5 (comprising F1f, F3c, F3d, and F4c) (Fig. 2.4, Fig. 2.5, Fig. 2.6, Fig. 2.10, and Fig. 2.11) consists of alternating bioturbated massive sandstone (F1f), variably bioturbated planar stratified mudstone (F4c),

homogeneously bioturbated sandstone and mudstone (F3c), and intensely bioturbated sandstone and mudstone (F3d). FA5 is the most common facies association in the upper McMurray Formation interval of the study area. The constituent facies commonly alternate with one other and do not form distinct coarsening-upward cycles in contrast to the typical successions of FA4. The base of FA5 is sharp, and locally overlain by variably bioturbated dark grey, planar stratified mudstone (F4c) (Fig. 2.10A). Varying expressions of FA5 can be observed (e.g., Fig. 2.10 and Fig. 2.11). Sedimentary structures are generally absent in FA5, except for minor syneresis cracks and evidence of soft-sediment deformation. Sandstone facies (F1f) commonly has a sharp basal contact with other facies, as shown in Fig. 2.11A and B. Soft-sediment deformation is commonly found to be associated with these sharp contacts. Ichnologically, mudstone-rich facies show variable intensities of bioturbation (BI 0-5). The ichnological suites in FA5 are generally diminutive but show the most diverse range of ethologies observed in the McMurray Formation. F3c is thoroughly and uniformly bioturbated, common ichnogenera include *Chondrites*, *Schaubcylindrichnus*, *Teichichnus*, *Planolites*, *Arenicolites*, *Asterosoma*, and *Phycosiphon*. It shares similar ichnogenera as mudstone-rich successions, but the most common trace fossils are *Cylindrichnus*, *Arenicolites*, and *Planolites*.

Interpretation

FA5 exhibits common facies expressions of a sheltered brackish-water embayment, including distal brackish bay deposits (F4c), storm-influenced marginal bay deposits (F3c), sheltered brackish bay margin deposits (F3d), and non-deltaic shoreface deposits (F1f). The predominance of thoroughly bioturbated facies F4c and F3c as well as the diverse trace fossil suites indicate a generally quiescent depositional environment with low deposition rates. The increased number of marine ichnogenera (e.g., *Chondrites*, *Schaubcylindrichnus*, *Teichichnus*, *Phycosiphon*, and *Asterosoma*) suggest salinities that were closer to normal marine and minimal fluvial influence. The diminutive traces are consistent with ichnological characteristics of an environment with brackish-water conditions. Common erosional surfaces within FA5 (e.g., the base of F1f) suggests reworking by high-energy events such as shoreface washovers and storms. These occasional events commonly produce soft-sediment deformation during periods of rapid sedimentation.

Figure 2.11 Variable core expressions of FA5 brackish-water embayment and FA6 shoreface to offshore in well 03-28-089-06W4, well 10-20-090-07W4, and well 13-11-089-06W4. **A)** Allomember A showing FA5 brackish-water embayment deposits, consisting of alternating homogeneously bioturbated sandstone and mudstone (F3c) and weakly bioturbated, planar stratified mudstone (F4c). **B)** Allomember A in well 00-20-090-07W4, consisting of alternating homogeneously bioturbated sandstone and mudstone (F3c) and bioturbated massive sandstone (F1f). Note the sharp contacts between facies. **C)** Allomember A in well 13-11-089-06W4, consisting of intensely bioturbated sandstone and mudstone (F3d) gradationally overlain by variably bioturbated, planar stratified mudstone (F4c). Green line marks the top of the McMurray Formation and yellow line corresponds to the base of Allomember A.



FA6: Lower shoreface to offshore

Description

FA6 (consisting of F4d, F3d, F1e, F1h, and F4c) (Fig. 2.4, Fig. 2.5, Fig. 2.6, Fig. 2.11 and Fig. 2.12) is the most common facies association of the Wabiskaw Member interval, which sharply overlies the McMurray Formation. FA6 is composed of 5 distinct facies. The base of FA6 succession is characterized by 2-20 centimetres thick, variably bioturbated planar stratified mudstone (F4c) that is gradationally overlain by coarsening-upward glauconitic sandstone (F1e). This succession is conformably overlain by unbioturbated, massive to fissile mudstone (F4d) (Fig. 2.11). In rare cases, FA6 clearly coarsens upward, and the planar stratified mudstone (F4c) grades into bioturbated, cross-stratified sandstone (F1h) (Fig. 2.12). Ichnologically, the basal planar stratified mudstone (F4c) is sparsely bioturbated (BI 0-2), with common *Chondrites*, minor *Planolites*, and minor *Arenicolites*. The overlying glauconitic sandstone facies (F1e) is characterized by robust trace fossils with BI ranges between 1-3. Common trace fossils observed in F1e include *Asterosoma*, *Chondrites*, *Cylindrichnus*, *Diplocraterion*, *Palaeophycus*, *Planolites*, *Teichichnus*, *Thalassinoides*, and *Scolicia*. The uppermost massive to fissile mudstone (F4d) is characterized by diminutive traces with BI of 0-2, including *Chondrites*, *Asterosoma*, and *Cosmorhappe*. In the rare coarsening-upward FA6 succession (Fig. 2.12), the glauconitic sandstone facies (F1e) is generally absent. The basal planar stratified mudstone (F4c) is up to 10m thick, which gradually grades into bioturbated sandstone (F1h). *Rosselia* and *Cylindrichnus* are the most common ichnogenera observed in F1h. Bioturbation intensity of the F4c increases upward with BI changes from 0 to 5, and the overlying bioturbated sandstone F1h has variable BI ranges from 0 to 3.

Interpretation

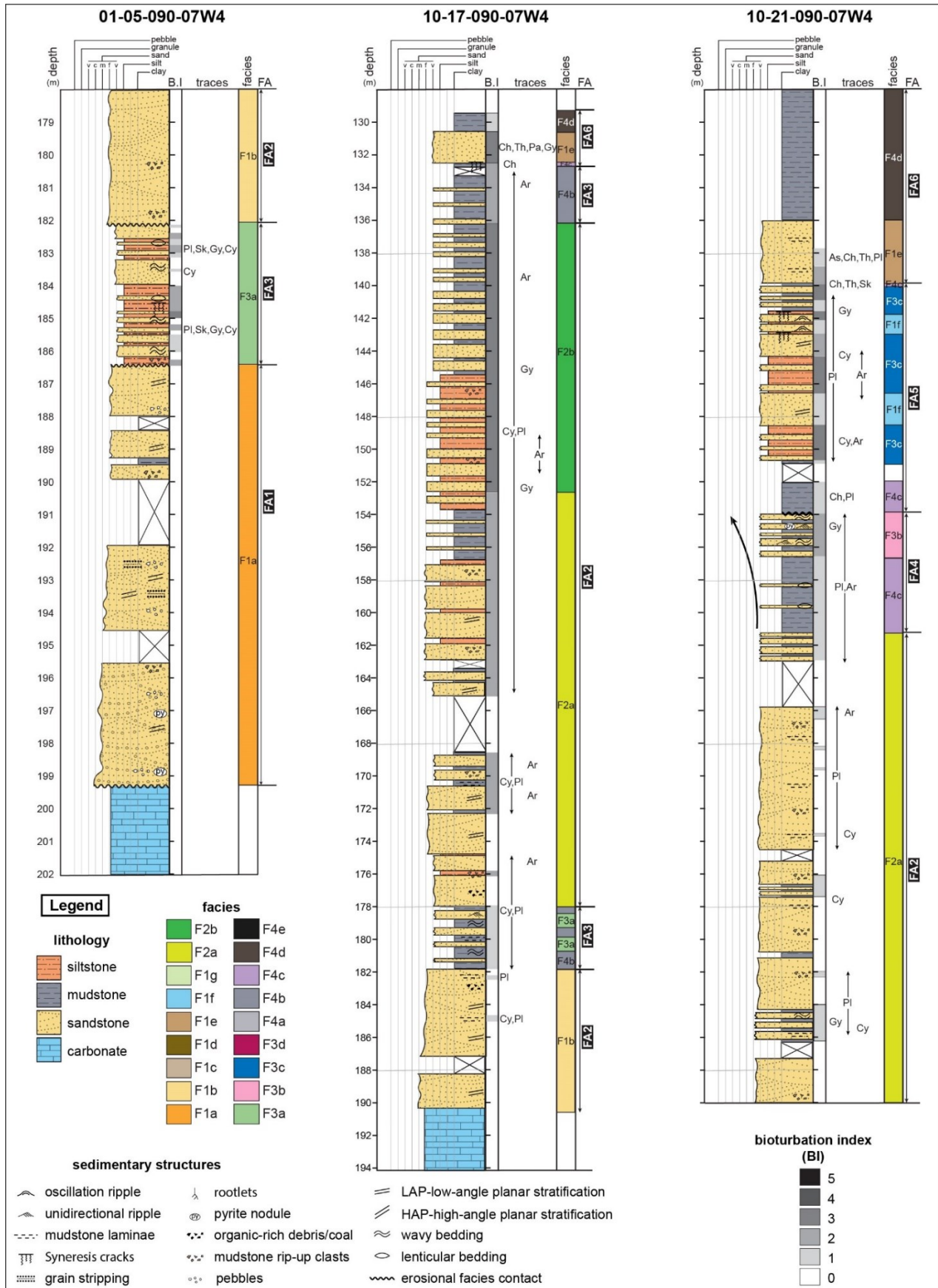
FA6 is interpreted to represent variable facies of the lower shoreface to offshore depositional environments. The robust and common marine trace fossils in FA6 exhibits elements of *Cruziana* Ichnofacies, suggest decreased environmental stress. The diverse trace fossil assemblage indicates a quiescent environment with generally low sedimentation rate. FA6 displays the most normal marine-associated ichnogenera and records the most distal facies expression of all observed facies associations.

According to the juxtaposition of all Facies Associations, FA5 is best interpreted as a succession of shoreface sandstone (F1e) grading upward into offshore deposits (F4d).

Figure 2.12 Core photos of a rare FA6 succession showing shoreface to offshore observed in the Wabiskaw Member.



Figure 2.13 Core lithologies for well 01-05-090-07W4, 10-17-090-07W4, and 10-21-090-07W4 showing lithology, sedimentary structures, bioturbation index (BI) and ichnofossils of the facies associations.



CHARACTERISTICS OF THE BOUNDING SURFACES

In previous studies of the McMurray Formation (e.g., Caplan and Ranger, 2001; Baniak and Kingsmith, 2018; Château *et al.*, 2020), the middle and upper McMurray Formation intervals have been interpreted as a series of either regressive (i.e., delta-dominated depositional model) or transgressive (i.e., incised valley depositional model) stratigraphic units. The foundation of establishing these sequence stratigraphic frameworks of the McMurray Formation is determining whether the bounding surfaces are allogenic. Many studies have proven that estuarine channel deposits of the middle to upper McMurray Formation successions are both allogenic (e.g., Ranger and Pemberton, 1997; Hein and Cotterill, 2006) and autogenic (e.g., Baniak and Kingsmith, 2018; La Croix *et al.*, 2019; Château *et al.*, 2020) origin.

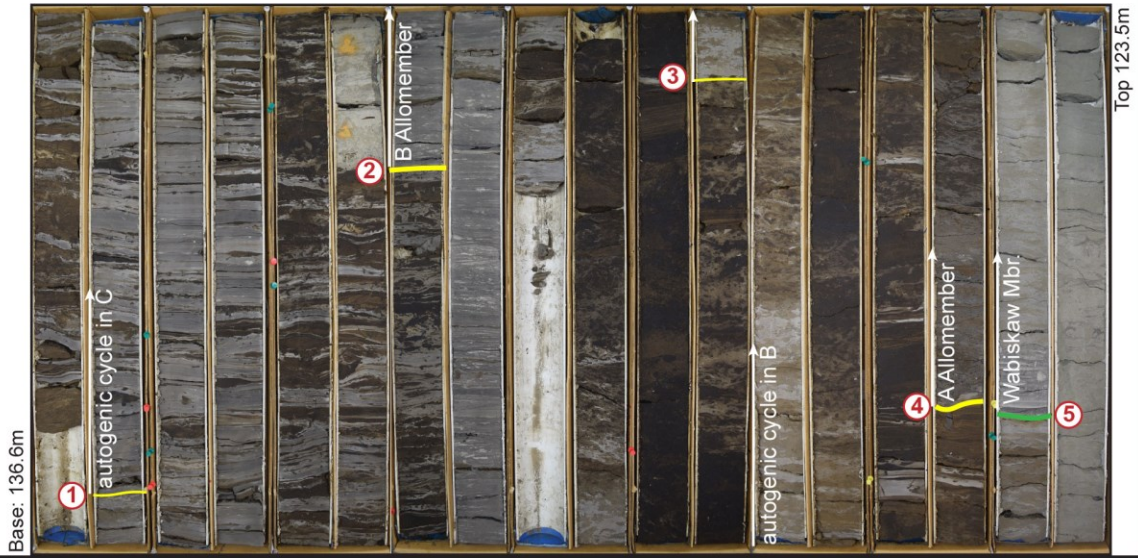
Allogenic flooding surfaces are sequence stratigraphically significant and are exclusively associated with base-level rises. Estuarine channels associated with (or are hung directly below) allogenic flooding surfaces have been commonly interpreted as valley incision linked to major sea-level drop in the McMurray paleovalley (e.g., Ranger and Pemberton, 1997; Hein and Cotterill, 2006; Hein *et al.*, 2013). Recent research has alternatively interpreted these channels as the youngest, basinward migrated fluvio-estuarine channel belt that was developed before the next episode of major base-level rise (e.g., Château *et al.*, 2020). On the contrary, autogenic flooding surfaces on top of estuarine channel deposits are developed due to delta lobe switching or shifts in the position of the shoreline during regression. The erosional bases of these channel complexes are results of lateral and downstream migration of channel belts, and their formation do not require significant base-level fluctuation. As such, the stratigraphic significance of allogenic and autogenic flooding surfaces is different: multiple autogenic flooding surfaces can be present within an allogenic stratigraphic unit (i.e., autogenic flooding surfaces are present A, B, and C units in this study). Detailed descriptions and comparisons of allogenic and autogenic surfaces within the McMurray Formation has been established by Château *et al.* (2020) in the west of Assiniboia Valley (south of the Athabasca Oil Sand Region). In their efforts, the lateral extent of

the flooding surfaces is one of the key criteria of determining whether a flooding surface is autogenic or allogenic: however it is challenging to differentiate them using solely core observations.

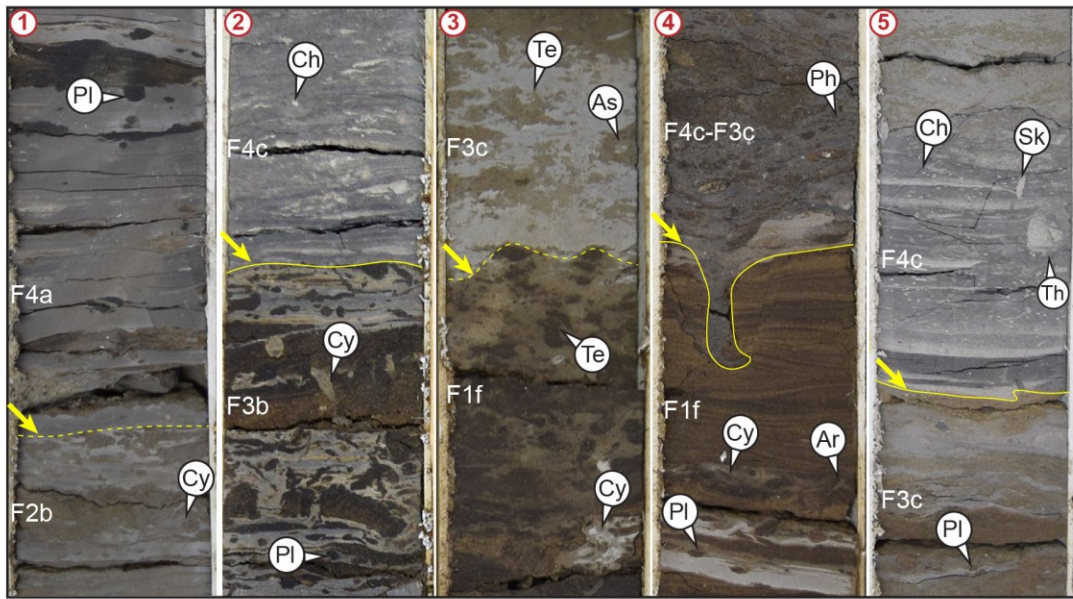
In this particular study, it is difficult to correlate most flooding surface because they are incised by deeply excavated fluvio-estuarine channel belts (as shown in Fig. 2.16). Therefore, the identification of these flooding surfaces, at least in part, is based on the contrasting sedimentological and ichnological characteristics above and below the surface. After detailed logging and facies analysis of the 67 cores in the study area, the characteristics of the two types of flooding surfaces are summarized below.

Figure 2.13 Details of the bounding surfaces observed in the cores in the study area (width of core: 6.5cm). **1)** An autogenic flooding surface separating bioturbated sandstone- to mudstone-dominated IHS (F2b) from overlying low to moderately bioturbated lenticular bedded mudstone (F4a). **2)** An allogenic flooding surface separating bioturbated wavy bedded sandstone and mudstone (F3b) from overlying weakly bioturbated dark gray mudstone (F4c). **3)** An autogenic flooding surface separating bioturbated massive sandstone (F1f) from overlying homogeneously bioturbated sandstone and mudstone (F3c). **4)** An allogenic flooding surface separating rippled sandstone in F1f from overlying bioturbated dark gray mudstone and sandstone (interbedded F4c and F3c). **5)** A regionally extensive transgressive surface of erosion marking the top of McMurray Formation. This separates the homogeneously bioturbated sandstone and mudstone (F3c) from the overlying dark grey mudstone containing marine trace fossils (F4c). Abbreviations: Pl-*Planolites*, Ch-*Chondrites*, Cy-*Cylindrichnus*, Te-*Teichichnus*, As-*Asterosoma*, Ar-*Arenicolites*, Ph-*Phycosiphon*, Sk-*Skolithos*, Th-*Thalassinoides*. (next page)

10-21-090-07W4



details of the bounding surfaces



Allogenic Flooding Surfaces

The youngest, regionally extensive flooding surface is identified at the contact between the McMurray Formation and the overlying Wabiskaw Member (surface 5 in Fig. 2.14). This contact is widely preserved in almost every core, except where is truncated by the Wabiskaw Member. This contact separates the brackish-water embayment associated with FA4 or FA5 from the overlying bioturbated, planar stratified mudstone of F4c. In particular, the mudstone of F4c is commonly dark grey color, and are commonly associated with trace fossils including *Chondrites* and minor *Skolithos*, *Thalassinoides*, and *Phycosiphon*. These ichnogenera are common elements of the *Cruziana* Ichnofacies and represent various types of ethnologies of their trace makers, such as deposit feeding, grazing, and horizontal and vertical dwelling traces. The dominance of structure produced by mobile fauna reflect accumulation of organic debris in a setting characterized by continuous, slow- to moderate-sedimentation in fully marine environment (Buatois and Mángano, 2011). In addition, the stressful conditions in the brackish embayment dramatically reduced the overall diversity and trace fossil sizes, resulting in impoverished assemblage (MacEachern and Pemberton, 1994). The general diminutive size and low-diversity trace fossil assemblage (especially monospecific *Chondrites*) can be associated with somewhat lowered dissolved oxygen levels (Savrda and Bottjer, 1986; Wignall and Myers, 1988; Dashtgard and MacEachern, 2016). The contact surface separates the normal marine succession (surface 5 in Fig. 2.14) from the underlying brackish-water succession and is interpreted as an allogenic flooding surface (FS) or transgressive surface of erosion (TSE).

Similar characteristics of flooding surfaces have also been identified in other stratigraphic intervals, such as the top of Allomember B and Allomember C (e.g., surface 2 and 4 in Fig. 2.14). In some cases, mudstones (F4c) occurring in stratigraphically older units (allomember B and C) show decreased proportions of normal marine traces (e.g., a paucity of *Chondrites* and *Phycosiphon*). Similar change in the marine expression of the transgressive mudstone underlying stratigraphic units have been previously observed in the McMurray Formation by Château *et al.* 2021. They interpreted this observation as one of the results of acceleration in the rate of the Boreal Sea transgression. It is more difficult to correlate these stratigraphically older flooding surfaces due to the complex cross cutting relation between channel belts.

Therefore, the juxtaposition of facies with contrasting trace fossil assemblage above and below the erosional surface suggest a transgression configuration (distal embayment deposit over proximal prodelta deposit) and make them good candidates for allogenic surfaces.

Autogenic Flooding Surfaces

Local flooding surfaces widely occur in stratigraphic units B and C. Surfaces 1 and 3 in Figure 2.14 show two possible candidates of this type of flooding surface. Facies observed above and below the surface share similar ichnological characteristics. In the case of surface 1 in Fig. 2.14, both the above F4a and underlying F2b show brackish-water trace fossil assemblages (e.g., *Planolites* and *Cylindrichnus*). In the case of Surface 3, the two facies above and below the bounding surface show similar diminutive normal marine ichnogenera (e.g., *Teichichnus*), except a slightly increased abundance of *Teichichnus* and *Asterosoma* in the F3c than the underlying F1f. The minor ichnological differences crossing the facies contact demonstrates that they are deposited in the same environment—that is, they record autogenic temporal and spatial changes in processes that occur within the same depositional environment. As such, comparing with the above allogenic flooding surfaces, these surfaces are more likely to be results of autogenic cycles that have been ascribed to channel avulsion in deltas or to shifting depocenters. Erosional down-cutting — owing to changes in the tidal prism or channel migration of an estuary channel, and basinward shifts of trunk channel system in regressive shoreline (e.g., Château *et al.* 2020; Pattison, 2020)— are equally viable. Correlations of autogenic flooding surfaces in these stratigraphically older units (Allomember B and C) are even more difficult due to the extensive excavation of channels.

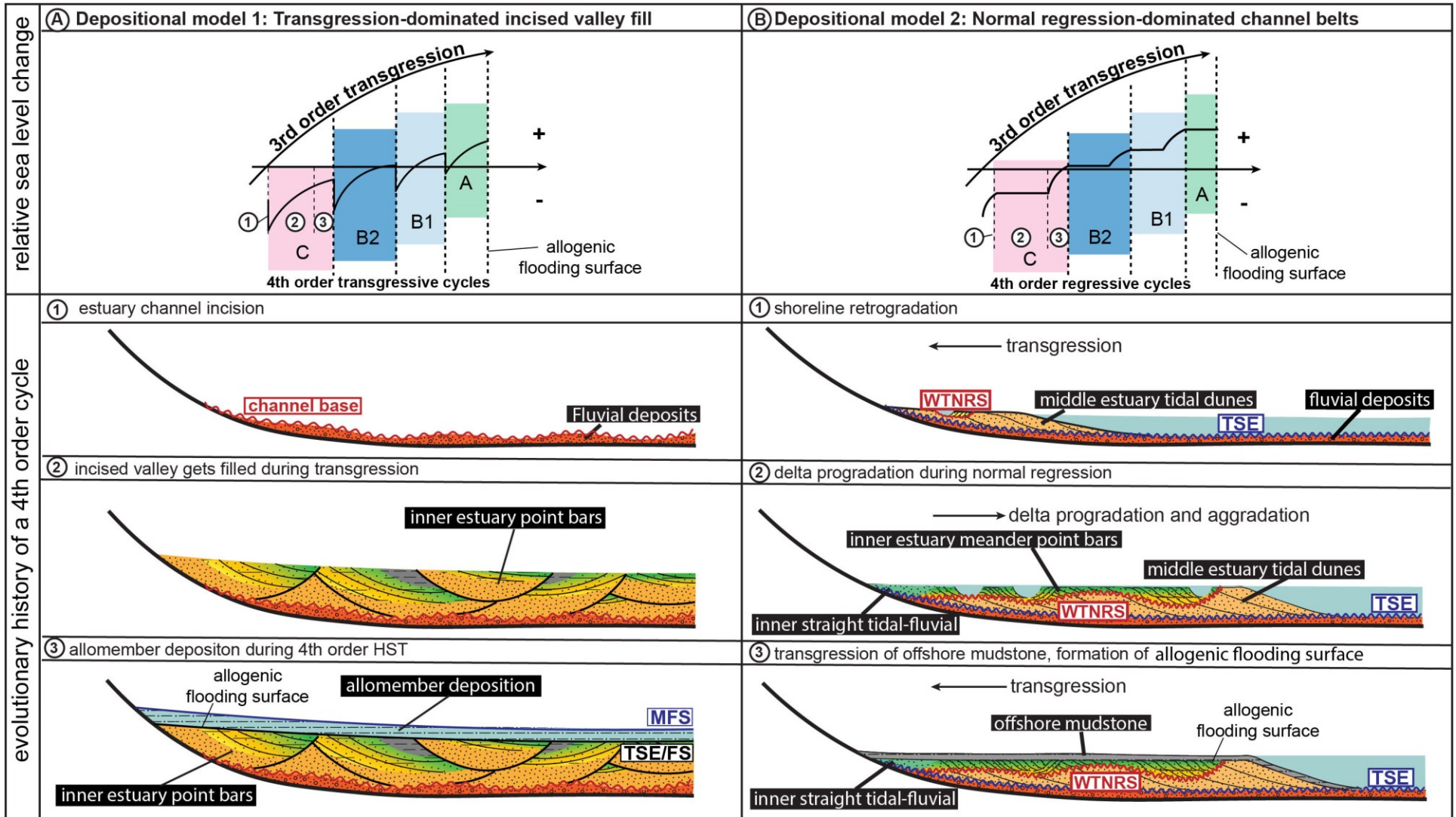
DISCUSSION

Stratigraphy and paleogeographic reconstructions of the estuary channels

A broad consensus has evolved regarding the depositional environments associated with the lower McMurray Member, and it is widely accepted that deposition occurred as fluviially dominated channel deposits based on the presence of alluvial plain facies including paleosols, coals, rootlets, organic-rich

mudstones, coarse-grained fluvial channel sandstone and non-marine trace fossils (e.g., Flach and Mossop, 1985; Ranger, 1994; Hein et al., 2000; Hein and Cotterill, 2006; Ranger and Gingras, 2010; Harris et al., 2016). As the most debatable interval of the entire McMurray Formation, the middle and upper McMurray has been variably interpreted as deposition of super-channel deposits of a fluvial system (Mossop and Flach, 1983; Flach and Mossop, 1985; Keith et al., 1988; Muwais and Smith, 1990; Blum and Jennings, 2016; Durkin et al., 2017), brackish-water estuarine valley-fill systems (Pemberton et al., 1982; Wightman and Pemberton, 1997; Crerar and Arnott, 2007; Hubbard et al., 2011; Labrecque et al., 2011; Martinius et al., 2015; Barton, 2016; Gingras et al., 2016), or deltaic systems (Carrigy, 1971; Gingras et al., 2003; Chateau et al., 2020). In this study, two depositional models are proposed to explain the architectural characteristics of the stacked point bars in the middle to upper McMurray Fm: 1) the transgressive incised valley-fill model; and 2) the regression-dominated fluvio-estuarine channel belt model. The relative sea-level curve and schematic diagrams of the two proposed depositional models are shown in Fig. 2.15. Supporting evidence is provided in this section to discuss the most feasible explanation for the observed stratigraphic architecture in the study area.

Figure 2.14 Relative sea-level curve and schematic diagram of the evolutionary history of two depositional models. **Left (A1-3)**: Sea-level curve and schematic diagram of depositional model 1 - Transgression-dominated incised valley fill model. **Right (B1-3)**: Sea-level curve and schematic diagram of depositional model 2: Regression-dominated fluvio-estuarine channel belt model.



Depositional Model 1: Transgression-dominated incised valley fill model

The transgression-dominated incised valley fill model was widely applied in regional stratigraphic studies by AEUB (2003). The stratigraphic units were picked by counting the number of nearshore coastal coarsening-upward sequences (their A1, A2, B1, and B2). The overall 3rd-order transgressive succession is composed of three episodic 4th-order transgressive cycles. As shown in the left column of Fig. 2.15, the valleys (A - C channels) were incised by fluvial erosion during the falling stage of sea level (FSST), and filled during a subsequent transgressive system tract (TST). The entire incised valley system is overlain by coarsening-upward nearshore coastal parasequences during the deposition of the highstand system tract (HST). These parasequences have been locally removed by subsequent forced regression.

In this dataset, the observed sedimentological characteristic of marginal marine deposits cannot be explained by this model. There is a general lack of coarsening-upward trends in the parasequences. Most allomembers (e.g., B1, B2, and C) are characterized by variable facies expressions of a brackish-water embayment system. The general lack of offshore mudstone above the flooding surfaces suggests only relatively minor base-level rises. Furthermore, evidence for interfluvial deposition between incised channels, such as pedogenic alteration, roots or coal, are not observed. As such, the incised valley model that assumes dramatic sea-level fluctuation does not well explain the observed stratigraphic framework in the study area. Notably, the depositional duration from the lower McMurray Formation ash to the coal seam in B1 has been dated approximately 6.32 ± 0.36 Ma by Rinke-Hardekopf *et al.* (2022). The interpreted 4th order stratigraphic cycles (scales of 100-200 thousand years) suggests that the incised valley model cannot be entirely excluded.

Depositional Model 2: Normal regression-dominated fluvio-estuarine channel belt model

An alternate depositional model that could have resulted in amalgamated channel belts is the normal regression-dominated fluvio-estuarine channel belt model. A schematic diagram summarizing the evolutionary history of this depositional model is shown in the right column of Fig. 2.15. Following the fluvial deposition during LST (3rd order), the allomember of the upper

McMurray Formation and middle estuary tidal sand bars were deposited landward during transgression (Fig. 2.15B2) and left behind a transgressive surface of erosion (TSE) at the base. During the succeeding normal regression, channels characterized by heterolithic point bars prograded over broader oceanward channels characterized by tidal dunes, thus truncating the more seaward units. The resulting truncation surface is expressed as an internal facies contact within the HST (Fig. 2.15 B2), which is defined as 'within-trend normal regressive surfaces' (WTNRS) (Catuneanu, 2006). The basinward progradation of trunk fluvio-estuarine channel system continued to feed the regressive shorelines during the prolonged HST. As the shoreline continued to move seaward, the channels increasingly excavated deeper into the previous allomembers. Similar examples have been shown in Castlegate Members in the Book Cliffs by Pattison (2020), and McMurray Formation in the southern part of the Athabasca Oils Sand deposit by Château *et al.* (2020). Applying this model, the stacked channel belts identified in this study are results of lateral and downstream migration of channel belts or simply lobe switching of delta lobes.

This model is a better fit for the observed stratigraphic architecture for the following reasons. First of all, the migration of channel belts results from autogenic cycles, which does not require significant base-level fluctuation. This can be evidenced by very similar sedimentological and ichnological characteristics observed in the different channel fills. Secondly, many flooding surfaces are not associated with an overlying offshore marine mudstone, which also suggests minor changes in base level. Thirdly, this depositional model better explains the erosional contacts (within-trend normal regressive surface (WTNRS)) between cross-bedded sandstone (CB) (equivalent to F1b in this study) and IHS (equivalent to F2a and F2b in this study) facies that are observed in outcrops (Ranger and Gingras, 2010; Hayes et al., 2018; Chen et al., 2022). The development of the WTNRS only requires minor base-level fluctuations. Finally, this model does not entirely exclude the existence of transgressive deposits. In other word, estuarine channel deposits of the McMurray Formation can be transgressive or regressive.

Stratigraphic architecture of the McMurray Formation in the Christina River region

A well-to-well stratigraphic correlation across the study area is presented in Fig. 2.16. To better illustrate the stratigraphic configuration, a schematic diagram showing the detailed architectures of the McMurray Formation in the Christina River study area is shown in Fig. 2.17. The middle to upper McMurray Formation interval records significant fluvio-tidal channel-belt incision and migration, which results in the poor preservation of allogenic and autogenic flooding surfaces. Allomembers observed in the dataset are relatively thin (approximately 2-10m), suggesting limited creation of accommodation spaces (Château et al., 2020). Allomember A is the best preserved and widely correlatable in almost every well, except where it is eroded by an A channel in the east of the study area. This youngest allomember is equivalent to the A1 and A2 sequences that have been previously defined by AEUB (2003). The differentiation between A1 and A2 are difficult to make in the study area due to the general lack of coarsening-upward lithological trends in the interval. In the Allomember B1 and Allomember B2, both allogenic and autogenic flooding surfaces are present, but their regional correlations are challenging due to the complex deep incisions and cross-cutting relation between channel belts. This correlation of flooding surfaces is even more difficult in the oldest Allomember C. As shown in Fig. 2.17, each stratigraphic unit is deemed to be a response to relative sea-level rise, with the new accommodation space quickly filled, indicating a progradational parasequence set and the establishment of an HST. The stacked stratigraphic units show a retrogradational stacking pattern, with the shoreline of A lying landward of B, and the shoreline of B lying landward of C. The transgression of the Boreal Sea is marked by regional flooding surfaces (equivalent to A, B, and C top). Autogenic surfaces 1-3 in the C unit are inferred flooding surfaces, which are interpreted to have been eroded by channel belt migration. Overall, the middle to upper McMurray succession records a gradual, incremental drowning of the estuary, which is composed of repeated regressive successions representing short-lived periods of shoreline progradation. Although it is not showing in Fig. 2.17, some

remnant transgressive tidal dune deposits were not entirely removed by the basinward progradation of fluvio-estuarine channel system are also present in the McMurray Formation.

Figure 2.15 West-to-East stratigraphic cross-section illustrating facies and estuarine channel architecture. The location of this cross-section is labeled in Fig. 2.3.

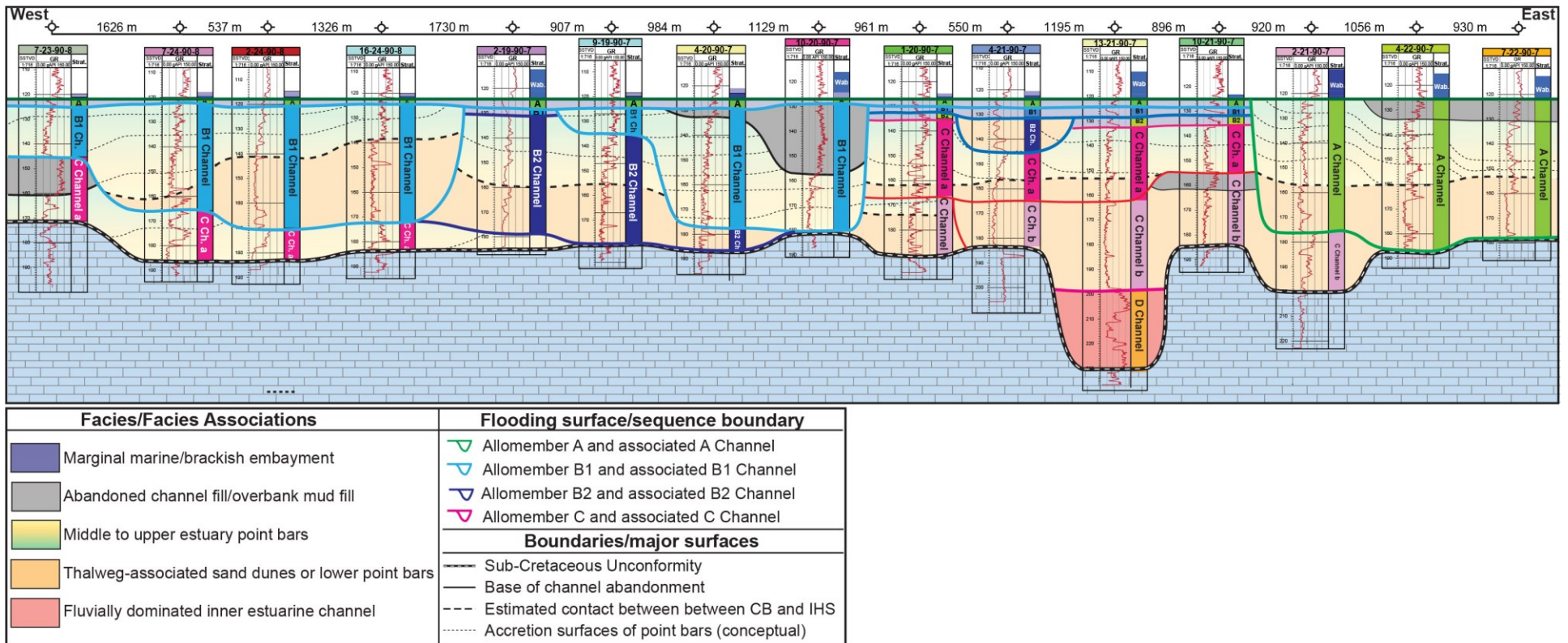
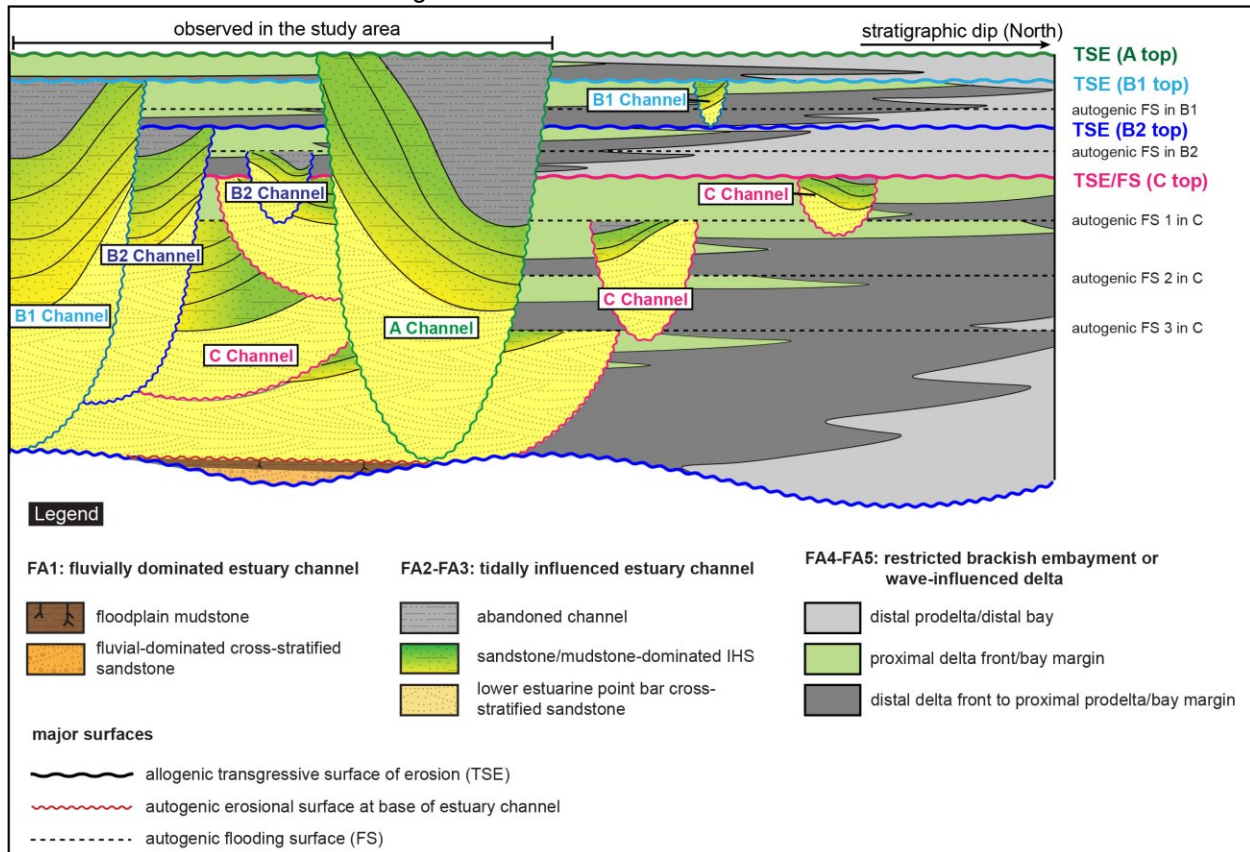


Figure 2.16 Schematic diagram showing the proposed stratigraphic architecture of the McMurray Formation in the Christina River region.



CONCLUSION

This study reveals three stratigraphic units (C, B, and A channels and their associated estuary point bars) in the middle McMurray estuarine channel succession, based on analysis of core-derived facies and petrophysical well logs. The sedimentological and ichnological characteristics of lithofacies suggest that the McMurray Formation in the Christina River area is dominated by deposits within tidally influenced fluvio-estuarine and brackish-water embayment settings. The complex cross-cutting relationships produced by estuarine channel incisions are developed at different stratigraphic levels during an overall transgression. The development of amalgamated estuary point bars is best explained by the regression-dominated fluvio-estuarine channel belts model, because it does not always require significant base-level fluctuations to achieve the resulting stratigraphic architecture. Pronounced fluvio-tidal channel-belt incision results in poor preservation of stratigraphic bounding surfaces within the McMurray Formation. The most important findings of this sedimentological and stratigraphic analysis in the study area include: 1) the relatively thin allomembers suggest that limited accommodation space was created during each base-level rise event; 2) the similar sedimentological and ichnological characteristics among channel belts and the general lack of well-defined coarsening-upward parasequences suggest the dominance of autogenic cycles; 3) both allogenic and autogenic flooding surfaces occurred in the McMurray Formation interval; and 4) stratigraphic units (allomembers and their associated channels) represent regressive cycles deposited under minor sea-level fluctuations, relict transgressive tidal dunes may have locally survived from progradational channel incisions in a regressive shoreline.

Chapter 3 : Integrating Facies Analysis with Dipmeter Data to Characterize Point Bars of the Lower Cretaceous McMurray Formation, Christina River, AB, Canada

INTRODUCTION

In the lower Cretaceous McMurray Formation, voluminous crude bitumen reserves are hosted in point-bar deposits of a fluvial-tidal channel depositional system (Pemberton et al., 1982; Wightman et al., 1987; Ranger and Pemberton, 1988; Hein et al., 2000). Large channels have been recognized in several studies, which variably focused on the stratigraphy, ichnology, and sedimentology of the McMurray Formation (e.g., Carrigy, 1963a, b; Hubbard et al., 1999; AEUB, 2003; Hein and Cotterill, 2006; Hein et al., 2006; Ranger and Gingras, 2008; Fustic et al., 2012; Durkin et al., 2017a; Durkin et al., 2017b). Large fluviotidal pointbars that sometimes display complex point-bar stacking patterns therein have been interpreted as amalgamation and migration of meandering channel belts in concert with overall sea-level rise.

Historically, dipmeter logs in the McMurray Formation have been used in combination with outcrop observation and image logs to identify dipmeter patterns and bedding architecture of the laterally accreted deposits (e.g., Muwais and Smith, 1990; Brekke and Evoy, 2004; Fustic, 2007; Nardin et al., 2013; Brekke et al., 2017; Brekke and Roenitz, 2021). High-quality seismic data allowed the identification of complex internal 3D point-bar architecture, various bar forms, and zone differentiation within a point bar (e.g., Fustic et al., 2008; Smith et al., 2009; Hubbard et al., 2011; Labrecque et al., 2011; Martinius et al., 2017).

Compared to seismic datasets, dipmeter-logs are more regionally available and they are very useful for the identification and demarcation of individual point bars, especially in cases where seismic data are absent in a dataset. In this study, dipmeter-log data has been used to interpret bedding and contact orientations to 1) interpret sediment transport directions; 2) indicate bedding orientation and bed-set architecture; 3) differentiate point bars and resolve their stacking patterns; and 4) infer aspects of sedimentary environments from those interpretations. Unlike other dipmeter papers using advanced microresistivity image logs to generate tadpole plots (e.g., Brekke et al., 2017; Brekke and Roenitz, 2021),

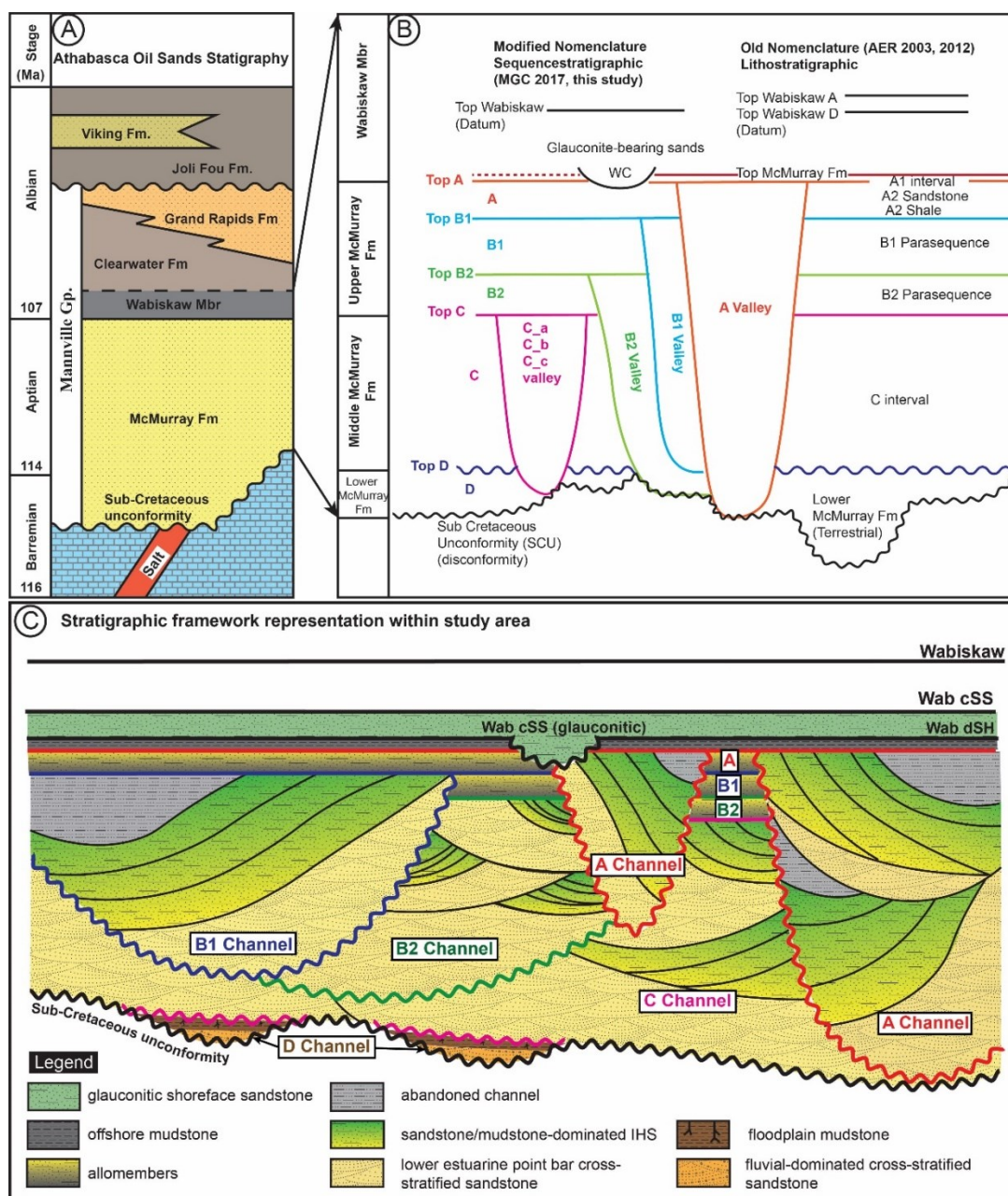
this study uses vintage dipmeter data collected by three armed dipmeter tools in the 1960s. These older tadpole data were manually digitized, and in the process we cleaned the dataset. Today, many wells penetrating the McMurray Formation only have vintage dipmeter data, and this paper provides an example of how these older dipmeter data can be used to assist analyses of point-bar stacking patterns and other facies assignments. In particular, this paper adds the dimensions of ichnology and sedimentology to understand how dipmeter data interpretations can be enhanced where augmented by core data. Importantly, this paper draws from earlier work by others that demonstrate the efficacy of using dipmeter data to mapping geobodies (e.g., Strobl et al., 1997; Fustic et al., 2008; Nardin et al., 2013; Brekke et al., 2017; Brekke and Roenitz, 2021).

GEOLOGICAL BACKGROUND

The McMurray Formation is deposited on top of the regionally truncated Upper Devonian carbonate strata of the Woodbend and Beaverhill Lake Groups in the Christina Lake area (Schneider and Grobe, 2013) (Fig. 3.1A). On a regional scale, the McMurray Formation has been informally subdivided into the lower, middle, and upper members (Carrigy, 1959; Wightman et al., 1995; Broughton, 2013). In general, the members represent the depositional system's evolution from fluvial (lower McMurray) to estuarine and coastal plain (middle McMurray), and ultimately to energy sheltered brackish embayment (upper McMurray) environments during the long-term southward transgression of the Boreal Sea (Fig. 3.2A) (Carrigy, 1959; Flach, 1977; James and Oliver, 1977; James, 1978; Flach and Mossop, 1985; Hein et al., 2006). Dissolution of the Devonian Prairie Evaporite Formation modified the paleotopography of the sub-Cretaceous unconformity by providing additional accommodation space locally. This is expressed as a structural low, the Bitumount Trough Basin, developed in the north of the study area (Christopher, 1974; Hein et al., 2000; Broughton, 2016) (Fig. 3.2B). According to outcrop and subsurface studies, it is accepted that the McMurray Formation was deposited within a broad paleo-valley and that the tributaries generally flowed to the north-northwest (Fustic et al., 2012; Hein et al., 2013; Martinius et al., 2015). These tributaries are similar in ages, and therefore referred to as the "Main Valley" in previous studies (Keith et al., 1990; Wightman and Pemberton, 1997; AEUB, 2003; Fustic et al., 2012).

Various stratigraphic models have been proposed to explain the repeated stacking patterns of transgressive-regressive cycles and complex cross-cutting relationships between estuarine point bars deposited in highly sinuous fluvial and estuarine channels of the middle McMurray (Hayes, 1975; AEUB, 2003; Ranger and Gingras, 2008; Nardin et al., 2010; Hein et al., 2013; Barton et al., 2014; Gingras, 2014; AER, 2015). The upper McMurray units are known to comprise stacked coarsening- and shallowing-upward allomembers that represent episodic progradational events of deltaic and shoreface environments (Ranger, 1994; AEUB, 2003; Ranger and Gingras, 2010; Weleschuk and Dashtgard, 2019; Château et al., 2020; Château et al., 2021). Being regionally extensive, these allomembers can normally be correlated at both local and regional scales. The associated middle McMurray estuarine channel fills can often be identified from underlying fining upward sandstone packages, although individual McMurray Formation point bars can be highly lithologically variable (Brekke et al., 2017; Brekke and Roenitz, 2021). The stratigraphic framework is based on that presented in Hein et al. 2006 (on the right of Fig. 3.1B) with minor changes to suit this local study (on the left of Fig. 3.1B). The stratigraphic framework for this study is shown in Fig. 3.1C. Stratigraphic units identified in this study are referred as allomembers herein (Allomember A, B1, B2, and C). Channel belts (A, B1, B2, and C Channels) are bounded at their bases by autogenic erosion surfaces, and by either an allogenic flooding surfaces or an autogenic flooding surface on their top. Allogenic flooding surfaces are indicative of major base-level rise, and at least in some regional studies, they are correlatable over thousands km² (Château et al., 2020). Autogenic flooding surfaces are much less correlatable over large area than allogenic flooding surfaces, and their development only requires minor or no base-level changes. They can be generated from shifting in depocenter or switching of delta lobes. The basal erosional surfaces of channel belts (colorful wavy lines) are exclusively autogenic, and they do not serve as allostratigraphic unit boundaries.

Figure 3.1 (A) Chronostratigraphy of the Athabasca Oil Sands deposit (modified from Wightman and Pemberton, 1997); **(B)** High-resolution stratigraphic model for the McMurray Formation. On the left is the lithostratigraphic/allostratigraphic model developed by the Alberta Energy and Utilities Board (2003; now Alberta Energy Regulator (AER)) (modified after Hein et al. 2006). On the left is a modified version of the AER model used by the McMurray Geology Consortium (MGC). In this modified model, the fluvial-tidal channels are labelled as McMurray channel belts instead of valleys (e.g., A Channel), implying incisions during relative base-level fall. The base of channels corresponds to autogenic erosion surfaces, and top of channels are represented by local flooding surfaces (i.e., allomembers overlying channel belts deposits); **(C)** Detailed lithostratigraphic/allostratigraphic relationships in the study area.



STUDY AREA AND METHODOLOGY

The study area is located 30 km east of Fort McMurray, covers approximately 2,500 km², and coincides with the “Main Valley” (Fig. 3.2A, B). It extends between ranges 7-8W4M and townships 89-90 (Figs. 3.2B, Fig. 3.3). The McMurray Formation within the study area is dominated by point-bar deposits displaying 20- to 65-metre thick successions of massive to cross-stratified sandstone, mud breccia, inclined heterolithic sandstone and mudstone, and pure mudstone. The dataset consists of 153 wells with petrophysical logs, of which 52 wells have dipmeter logs, 47 wells have logged cores, and 12 wells have both core and dipmeter data, which were used for detailed facies calibration (Fig. 3.3). Petrophysical logs were analyzed in combination with core data to establish a well-to-well stratigraphic correlation across the study area (Fig. 3.1B). Forty-seven cores were logged in detail to record sedimentology and ichnology of different sedimentary facies. Unfortunately, the core cannot be oriented due to their age and the lack of orientation data from retrieval. Thus, the criticality of using dipmeter data is underscored in this study. Where available, dipmeter data are used to refine the stratigraphic correlations that were established using petrophysical logs and core data. They also help demarcate individual point-bar deposits within the amalgamated meandering belts of the middle and upper McMurray units. The resulting tadpole characteristics were compared to core observations to establish an integrated facies-dipmeter framework.

Figure 3.2 (A) Paleogeographic reconstruction of the Early Cretaceous Western Canada Sedimentary Basin (WCSB), including the location of the ancient meander-belt deposit of the study (modified from Durkin et al., 2017); **(B)** Paleogeographic reconstruction of Alberta in the Lower Cretaceous showing stratigraphic thickness of the McMurray-Wabiskaw interval and the dashed green line shows the extent of bitumen-bearing McMurray Formation (>10m). Several structural elements are shown, including the Bitumount Trough, Salt Scarp and dissolved salt beds. Modified from Ranger (2006), Hein et al., (2013), Alberta Energy and Utilities Board (2015), Martinius et al., (2015), and Broughton (2016). The study area is indicated in the blue box.

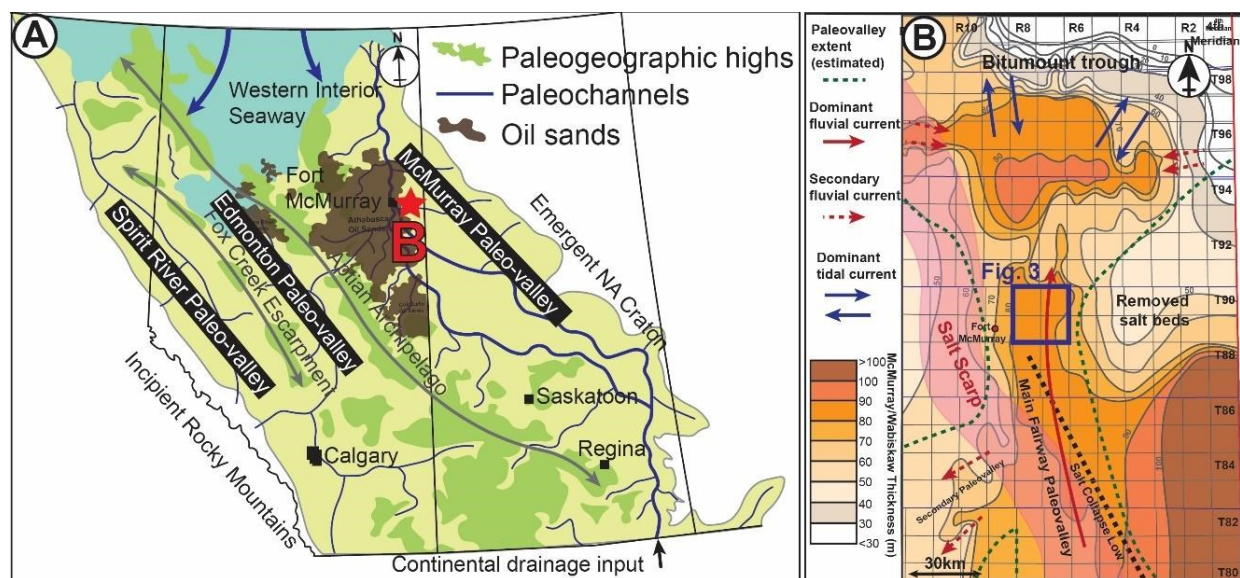
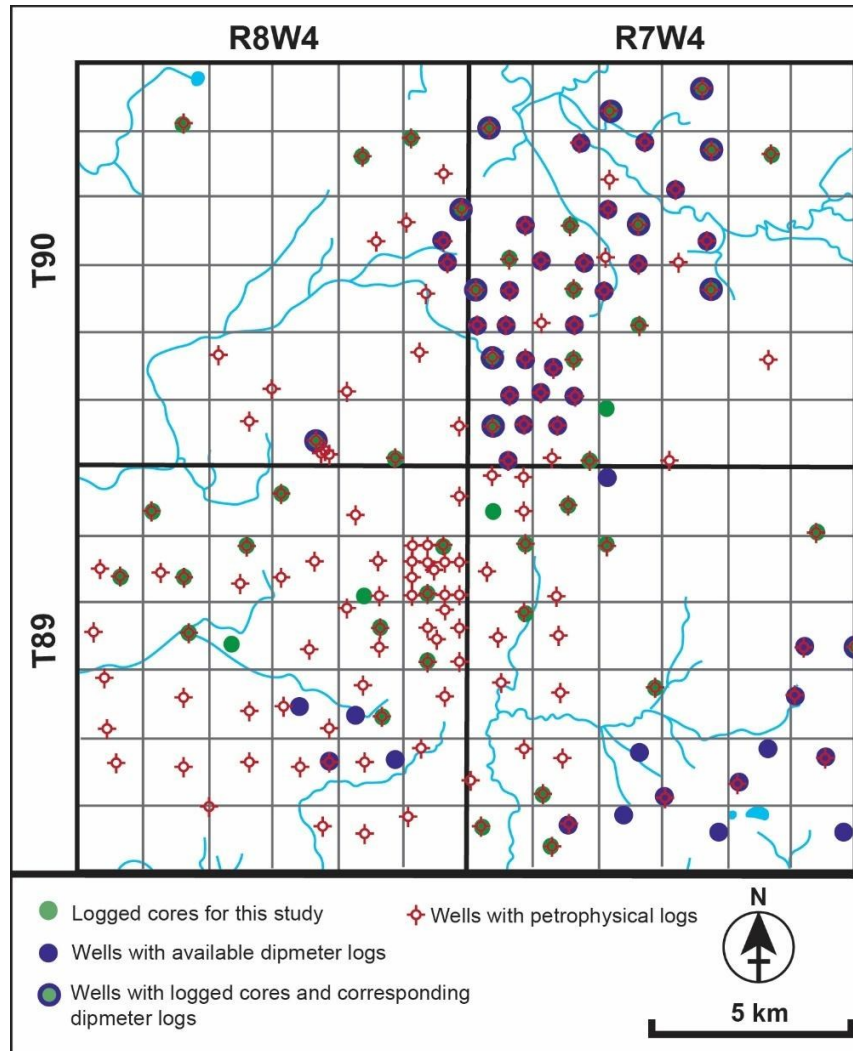


Figure 3.3 Basemap of study area showing wells with petrophysical data, dipmeter logs and logged cores used in this study.



Dipmeter tadpole data representing dipping angle and azimuth are used to track changes in geological bed orientation, making them particularly useful for identifying genetically related point-bar deposits within the middle McMurray. In particular, inclined heterolithic stratification (IHS), which is the main constituent of McMurray fluvio-tidal point bar deposits, show consistently dipping bedding surfaces defined by alternations of sandstone and mudstone.

Dipmeter analyses have been used in the McMurray Formation for three decades. Muwais and Smith (1990) recognized that shallowing upward and steepening upward dipmeter patterns were diagnostic of vertically accreted and laterally accreted point bar deposits respectively. Later, Brekke and Evoy (2004) used dipmeter characteristics to map and prove the presence of large-scale continuous point-bars within

the McMurray Formation, showing the contact between IHS deposits from different channels could be difficult to identify without bedding architecture data. Importantly, this demonstrated the existence of large point bars, which is consistent with what was identified from 3D seismic data (Langenberg et al., 2002). A recent study by Brekke and Roenitz (2021) stressed that it is inaccurate to resolve the complexities associated with point-bar macroforms solely using conventional core and petrophysical logs which are heavily based on lithological changes. Additional analytical tools, such as dipmeter logs or high-resolution microresistivity image logs are being increasingly used, and indeed are requisite, to better resolve complex point-bar stacking patterns.

In this study, we digitized and interpreted the available dipmeter logs within the study area and present a framework for classifying dipmeter data of the McMurray Formation. The resulting dipmeter characteristics, as well as core observations of facies, are used to differentiate and interpret different point bars and stratigraphic units. A schematic estuarine point-bar facies model and stacking-pattern model are proposed in this paper with details of the sedimentology, ichnology, and petrophysical log characteristics for different parts of point bars and in the upper McMurray, shoreline-associated deposits.

DATA ACQUISITION AND PROCESSING

Dipmeter principle and risks

The dipmeter was developed in 1930 and was later refined such that the dip and azimuth of sedimentary beds and contacts could be determined in subsurface datasets. The dip azimuth and direction are derived from correlations of microresistivity logs, which record resistivity contacts at different points in the borehole. The azimuth and direction data are typically represented as vector plots which are commonly called “tadpole plot”. The IHS dominate the McMurray Formation. The bedding dip orientation of IHS facies (middle to upper point bar deposits) indicates the direction of lateral accretion and, in the case of cross stratified sandstone facies (compound dunes of the thalweg and lower point bar deposits), paleocurrent flow direction. Since these bedding orientations provide important information of depositional processes, diagnostic tadpole patterns can be recognized in corresponding facies of point bar deposits. In

particular, the bedding orientation is very useful in recognizing sandstone-mudstone contacts within the IHS, which dominates the point bar deposits of the McMurray Formation.

Since the dipmeter tool is sensitive to conductivity of different lithologies and pore-filling fluids, issues associated with dipmeter measurements may include: 1) difficulties measuring the orientation of homogenous units such as mud-dominated abandoned channel facies; and 2) inaccurate measurement of non-bedding features, such as breccia-rich units, fractures and faults. The first issue results in unreliable bedding azimuth data which is estimated from flat-lying laminated mudstones. The second issue is associated with the limited resolution of dipmeter tadpole plots, and the presence of non-bedding features such as fractures and intraformational breccia. Small breccia clasts do not span the wellbore and generate a surface to be picked. Dipmeter logs available in the area are collected by a three-arm slimline dipmeter tool that samples at 0.5cm. The correlation step of the dipmeter log is 0.26m and the vertical resolution is about 1cm, so the dataset does not have the ability to resolve small sedimentary features such as ripples or micro-fractures. However, dipmeter datasets are useful to represent the orientation of IHS bedding within the meander belts of the McMurray Formation when modern micro-resistivity image logs with higher resolution are not available. By comparison, modern micro-resistivity image logs sample at 0.25 cm and have 0.5cm resolution. Integration of core analyses should help to address the above limitations of dipmeter data, and this paper brings together both datasets to arrive at a more substantive sedimentological interpretation.

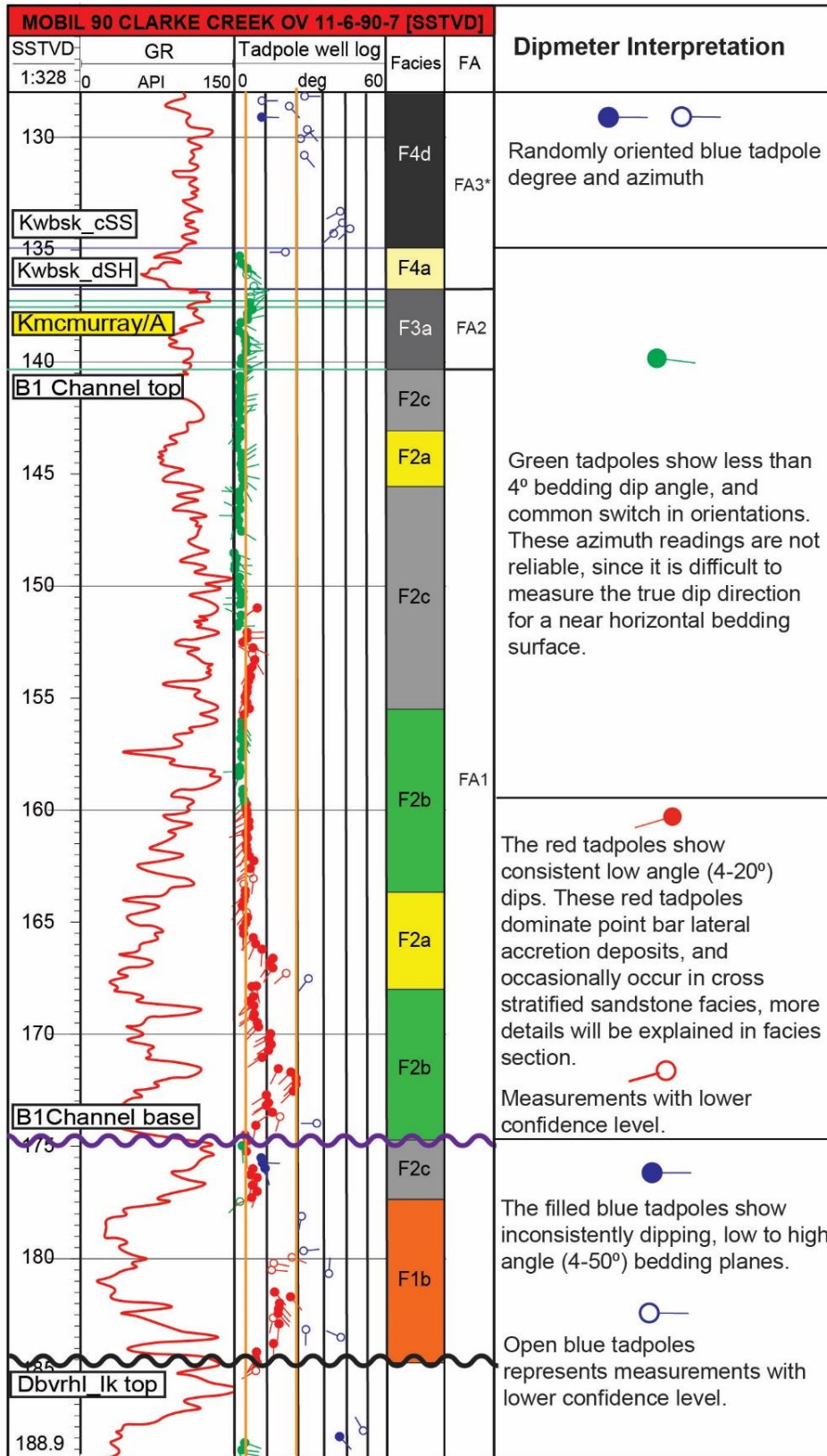
Tadpole plot reclassification

The most common representation of the dipmeter data is the tadpole or stick plots. The head of the tadpole represents the magnitude of a dip of a bedding plane, and the dip azimuth is represented by the direction of the tadpole tail. An example tadpole plot interpretation is presented in Fig. 3.4.

Reclassification of dip angles and orientations in 52 wells followed the method introduced by Brekke et al., (2017) with slight modification to suit this case study. According to their approach, dip angles are classified into three major groups: horizontal bedding ($<4^\circ$), low-angle (4° - 20°), and high-angle ($\geq 20^\circ$). In this paper, the 4° and 20° cut-off lines are drawn on each tadpole plots. Different color coding was applied for dip direction classification: green tadpoles represent flat-lying dips with unreliable dip azimuth values,

red tadpoles show consistent, low- to rarely high-angle dips, and blue tadpoles denote randomly orientated, low to high angle dips. Color coding was useful for the following reasons: 1) color coding assists in visually identifying and classifying the bedding types; 2) flat-lying dipmeter readings can be identified and interpreted in their appropriate context; 3) subtle patterns in intervals with random dip directions (e.g., consistently dipping lateral accretionary surfaces embedded in the cross-stratified sandstone) are readily discerned, thereby contributing to the identification and interpretation of genetically related bedsets (e.g. depth 175-180m in Fig. 3.6A).

Figure 3.4 A sample dipmeter log interpretation from the study area. The example log shows gamma-ray (GR), dipmeter tadpole plot, facies, and facies associations (FA) in this study. Two cut-off lines used for dipmeter classification (4° and 20°) are represented by orange vertical lines. They are used to guide the reclassification of tadpoles: green (disorganized tadpole azimuth and flat-lying to gently dipping $<4^{\circ}$), red (organized tadpole azimuth and dipping angle between 4° - 20°), and blue (disorganized azimuth with dip-angles from 4° up to 60°). Filled and open tadpoles represent different confidence levels for the measurements. Filled tadpoles are confident measurements and open tadpoles are less certain. (next page)



* FA3 represents marginal embayment facies in Upper McMurray Formation unit, and its dipmeter characteristics are not discussed in this study due to thin thickness and poor data quality.

RESULTS AND INTERPRETATION

This section summarises eight recurring lithofacies (F1a, F1b, F2a, F2b, F2c, F2d, F3a and F3b) observed in the McMurray Formation within the study area. Recurring facies successions are grouped into two facies associations (FA1 and FA2). FA1 comprises the dominant McMurray Formation interval and presents fluviotidal point bar complexes (presented and interpreted below). Below, core and dipmeter tadpole characteristics are summarized for each facies of FA1. A synthesized interpretation from core and dipmeter characteristics is provided after each facies description. In the case of FA2, facies identification relied heavily on core observation since FA2 facies are variably present in the study area and their dipmeter characters less clear. Therefore, core examples are shown for each facies, but dipmeter tadpole example is only provided for FA1 facies. The facies associations and their constituent lithofacies are presented in Table 3.1.

Table 3.1 Facies association and their constituent lithofacies in the north of Christina River region.

Stratigraphic unit		Facies association	Lithofacies	Interpretation
McMurray Formation	upper	FA2	F3b	brackish-water embayment to proximal offshore
			F3a	
	lower-middle	FA1	F2d	tidally and fluviually influenced estuary point bar complex
			F2c	
			F2b	
			F2a	
			F1b	
			F1a	

Facies Association 1

F1a: mud-breccia dominated sandstone

Description

Facies F1a comprises sandstones with abundant intraformational breccia. The important sedimentological and ichnological characteristics observed from cores, and dipmeter tadpole

characteristics observed from petrophysical logs are presented in Table 3.2. A real example including GR, dipmeter tadpole, and core expressions of this facies is shown in Fig. 3.6.

Table 3.2 Core and dipmeter tadpole characteristics of facies F1a mud-breccia dominated sandstone.

F1a: mud-clast breccia-dominated sandstone		
Core characteristics		Dipmeter tadpole characteristics
Bedset thickness	<ul style="list-style-type: none"> • from 10cm to >10s of metres 	<ul style="list-style-type: none"> • disorganized dip directions with dip angles up to 60° • dominated by tadpoles with less confidence level (blue open tadpoles)
Occurrence and contacts	<ul style="list-style-type: none"> • sharp contact to F1b 	
Sedimentary structures	<ul style="list-style-type: none"> • rare low- to high-angle cross stratification within sandstone matrix 	
Other sedimentological observations	<ul style="list-style-type: none"> • common mud-clast breccia, size of the mudstone clasts ranges from a few centimetres to 10s of centimetres in size, observed in two expressions: large, massive unburrowed clasts (Fig. 3.5B, D1), and small, bladed to oblate, laminated clasts with primary bioturbation (Fig. 3.5C, D2) • local pyrite nodules and coal fragments (Fig. 3.5D3-5) • rare collapsing or slumping features (Fig. 3.5D4-5) 	
Ichnological characteristics	<ul style="list-style-type: none"> • trace fossils are generally absent in the sandstone matrix (BI:0-1) • primary bioturbation locally preserved in mud clasts, including <i>Planolites</i>, <i>Cylindrichnus</i> and <i>Gyrolithes</i> 	

Integrated discussion and interpretation

The abundance of mudstone breccia is commonly associated with energetic and erosive events, such as bank erosion associated with fluvial channel margins, top-of bar erosion in tidal settings and even exhumation of IHS on point bar facies (Labrecque et al., 2011; Brekke et al., 2017; Broughton, 2018). The locally preserved cross-stratification within the sandstone matrix confirms sediment transport as bedload although the sand-transport mechanism may differ from that of the mudstone clasts. The mudstone clasts likely represent a diversity of processes including *in-situ* current-fragmentation of mud beds and partial winnowing, bank and bar erosion with gravitational collapse or slumping and some amount of current reworking occurring at bed contacts (Labrecque et al., 2011; Broughton, 2018). Abundant coalified plant fragments are derived from continental plant materials and their abundance is consistent with a fluvial

sediment source. The general absence of trace fossil also implies extremely stressful physicochemical conditions, which support the energetic freshwater dominated fluvial system.

The mudstone breccia is subdivided into two major types: (1) large, massive unburrowed mud clasts (10s of centimetres in diameter) (Fig. 3.5B); and (2) small, bladed to oblate, laminated mud clasts with primary bioturbation (1-5 cm in diameter) (Table 3.1, Fig. 3.5C). The large mudstone clasts contain coal fragments and are associated with deformed sediment, and the clasts commonly mark the channel base (Fig. 3.5D1) (Brekke et al. 2017): these are taken to be relict of channel-margin erosion (Hubbard et al., 2011; Broughton, 2018). Small, laminated mud clasts are commonly centimetre scale, and tend to occur in the middle to the upper part of a continuous estuarine point bar succession (Brekke et al. 2017): we interpret these to generally represent the hydraulic erosion and fragmentation of mud beds on the accreting bar surfaces (Broughton, 2018). Minor bioturbation and sandstone lenses are commonly observed within this type of mudstone clast (Fig. 3.5D2) implying that their primary depositional origins are associated with estuarine point bars (Gingras et al., 2016).

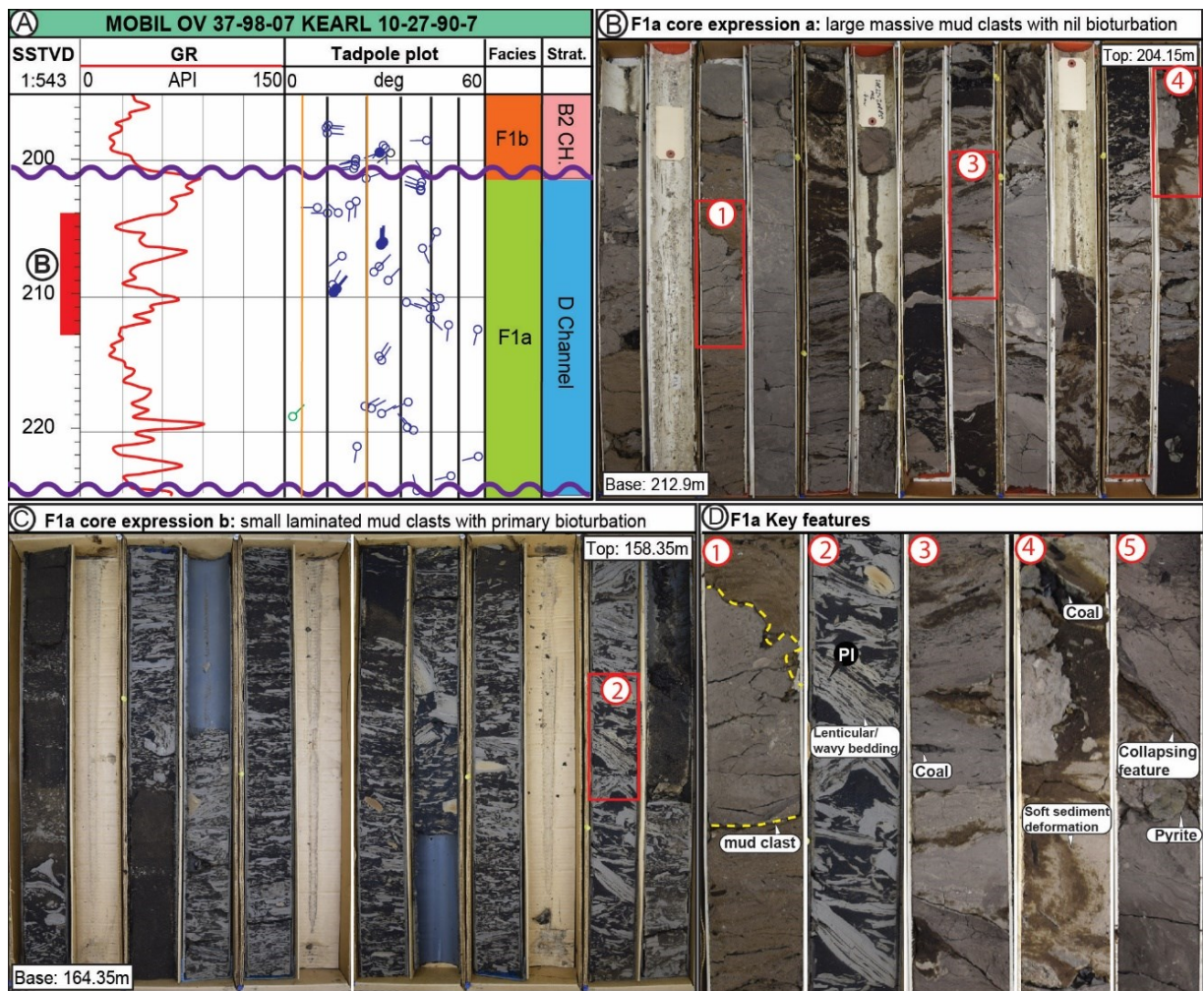
Dipmeter orientations observed in F1a represent the orientation of contacts between the variably oriented mudstone clasts and the sandstone matrix (figs 5A, 5D1), and primary bedding of the matrix and possibly laminations within larger mudstone clasts (figs 5A, 5D2). The dipmeter tadpole logs of F1a are characterized by disorganized, low- to high-angle dips (5-60°) (blue tadpoles), and most of them show low-confidence dipmeter measurements represented by open blue tadpoles (Fig. 3.5A). The low-confidence tadpoles cannot be used to interpret bed orientations, however they are characteristic of mudstone breccia facies within the McMurray Formation.

The low-confidence tadpoles (open blue tadpoles) are ascribed to the variably oriented mudstone clasts / sandstone matrix contacts (Fig. 3.5D1). Where coherent, similarly oriented, and gently to moderately dipping beds can be discerned, these might be interpreted to represent cross-bed foresets (higher angle) or inclined stratification (lower angle) in these facies: but this observation maybe difficult to make. Notably, low-confidence dip measures are not solely due to the presence of mud clasts.

Measurement error may be exacerbated by the poor lithology (resistivity) contrast in such mudstone breccia-rich facies, poor pad contact with the wellbore, or hole washouts. Notably, CBB and PBB share

similar dipmeter characteristics, therefore, core analysis or other types of image-log analyses are complimentary in resolving their distributions and significances (Brekke et al., 2017).

Figure 3.5 Mud breccia-dominated sandstone – Facies 1a: core and wireline perspectives. **(A)** Composite log including gamma ray, tadpole plot, facies, and stratigraphic context of F1a mud breccia dominated sandstone in well 10-27-090-07W4, red bar in the depth column indicates the location of figure B; **(B)** photo of the core expression a of F1a: large, massive unburrowed clasts, red rectangle indicate locations of detail photos in D; **(C)** photo of the core expression b of F1a: small, bladed to oblate, laminated clasts with primary bioturbation, red rectangle indicates locations of detail photos in D; **(D)** detail photos of F1a facies showing large massive-appearing mud clast (1), lenticular to wavy bedding within small laminated, bladed mud clasts (2), common coal fragments (3, 4), soft sediment deformation (4, 5), and centimetre-scale pyrite nodules (5). Abbreviations: PI-Planolites. Width of core: 7cm.



F1b: massive to cross-stratified sandstone

Description

Facies F1b comprises massive to low- to high- angle cross-stratified sandstone with minor mudstone clasts. The important sedimentological and ichnological characteristics observed from cores, and dipmeter tadpole characteristics observed from petrophysical logs are presented in Table 3.3. An example of F1b including GR, dipmeter tadpole, and core expressions is shown in Fig. 3.6.

Table 3.3 Core and dipmeter tadpole characteristics of facies F1b massive to cross-stratified sandstone.

F1b: massive to cross-stratified sandstone		
Core characteristics		Dipmeter tadpole characteristics
Bedset thickness	<ul style="list-style-type: none"> • 9-30m thick sandstone with cm scale mud lamination 	<ul style="list-style-type: none"> • disorganized high-angle and low-angle beds (blue tadpoles): 6°-55° dip angle • common low-angle organized beds (red tadpoles): 4-22° dip angle • red and blue tadpoles can be grouped into metre-scale packages, each package has a preferred tadpole orientation. (examples are highlighted in red and blue shades in Fig. 3.6) • wherever F1b is associated with overlying F2a and F2b, red tadpole packages show consistent dipping orientation with F2a/F2b • rare tadpoles with low confidence level (open blue tadpoles)
Occurrence and contacts	<ul style="list-style-type: none"> • prevalent gradational contact with F1a and F2a/F2b • rare sharp contact with F2a/F2b 	
Sedimentary structures	<ul style="list-style-type: none"> • dominant low- to high-angle cross stratification is common core expression of trough or planar tabular bedding (Fig. 3.6B, C4), commonly show opposing dipping beds as shown in Fig. 3.6B • local unidirectional ripples and minor climbing ripples (Fig. 3.6C6) • common grain size stripping between very fine- and fine-grained sandstone (Fig. 3.6C5) • overall fining upward 	
Other sedimentological observations	<ul style="list-style-type: none"> • common mudstone clasts • local coal fragments and laminae • common mud laminae • rare pebble-sized lag deposit at the base (Fig. 3.6C3) 	
Ichnological characteristics	<ul style="list-style-type: none"> • trace fossils are generally absent • common ichnofossils are confined in mudstone breccia and laminae, trace fossils consist of <i>Planolites</i>, <i>Arenicolites</i>, <i>Cylindrichnus</i>, and apparent <i>Gyrolithes</i>. (Fig. 3.6C2-3) 	

Integration of facies analysis and dipmeter data

Large scale trough and high angle planar tabular cross-stratification cannot easily be differentiated from the dipmeter and core datasets. The most dominant sedimentary structure identified from F1b, is

low- to high-angle cross-stratified sandstone (Fig. 3.6B), which is interpreted as the core expression of trough cross-stratification or planar tabular bedding resulting from the migration of large-scale subaqueous dunes. The apparent opposing dipping beds (highlighted with yellow dash lines in Fig. 3.6B) represent variably oriented dunes (Hein et al., 2001), or can simply be the relict of the core slabbing process: orientations within continuous core segments provide dependable data in any case. In some of those examples, divergent dipping directions can result from three-dimensional dune and compound-dune migration (Dalrymple and Choi, 2007; Ranger and Gingras, 2010) and variable sediment transport directions. The common occurrence of grain striping (Fig. 3.6C5) also supports the migrating dune interpretation, because the alternating lower medium and very fine sandstone are commonly observed in the foresets of migrating bar forms, which results from sorting associated with small bedforms on the dune's stoss surface (Smith, 1972). Pebbles are locally present overlying basal erosional contacts (Fig. 3.6C1). Coal (Fig. 3.6C3) and mudstone fragments are also concentrated on the erosional surface, a result of settling in the lowered current energies near the toesets of the dunes. The overall fining-upward grain size trend suggests a gradual decrease in energy level, and this interpretation is supported by the occurrence of unidirectional ripples (Fig. 3.6C6) identified in the upper part of the succession.

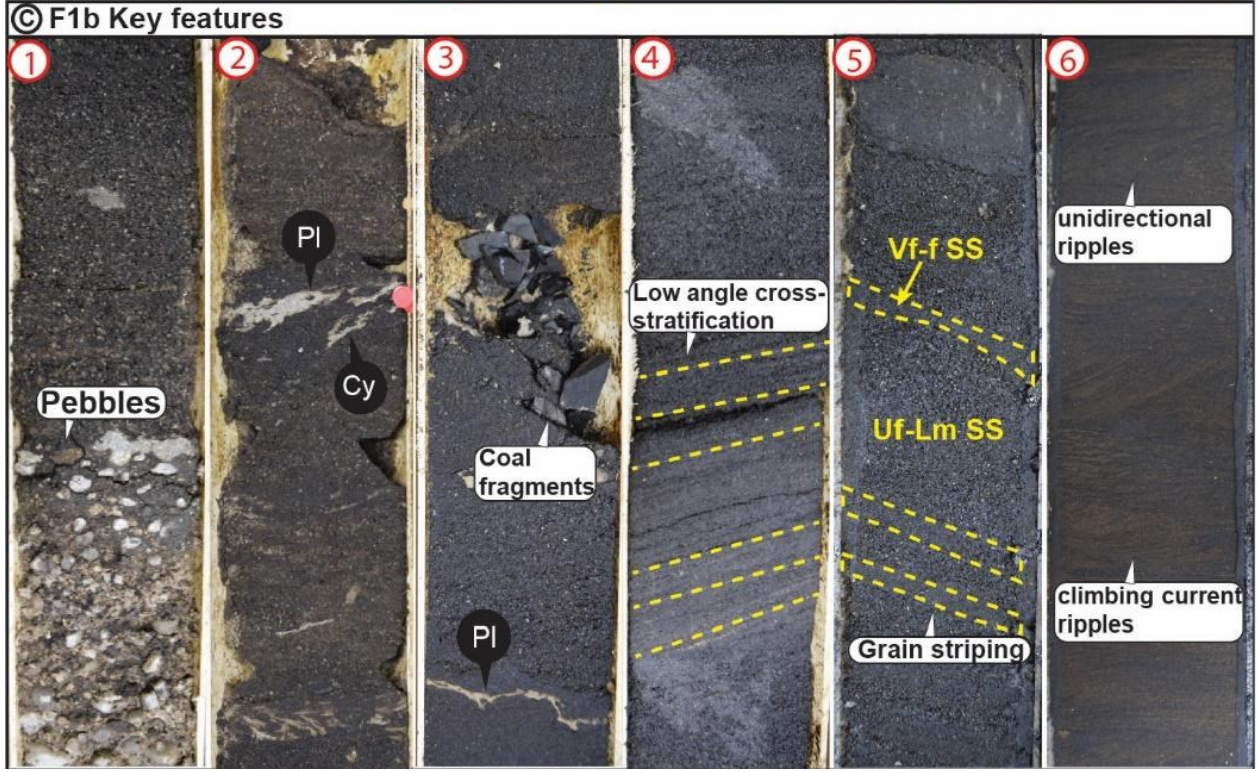
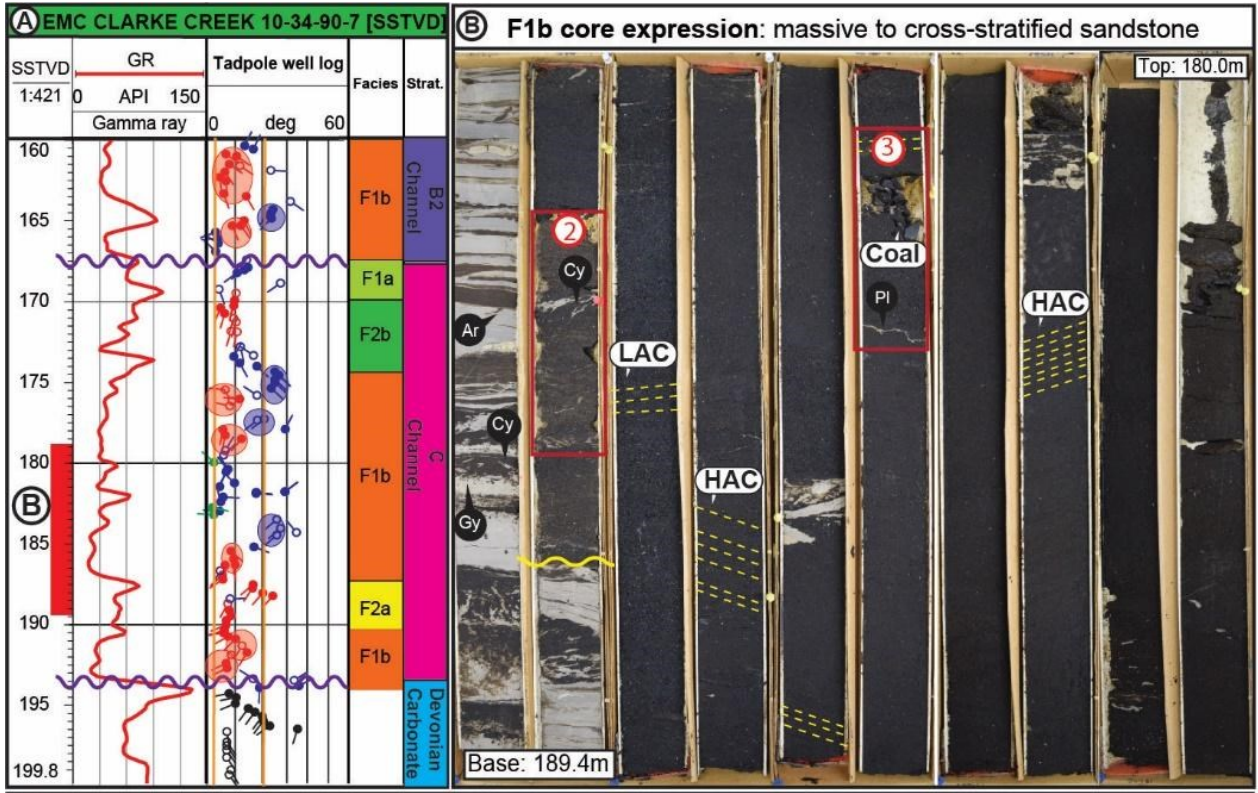
The general paucity of bioturbation can be explained by rapid depositional rates and shifting sediments. As a result of sedimentation stresses, only sporadically distributed *Planolites* (Fig. 3.6C2, 3), *Arenicolites*, *Cylindrichnus* (Fig. 3.5C2), and *Gyrolithes* are preserved within mudstone laminae. Organisms cannot readily inhabit and maintain domiciles in such high-energy mobile substrates (Gingras et al., 2008; Buatois and Mángano, 2011). The presence of such low ichnodiversity and diminutive brackish trace-fossils are best explained by the presence of brackish water (Pemberton et al., 1982; Gingras et al., 2016). The ichnology, sedimentology, and the spatially close association of F1A immediately below the heterolithic facies F2a and F2b suggests that F1b represents the lower part of fluviotidal to inner estuarine point bars and these deposits may interfinger with thalweg-associated compound dunes.

Regarding the dipmeter expressions, an example is shown in Fig. 3.6A. The low- to high-angle disorganized beddings (blue tadpoles in Fig. 3.6A) correspond to beds and bedsets dominated by high- to low-angle cross-beds indicating paleocurrent flow directions. Similarly to F1a, the uncertain tadpoles

(open blue tadpoles) possibly result from minor resistivity contrasts within sandstone-dominated facies, or rare mudstone fragments where a continuous lithological contact does not span the entire wellbore. In this example, the blue tadpoles (or blue tadpole packages) alternate with low-angle consistently dipping metre-scale red tadpole packages which may indicate the orientation of inclined stratified bounding surfaces between cross-bedsets: this cannot be observed in the core. These red tadpole packages are characterized by a unidirectional SW direction, implying a SW lateral accretional migration of point bars (Fig. 3.6A). In this example, the dipmeter tadpole pattern supports an interpretation of cross bedded sandstone in the lower point bar. However, the identification of consistently dipping red tadpole packages is sometimes difficult to make due to limited resolution of dipmeter tadpole log at some wells. In such cases, this facies may be mis-identified as cross-stratified fluvial channel fill deposits if the identification is solely based on core observation.

Figure 3.6 Massive to cross-stratified sandstone - Facies F1b: core and wireline perspectives. **(A)**

Gamma ray, dipmeter log, facies and stratigraphic context of F1b massive to cross-stratified sandstone in well 10-34-090-07W4, red bar in the depth column indicates the location of figure B. The red tadpoles are grouped into metre-scale packages (red shade) with a unidirectional SW direction. Blue tadpoles are grouped into dm-scale packages (blue shade) oriented $\sim 90^\circ$ from red tadpoles and dip to the SE in the C Channel unit. Note the southwest-dipping lateral accretion surfaces (indicated with consistently dipping red tadpoles) from 175-194m are inconsistent with the overlying southeast-dipping lateral accretion succession above 164 m, and indicates a contact between two point-bars. **(B)** Core photos of F1b showing lithological characteristics of cross-stratified sandstone, which contrasts with dipmeter tadpole patterns of the corresponding interval, suggesting lateral accretionary behavior; **(C)** Detailed photos of common sedimentary features identified from F1b facies showing pebbles (1), trace fossils within mud laminae (2), coal fragments (3), low angle cross stratification (4), grain striping (5), and unidirectional or climbing ripples (6). Purple wavy lines represent the base of channel. Abbreviations: LAC-Low angle cross-stratification, HAC-High angle cross-stratification, Vf-very fine-grained, Uf-upper fine-grained, f-fine-grained, Lm-lower medium-grained, SS-sandstone, Cy-*Cylindrichnus*, Pl-*Planolites*, Ar-*Arenicolites*, Gy-*Gyrolithes*. (next page)



F2a: sandstone-dominated IHS

Description

Facies F1b is characterized by shallowly dipping, alternating dm-scale sandstone and cm-scale mudstone beds. The important sedimentological and ichnological characteristics observed from cores, and dipmeter tadpole characteristics observed from petrophysical logs are presented in Table 3.4. An example of F2a including GR, dipmeter tadpole, and core expressions is shown in Fig. 3.7.

Table 3.4 Core and dipmeter tadpole characteristics of facies F2a sandstone-dominated IHS.

F2a: sandstone-dominated IHS		
Core characteristics		Dipmeter tadpole characteristics
Bedset thickness	<ul style="list-style-type: none"> • 10-30m (sand: 2-80cm; mud: 1-15cm) 	<ul style="list-style-type: none"> • dominant organized low angle beds (red tadpoles): 5°-18° dip angle, variability of angle is normally within ±20°. • uncommon disorganized high to low angle beds (green and blue tadpoles): 3°-22° dip angle • common overall steep-upward pattern, occasional shallow-steep-shallow pattern (Fig. 3.7A) • tadpole directions show subtle clockwise or counterclockwise rotation • rare disorganized blue tadpoles • red tadpoles show abrupt shift in dip angle
Occurrence and contacts	<ul style="list-style-type: none"> • gradational contact with F2b, sharp or gradational contact with F1b 	
Sedimentary structures	<ul style="list-style-type: none"> • sandstone-dominated IHS • common parallel to sub-parallel wavy bedding near base and flaser bedding the middle and upper succession • common apparent low-/high-angle cross stratification within sandstone interval • sandstone/mudstone contact nature is variable due to bioturbation intensity, three core expressions are observed: sharp (Fig. 3.7B and Fig. 3.7E1-3), burrowed (Fig. 3.7C and Fig. 3.7E4-5), and heavily burrowed contacts (Fig. 3.7D and Fig. 3.7E6) • local current ripples (Fig. 3.7E1) 	
Other sedimentological observations	<ul style="list-style-type: none"> • local compressed syneresis cracks occur in mud laminae • common mud drapes and minor double mud drapes (Fig. 3.7E7) • minor coal fragments and laminae (Fig. 3.7E2) 	
Ichnological characteristics	<ul style="list-style-type: none"> • consists of variably distributed diminutive trace fossils (BI:0-5) • mudstone beds show moderate to high degree of bioturbation intensity and diversity (BI: 2-5); sandstone intervals are nearly devoid of bioturbation (BI:0-1) • common <i>Planolites</i>, <i>Arenicolites</i> • <i>Gyrolithes</i> is locally monospecific and abundant • <i>Cylindrichnus</i> is commonly monospecific and abundant throughout F2a, composed of multiple clays and silt lining • minor <i>Skolithos</i>, <i>Thalassinoides</i> 	

Integrated discussion and interpretation

Facies 2a is characterized by mildly dipping, sandstone-dominated, inclined heterolithic stratification (IHS). The alternation between sandstone and mudstone intervals signifies deposition associated two modes of sedimentation: a freshet and a tide-dominated interval. It is conventional to interpret the sandstone beds to have been deposited during high fluvial discharge (i.e., during freshet-dominated seasons), and the thinner silty mudstone as deposited during sustained base flow periods and influenced by tidal currents (Ranger and Pemberton, 1992; Sisulak and Dashtgard, 2012; Johnson and Dashtgard, 2014). Importantly, this relationship can change depending on the nature of sediment loads carried by the river and the position of the core in the paleo fluviotidal setting (Melnyk and Gingras, 2020). Freshet-associated sandstones are cross bedded and unburrowed, freshet-mudstones are unburrowed, whereas tide dominated examples of either the sand- or mud-lithosome are bioturbated (Melnyk and Gingras, 2020). In this dataset, sandstone is generally cross-laminated or cross-bedded.

The presence of cross-stratification (Fig. 3.7B, C and E4) and minor unidirectional ripples (Fig. 3.7E1) imply sedimentation from traction and are the result of unidirectional (locally variably oriented) currents. The thin mudstone intervals are generally burrowed, resulting in the destruction of primary sedimentary structures. F2a is the most common component of tidally influenced estuary channel point bars, and it does have variable core expressions, which are characterized by different types of sandstone/mudstone contacts, including sharp (Fig. 3.7B and Fig. 3.7E1-3), burrowed (Fig. 3.7C and Fig. 3.7E4-5) and heavily burrowed contacts (Fig. 3.7D and Fig. 3.7E6). The bed contact expression is determined by variations in fluvial *versus* tidal energy, and water salinity during a fluvial event and are related to the variations in lithosome sedimentation alluded to above. Sharp basal bed contacts (Fig. 3.7B) tend to be related to the onset of freshets and bioturbated contacts (Fig. 3.7C) are associated with the return to ambient fluviotidal conditions (Melnyk and Gingras, 2020). Although a variety of depositional environments can result in the deposition of IHS, lateral and downstream accretionary deposits of estuarine point bars are inferred *herein* due to the presence of bioturbation, syneresis cracks, mudstone drapes (Fig. 3.7E7), wavy bedding (Fig. 3.7E1), and coal clasts (Fig. 3.7E2). The sum of these is consistent with the presence of brackish water and salinity fluctuations (MacEachern et al., 2005; MacEachern et al., 2008; Bhattacharya

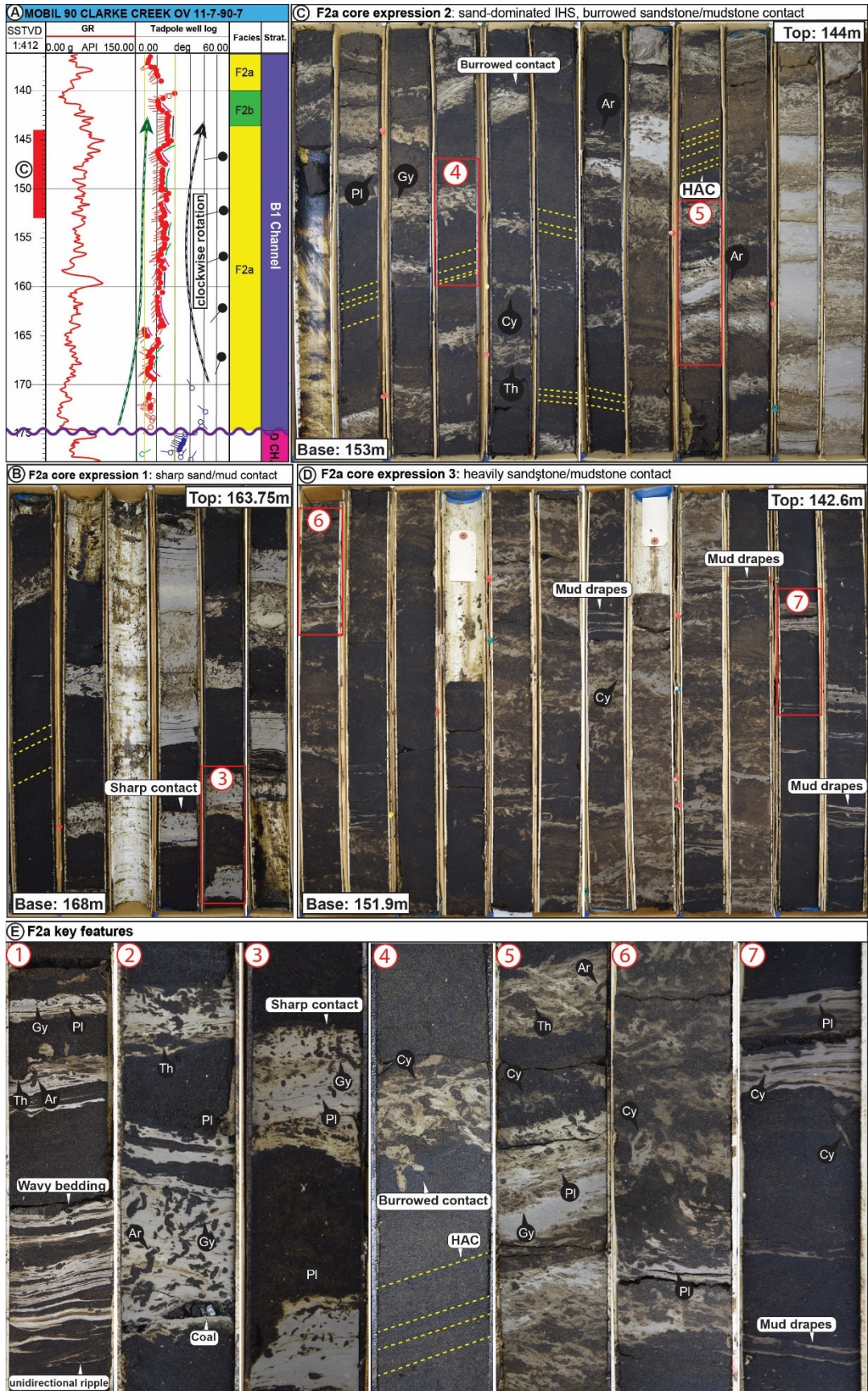
and MacEachern, 2009), rhythmic fluctuations in depositional energy and proximity to a fluvial setting. Based on the predominant sandstone composition of F2a, this facies is interpreted as the lower to middle part of the lateral accretion deposit of fluvio-tidal point bars.

As alluded to above, the distribution of trace fossils also evidences regular variations in fluvial inflow. Bioturbation is significantly more common in mudstone beds (BI 2-5) than in sandstone beds (BI 0-1). Trace fossils in the mudstones are dominated by millimetre-scale ichnofossils made by suspension- and deposit- and interface-feeding organisms, including *Planolites*, *Arenicolites*, *Thalassinoides*, and *Gyrolithes* (Fig. 3.7E1-3). The diminutive size and low diversity are characteristic of brackish-water trace-fossil assemblages. Unburrowed sandstones indicate the presence of physico-chemico stresses such as fresh-water and / or rapid sedimentation and shifting sediments (Fig. 3.7E2-3). Notably, higher up in the point bar (e.g. F2b discussed below) a very subdued freshet signature, indicates that for F2a, rapid sedimentation and shifting substrates are the best explanation for the sparse ichnofossils in the sandstones, as reduced salinities would influence the entire pointbar, an observation that cannot be inferred from F2b (see below). Trace fossils in mudstone beds may extend into underlying sandstone intervals lending the sandstones a bioturbated appearance (Fig. 3.7E4-5).

Tadpoles of F2a show coherent dips and dip directions (Fig. 3.7A). Similar low-angle dipmeter tadpoles have been interpreted to represent the lateral accretion surfaces of a point bar (Muwais and Smith, 1990; Brekke and Evoy, 2004; Fustic, 2007; Fustic et al., 2008; Brekke et al., 2017). This observed dipmeter pattern is consistent with IHS beds observed from cores, although there is no way to assess the true dip, dip direction and vertical coherency in the core datasets. The consistent low-angle dips are commonly observed within laterally accreted point bars in meandering channel belts (e.g. Donselaar and Schmidt, 2010) (an example is shown in Fig. 3.7A). A subtle steepening-upward trend (Fig. 3.7A) is interpreted as partial preservation of a shallow-to-steep-to-shallow dip pattern, which is expected in IHS (or epsilon cross-bedding) of point bars (Allen, 1963; Flach and Mossop, 1985; Thomas et al., 1987; Brekke and Couch, 2011). Bedding angles that only display steepening upward pattern are a potential indication of a truncated point bar. Abrupt shifts in red tadpole dip angles indicate erosional breaks of lateral accretion surfaces (at 164m in Fig. 3.7A). Where present, a subtle clockwise or counterclockwise rotation (e.g.,

~30°; Fig. 3.7A, 8A) is observed and can be interpreted as changes in point bar topography or natural variations in lateral-accretion beds.

Figure 3.7 Facies F2a of Facies Association 1: core and wireline perspectives. **(A)** Gamma ray, dipmeter log, range of facies, and stratigraphic context of F2a sandstone-dominated IHS in well 11-07-090-07W4, red bar in the depth column indicates the location of figure C. The subtle steepening upward tadpole pattern is indicated by the green arrow. The black tadpoles represent the average dip direction over a 5m interval. The rotation pattern is indicated by the black arrow. Note there is an approximately 30° clockwise rotation observed, and increase of dip angle from 6° to 16° within depth 142m-175m. The contact between sandstone and mudstone can be sharp **(B)**, burrowed **(C)** or heavily burrowed **(D)**. **(E)** Detailed photos of common sedimentary features identified from F2a facies showing low- to high-angle cross-stratification within sandstone interval (4), variety of trace fossils preferentially present in mudstone (1-7), homogeneous trace fossil distribution observed in D (E6), local wavy bedding (1), minor current ripple (1), rare coal fragment (2), mudstone bed with erosional upper and lower contact (3), and mud drapes (7). The wavy purple line represents a contact between different channels. Abbreviations: HAC- High angle cross-stratification, *Cy-Cylindrichnus*, *Pl-Planolites*, *Ar-Arenicolites*, *Gy-Gyrolithes*, *Th-Thalassinoides*. (next page)



F2b: mudstone-dominated IHS

Description

Facies F2b is characterized by alternating dm-scale mudstone and cm-scale sandstone beds with low bedding angle, comprising mudstone-dominated IHS. The important sedimentological and ichnological characteristics observed from cores, and dipmeter tadpole characteristics observed from petrophysical logs are presented in Table 3.5. An example of F2b including GR, dipmeter tadpole, and core expressions is shown in Fig. 3.8.

Table 3.5 Core and dipmeter tadpole characteristics of facies F2b mudstone-dominated IHS

F2b: mudstone-dominated IHS		
Core characteristics		Dipmeter tadpole characteristics
Bedset thickness	<ul style="list-style-type: none"> • 2-10m (sand: variable, ~0.5-15cm; mud: variable, ~0.5-25cm) 	<ul style="list-style-type: none"> • dominant low-angle beds with random orientations (green tadpoles): mixing of 4-6° dip angle and rare horizontal beds with <4° dip angle • local consistently dipping, low-angle beds (red tadpole groups in Fig. 3.8A) • uncommon disorganized high- to low- angle blue tadpoles with low confidence level: 6°-40° dip angle • often found in association with F2a/F1b, observed in the upper part of a shallow-steep-shallow dipping angle pattern • tadpole directions show subtle clockwise or counterclockwise rotation
Occurrence and contacts	<ul style="list-style-type: none"> • commonly associated with F1b/F2a below and F2c/F2d above • gradational contact with underlying F1b/F2a, F2c and F2d, rare sharp contact with F2a (Fig. 3.8C5) 	
Sedimentary structures	<ul style="list-style-type: none"> • rare poorly preserved wavy to lenticular bedding due to intense bioturbation (Fig.8C2) • rare mud drapes 	
Other sedimentological observations	<ul style="list-style-type: none"> • minor pyritized mudstone • minor mud clasts • rare compressed syneresis cracks (Fig. 3.8C5) 	
Ichnological characteristics	<ul style="list-style-type: none"> • homogeneously distributed, diminutive trace fossils, moderate to intense bioturbation intensity (BI: 3-5) • common <i>Cylindrichnus</i>, <i>Planolites</i>, <i>Gyrolithes</i>, <i>Skolithos</i> and <i>Arenicolites</i> (Fig. 3.8C) • minor <i>Skolithos</i>, <i>Asterosoma</i>, <i>Palaeophycus</i>, <i>Lockeia</i> • <i>Cylindrichnus</i> is commonly lined with clay/silt 	

Integrated discussion and interpretation

Compared to F2a, F2b shows increased mudstone beds, increased levels of bioturbation and a minor increase in ichnodiversity. These features suggest reduced influence of freshets (which seem to most affect lower point-bar deposits of F2a) and sedimentation that is more consistently in brackish-water and

under the influence of tidal modulation. The common presence of poorly preserved wavy to lenticular bedding (Fig. 3.8C2) further indicate variable depositional energies within the depositional environment. Notably, there are minor intervals (cm-scale of sandstone or mudstone) that are sharp-based and unburrowed. As with F2a, these are interpreted as freshet sediments. They are much rarer and thinner in F2b compared to F2a, indicating that freshets abruptly accumulated in F2a but did not substantially accumulate in F2b, Furthermore, the persistent ichnological expression suggests that salinity was generally brackish, but stable.

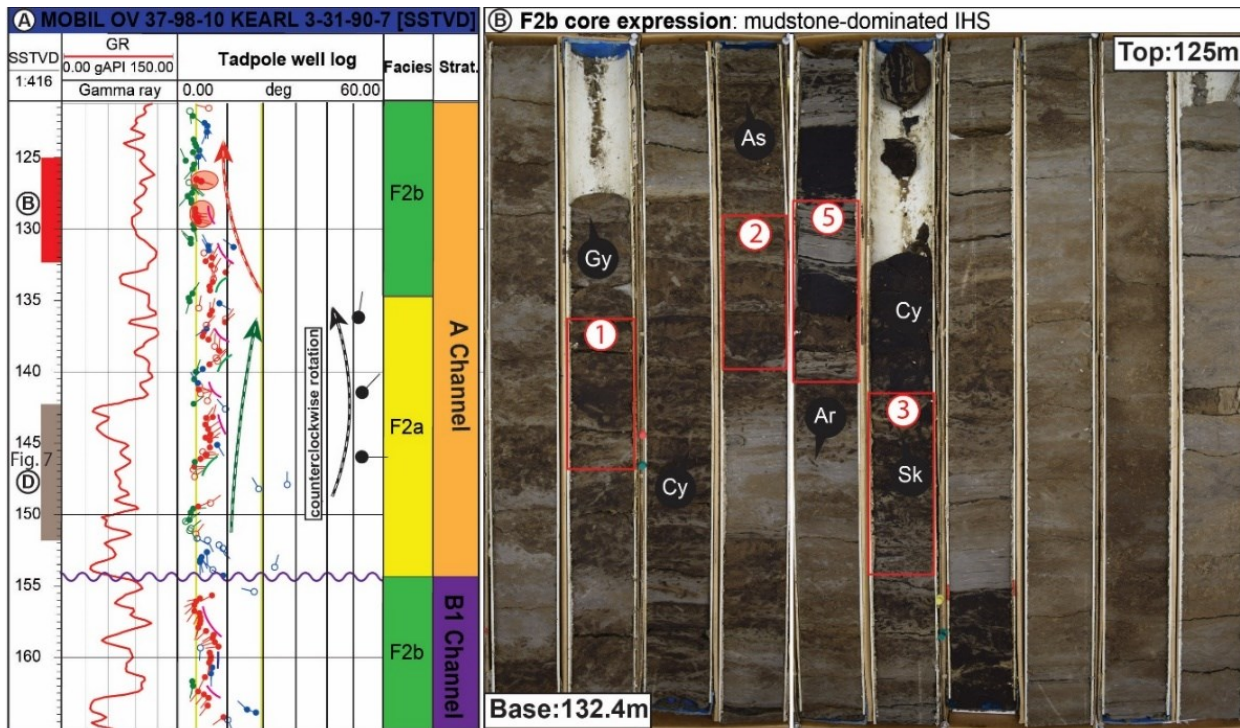
Facies 2b displays a trace-fossil assemblage that is similar to F2a (dominated by *Cylindrichnus*, *Planolites*, *Gyrolithes*, *Skolithos*, *Arenicolites*), representing a brackish water depositional environment. However, trace fossils such as *Cylindrichnus* (Fig. 3.8C1-5), *Teichichnus* (Fig. 3.8C1-3), *Asterosoma* (Fig. 3.8C1) and minor *Palaeophycus* appear or are more common. The homogeneously distributed trace fossils characterized by high bioturbation intensity (BI: 3-5) and low diversity suggest lowered depositional energy and sedimentation rates. In some examples, bioturbation is pervasive upwards. Along with systematically reduced to nearly horizontal dips (discussed below), F2b is interpreted to represent a transition to intertidal flat deposits (Gingras et al., 1999; MacEachern and Gingras, 2007; Gingras et al., 2016; Gingras and Leckie, 2017). F2a facies rarely occurs with F2b, sharp facies contacts (Fig. 3.8B, 8C5) were developed as a result of pulses of stronger currents which were brought in from the main thalweg.

The predominant gently dipping to horizontal bedding represents increasing percentage of vertical accretion, which signifies the transition to the upper point bar or intertidal flat deposit, where bedding becomes horizontal and parallel to the bartops. Metre-scale groups of red tadpoles showing low-angle consistently dipping F2a characteristics are locally observed, indicating lateral accretion surfaces. An example is indicated by red cycles in Fig. 3.8A. The consistently dipping low-angle beds are highlighted in red circles at depth 126.5m and 128.5m, indicating an eastward lateral accretion direction. This dipping orientation is consistent with the lateral accretionary surfaces from F2a (red tadpoles at depth 133-150m), suggesting the two facies are genetically related and represent a continuous point bar. Local, disorganized, high- to low-angle dips are possibly due to difficulties in recognizing lithological contacts in heavily burrowed facies, or local soft-sediment deformation of unconsolidated mudstone intervals. The

continuum of F2a through F2b better exemplify the shallow-to-steep-to-shallow dipmeter pattern (epsilon cross-bedding; Allen, 1963; Flach and Mossop, 1985), strongly supporting the notion that F2b represents the upper part of a point bar. As with F1a subtle rotations of tadpole orientations are rarely observed, which represent local changes in topography or natural variation of the lateral accretionary surfaces of the point bars. The complete shallow-to-steep-to-shallow dipmeter pattern may not be well preserved since the top of the point bar is often truncated by other facies (i.e., F1b or F2a of younger point bars).

In summary, the close relationship between F2a and F2b suggests that F2b is preserved in the middle or upper part of thick, laterally accreted point bars. The transition from F2a to F2b indicates a progressive decrease in depositional energy upwards.

Figure 3.8 Facies F2b of Facies Association 1: core and wireline perspectives. **(A)** Gamma ray, dipmeter log, range of facies, and stratigraphic context of F2b mudstone-dominated IHS in well 03-31-090-07W4, the upper red bar in the depth column indicates the location of figure B. The subtle steepening upward tadpole pattern is indicated by the green arrow, and the overlying shallowing upward tadpole pattern is indicated by the red arrow. The black tadpoles represent the dominant dip direction (or azimuth) of the consistently dipping red tadpoles averaged from nearby 5m interval, and the rotation pattern is indicated by the black arrow. **(B)** Core photo of F2b. **(C)** Detailed photos of common sedimentary features identified from F2b facies showing dominant trace fossils (1-5), wavy to lenticular bedding (2), sharp contact with facies F2a (5). The purple wavy line represents the base of the channel. Abbreviations: HAC-High angle cross-stratification, Cy-*Cylindrichnus*, Pl-*Planolites*, Ar-*Arenicolites*, Gy-*Gyrolithes*, Th-*Thalassinoides*, Sk-*Skolithos*, As-*Asterosoma*, Te-*Teichichnus*. (next page)



F2c: massive to laminated mudstone

Description

Facies F2c is characterized by metre-scale massive to laminated mudstone with sporadically distributed bioturbation. The important sedimentological and ichnological characteristics observed from cores, and dipmeter tadpole characteristics observed from petrophysical logs are presented in Table 3.6. An example including GR, dipmeter tadpole, and core expressions of this facies is shown in Fig. 3.9.

Table 3.6 Core and dipmeter tadpole characteristics of facies F2c massive to laminated mudstone.

F2c: massive to laminated mudstone		
Core characteristics		Dipmeter tadpole characteristics
Bedset thickness	<ul style="list-style-type: none"> • 3-15m 	<ul style="list-style-type: none"> • dominant horizontal beds with unreliable orientations (green tadpoles): <4° dip angle • uncommon disorganized/organized low-angle beds (blue tadpoles): 5°-10° dip angle
Occurrence and contacts	<ul style="list-style-type: none"> • gradational contact with F2b/F2a • this facies is locally preserved 	
Sedimentary structures	<ul style="list-style-type: none"> • massive to planar parallel laminated mudstone with mm-scale diffuse sand laminae (Fig. 3.9B, C1) • local lenticular bedding 	
Other sedimentological observations	<ul style="list-style-type: none"> • local pyritization zone (Fig. 3.9C2) • minor syneresis cracks • common coal fragments (Fig. 3.9C2, 6) 	
Ichnological characteristics	<ul style="list-style-type: none"> • absent to rare, sparsely bioturbated sandstone laminae, moderate bioturbation in sand-rich succession (BI: 0-3) • trace fossil assemblage includes <i>Planolites</i>, rare <i>Teichichnus</i>, <i>Arenicolites</i>, <i>Cylindrichnus</i> and <i>Skolithos</i> (Fig. 3.9C) • locally deformed traces or strain-deformed traces (Fig. 3.9C4-5) 	

Integrated discussion and interpretation

The dominance of mudstone and common occurrence of planar parallel lamination (Fig. 3.8C1) and common bioturbation implies an overall low depositional energy. The presence of syneresis cracks are indicative of salinity fluctuation (MacEachern et al., 2005; MacEachern and Bann, 2008; Bhattacharya and MacEachern, 2009). Coal fragments are often observed as very small clasts or more commonly as laminae composed of coarse sand-sized coal grains: both are interpreted to have been transported by fluvial processes into the fluvio-tidal setting. F2c is characteristically on top of F2a and F2b, forming an overall fining upward grain size trend (F2a through F2c) that is indicative of energy decreasing upwards.

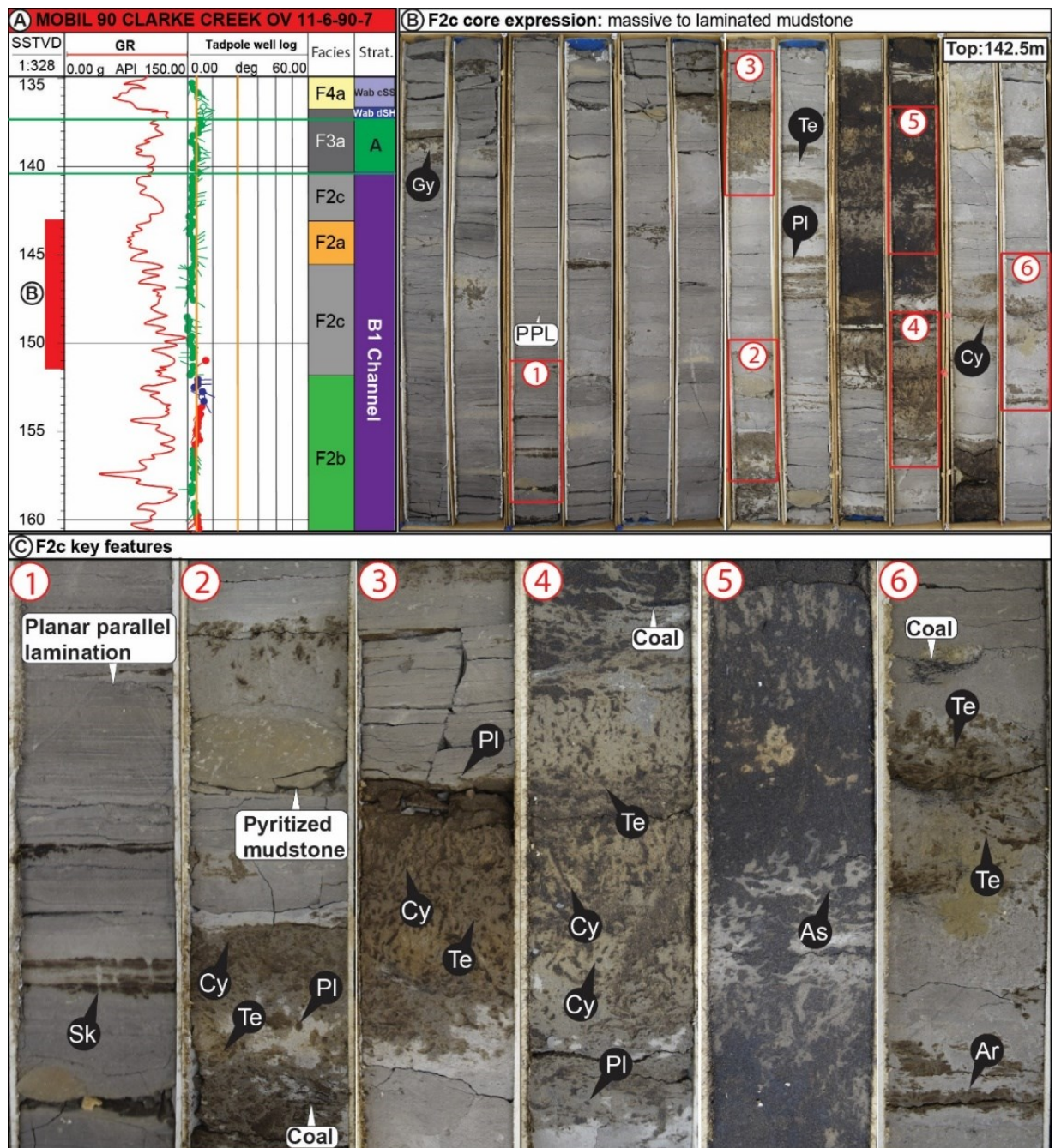
With ichnological characteristics similar to F2b, F2c is correspondingly ascribed to brackish-water sedimentation. Mudstones of F2c are characterized by unburrowed to low intensities of bioturbation, although heavily bioturbated beds are moderately common. Some ichnogenera observed, such as *Teichichnus*, *Arenicolites*, *Asterosoma*, and *Skolithos* (Fig. 3.8C1-6) suggest food is available both at the sediment-water interface (*Arenicolites* and *Skolithos*) and within the accumulated strata (*Asterosoma* and *Teichichnus*) (Gingras et al., 2007). The burrows display consistent bending/deformation direction (e.g., *Teichichnus* and *Cylindrichnus* in Fig. 3.8C3-5), which may be attribute to downslope sediment strain (Gingras and Bann, 2006). All of the above observations suggest a sedimentologically complex unit. Bioturbated horizontal beds and sparsely burrowed mudstones with minor sandstones may represent intertidal bar-top units that represent ambient tidal flat, which are commonly heavily burrowed, and run-off features (e.g., tidal creeks, that feature much less bioturbation). Indeed, the types of trace fossils that reflect an abundance of food resources and their availability on and within the sediment can be associated to intertidal flats as well (Gingras and MacEachern, 2012). It is notable that some of these mudstone beds lack bioturbation altogether and those are taken as a transition to channel abandonment.

The predominance of horizontal tadpole readings is a common dipmeter tadpole characteristic of flat-lying planar parallel laminated mudstone facies. Random orientation of these green tadpoles is derived from a general lack of lithological/resistivity contrast of this facies. Both abandoned channel deposits and intertidal flat strata (top of point bar) share similar flat-lying dipmeter tadpole characteristics. To differentiate one from the other, the context of the underlying facies is required. If a thin F2c (roughly

<2m) overlies a thick F1b/F2a and F2b, further showing the shallow-to-steep-to-shallow dipmeter pattern of epsilon cross-bedding, the F2c might indicate the top of the point bar. The overall dipmeter pattern of this point bar displays a transition of depositional pattern: steeply dipping lateral accretion to flat-lying vertical accretion (Brekke et al., 2017). In cases where the F2c interval is >5m thick, and overlies facies F1b, this facies may indicate channel abandonment. F2c shows a typical example where core and tadpole data should be used together to make a certain environment interpretation. These scenarios can be integrated with core observations, as heavily bioturbated media is normally excluded from abandonment-phase channel fills.

F2c is interpreted as top of estuarine point bar or abandoned channel deposits. Interbeds of sand in F2c can be explained as variations in sediment distribution at the point bar-tidal intertidal flat transition.

Figure 3.9 Facies F2c of Facies Association 1: core and wireline perspectives. **(A)** Gamma ray, dipmeter log, range of facies, and stratigraphic context of F2c massive to laminated mudstone in well 11-06-090-07W4, red bar in the depth column indicates the location of figure B. **(B)** Core photo of F2c, note that F2c locally interbeds with F2a or F2b. **(C)** Detailed photos of common sedimentary features identified from F2c facies showing planar laminated mudstone (1), a trace fossil assemblage preferentially observed in sand laminae or sandstone-rich intervals (1-6), local coal fragments (2, 4, 6), and rare pyritized mudstone (2). Abbreviations: PPL- planar parallel lamination, Cy-*Cylindrichnus*, Pl-*Planolites*, Gy-*Gyrolithes*, Te-*Teichichnus*, Ar-*Arenicolites*, As-*Asterosoma*.



F2d: lenticular to wavy bedded mudstone/sandstone

Description

Facies F2d is characterized by alternating dm-scale mudstone and cm-scale sandstone with low bedding angle, comprising mudstone-dominated IHS. The important sedimentological and ichnological characteristics observed from cores, and dipmeter tadpole characteristics observed from petrophysical logs are presented in Table 3.7. An example of F2d, including GR, dipmeter tadpole, and core expressions is shown in Fig. 3.10.

Table 3.7 Core and dipmeter tadpole characteristics of facies F2d lenticular to wavy bedded mudstone and sandstone.

F2d: lenticular to wavy bedded mudstone and sandstone		
Core characteristics		Dipmeter tadpole characteristics
Bedset thickness	<ul style="list-style-type: none"> • 1.5-6m 	<ul style="list-style-type: none"> • dominant horizontal beds: <4° dip angle • local organized low-angle beds: 5°-8° • very uncommon disorganized low-angle beds: 5°-10° dip angle • need to confirm with core observation to distinguish this facies from F2c
Occurrence and contacts	<ul style="list-style-type: none"> • poor preservation, gradational contact with F1b, F2a or F2b 	
Sedimentary structures	<ul style="list-style-type: none"> • common wavy and lenticular bedding • local oscillation ripples and current ripples • rare mud drapes 	
Other sedimentological observations	<ul style="list-style-type: none"> • rare mud rip-ups • soft sediment deformation • compressed syneresis cracks 	
Ichnological characteristics	<ul style="list-style-type: none"> • low to moderate bioturbation (BI: 1-3) • diminutive trace fossil sizes, common <i>Planolites</i>, <i>Cylindrichnus</i>, minor <i>Arenicolites</i>, <i>Skolithos</i> • common <i>Planolites</i> occur at the interface between sandstone and mudstone laminae • Other trace fossils extend from the tops of the mudstone laminae/beds, are filled with sandstone from overlying sandstone interval • Assemblages dominated by facies crossing trace fossils 	

Integrated discussion and interpretation

F2d is predominantly wavy to lenticular bedded (Fig. 3.10B) suggesting repetitive alternation between bedload sedimentation and fallout from suspension (MacEachern and Bann, 2008; Deschamps et al., 2012; Flemming, 2012). Similar bedding has been interpreted as the result of semidiurnal fluctuations of tidal currents (Reineck and Singh, 1980; Dronkers, 1986; Armenio et al., 2017), however clear tidal

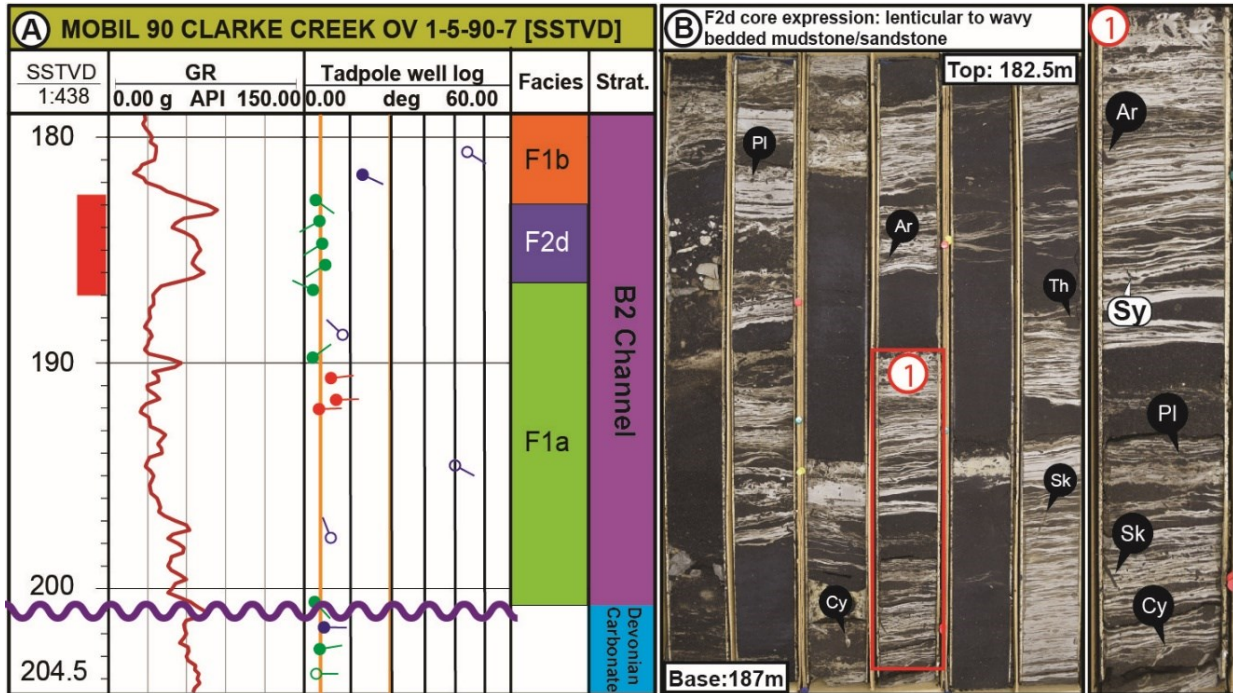
rhythms are not observed in this facies. Syneresis cracks are common (Fig. 3.9a) and are indicative of salinity fluctuation. Massive-appearing, dm-scale sandstone beds are present. Although the sandstone beds can be enigmatic, they clearly interfinger with the wavy to lenticular bedded mudstone, and are interpreted as evidence of episodic transport of sand to the sedimentary environment.

The trace fossil assemblage observed within F2d shows bioturbation intensities (BI) of 1-3. Major traces include *Planolites*, *Cylindrichnus*, minor *Arenicolites*, *Skolithos*, and *Thalassinoides*, representing an assemblage of trophic generalists engaging in filter-, interface- and deposit-feeding and point to an abundance of food resources (Fig. 3.10B). Again, the low to moderate trace-fossil abundance, diversity and diminutive ichnofossil sizes, imply variabilities in salinity under the convergence of fresh and saline water (Gingras et al., 2011).

It is easy to mis-identify F2d as F2a/F2b based solely on core, since they all comprise interbedded sandstone and burrowed mudstone intervals (Fig. 3.10B). However, unlike organized low-angle dipping of lateral accretionary surfaces in F2a/F2b, both the wavy-to lenticular bedded intervals and clean sandstone intervals are characterized by flat-lying tadpoles (see green tadpoles in Fig. 3.10A), which indicate vertical accretion. Such dipmeter tadpole patterns signifies a relatively low energy depositional system. Rarely observed low-angle dips are possibly derived from the cross-stratified sandstone intervals (red tadpoles) representing lateral migration direction of localized tidal runoff creek drainage. The difference between the dipmeter tadpole characteristics of F2c and F2d is very small since both facies are dominated by horizontal beds. Therefore, core observation can be utilized in turn to differentiate F2c from F2d by its much higher sandstone percentage in F2c. F2d shows a great example where core and dipmeter data should be analyzed together to achieve an accurate facies identification.

Altogether, the trace fossil assemblage, the overall high degree of bioturbation, the variable dip angles in places, the presence of tidal run-off creek stratification are most consistent with a tidal flat depositional environment.

Figure 3.10 Lenticular to wavy bedded mudstone and sandstone - Facies F2d: core and wireline perspectives. **(A)** Gamma ray, dipmeter log, range of facies, and stratigraphic context of F2c massive to laminated mudstone in well 01-05-090-07W4, red bar in the depth column indicates the location of figure B. **(B)** Core photo of F2d, a zoom in figure is shown on the right. **(C)** Detailed photos of common sedimentary features identified from F2d facies showing wavy to lenticular bedding, compressed syneresis cracks, and trace fossils. Abbreviations: Sy-Syneresis cracks, Cy-Cylindrichnus, Pl-Planolites, Ar-Arenicolites, Sk-Skolithos, Th-Thalassinoides.



Facies Association 1 Interpretations

FA1 comprises stacked metre-scale successions of F1a through F2d. The base of the succession is characterized by massive to cross-stratified sandstone (F1b) with local mudstone breccia-dominated sandstone (F1a). Inclined Heterolithic Stratification (IHS), interpreted to represent lateral accretion (F2a and F2b) of the middle to the upper parts of the point bar, comprises the bulk of the McMurray Formation (Fustic, 2007; Hubbard et al., 2011; Brekke et al., 2017). The uppermost part of the point-bar deposits is overlain by abandonment channel mudstones of F2c or intertidal flat sediments of F2d. Alternatively, FA1 may be truncated by cross-cutting channels containing FA1. There is an overall increase in bioturbation intensity and diversity from the base to the top of a point bar, suggesting gradual decrease in hydrodynamic energy and slower sedimentation rate towards top. The observed trace fossil suites are

characterized by diminutive trace fossils and their sedimentological context suggests fluctuating energy conditions, variable sedimentation rates, and abundant food resources (MacEachern et al., 2006). The range of facies (F1a, F1b, F2a, F2b, F2c, and F2d) of FA1 is interpreted here as a tidally and fluviually influenced, estuary point bar complex.

Facies Association 2

F3a: bioturbated to lenticular bedded mudstone/sandstone

Description

Facies F3a is characterized by bioturbated to lenticular bedded mudstone and sandstone. The important sedimentological and ichnological characteristics observed from cores, and dipmeter tadpole characteristics observed from petrophysical logs are presented in Table 3.8. Core examples of this facies are shown in Fig. 3.11A-B, Fig. 3.12A.

Table 3.8 Core and dipmeter tadpole characteristics of facies F3a bioturbated to lenticular bedded mudstone and sandstone.

F3a: bioturbated to lenticular bedded mudstone/sandstone		
Core characteristics		dipmeter tadpole characteristics
Bedset thickness	• 1.5-8m	<ul style="list-style-type: none"> • dominant horizontal beds (green tadpoles): <4° dip angle • local low- to high-angle dipping beds (blue tadpoles): 10°-50° dip angle • identification of this facies requires integrating core observations.
Occurrence and contacts	• sharp contact with the middle McMurray estuarine point bar facies F2a-d	
Sedimentary structures	<ul style="list-style-type: none"> • common diffuse heterolithic bedding • locally preserved flaser and lenticular bedding • local rippled laminated sandstone 	
Other sedimentological observations	<ul style="list-style-type: none"> • minor soft sediment deformation (flame structure) • mud drapes 	
Ichnological characteristics	<ul style="list-style-type: none"> • moderate to intensively bioturbated (BI:0-4) • trace fossils include <i>Planolites</i>, <i>Gyrolithes</i>, <i>Skolithos</i>, minor <i>Arenicolites</i>, <i>Lockeia</i>, <i>Teichichnus</i>. (Fig. 3.11A-B) 	

Integrated discussion and interpretation

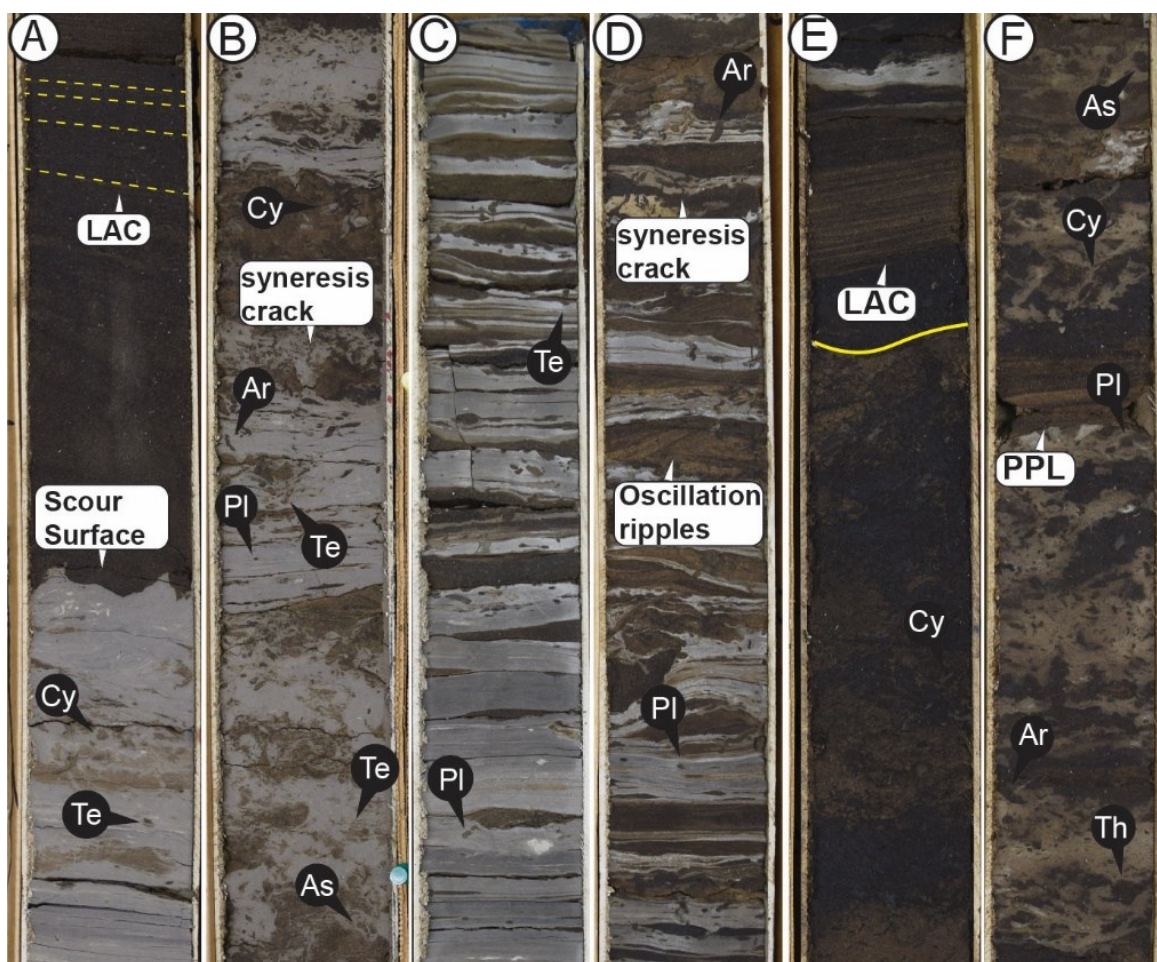
F3a is characterized by moderately to intensively bioturbated silty mudstone interbedded with significant portions of low-angle cross-stratified sandstone, which are interpreted as wave reworked. The chaotic bedding of mudstone (Fig. 3.11B) and common erosional contacts/scour surfaces with cross-stratified sandstone (Fig. 3.11A) are indicative of rapid/episodic sedimentation processes, such as tempestites and freshets. The common presence of syneresis cracks results from fluctuating salinity in brackish water conditions.

The trace-fossil assemblage of F3a is characterized by diminutive trace fossils, low to moderate bioturbation intensity (BI 0-3), and limited ichnodiversity. Trace fossils include *Teichichnus*, *Planolites*, *Gyrolithes*, *Skolithos*, *Asterosoma*, *Cylindrichnus*, with subordinate *Arenicolites*, and *Lockeia*. As with FA1, the trace-fossil assemblage of F3a is interpreted to represent brackish water conditions, although F3a is slightly more diverse. Moderate ichnodiversity and regularly heterogeneous to homogeneously distributed trace fossils in mudstone beds indicate that lowered and fluctuating salinities were generally present (Buatois and Mángano, 2011; Gingras et al., 2011; Tonkin, 2012). The increasing abundance of marine traces compared to FA1 is interpreted to result from the transition from the inner/middle estuary to a shallow-water and sheltered marginal marine environment. Overall, the trace fossil assemblage observed in F3a also supports a proximal brackish-embayment interpretation.

The dominant horizontal beds are the result of silty mudstone deposited from suspension fallout, therefore, no preferred bedding orientation is generated within the mudstone intervals. The local disorganized low- to high-angle dipping beds are possibly derived from poor lithological contacts that were bioturbated.

Evidence for wave reworking along with freshet-associated tempestite deposits is interpreted as the depositional environment stepping landward with the channel environments (F2a,b,c) supplanted by a coastal shoreline. Bioturbation is still brackish in nature and the instances of this facies that occur in the study area are referred to a shallow brackish-embayment and bay margin (i.e., low-energy shoreface).

Figure 3.11 Core photos of Facies F3a and F3b of Facies Association 2. **A)** Core expression of F3a showing a scour surface at the contact between cross-stratified sandstone and bioturbated mudstone. Well 10-20-090-07W4, depth 129.4-129.8m. **B)** Core expression of F3a showing massive to lenticular bedded mud/sand. Well 10-20-090-07W4, depth 127.9-128.3m. **C)** Core expression of F3b showing minor bioturbated lenticular to wavy bedded mud/sand, normally occurring at the base of coarsening-upward allomembers in Upper McMurray Formation. Well 10-21-090-07W4, depth 133.60-134.0m. **D)** Core expression of F3b showing wavy bedded sand/mud with oscillation ripples observed in sandstone interval, syneresis cracks are observed in mudstone interval, this facies normally represent the middle section of the coarsening-upward allomembers. Well 10-21-090-07W4, depth 132.7-133.1m. **E)** Core expression of F3b displaying low angle cross-stratified sandstone and an erosional contact (indicated with yellow line) with the underlying bioturbated sandstone. This is commonly observed in the upper part of coarsening-upward allomembers. Well 10-21-090-07W4, depth 128.0-128.4m. **F)** similar to (E), moderate to high bioturbation destroys primary sedimentary structures. Well 10-21-090-07W4, depth 128.4-129.0m. Abbreviations: LAC-Low angle cross-stratification, PPL-Planar parallel lamination, Sy-Syneresis cracks (commonly compressed), Cy-Cylindrichnus, Pl-Planolites, Ar-Arenicolites, Gy-Gyrolithes, Th-Thalassinoides, Te-Teichichnus, Sk-Skolithos, As-Asterosoma.



F3b: heterolithic coarsening upward mudstone/sandstone

Description

Facies F3b is characterized by heterolithic mudstone and sandstone with coarsening upward grain size trend. The important sedimentological and ichnological characteristics observed from cores, and dipmeter tadpole characteristics observed from petrophysical logs are presented in Table 3.9. Core examples of this facies are shown in Fig. 3.11C-F, Fig. 3.12B.

Table 3.9 Core and dipmeter tadpole characteristics of facies F3b heterolithic coarsening upward mudstone and sandstone.

F3b: heterolithic coarsening upward mudstone/sandstone		
Core characteristics		Dipmeter tadpole characteristics
Bedset thickness	<ul style="list-style-type: none"> coarsening upward allomembers range between 6-8m. 	<ul style="list-style-type: none"> dominant horizontal beds (green tadpoles): <4° dip angle local low- to high-angle dipping beds (blue tadpoles): 10°-50° dip angle identification of this facies requires integrating core observations.
Occurrence and contacts	<ul style="list-style-type: none"> sharp contact with FA1 	
Sedimentary structures	<ul style="list-style-type: none"> massive to planar laminated mudstone at the base, and grades upward into heterolithic bedded sand/mud, forming coarsening-upward cycles local oscillation ripples local low-angle cross stratification, and apparent planar parallel lamination in discrete sandstone interval 	
Other sedimentological observations	<ul style="list-style-type: none"> common soft sediment deformation local scour surfaces minor mud rip-ups 	
Ichnological characteristics	<ul style="list-style-type: none"> sporadically distributed trace fossils (BI: 1-4) common <i>Planolites</i>, <i>Arenicolites</i>, <i>Thalassinoides</i>, minor <i>Asterosoma</i>, <i>Gyrolithes</i>, <i>Diplocraterion</i>, and <i>Teichichnus</i> (Fig. 3.11C-E) 	

Integrated discussion and interpretation

F3b is composed of stacked coarsening-upward cycles, among which, each cycle signifies a depositional package within a deltaic environment. The base of the cycles is characterized by heterolithic bedded mudstone and sandstone intervals, and the abundance of mudstone (Fig. 3.11C-D) implies a distal subenvironment of deltaic systems. The discrete low-angle cross-stratified sandstone beds (Fig.

3.11E), planar-parallel lamination (Fig. 3.11F) and oscillation ripples (Fig. 11D) are more commonly observed in upper part of the coarsening-upward cycles. This observation is suggestive of episodic storm influenced and persistent wave reworking within the proximal delta front environment. Other sedimentary accessories, such as soft-sediment deformation structures and local scour surfaces, are also common features identified in storm influence environment representing rapid sedimentation rates within delta front settings. The observed coarsening-upward cycles of F3b show great consistencies with previous studies that suggest an incised valley depositional model (Mossop and Flach, 1983; Flach and Mossop, 1985; Ranger and Pemberton, 1988; Ranger, 1994; AEUB, 2003; Ranger and Gingras, 2010). These coarsening-upward cycles are interpreted as allomembers deposited during a high stand systems tract (HST) and bounded by flooding surfaces during the overall transgression of the McMurray Formation. Herein, The approximately 3-4m thick (see examples in Fig. 3.12A) allomembers recognized from facies 3b can be interpreted as a result of repeated lobe switching within a wave- and storm-influenced deltaic environment.

The diminutive and low ichnodiversity ichnofossil assemblage of F3b point to brackish-water conditions (Pemberton et al., 1982; MacEachern and Bann, 2008). The slight increase in trace fossil sizes and diversity in the upper part of the cycles is a result of higher organic content (more sufficient food availability) within the substrate and water column of the distal delta front *versus* proximal prodelta (Tonkin, 2012). The general paucity of burrows in cross-stratified or rippled sandstone intervals indicates local energetic events (storms or wave reworking), and again this is consistent with the deltaic setting interpretation made from sedimentary observations (Reading, 1996). Unlike the typical trace fossil assemblages identified on prodelta and delta front environments that characterized by brackish water to fully marine environments (MacEachern and Bann, 2020), facies F3b is solely characterized by brackish-water suite. This observation can be interpreted as the delta prograding into a brackish-water embayment.

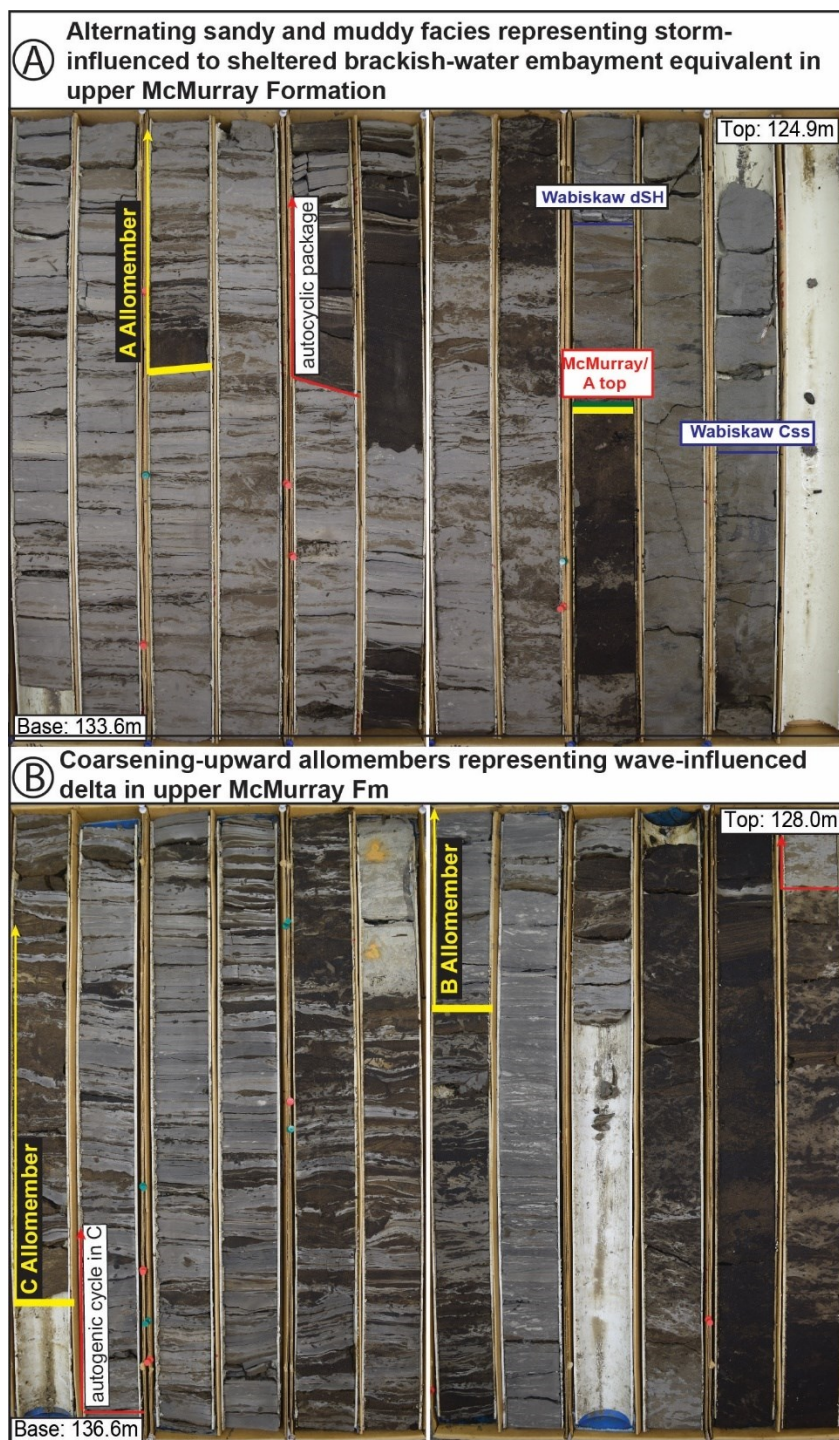
The dominant flat-lying beds are derived from the mudstone and sandstone contacts of heterolithic bedding deposited within the proximal prodelta environment. The characteristic low energy depositional environment induced the mudstone deposition from suspension fallout, and results in such horizontal beds.

Facies Association 2 Interpretations

Facies association 2 (FA2) caps the fluvio-tidal estuarine point-bar complex of FA1. It consists of two major facies expressions: 1) alternating cross-bedded sandstone and intensely bioturbated to lenticular bedded mudstone and sandstone (F3a) (Fig. 3.12A); and 2) regionally correlatable (in most regional studies), coarsening-upward allomembers (F3b) (Fig. 3.12B) (Table 3.1). Details of the two facies expressions are presented in Fig. 11. Unlike the brackish-water trace fossil assemblages identified in FA1, both facies (F3a and F3b) in FA2 are signified by increased but extremely variable bioturbation intensities and in some instances diversity, additional ichnogenera, such as *Teichichnus* and *Thalassinoides*, are observed. Nevertheless, the trace fossil assemblage associated with FA2 is similarly brackish in nature, but potentially evidencing increased marine influence.

This trace fossil evidence is the key to differentiate FA2 from underlying FA1, suggesting a marine to marginal settings (i.e., proximal offshore to shoreface). The heterolithic-dominated, wave- and storm-influenced coarsening-upward packages of F3b reflect an energy sheltered shoreface (i.e., delta) that prograde into a normally quiescent shallow brackish-water embayment (Château et al., 2019; Château et al., 2021). Facies 3a does not show any grain size trend and is interpreted as storm-influenced aggradational proximal offshore or brackish water embayment (Weleschuk and Dashtgard, 2019; Château et al., 2020; Château et al., 2021).

Figure 3.12 Core examples of Facies 3 of Facies Association 2. **(A)** core expression of F3a at well 10-20-090-07W4: alternating cross-bedded sandstone and intensively burrowed mudstone and sandstone facies, representing storm-influenced to sheltered brackish-water embayment. **(B)** core expression of F3b at well 10-21-090-07W4: correlatable, coarsening-upward allomembers in Upper McMurray Formation. Note the presence of autogenic cycles present within each allomember.



Comparing core and dipmeter characteristics of sedimentary facies

Core- and wireline-based facies analyses draw great attention to changes in lithology, and thereby may be inadequate or misleading with respect to identifying vertically and laterally heterogeneous point-bar deposits. This is exacerbated in some lithologies. For example, our core analysis identifies any low- to high-angle cross stratified as F1b and potentially as simple- or compound-dune deposits (as shown in Table 3.1). However, the corresponding dipmeter tadpole plot shows two different characteristics: 1) low- to high-angle disorganized blue tadpoles (F1a in Table 3.2); 2) alternating dm-scale blue and red tadpole groups (Fig. 3.6 and F1b in Table 3.3). The blue tadpoles indicate paleocurrent directions measured at cross beds. The red tadpoles are characterized by low dips, and are consistent with the bedding orientation of the overlying lateral accretion surfaces of IHS facies (F2a/F2b). Supported with these observations, the cross-bedded sandstone is clearly genetically related to IHS facies, and thereby represents point-bar associated strata. An issue we encounter with the thick point-bar deposits is that the scale of observation within core datasets can lead to inadvertent splitting of genetically related successions. Similar observations have been made by Brekke et al., (2017).

The other advantage of analyzing dipmeter tadpoles is to determine whether the nearby wells can be stratigraphic correlated. In most core and wireline based McMurray studies, only channels directly underlying Upper McMurray allomembers can be stratigraphically named or recognized. Once the allomembers were removed by younger incisions, the remnant point bars become difficult to differentiate. If there is sufficient dipmeter tadpole data available in nearby wells, this gap can be closed. An example is shown in cross section Fig. 3.14, where the lateral accretion beds (red tadpoles) at depth 167-190m of well 01-20-090-07W4 can be correlated across younger (cross-cutting) channel sets with 07-24-090-08W4 to the west.

There are also some limitations of the dipmeter tadpole analysis. First of all, its application is limited in recognizing the upper McMurray allomembers at least in this case study. The allomembers are recognized by: 1) local coarsening-upward grain size change; 2) occurrence of marine trace fossils (e.g., *Teichichnus* and *Thalassinoides*); 3) sign of storm influences (local scour surfaces). In such energy sheltered brackish embayment, the dipmeter tadpoles commonly have flat-lying tadpole patterns, but

wherever there is a local storm influence or heavy bioturbation interval, the dipmeter tadpole characteristics may be variable. As a result, the identification of Upper McMurray allomembers heavily relies on the core (and wireline) analyses.

Core analyses were critical in identifying environmental details, such as differentiating freshet-associated lithosomes to interpret influence of the fluvial system, the identification of brackish-water trace fossils, discriminating between bar-top intertidal facies and channel abandonment phases. Also, core is critical in determining whether 'upper' McMurray parasequences had more of a shoreface, offshore or deltaic character. But particularly regarding lithofacies variability within pointbars could be misleading.

Overall, the dipmeter characteristics helps to refine the identification of point bars, and differentiate channel bar sets. Most importantly, the vintage dipmeter dataset contributes greatly to resolving point bar stacking patterns and architectures in the McMurray Formation. Core analyses contribute to the overall understanding of sedimentary processes interpreted from small scale sedimentary structures (e.g. ripples, syneresis cracks), and ichnofossils, which greatly enhances our ability to interpret details of the sedimentary environment.

DISCUSSION

Estuarine point bar geometry

Detailed facies analysis integrated with dipmeter data supports an interpretation of the estuarine point-bar model for much of the middle McMurray member. The point bar comprises 1) a lower section represented by cross-stratified sandstone of facies F1a; 2) a middle section with heterolithic sandstones and mudstones of facies F1b, F2a and F2b; and 3) an upper section constituting massive to bioturbated mudstone of facies F2c and F2d. Thicknesses of point bars range from 6-65m (see examples in Fig. 3.13 and Fig. 3.14).

In the absence of lateral-accretion characteristics, the lower section is interpreted to represent channel-thalweg dunes (i.e., trough cross-stratified and/or planar tabular sandstone of F1a). This section can be easily identified on the dipmeter logs by the presence of disorganized and variably dipping tadpoles presumably measured from cross-bedding (Figs. 3.5-3.6).

The gradational contact between the lower and middle is observed in tadpoles showing transition from unorganized to organized patterns (Figs. 3.4, 3.6-3.7). Previous outcrop and image log analyses have further shown that the heterolithic facies F2a and F2b can be traced laterally into the underlying F1a/F1b cross-stratified sandstone unit (Mossop and Flach, 1983; Nardin et al., 2013; Brekke et al., 2017). The middle section consists of a transition from the sandstone-dominated IHS (F1b/F2a) to mudstone-dominated IHS (F2b). If preserved, this section is characterized by a general shallow-to-steep-to-shallow dipmeter pattern, and consistent dipping direction with occasionally subtle changes in dip direction due to natural variations commonly observed in lateral accretion beds in point bars (Muwais and Smith, 1990; Brekke et al., 2017) (Fig. 3.8).

The upper section is observed locally, but only where a complete estuarine point bar is well preserved. The facies identified in this section include dominant F2c and minor F2d, and represent the uppermost part of the shallow-to-steep-to-shallow dip pattern of laterally accreted beds, which marks the final steps of point-bar development. The flat-lying dipmeter pattern thereby represents bar top units and can be considered to be the intertidal flat portion of the point-bars laterally accrete bar owing to other facies characteristics such as the presence of brackish-water bioturbation (Fig. 3.9).

Stratigraphic correlation has been conducted using the petrophysical well logs and core analysis, dipmeter tadpole data has been used to aid point bars correlation in areas where they are available. Five channel belts (Channel A-Channel D) and three allomembers (A1-B2) have been identified within the study area with Channel A being the youngest and Channel D being the oldest. Each channel incision is characterized by single point bar or amalgamation of multiple meandering point bars. According to the dipmeter characteristics of the point bar deposits, same point bar occurs at different wells can be correlated by identifying similar lateral accretion directions indicated by IHS facies. The dipmeter characteristics alone permit identification of stacking patterns and lateral distributions of individual point bars. A north-south interpreted cross section with classified dipmeter tadpole data is illustrated in Fig. 3.13, and a west-east interpreted cross section with dipmeter tadpole plots is illustrated in Fig. 3.14. The location of each channel incision has been established to show correlation between wells in these cross sections.

Channel D is preserved only within the stratigraphic lows, and is characterized by cross-bedded, unburrowed fluvial deposits. Overlaying C, B2, B1 and A channels show variable thicknesses (6-65m) and different IHS dipping directions (Wightman, 1995; Ranger and Pemberton, 1997; Strobl et al., 1997; Hein et al., 2000; Hein et al., 2001; Brekke and Evoy, 2004; Fustic, 2007; Fustic et al., 2012). The older channel deposits Channel C is locally preserved due to incision by the younger channels (Channel A, B1 and B2), and is characterized by NW- to W-dipping lateral accretion orientation (Fig. 3.13 and Fig. 3.14). Channel B2 show consistently NE- to E-dipping lateral accretion direction (Fig. 3.13 and Fig. 3.14). Point bars of Channel B1 spatially dominate the study area, showing consistently SW-dipping lateral accretionary surfaces (Fig. 3.13 and Fig. 3.14). The youngest Channel A is characterized by SE- to NE-dipping lateral accretion beds (Fig. 3.13 and Fig. 3.14). Examples of complete point bar preservation are observed in the younger channel sets A and B1, in contrast, older channels B2 and C are preserved in most cases as background point bars.

Previous works indicate that the basinward paleoflow is characterized by north-northwest oriented paleoflow within the "Main Valley", with likely distributaries sourced from paleo-topographic-highs to the west and east (Wightman, 1995; Ranger and Pemberton, 1997; Hein et al., 2000; Fustic et al., 2012). In this particular study, the orientation of IHS facies in Channel B1 and C consistently dip NW-SW, and point bars of Channel A and B2 dip consistently towards NE-SE (Fig. 3.13 and Fig. 3.14). These IHS dipping directions are consistent with a preferred lateral migration of meander belts in a northward flowing "Main Valley" (Keith et al., 1990; Ranger, 2006; Ranger and Gingras, 2010).

Figure 3.13 Interpreted north-south cross section with classified tadpole plots. Note the IHS facies bedding orientation represented by red tadpoles display a predominant lateral accretion direction of point bars (red tadpoles). The cross-section tracks for each well are gamma ray (GR) and dipmeter tadpoles. The datum for the cross section is the top of allomember A. The cross section displays stratigraphically defined B2 channel incised by younger B1 and A channels. B2 channel is characterized by southeast- to east-dipping lateral-accretion beds. B1 is characterized by southwest- to west-dipping lateral accretion beds. The youngest A channel is dominated by southeast-dipping lateral accretion beds.

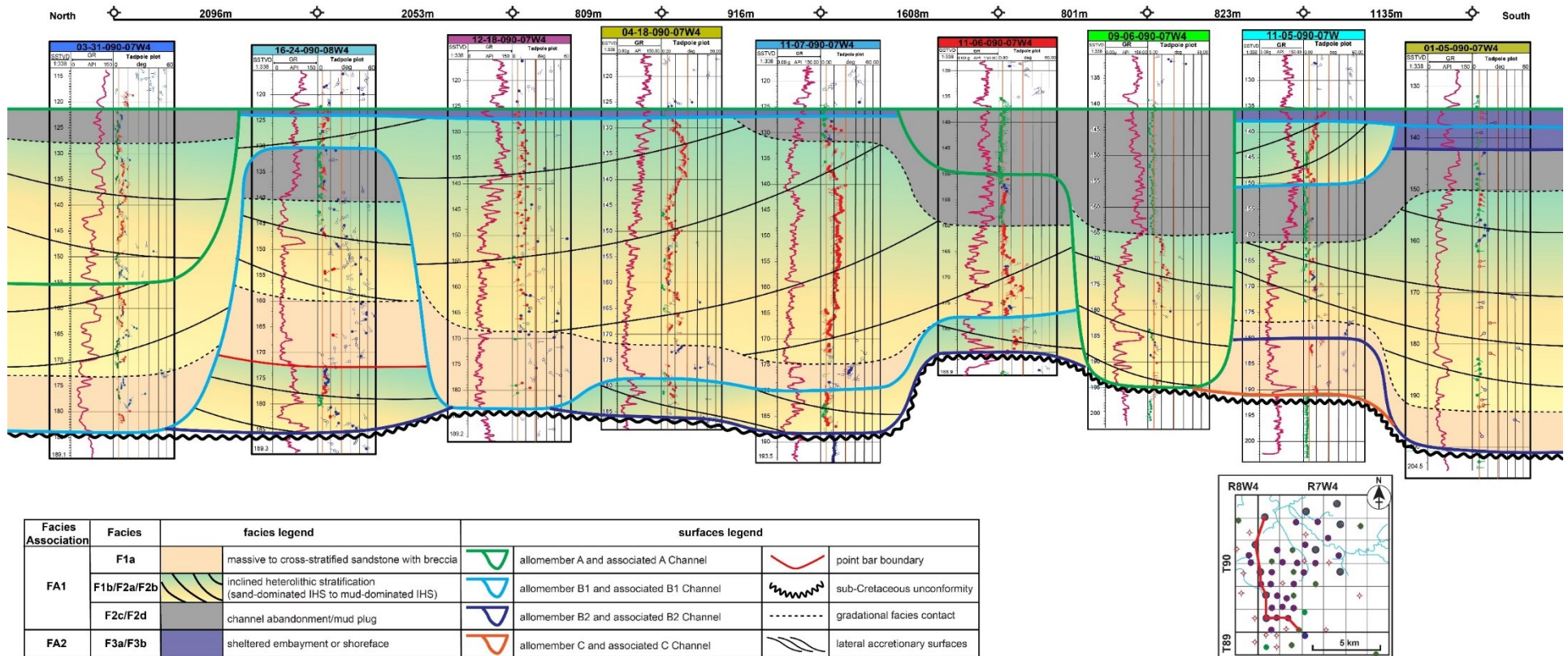
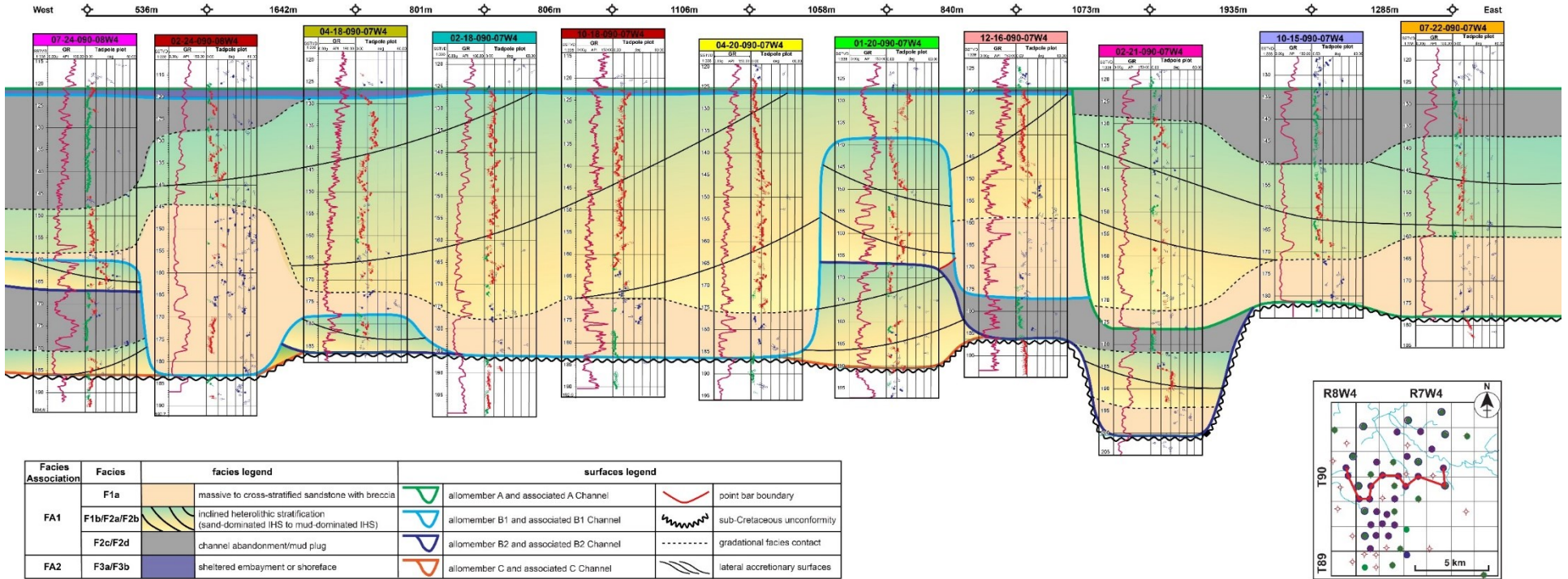


Figure 3.14 Interpreted west-east cross section with classified tadpole plots. Note the IHS facies bedding orientation represented by red tadpoles display a predominant lateral accretion direction of point bars (red tadpoles). The cross-section tracks for each well are gamma ray (GR) and dipmeter tadpoles. The datum for the cross section is the top of allomember A. The cross section displays stratigraphically defined C and B2 channel incised by younger B1 and A channels. C channel is characterized by northwest- to west-dipping lateral accretion beds. B2 channel is characterized by southeast- to east-dipping lateral accretion beds. B1 is characterized by southwest- to west-dipping lateral accretion beds. The youngest A channel is dominated by southeast- to northeast-dipping lateral accretion beds.



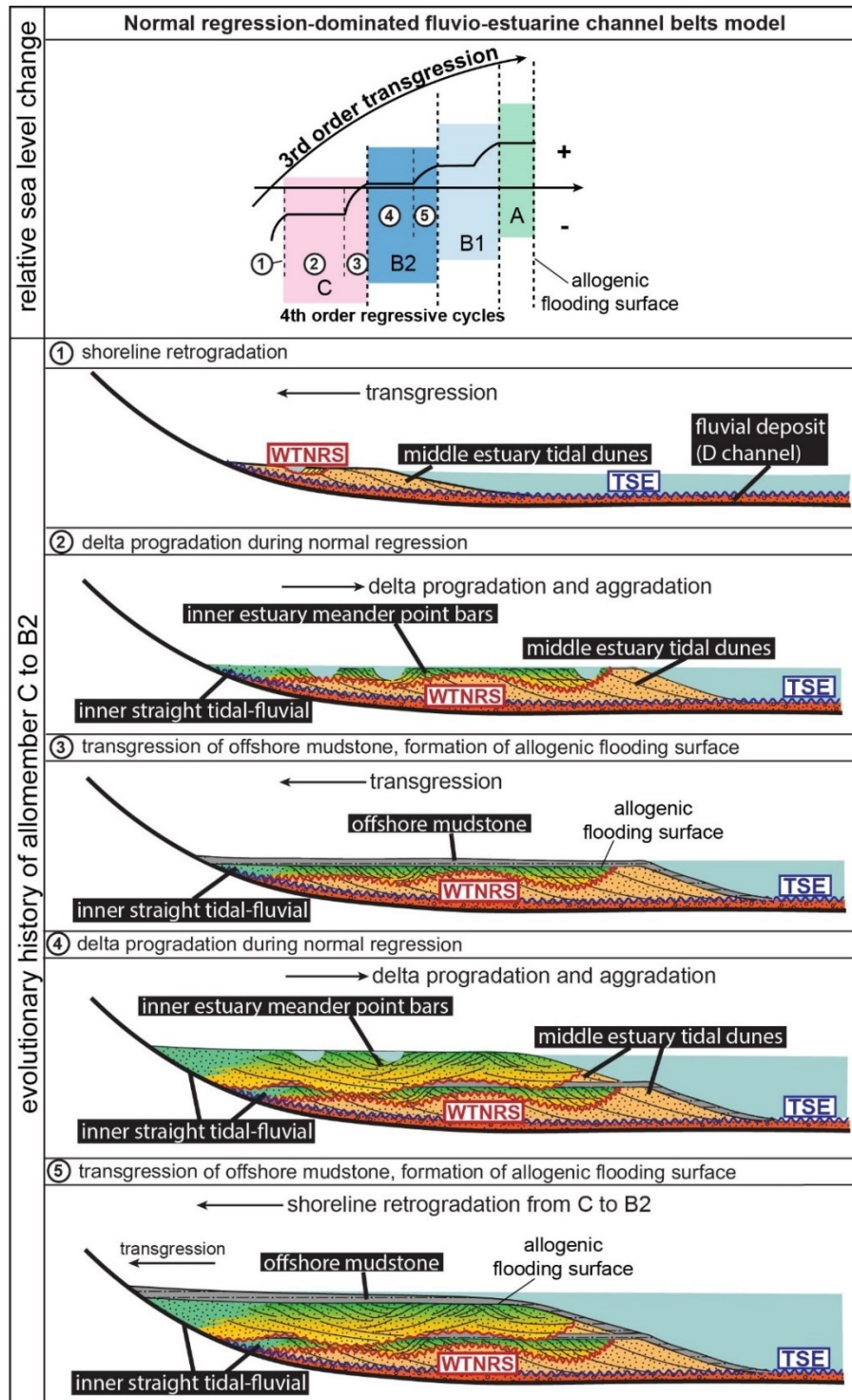
McMurray Formation depositional model

The depositional interpretation of the McMurray Formation has been ongoing for decades. A northward prograding deltaic system (Carrigy, 1971) was proposed as early as the 1970s, whereas later McMurray interpretations suggested an estuarine channel-bar model (Pemberton et al., 1982; Mossop and Flach, 1983; Flach and Mossop, 1985; Thomas et al., 1987; Ranger and Pemberton, 1988; Ranger, 1994; Hein, 2015; Martinius et al., 2015; Gingras et al., 2016; Shchepetkina et al., 2016; Brekke et al., 2017; Hayes et al., 2018). More recently ongoing outcrop, seismic, and dipmeter log studies imply a general acceptance that the IHS facies represent fluvial or fluvio-tidal, brackish-water point bar deposits (Nardin et al., 2013; Brekke et al., 2017; Hayes et al., 2018; Brekke and Roenitz, 2021). According to the core-based sedimentological and ichnological analysis described in Chapter 2 and this study, the observed middle to upper McMurray Formation represents basinward progradation of fluvio-estuarine channel belts resulting from episodic 4th order sea-level fluctuation during an overall 3rd order transgression of the Boreal Sea. A relative sea-level curve and schematic diagram depicting the evolutionary history and the resulting stratigraphic configuration on the shoreline during the deposition of Allomember C and Allomember B2 are summarized in Fig. 15. The deposition of successive allomembers and their associated channels follow the same fashion as C and B2.

As shown in the sea-level curve figure (Fig. 15), the evolutionary history of the McMurray Formation can be divided into several normal-regression dominated episodes (C, B2, B1 and A), each of which is a result of a 4th order sea-level fluctuation cycle. The initial deposition of the McMurray Formation is marked by paleogeography-constrained fluvial channels and associated floodplain deposits (Channel D) as evidenced by the presence of continental trace fossils, coal and wood fragments and immature paleosols (Flach and Mossop, 1985; Harris et al., 2016). Following the deposition of fluvial deposits, the allomember C and middle estuary tidal sand bars were deposited landward during transgression (time 1 in Fig. 15). And left behind a transgressive surface of erosion at the base. As the rate of sea level rise decreases, channel-fill deposit of Channel C, characterized by heterolithic point bars, were deposited as results of amalgamated, lateral and downstream migrated channel belts during normal regression (NR) (time 2 and time 4 in Fig. 15). As the shoreline prograded basinward, a truncation surface is developed as internal

facies contact separating the broader oceanward channel deposits below from the overlying inner estuary point bars. Such surface has been observed at Amphitheatre and Christina River outcrops (Hayes et al., 2018; Chen et al., 2022), and is defined as 'within-trend normal regressive surfaces' (WTNRS) (Catuneanu, 2006) (as shown in time 2-4 of Fig. 15). Each 4th order cycle is terminated by the deposition of transgressive offshore mudstone deposits (time 3 and 5 of Fig. 15), and the base of the marine mudstone is defined as an allogenic flooding surface. Additionally, contacts between channels identified from the dipmeter tadpole analysis correspond to autogenic erosional surfaces that are caused by channel-belt migration. The upper boundary of channel belts can be either allogenic or autogenic flooding surfaces. The differentiation between them requires detailed sedimentological and ichnological examination of contrasting facies across the contact. Details regarding this differentiation is discussed in Chapter 2.

Figure 3.15 Relative sea-level curve and schematic diagram depicting the evolutionary history and the resulting stratigraphic configuration during the deposition of Allomember C and Allomember B2. The successive allomembers (B1 and A) are their associated channel belts evolved in the same fashion.



CONCLUSION

This paper provides a detailed description of the middle McMurray facies in the Christina River area using the sedimentological, ichnological, and dipmeter characteristics. This study, which follows on earlier efforts such as Muwais and Smith (1990), Fustic et al., (2008), Brekke et al., (2017), and Brekke and Roenitz (2021), provides an example of how vintage dipmeter tadpole logs can be used to support and refine facies interpretations in core datasets, and to discriminate between different estuarine point bars of the middle McMurray Formation. Particularly, similar point-bar stacking patterns are identified in four channel sets, which allows provides the basis for the reconstruction of the paleodepositional history and relative sea-level changes.

A normal regression-dominated fluvio-estuarine channel belts model has been proposed based on sedimentology, ichnology and dipmeter patterns. Four repeated 4th order cycles have been recognized over the major 3rd order transgression. The IHS facies display a predominant either NW-SW or NE-SE lateral accretion direction which is consistent with an overall N-NW paleoflow direction within the Main Valley.

This local study particularly highlights one of the challenges of applying a normal regression-dominated model to areas within or near the main valley system of the McMurray Formation. Deep channel incision, together with intense amalgamation and migration of estuarine channels, contributes to poor preservation of allomembers in the upper McMurray succession. Lateral variation within allomembers makes the identification of allomembers even more challenging, the result of which can be uncertainty in the identification of discrete channel-fill deposits and the stratigraphic levels to which they correspond. With the assist of dipmeter tadpole data, the stratigraphic correlation can be ensured by identifying individual point bars associated with corresponding stratigraphic units. With sufficient dipmeter tadpole data, well-to-well can resolve some remnant point bars in the regional background of the McMurray Formation by correlating the same point bars which are crosscut by younger channels. This study gives other subsurface workers another analogue study that dipmeter tadpole data can help to

refine core-based facies analysis, enhance wireline- and core-based stratigraphic correlation, and support subsurface interpretations of other channelized estuary deposits.

Chapter 4 : Recognizing Genetically Related Depositional Packages Using 3D Photogrammetric Outcrop Models in a Fluvially Dominated, Tidally Influenced Meander-Belt Succession.

INTRODUCTION

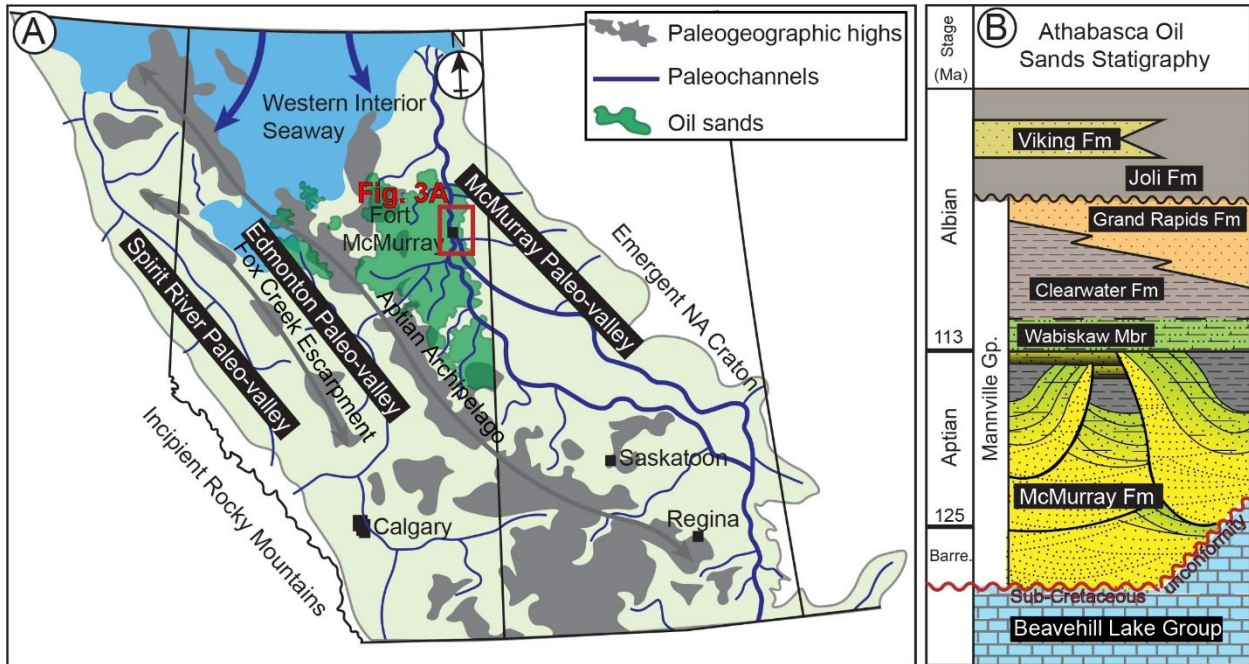
Estuary channels in fluvio-tidal settings are commonly composed of thalweg-associated dune and point-bar deposits (e.g., Carling et al., 2015; Shchepetkina et al., 2016). The migration and amalgamation of tide-influenced fluvial meander belts result in complex stacking patterns of point bars and dune deposits. For this reason, estuary deposits can be stratigraphically complex. This is exacerbated by the facts that not all fluvio-tidal channels contain cross-bedded sandstone in the thalwegs and that IHS (Inclined Heterolithic Stratification) in such channels is sedimentologically variable, even along individual point bars (Gingras et al., 1999; Choi et al., 2004; Labrecque et al., 2011). As a result of these factors, identifying different channel stories can be challenging, yet this is requisite to determine an estuary deposit's stratigraphic architecture and establish a paleogeographic understanding.

Previous studies have delineated boundaries between different point bars or genetically unrelated packages using petrophysical logs, dipmeter logs, micro-resistivity image logs, seismic data, and outcrop-based bedding orientation data analysis (Crerar and Arnott, 2007; Hubbard et al., 2011; Nardin et al., 2013; Brekke et al., 2017; Brekke and Roenitz, 2021). Among these studies, subsurface studies have limitations, particularly where similarly dipping bars are superimposed on each other wherein unit contacts maybe difficult to observe. In contrast, outcrop-based studies in part rely on the identification of contacts that can be traced across the outcrop to facilitate the identification of depositional units. An early model for point-bar deposits is underlying thalweg-associated cross-bedded sandstones that intercalate with inclined heterolithic stratification (IHS) of point bars upwards (Hein et al., 2006): this model generally supports subsurface studies in the McMurray Formation. Generally not identified in McMurray subsurface studies are the following features observed in outcrop: 1) the discontinuities within the successive point bar facies, at least in some cases, favor a model of channel deposits represented primarily by IHS without substantial thalweg deposits (Ranger and Gingras, 2010); and, 2) sedimentological analyses of the cross

bedded sandstone suggests the presence of laterally accreted tidal bars and forward-accreted tidal dunes in large tidal channels (Olariu et al., 2012; Longhitano et al., 2014; Hayes et al., 2018). Few outcrop studies have attempted to provide integrated interpretations combining sedimentological, ichnological, and bedding orientational analyses, to understand the various depositional models that can be supported by the datasets. This study focusses on integrating these characteristics to identify and interpret stratigraphic complexities for the purpose of identifying genetically related stratigraphic units with greater certainty.

Subaqueous fluvio-tidal deposits can be broadly divided into 2 facies: 1) dune-scale, cross-bedded sandstone (CB); and 2) inclined heterolithic stratified sandstone and mudstone bedsets (IHS). Numerous outcrops and subsurface studies have shown that the IHS facies commonly overlie the cross-bedded sandstone facies, and form conspicuously stacked fining-upward grain size trends. Several of these studies suggested that the two dominant facies thereby belong to the same genetic package and represent a continuous estuary point bar (Mossop and Flach, 1983; Langenberg et al., 2002; AEUB, 2003; Crerar and Arnott, 2007; Hubbard et al., 2011; Fustic et al., 2012; Musial et al., 2012; Jablonski and Dalrymple, 2016). Nonetheless, several studies have also shown that fluvio-tidal channel fills can be composed almost entirely of IHS, with no notable sand-dominated thalweg unit (Pearson and Gingras, 2006; Ranger and Gingras, 2010; Hayes et al., 2018): this is particularly true in mud-dominated channel settings (Gingras et al., 1999; Pearson and Gingras, 2006). This results in channel contacts commonly expressed as IHS cut into IHS and these contacts can be difficult to identify in wireline, core and even outcrop datasets. For example, subsurface studies tend to recognize nearly ubiquitous large-scale point bars, whereas smaller-scale point-bar stacking and amalgamation seem to be overlooked compared to observations from outcrops (Hein and Cotterill, 2006; Hein et al., 2013). To understand the outcrop dataset more fully, the primary objective of this study is to investigate the genetic relationship between the cross-bedded and IHS units of the McMurray Formation exposure at the Christina River outcrop, and establish the likely geological relationship between the two; namely are they unrelated, or genetically related? With respect to the point-bar succession, integrated ichnological, sedimentological, and bedding architectural characteristics are analyzed to explore feasible solutions to the depositional model.

Figure 4.1 (A) Paleogeographic reconstruction of the Early Cretaceous Western Canada Sedimentary Basin (WCSB), including the location of the ancient meander-belt (modified from Durkin, Boyd et al., 2017). **(B)** Stratigraphy of the Athabasca Oil Sands deposit near the study area.



GEOLOGICAL BACKGROUND

Depositional setting of the McMurray Formation

The lower Mannville Group in northern Alberta is characterized by paleogeographic topographic highs that bound three north-trending paleo-valleys (i.e., McMurray, Edmonton and Spirit River paleo-valleys) (Williams, 1963; McLean, 1977). The McMurray Formation deposit in this study belongs to the easternmost McMurray Paleo-valley (alternatively known as the Assiniboia paleo-valley), which is commonly referred to as the "Main Valley" in previous studies (Keith et al., 1990; Wightman and Pemberton, 1997; Fustic et al., 2012). In the Christina River area, the McMurray Formation is deposited on top of the regionally truncated Upper Devonian carbonate strata of the Beaverhill Lake Group (Schneider and Grobe, 2013) (Fig. 1B). Dissolution of the underlying Devonian Prairie Evaporite Formation, as well as the paleographic highs dictated the trend of the major paleo-valleys (Christopher, 1974; Hein et al., 2000) (Fig. 1A).

The McMurray Formation is, in large part, represented by the point bar deposits of a Cretaceous fluvio-tidal channel system that flowed northwards in NE Alberta, Canada (Stewart and MacCallum, 1978; Pemberton et al., 1982; Wightman et al., 1987; Ranger and Pemberton, 1988; Hein et al., 2000). The McMurray Formation has been informally subdivided into the lower, middle, and upper members (Carrigy, 1959), which has been generalized to represent an increase in marine influence throughout the succession during the long-term southward transgression of the Boreal Sea (Fig. 1), although this is a simplification. For instance, the fluvio-tidal system has generally been assigned to the middle McMurray, however stratigraphic analyses conducted over the last 20 years shows that fluvio-tidal deposits are associated with both the middle and upper McMurray units (Carrigy, 1959; Carrigy and Kramers, 1973; Wightman and Pemberton, 1997; Hein et al., 2006)

A representative stratigraphic framework which largely follows the Alberta Geological Survey (AGS) model is illustrated in Fig. 2 and represents the succession of depositional packages in the Christina River region. Similar to other local or regional studies of the McMurray Formation, the upper McMurray interval is known to comprise stacked highstand coarsening-upward parasequence sets (A, B1, B2 and C) that represent episodic progradation of deltaic and shoreface environments (Ranger, 1994; Caplan and Ranger, 2001; AEUB, 2003; Ranger and Gingras, 2010; Baniak and Kingsmith, 2018; Château et al., 2020). The underlying upper and middle McMurray estuarine channel fills (A, B1, B2 and C channels) are either associated with these parasequences, or had been associated and then decoupled from parasequences due to later channel incisions. As shown in the diagram, the McMurray Formation near the study area is characterized by stacked estuarine point bars deposited in highly sinuous fluvio-tidal and estuarine channels. The regionally correlatable McMurray parasequence sets identified in other studies (Ranger, 1994; AEUB, 2003; Baniak and Kingsmith, 2018; Hagstrom, 2019; Château et al., 2020) are commonly absent in the area, and the facies identified at the Christina River outcrop possibly correspond to the incised valley fill of the stratigraphically youngest channel A, although that can not be definitively demonstrated (Fig. 2). Channel A has also been documented as the thickest channel fill deposit of the McMurray Formation at least in the eastern Athabasca Oil sands deposit (Hagstrom, 2019).

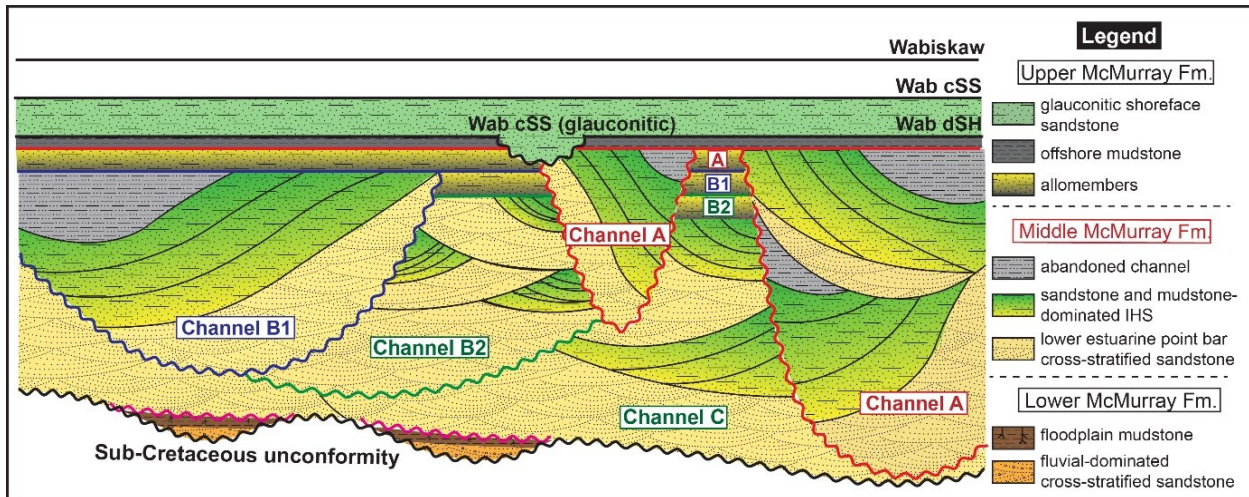
The most recent studies conducted in the Christina River outcrop are by Martinius *et al.* (2015) and Hayes *et al.* (2017). According to their findings, the lower section of the outcrop shows strong evidence of

tidal influence (i.e., tidal reactivation surfaces, reverse flow ripples), and was interpreted to reside in the fluvial to tidal transition zone (FTT), where sediment deposition occurred under combined influences of fluvial discharge and variable degrees of tidal current flow (Martinius et al., 2015; Hayes et al., 2017). Their observations generally agree with the widely accepted inner estuary meander belt model, but there is a lack of discussion regarding the overlying IHS dominated succession in the upper section of the outcrop. The relationship of these IHS units to the cross-bedded sandstone facies is important for the interpretation of the McMurray depositional model. In addition, the Christina River outcrop provides a great opportunity to assess the sedimentology of a relatively younger channel deposit in the McMurray Formation.

Controversy of the McMurray Formation depositional environment

The paleogeographic interpretation of the McMurray Formation has been debated since the early 1980s when Mossop and Flach (1983) proposed a fluvial model and Pemberton et al. (1982) interpreted the formation as emblematic of estuary sedimentation. In the past decade, the origins of McMurray strata have been much more intensely debated. Interestingly the discussion has returned to the original debate with two competing depositional models for the middle McMurray Formation strata: 1) a fluvial channel belt; and 2) a hundreds-of-kilometres long estuarine marine-fluvial transition zone setting. These interpretations are well discussed in several studies, including (Blum and Jennings, 2016; Gingras and Leckie, 2017; Broughton, 2018; Broughton, 2019; La Croix et al., 2019; Durkin et al., 2020; La Croix et al., 2020) The presence of seismically imaged highly sinuous meander belts support a fluvial channel original (Blum and Jennings, 2016; Durkin et al., 2017b). However, the presence of an abundant brackish-water trace fossil assemblage and various tidally associated sedimentary structures support an estuary origin (Hayes et al., 2017; La Croix et al., 2019). As noted above, this study focusses on integrating trace fossil and sedimentological data and thereby should contribute to this discussion.

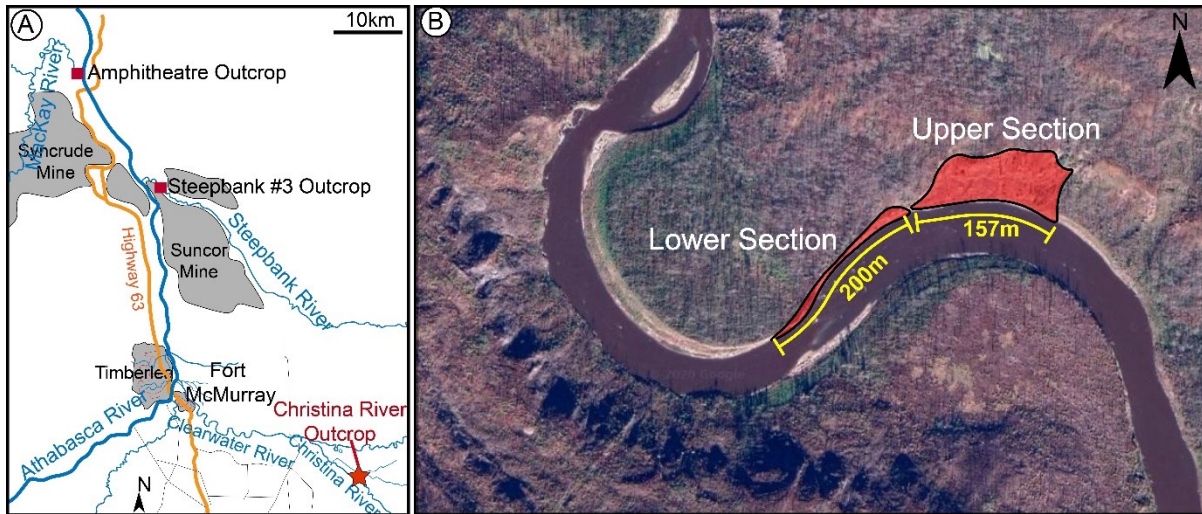
Figure 4.2 Stratigraphic framework representation near the Christina River region. The Christina River outcrop sections correlate to the middle McMurray Formation interval.



STUDY AREA

The McMurray Formation sections are exposed along Christina River in the northeast Alberta, Canada (Fig. 3A), located approximately 25.8km west-southwest of the town of the Fort McMurray in Township 88, Range 6W4M (coordinates: 56.620926, -100.959647). Two sections on the cut bank side of the Christina River were studied, and named as the lower and upper Christina River sections, respectively (see detailed location in Fig. 3B). The 200 metres-long lower Christina River section displays the cross-bedded sandstone facies of the middle McMurray member. The upper Christina River section lies directly adjacent to the lower section and extends 157 metres further east (upstream) along the Christina River (Fig. 3B). This outcrop not only includes a basal extension of the cross-bedded sandstone facies of the lower section, but also displays a large portion of the overlying IHS facies. In particular, the contact between the two facies is clearly represented in the upper Christina River section.

Figure 4.3 (A) relative location of Amphitheatre, Steepbank and Christina River outcrops; **(B)** Christina River outcrop satellite image showing the lower and upper section along the cutbank.



METHODS

Photogrammetry is used to construct a 3D photogrammetric outcrop model of the Christina River outcrop following Hayes et al. (2018). Bedding orientation analysis is conducted for the two dominant facies (i.e., cross-bedded sandstone facies and IHS facies). *Pseudo*-dipmeter tadpole logs are generated from the model and calibrated with the actual dipmeter tadpole logs from nearby wells. The bedding orientations are analyzed in combination with sedimentary and ichnological characteristics of the outcrop to form a synthesized depositional interpretation of the McMurray Formation in the Christina River area. Detailed descriptions of the analytical method and error control are present below.

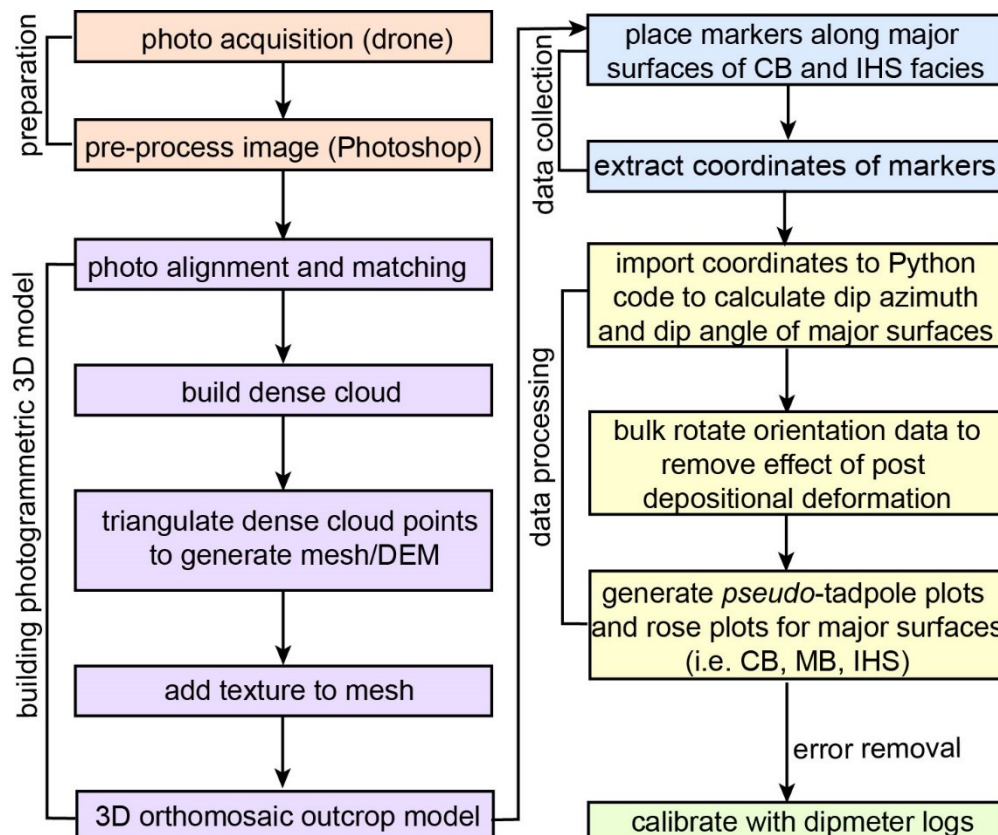
Photogrammetry

Instead of traditional field logging and bedding orientation data collection methods, this study utilized Structure-from-Motion (SfM) photogrammetry to produce a 3D model of the outcrop. The equipment used to capture the outcrop photos is a DJI Mavic 2 Pro Drone Quadcopter equipped with a Hasselblad L1D-20c camera with a 20MP 1 COMS sensor. Hundreds of photos were taken from each outcrop section as the drone moves at a meter scale both vertically and horizontally. A minimum of 30% overlap was maintained in successive photos to ensure the quality of later photo alignment. Detailed principles and

discussion of the application of SfM photogrammetry-to-outcrop are documented in Hayes *et al.* (2017). Once the photos were acquired from the outcrop, they were processed using Adobe Photoshop to adjust photo properties (e.g., brightness, contrast, and color tones, etc.) and to remove significant shadows for the purpose of avoiding bias due to sunlight changes during photo acquisition.

The processed photos were then imported into a commercial SfM photogrammetry software, Metashape 1.7 (© Agisoft) to generate a 3D model of the outcrop. During the processing stage, the software first uses implemented algorithms to extract pixels of the 2D photos and generate a dense point cloud across the outcrop area. Then the subsequent step triangulates these dense cloud points to create a mesh to represent the surficial topography of the outcrop. Textures are added to the mesh at the end to improve the overall resolution of the outcrop. Finally, a high-resolution 3D orthomosaic outcrop model can be generated for bedding orientation analysis. For the detailed principles of the software, refer to Tavani *et al.* (2014).

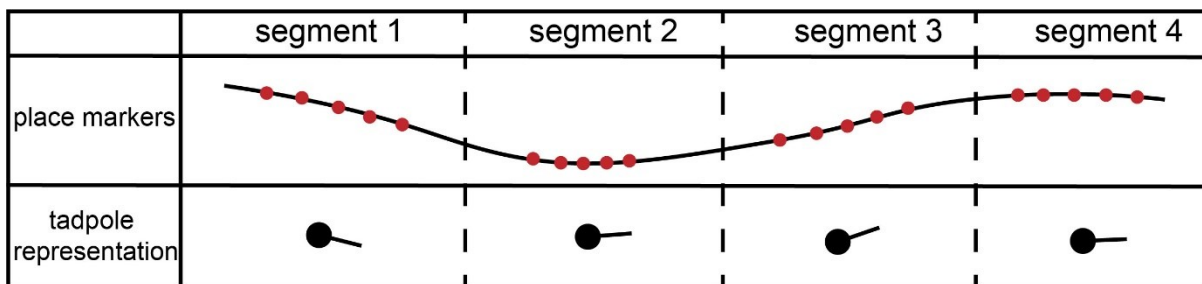
Figure 4.4 Schematic workflow for generating the 3D photogrammetric outcrop model to characterize McMurray Formation deposits at the Christina River outcrops.



Bedding orientation calculation

Once the 3D orthomosaic model of the outcrop is generated, markers can be placed using Metashape 1.7 along any surfaces of interest. Since sedimentary surfaces are commonly undulatory, each surface is divided into smaller measuring segments, which are selected from a portion of the surface that have consistent dipping orientations (Fig. 5). At least 3 markers are required to estimate strike and dip of a best-fit plane. In this study, we placed as many markers as possible along the surface, as the more markers there are, the better the estimation of the bedding orientations. To obtain the most accurate estimation of bedding orientations, markers are placed preferentially in locations where there is three-dimensional outcrop relief along the length of each segment. Metashape 1.7 calculates the coordinates of each marker. These coordinates are then imported into a Python script, which allows bulk conversions to dip and dip azimuth of measured surface segments. Finally, a tadpole representation is used to generate a pseudo-dipmeter log, which is overlaid on the outcrop model. At the lower Christina River outcrop section, cross beds (CB) and cross-set boundary (CsB) (i.e., master bedding planes) are marked in the dominant cross-bedded sandstone facies. With respect to the upper Christina River Outcrop section, lateral accretion surfaces (LASs) in the IHS facies marked by lithological changes between sandstone and mudstone are measured to represent the direction of point bar migration.

Figure 4.5 Schematic diagram showing marker placement along a measured surface. A surface is divided into measuring segments, and at least 3 markers are placed for each segment. This method collects multiple bedding orientation data for a surface to ensure accuracy.



Since the McMurray Formation has undergone pre-, syn-, and post salt tectonic events throughout the region (Broughton, 2013), corrections of bedding measurements need must be applied in order to remove deformation. To do this, we collected bedding orientation data from dipmeter logs in nearby wells located approximately 10km north of the outcrop, which were the closest bedding orientation data available. The

dipmeter data of the upper McMurray interval indicates that the strata are gently dipping WSW in the area. The average rotation axis is estimated as 175.3°S with plunge of 4.13° . To restore the bedding orientations to their original status prior to deformation, our orientation data are rotated around the axis using open-source structural geology software (Stereonet v.11). Finally, the measured strikes and dips of these surfaces are converted to tadpole representations to generate *pseudo*-dipmeter logs of the measured sections. To statistically investigate the dominant bedding dip orientations and relationships between different types of bedding, rose diagrams and poles-to-beddings are generated with respect to individual depositional packages.

Bedding measurement error control

Potential errors associated with this photogrammetric method are derived from: 1) building the photogrammetric 3D model using Metashape 1.7; and 2) calculating dip and dip azimuth values using Python script.

During the photogrammetric model building process, systematic errors that need to be considered including camera-lens distortion, photo resolution, photo shooting distance, the amount of overlap between photos, intersection angles, et al (Dai et al., 2014). To minimize the effect of these errors associated with camera factors, Metashape 1.7 features a camera calibration function during photo alignment step to group photos with consistent camera types and settings, autocorrect lens-associated distortion factors. Therefore, the precision of the 3D model can be ensured. Since the photos and the resulting models are georeferenced, the accuracy of the marker coordinates can be calculated using the software. The Metashape 1.7 calculated accuracy of the marker is 5mm, and the error is generally less than 0.15mm. This amount of error is negligible for the purpose of this study.

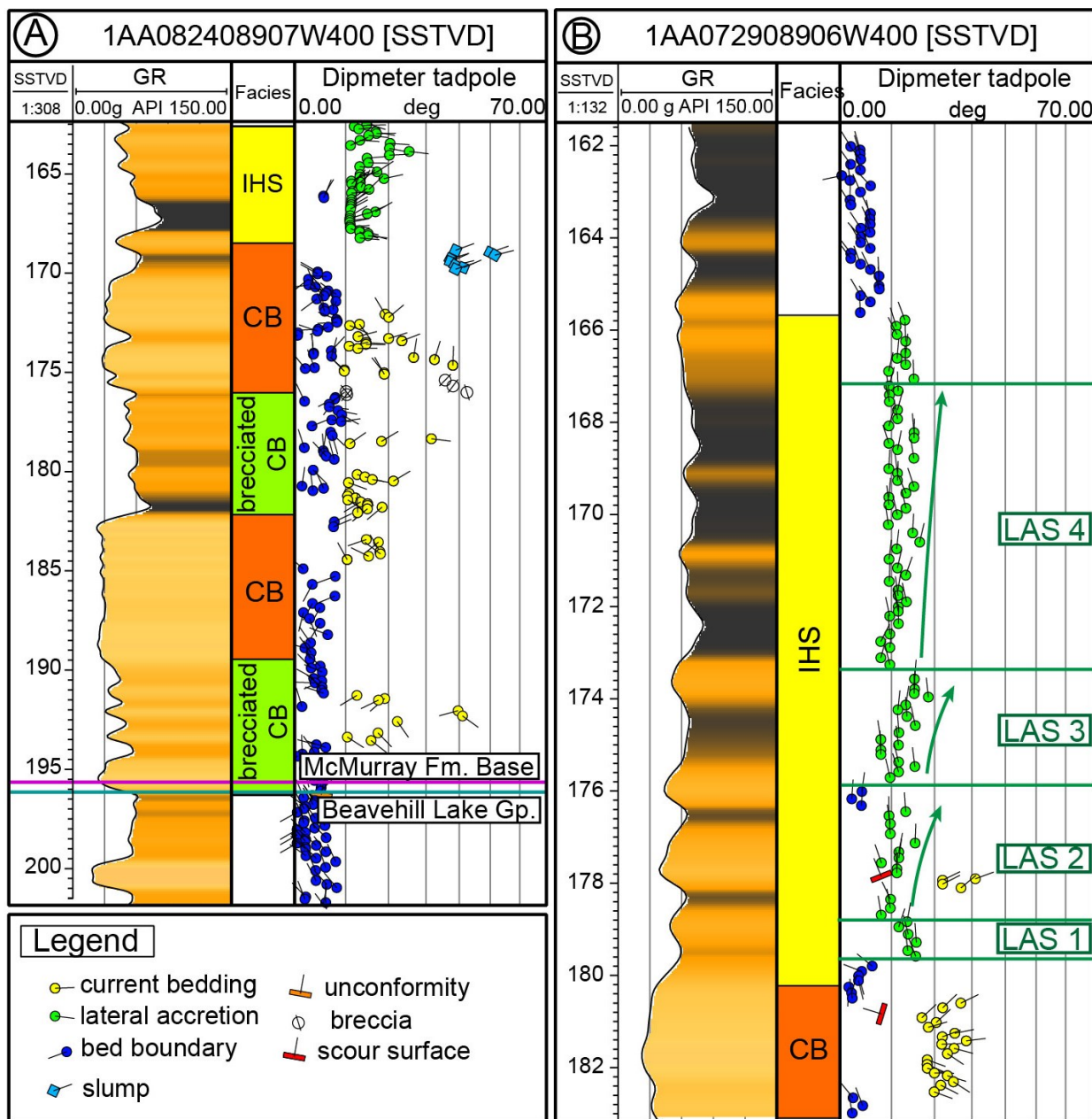
After obtaining the coordinates of markers, the Python script features algorithms to estimate the orientational data of best-fit plane. This script adopts the principle of moment of inertia analysis, which estimates the moment of inertia of a set of markers and using the axis of maximum moment of inertia as the pole to the best-fit plane (Fernández, 2005). Using this method, two values are calculated to describe the degree of fit and reliability for moment of inertia analysis: degree of fit described by M and reliability (degree of co-linearity of a point) described by K. For the purpose of this study, the M and K values are

controlled within the following range: M is greater than 4, and K is less than 2. At this step, the accuracy and error control of the orientational data are ensured by eliminating data with M and K values outside of this range. For a more detailed discussion of these value ranges, readers are directed to Fernández (2005).

Tadpole log calibration

The nearest 4 wells with drilled cores are located 2-3km in the NE of the Christina River outcrops. Detailed logging of these cores allows comparison of different core and outcrop facies expressions. *Pseudo*-dipmeter tadpole logs derived from the 3D photogrammetric outcrop model are calibrated with subsurface dipmeter logs of similar facies observed in nearby wells (Fig. 6). The cross-bedded sandstone consists of two groups of data (represented by blue and yellow tadpoles) (Fig. 6A). Red tadpoles represent cross beds measured from the outcrop. They are characterized by disorganized, low- to high-angle tadpoles (5°-40°). Blue tadpoles represent bed boundaries, which are equivalent to low-angle dipping cross-set boundaries separating cross-bed sets. Dipmeter representation of IHS sandstone and mudstone bedsets is illustrated in Fig. 6B. The dipmeter log is dominated by consistently dipping, low-angle beds that vary between 3° and 18°. Abrupt changes in dip angle have been interpreted as natural breaks separating stacked accretionary sets in previous dipmeter log studies (Brekke et al., 2017; Brekke and Roenitz, 2021). These sample tadpole plots serve as analogues of typical dipmeter expressions of cross-bedded sandstone and IHS facies. Large deviations between the *pseudo*-dipmeter expression and predicted or typical expressions are investigated for their accuracy and excluded if merited.

Figure 4.6 Sample subsurface dipmeter tadpole data that have been used to calibrate *Pseudo*-dipmeter tadpole logs of the outcrop in this study. **(A)** Dipmeter tadpole log example of the cross-bedded sandstone facies in the McMurray Formation. Note the coexisting measurements of cross-bed (current bedding) and master bedding surfaces (bed boundary) in the cross-bedded sandstone facies. **(B)** Dipmeter tadpole log example of the inclined heterolithic stratified sandstone and mudstone facies. Note that lateral accretion sets can be identified by abrupt change in the dip angle. Abbreviations: Md-mudstone, CB-cross-bedded sandstone, LAS-lateral accretion set.



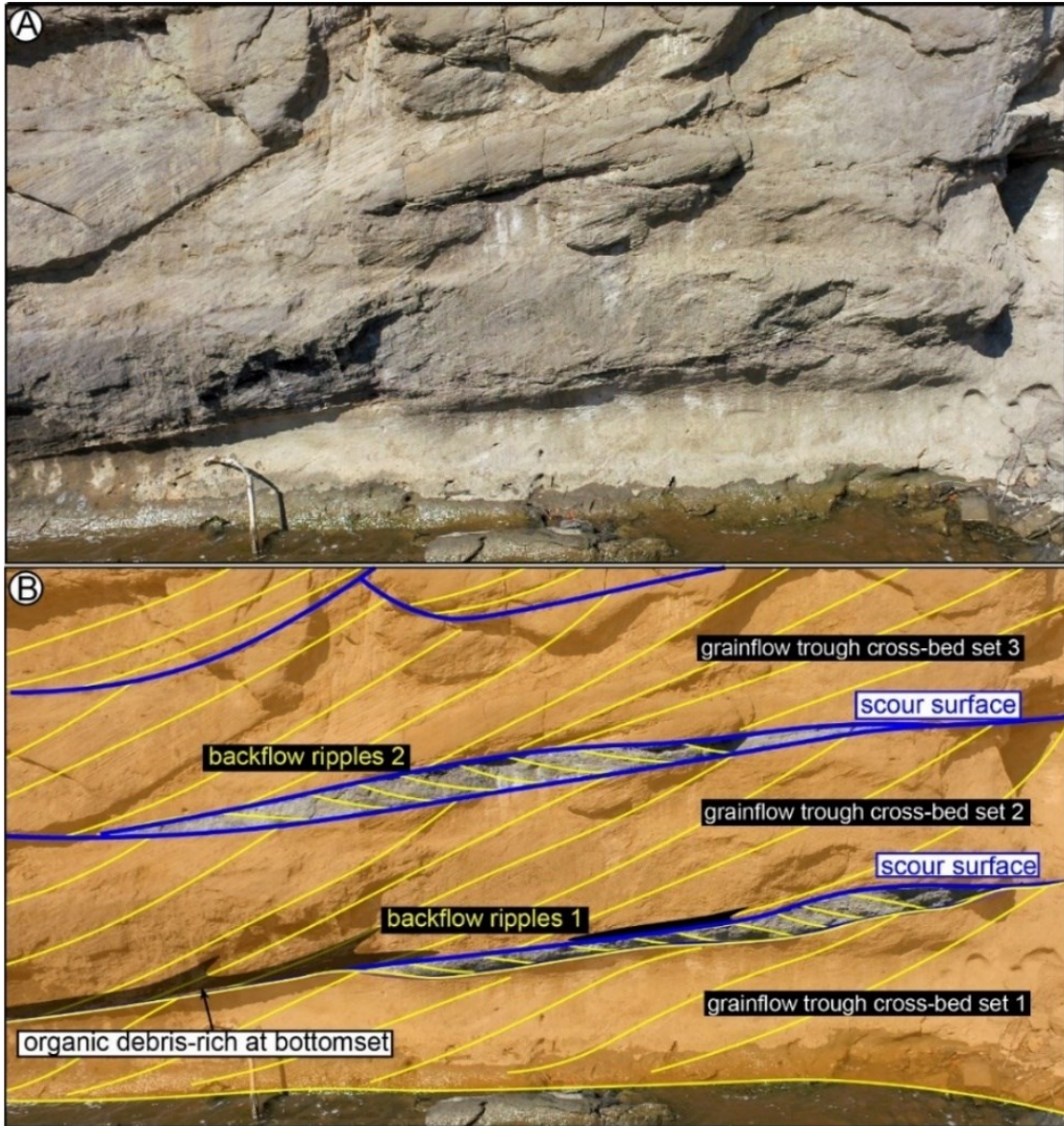
OBSERVATIONS AND INTERPRETATION

Lower Christina River Section

Description

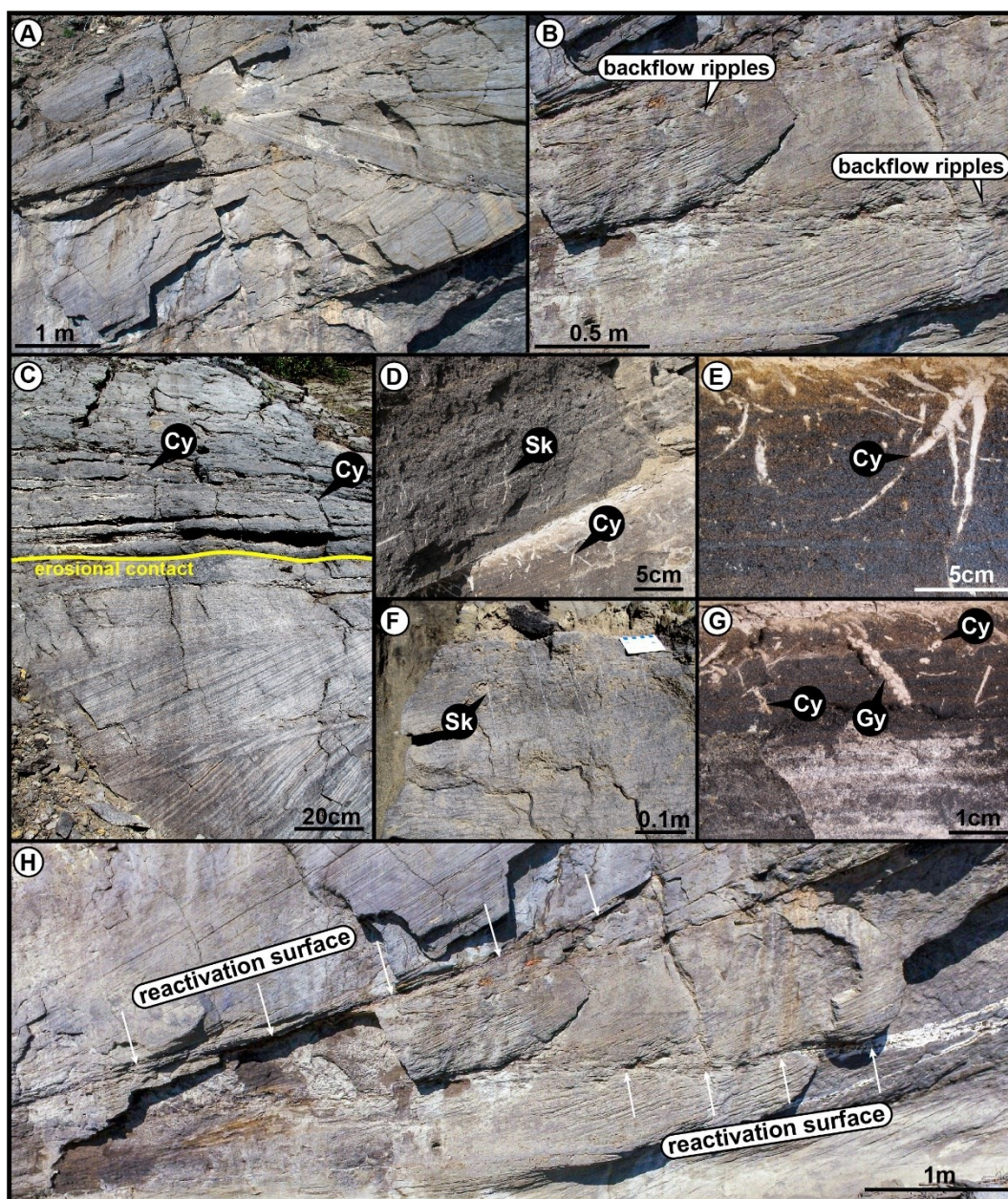
The measured lower Christina River outcrop section is characterized by metre-scale, fine- to lower coarse-grained cross-bedded sandstone. Sedimentary structures are dominated by trough and planar tabular cross stratification (Fig. 7, Fig. 8A, and Fig. 10). The thicknesses of sandstone bedsets range from a few decimetres to up to 3 metres, and their average thicknesses decrease from bottom to top of the succession (Fig. 10B). Locally, adjacent cross beds display divergent dipping directions as shown in Fig. 8A and Fig. 10. Of particular note is that the divergently dipping cross bedsets are generally associated with concave-upward basal bounding surfaces. Centimetre- to decimetre-scale counter-current (backflow) ripples are locally observed at the bases of cross-bed sets, displaying opposite dipping orientations compared to the cross-bed foresets (Fig. 7 and Fig. 8B). The cross-beds are commonly characterized by tangential bases with abundant organic-rich debris (Fig. 7). A sharp contact between this unit and the overlying IHS (Fig. 8A) can be observed locally. Reactivation surfaces are inconsistently arranged in the CB unit without regular spaces, an example is shown in Fig. 8H. Frequency analyses of foreset thickness variations show a single, strong periodic cycle occurs at a period of approximately 56 foresets per cycle, strongly supporting neap-spring diurnal cyclicity (Hayes et al., 2017).

Figure 4.7 Outcrop photo of the cross-bedded sandstone in the lower Christina River section with interpreted cross-beds (yellow lines) and cross-set boundaries (blue lines). **(A)** Uninterpreted **(B)** Interpreted. Note the backflow ripples present at the base of cross-bed sets.



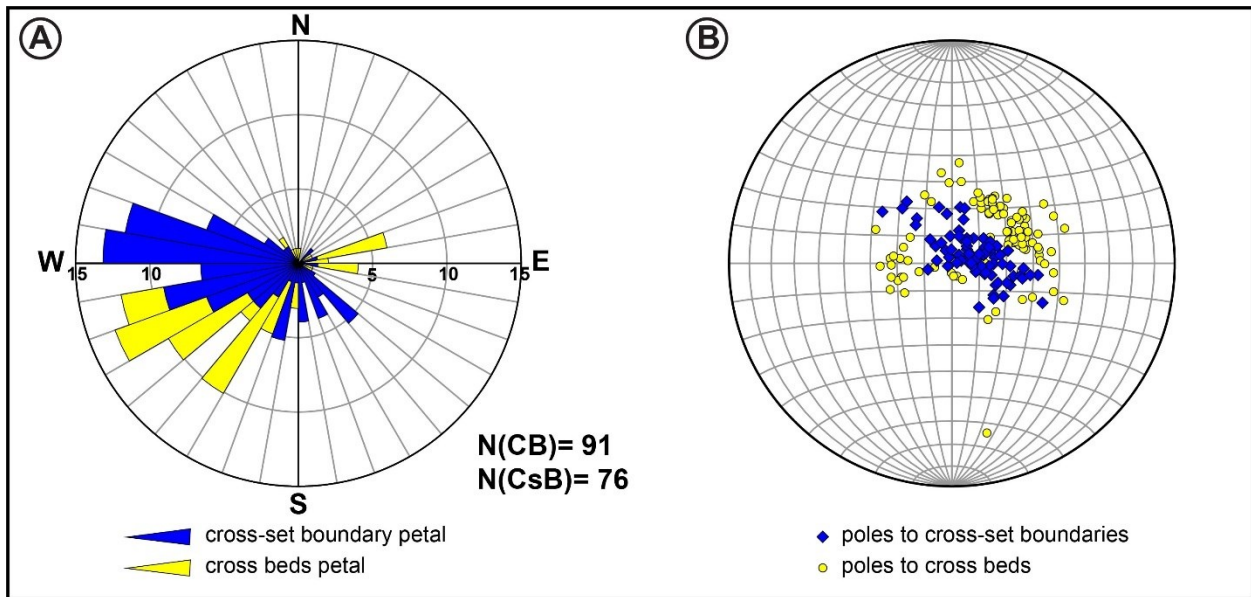
Trace fossils are rare or absent throughout the CB unit. Where present, they are commonly associated with the upper boundary of cross-bed sets (Fig. 8D-G). Overall, the bioturbation intensity observed in this unit is assigned between BI 0 to 1. *Cylindrichnus*, *Skolithos*, *Planolites*, and *Gyrolithes* are observed in descending order of abundance (Fig. 8B-E). In particular, *Skolithos* can be up to 30cm long (Fig. 8D).

Figure 4.8 Detailed outcrop photos of the cross-bedded sandstone in the lower Christina River Outcrop section. **(A)** Trough cross-bedded sandstone showing successive bedsets with some stratification showing divergent dipping orientations. **(B)** Backflow ripples at the base of cross-bed sets. **(C)** Metre-scale cross-bedded sandstone erosionally truncated by a WTNRS and overlain by IHS facies. **(D)** Cross-bedded sandstone facies. *Skolithos* penetrates the sandstone cross-bed sets, and *Cylindrichnus* are commonly associated with the upper bed set boundary. **(E)** Close-up photo of *Cylindrichnus* in cross-bedded sandstone. **(F)** *Skolithos* identified in mudstone laminae of metre-scale cross-bedded sandstone. **(G)** Close-up photo of *Gyrolithes* and *Cylindrichnus*. Trace fossils subtend into the sandstone from the overlying mudstone beds. **(H)** Reactivation surfaces indicated by white arrows. Abbreviations: Cy-*Cylindrichnus*, Sk-*Skolithos*, Gy-*Gyrolithes*



Bedding orientations are collected from cross-set boundaries and cross-beds of this unit using the 3D model. Backflow ripples are not measurable on the photogrammetry models since 1) it is difficult to produce enough markers for such small structures; and 2) there is a general lack of 3D relief in the small cross-laminae of ripples. Dip angle and azimuth of the measured surfaces are represented in *pseudo-dipmeter tadpole logs* (e.g., Fig. 10). Orientational analyses of these data are conducted using rose plots (Fig. 9). In this CB unit, cross beds show unimodal orientations towards the southwest (strongest at 240°), with a minor subordinate set dipping northeastward (approximately 80°) (Fig. 9A). The poles to these cross beds show variable dip angles (majority of data are <40°). The cross-set boundary display slightly variable directional characteristics, which dip strongest at 260°SW to 290°NW, with a subordinate set that dips at 130° SE. Their poles-to-bedding are not as scattered as the cross beds and show dip angles generally <20°. There is a clear oblique relationship between the cross beds and the cross-set boundaries. Some cross-set boundaries identified in the CB unit are laterally continuous whereas some are discontinuous. In this study, a 20m cut-off is used to differentiate them. In Fig. 11B, cross-set boundaries that are laterally correlatable over distances of 20m or more are highlighted in red lines, which are accretionary surfaces dipping in the migration direction of sand dunes. The remaining blue lines (<20m long) are master bedding surfaces separating cross-bed sets. Their dipping azimuths are represented in a separate rose plot on the right side of the diagram. The laterally extensive master-bedding surfaces show strong unimodal characteristics and consistently dip in the NW direction.

Figure 4.9 Rose and poles-to-bedding diagrams of the cross-bedded sandstone facies at Christina River Outcrop section. **(A)** Rose plot for the cross-bedded sandstone facies. Cross-set boundaries (n=62) are represented by blue petals indicating predominant WNW direction. Cross-beds orientations (n=91) are indicated by yellow petals. Note that the bedding measurements are derived from cross-bedded sandstone facies in the lower Christina River and the upper Christina River section. The cross-bedded sandstone facies in both sections are genetically related, they are combined to form CB1 unit. Note that the cross-set boundaries are oblique to subparallel to the orientation of cross-beds. **(B)** Poles-to-bedding of the cross-set boundaries, and cross-beds are represented by blue and yellow dots, respectively.



Interpretation

An interpreted photomosaic section of the lower Christina River outcrop is shown in Fig. 10. Consistently SW-dipping cross beds of the trough cross bedding indicate moderately high energy, unidirectional flow to the SW. Such conditions are commonly associated with channel environments, and the CB unit is interpreted as migrating subaqueous sand dunes. The concave-upward bounding surfaces filled with variably dipping foresets are common expressions of three-dimensional sand dunes (Longhitano et al., 2014). The upward thinning of cross-bed sets and increasing abundance of current ripples suggest a gradual decline in flow energy, which is consistent with the characteristics of fluvial channel, tide-influenced fluvial channel, and tidal-channel deposition. The backflow ripples (Fig. 7 and 8B) are the result of vortex flow in the troughs of large-scale dunes where the near-bed backflow direction is opposite to the dominant current flow (Martinius et al., 2015). Such backflow resulted from flow separation

starting at the brink point of dune summit, with vortex flow generated in the trough area between sand dunes. Although the occurrences of reactivation surfaces are not regularly spaced, Hayes et al. (2017) have quantitatively measured the strong periodic cycles that occurred at periods of 56 foresets in dunes at the same outcrop. Their study strongly supports an interpretation of semi-diurnal synodic deposition at this locale. Based on the above sedimentological characteristics, we interpret the migrating sand dunes were subjected to tidal influences.

Trace fossils (i.e., *Cylindrichnus*, *Skolithos*, *Gyrolithes*, and *Planolites*) identified in this unit are common dwelling burrows made by suspension feeders and indicate minor but extensive brackish-water influences. In particular, *Cylindrichnus*, is a common element of suites assigned to the *Skolithos* ichnofacies and extends into the proximal expression of the *Cruziana* ichnofacies, and is an indicator of marine influence. These normally marine trace fossils are interpreted to be advected by tidal currents into the estuarine locale and thereby are evidence of the presence of tidal currents (Gingras et al., 2016).

The consistently dipping cross beds suggest a SW-oriented dominant and an ENE-oriented subordinate paleocurrent directions. In a tide-influenced fluvial channel environment, the rare ENE-dipping dune-scale cross-beds (as seen in section 4 in Fig. 10B) are interpreted as the result of local occurrence of three-dimensional sand dunes. The laterally extensive cross-set boundaries (red lines in Fig. 11B) form a predominant acute angle (<45°) with the cross beds, and are interpreted as evidence of forward/oblique migration of subaqueous sand dunes. Such subparallel relationships between paleocurrent and sand dune accretion orientation is commonly observed in the tide-dominated estuary compound dunes (Olariu et al., 2012). The cross-set boundaries (blue lines in Fig. 11B) display random orientations that are ascribed to intense scouring and shifting of sand dunes in a dynamic channel. There is also a minor lateral accretion element evidenced by the SE-dipping master bedding subset and the SW-dipping paleocurrent. These are caused by flow separation and lateral drift in three-dimensional tidal dunes (Longhitano et al., 2014). Based on the above interpretations, the CB facies is best interpreted to record two-dimensional (planar tabular cross-stratified sandstone) and three-dimensional (trough cross-stratified sandstone) sand dunes on large sand bars in a tide-dominated estuary environment. Given an inferred northward-facing estuary funnel, the orientation of the cross beds suggests a SW-oriented flood-dominated tidal currents and subordinate NE-oriented ebb currents.

Figure 4.10 Interpreted photomosaics of the lower Christina River outcrop section generated using Metashape 1.7. **(A)** Overview of the lower Christina River outcrop section with locations of measured *pseudo*-dipmeter log sections. **(B)** Interpreted *pseudo*-dipmeter tadpole log section, cross-set boundaries and cross beds were traced on the outcrop model. Open tadpoles represent measurements with low confidence levels.

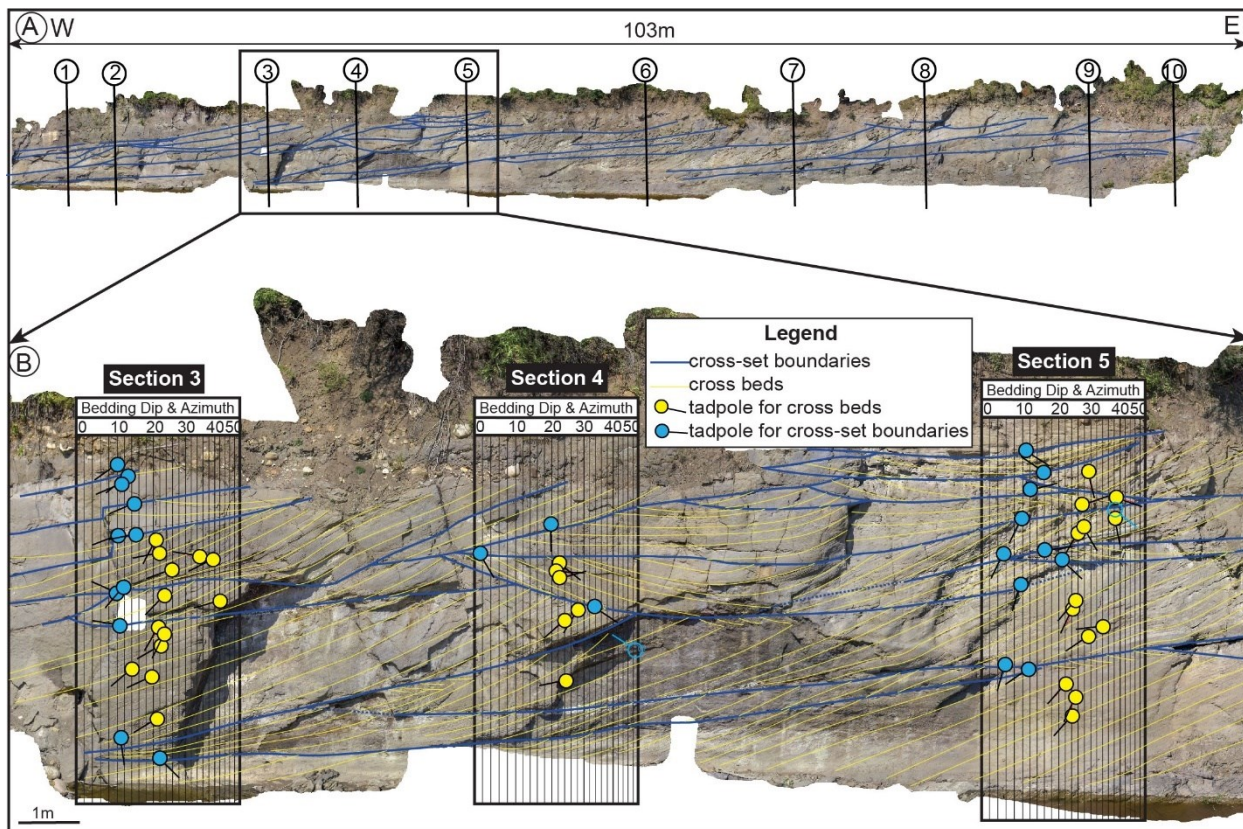
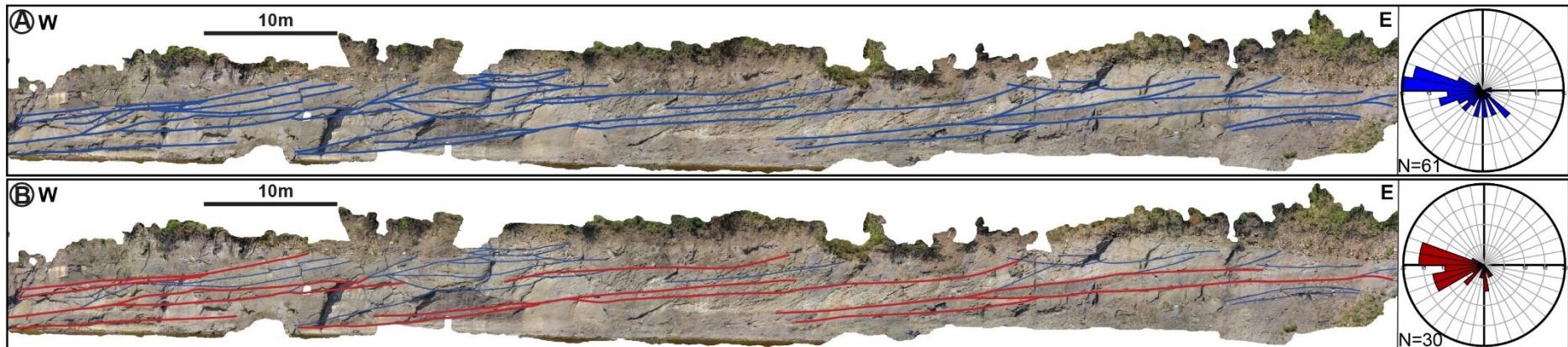


Figure 4.11 Photomosaic of the lower Christina River outcrop section showing interpreted cross-set boundaries and accretionary surfaces. **(A)** Interpreted photogrammetric 3D model of the lower Christina River outcrop model. Blue lines represent cross-set boundaries separating successive cross-bed sets. **(B)** Cross-set boundaries that are correlatable over 20m are highlighted with red lines, which are interpreted as accretionary surfaces in the cross-bedded sandstone facies. The remaining blue surfaces are results of changes in topography or switching direction of sand dunes.



Upper Christina River Section

Description

An overview of the upper Christina River outcrop section is shown in Fig. 12, along with the locations of *pseudo*-dipmeter tadpole logs. The actual data and interpretation of the outcrop are presented in Fig. 15. Two cross-bedded sandstone units (CB1 and 2) and three IHS units (IHS1-3) are identified based on their sedimentary and dipmeter tadpole characteristics. The basal CB unit 1 is associated with the same facies present in the lower Christina River outcrop section to the west, and has similar sedimentary characteristics (i.e., trough to planar tabular cross stratification, backflow ripples, and local organic debris). In the upper Christina River section this unit is approximately 12 metres thick and comprises thickly (metre-scale) to thinly (decimetre-scale) bedded cross-stratified sandstone (Fig. 13 and 17). It is erosionally overlain by IHS unit 1 (see details in Fig. 13A-B). This contact is discernable throughout the outcrop (Fig. 15) and interfingering at the contact is not observed. A thinner cross-bedded sandstone unit (CB2) is observed on top of IHS1, which gradually pinches out to the east. This unit scours across the underlying IHS unit 1, forming an undulatory basal contact (Fig. 13C). The bedsets in CB2 are significantly thinner than those of CB1. Both units (CB1 and CB2) locally show divergent dipping directions of cross-bed sets (Fig. 13 and Fig. 15).

Figure 4.12 Upper McMurray Formation outcrop overview showing the locations of *pseudo*-dipmeter tadpole logs. Interpretations are provided in Fig. 4.15.

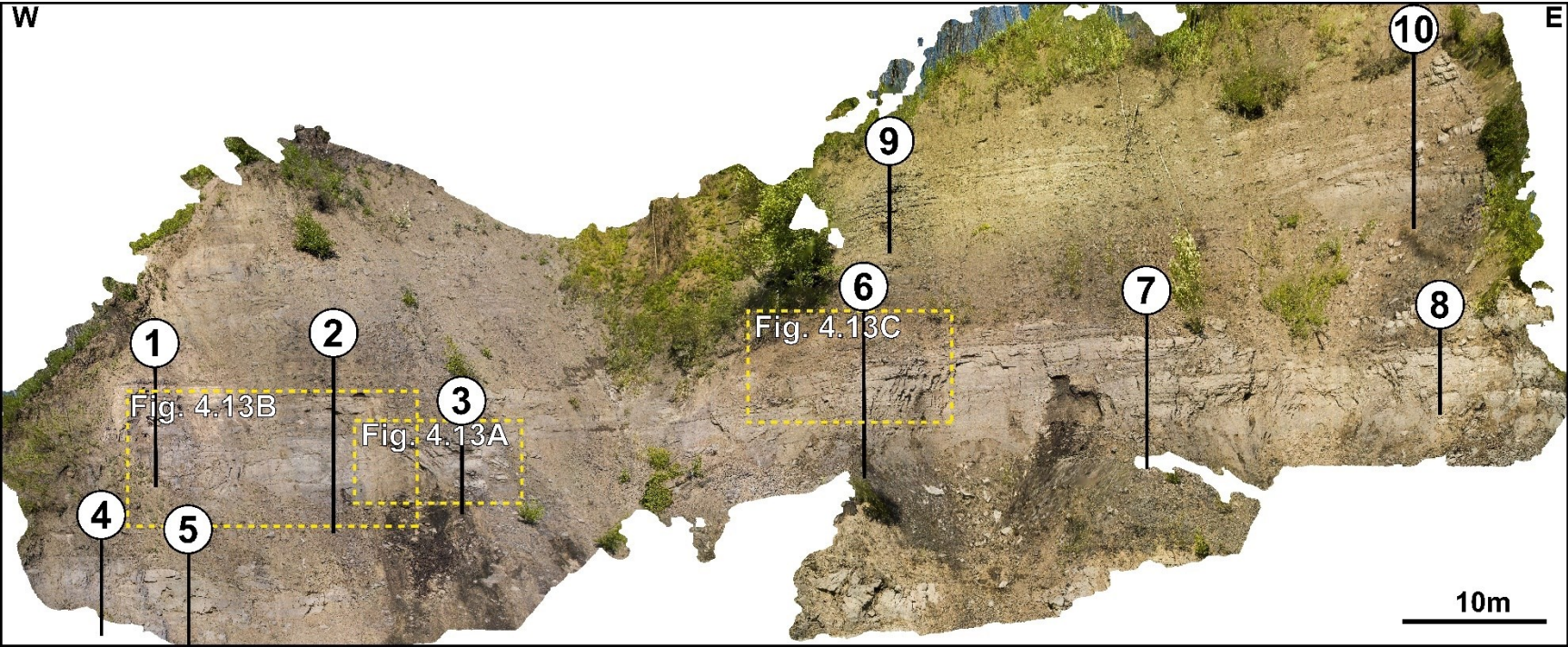
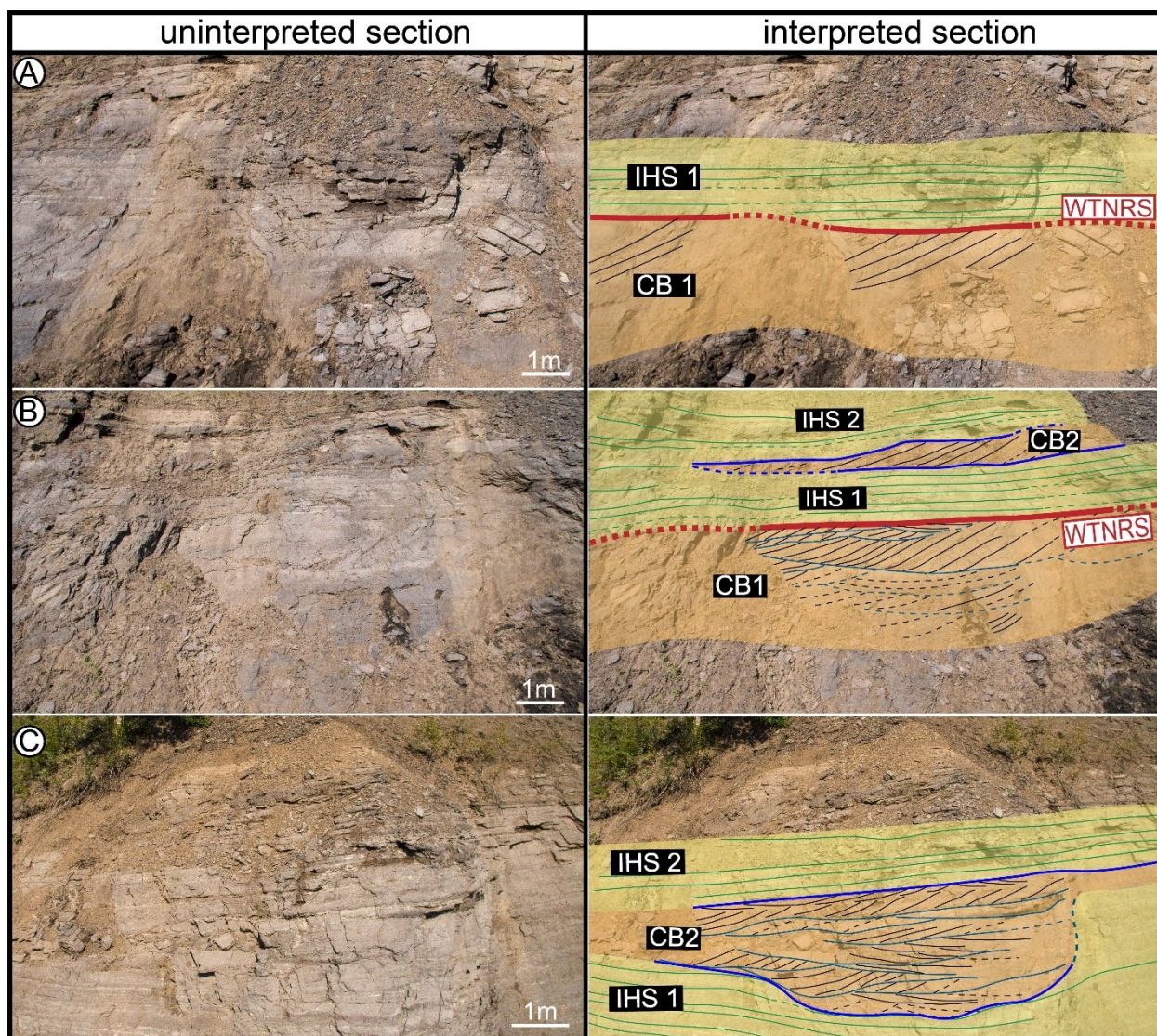


Figure 4.13 Close-up photos of contacts between the different depositional units. **(A)** Sharp contacts are marked with thick blue lines. The sharp contact separating cross-bedded sandstone 1 (CB1) and the overlying IHS1 facies is interpreted as a WTRNS (thick red line). **(B)** The lower CB 1 is not genetically related and is truncated by within-trend normal regressive surface (WTNRS), which separates middle estuary from inner estuary. The overlying IHS1, CB2, and IHS2 units are also in sharp contacts (thick blue lines) with each other, representing stacked lateral accretion sets of a single bar or stacked multiple bars. **(C)** The scour surface (blue line) is locally identified at the base of cross-bedded sandstone 2 (CB2). Locations of the photos are shown in Fig. 12. Abbreviations: CB-cross-bedded sandstone, IHS-inclined heterolithic stratified sandstone and mudstone, WTRNS-within-trend normal regressive surface.



IHS units are characterized by inclined interstratified decimetre- to centimetre-scale sandstone and mudstone beds. Sandstone content in these units varies from approximately 80% in IHS facies to 20% in mudstone-dominated end members (visual estimate). Sandstone and mudstone bed thicknesses gradually decrease upward in each unit. IHS units are sharp based with thickness ranging from 2-10m. Of particular note is the contact between IHS2 and IHS3, which occurs as a steeply dipping erosional discontinuity (Fig. 15B). In each IHS unit, sandstone and mudstone bedding thicknesses generally decrease upward and fall within the range of 10cm to 50cm. No clear difference of bedding thicknesses is observed between the identified units. A planar laminated sandstone and mudstone unit is located in the west end of the outcrop (Fig. 15A), which gradually transitions eastward into adjacent IHS2 unit.

Trace fossils identified in CB units are similar to those of the lower Christina River outcrop, consisting of rare numbers of *Cylindrichnus* and *Skolithos*. IHS units are characterized by *Cylindrichnus* - *Planolites* - *Teichichnus* associations. Trace fossils are generally diminutive size, and bioturbation intensities increase upward in each IHS unit.

Bedding orientations of different units (cross-bedded sandstone 1-2, IHS1-3) are summarized in Table 1. Synthesized rose diagrams and poles-to-bedding plots of all IHS units are presented in Fig. 14. The *pseudo*-dipmeter tadpole log (section 1-10 in Fig. 15) of the CB sandstone facies is dominated by disorganized, low- to high-angle tadpoles (2-40°). Measurements from a single cross-bed set show consistent dipping orientations. Cross beds of the CB1 unit at the upper Christina River section dip predominantly to the WSW (Fig. 15A). The cross beds of the CB2 unit are slightly more variable with dipping orientation ranging from SW to NW directions. Cross-set boundaries of the CB2 are dominated by NW-oriented direction, with a subordinate dataset oriented in the SW direction. Tadpole plots of IHS units display a dominance of low-angle dipping beds varying between 0° and 30°. After plotting the orientation data separately with respect to each unit, the following characteristics are observed: 1) all IHS units share a similar NNW-oriented dip direction; and 2) all cross-bedded sandstone packages indicate consistently WSW-dipping cross beds and NW- or SE-dipping cross-set boundaries.

Figure 4.14 Synthesized rose diagrams and poles-to-bedding diagrams of the cross-bedded sandstone packages and LASs in IHS packages at upper Christina River outcrop section. **(A)** Rose diagram of lateral accretion surfaces (LASs) in IHS facies. Lateral accretionary surfaces (n=84) are represented by green petals, indicating a NW direction. The orthogonal relationship between LAS and paleocurrent direction indicate the inferred paleocurrent direction is oriented SW or NE (approximately 50°NW or 230°SW, indicated by orange arrow). Note that bedding measurements are derived from all IHS units (1-3). Plots for individual depositional packages are summarized in Table 1. **(B)** Poles-to-bedding measurements for lateral accretion surfaces (LASs) of IHS units are represented by green dots.

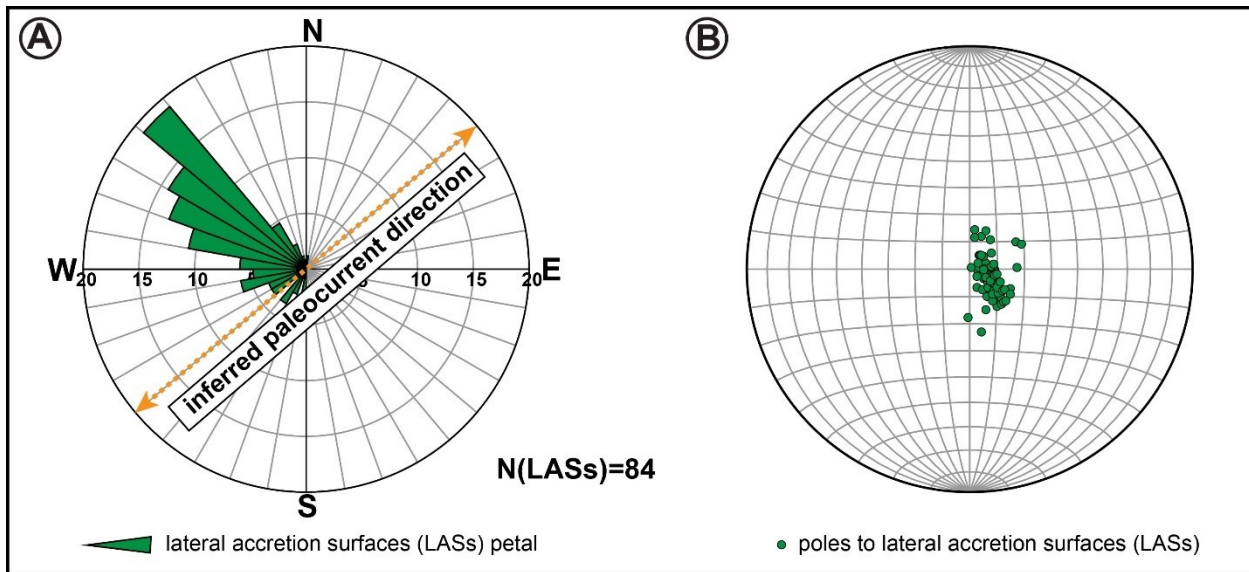


Table 4.1 Summary of the measured beddings and surfaces of the sedimentary packages identified from the lower and upper Christina River outcrop sections. In the rose plots, cross-beds and master bedding planes of the cross-bedded sandstone packages are represented by yellow and blue petals. IHS bedding surfaces of the sand-dominated IHS packages are represented by green petals.

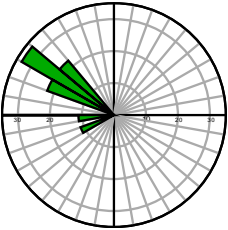
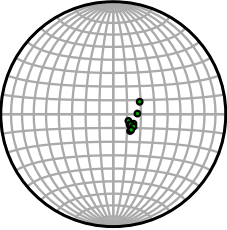
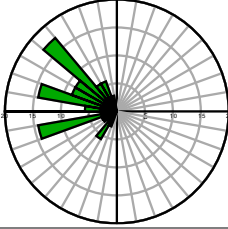
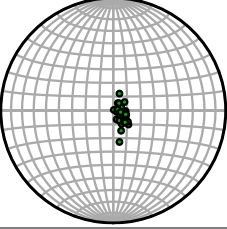
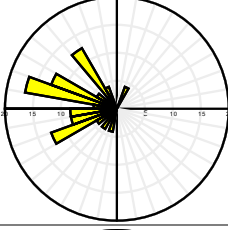
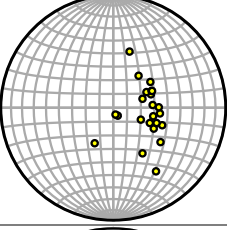
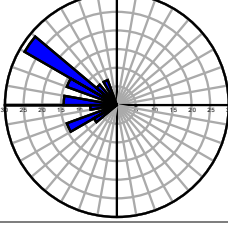
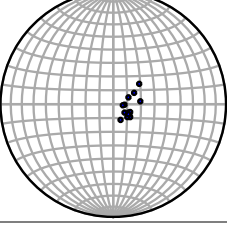
depositional packages	measured surfaces	n	rose diagram representation	poles-to-beddings	bedding characteristics	interpretation
IHS 3	LASs	9			<ul style="list-style-type: none"> • predominantly NW dipping lateral accretion surfaces in IHS 3 • low-angle dipping beds (0°-9°) • suggest SW/NE-oriented paleocurrents 	<ul style="list-style-type: none"> • gently dipping lateral accretion surfaces in IHS are consistent with laterally accreted point bars
IHS 2	LASs	35			<ul style="list-style-type: none"> • lateral accretion surfaces predominantly dip in a SW- to NW-oriented direction • low-angle dipping beds (0°-8°) • suggest SW/NE to NW/SE oriented paleocurrents 	<ul style="list-style-type: none"> • gently dipping lateral accretion surfaces in IHS are consistent with laterally accreted point bars
cross-bedded sandstone 2 (CB 2)	cross-beds (CB)	24			<ul style="list-style-type: none"> • variable cross-beds orientations range from NW to SW directions • cross-beds have variable dipping angles of less than 35° 	<ul style="list-style-type: none"> • westward sediment transport direction • indicates unidirectional current in fluvial dominated channel system
	Cross-set boundaries (CsB)	14			<ul style="list-style-type: none"> • predominantly NW dipping cross-set boundaries with subordinate dataset showing variable directions between SW to NW • low-angle dipping cross-set boundaries (0°-20°) • the cross-set boundaries are oblique/orthogonal to paleocurrent directions 	<ul style="list-style-type: none"> • indicate oblique/lateral accretion of sand dunes of estuary point bar deposit.

Table 4.1. (continued)

IHS 1	LASs	40			<ul style="list-style-type: none"> • predominantly NW dipping LASs • gently dipping angles of IHS bedding planes (0°-13°) • inferred paleocurrent direction is orthogonal to lateral accretion surfaces of IHS, dipping in the NE or SW direction 	<ul style="list-style-type: none"> • gently dipping lateral accretion surfaces in IHS is consistent with laterally accreted point bars
cross-bedded sandstone 1 (CB 1)	cross-beds (CB)	91			<ul style="list-style-type: none"> • dominantly SW dipping cross-beds, subordinate dataset dipping in the NW direction • low- to moderate-angle dipping beds (2°-40°) 	<ul style="list-style-type: none"> • sediment transport direction predominantly to the SW • commonly observed in migrating sand dunes associated with flood-dominated estuaries, minor ebb currents are oriented NW.
	Cross-set boundaries (CsB)	62			<ul style="list-style-type: none"> • cross-set boundaries predominantly dip in the W direction • low to moderate angle dips of cross-set boundaries (0°-30°) • oblique relationship between cross-set boundaries and cross bed orientations in the CB1 unit 	<ul style="list-style-type: none"> • The oblique relationship between paleocurrents and cross-set boundaries is interpreted as forward/oblique accretion of sand dunes.

Interpretation

The tidal sand dunes interpretation of the CB1 unit also applies to the same facies in the upper Christina River section. The divergent dipping beds (represented in tadpole plots in Fig. 15A) result from randomly stacked, variably oriented, sand dunes. The upward thinning of cross-bed sets indicates a decrease in flow energy, which conforms to a channel interpretation. Locally preserved backflow ripples are commonly present in the troughs of sand dunes, owing to flow separation over the bedform's crest.

IHS units are characterized by alternations between sandstone and mudstone beds, indicating deposition of seasonal and/or episodic events. Sandstone beds are deposited during high fluvial discharge, whereas mudstone beds represent deposition during sustained base flow periods influenced by tidal currents (Ranger and Pemberton, 1992; Sisulak and Dashtgard, 2012; Johnson and Dashtgard, 2014). Sharp contacts between the depositional units potentially indicate they are possibly deposits formed by genetically unrelated channels. In a tide-influenced fluvial channel context, these units may represent different point bar deposits or successive point-bar stories that occurred in one single bar form (Crerar and Arnott, 2007). The consistent range of bedding thicknesses in all IHS units suggest similar hydrodynamic conditions (i.e., similar tidal and fluvial intensity). The planar laminated sandstone and mudstone unit is interpreted as mixed tidal flat deposits that commonly flank the meander channels.

The ichnological characteristics indicate the presence of brackish-water and potentially tidal currents, which is based on the low diversity and diminutive size of trace fossil assemblages. Bioturbation intensity does increase upwards in each unit; an observation that implies reduction in sedimentation rates as the bar shoals, and that shoaling occurs at the metre scale, which is consistent with smaller channels (e.g., the reported observed IHS sets are 3 to 8m thick).

Bedding orientations of cross beds in CB1 unit suggest a uniform paleocurrent that flowed to the WSW (Table 1). Cross-set boundaries in this unit display dominantly WNW- oriented orientation, suggesting oblique/forward accretion of the tidal compound dunes. The relationships between cross beds and cross-set boundaries of the CB2 have both oblique and orthogonal components, which imply laterally, and forward accreted subaqueous sand dunes associated with tide-influenced fluvial channel belts. Since the IHS units have been interpreted as point-deposit of these fluvio-tidal meander belts in the previous section, the paleocurrent direction inferred from this facies is parallel to the strike of these lateral accreted

units. These IHS-inferred paleocurrent directions parallel those derived from CB2 unit (Fig. 14 and Table. 1), suggesting two interpretations: 1) all depositional units are genetically related; or 2) multiple channel events shared similar flow directions over time.

Figure 4.15 Interpreted photogrammetric outcrop model of the upper Christina River section with *pseudo*-dipmeter tadpole plots. Major surfaces are traced throughout the outcrop, including contacts between depositional units, and cross-beds and cross-set boundaries within cross-bedded sandstone facies and IHS facies. The inferred contacts are represented by dashed lines. **(A)** Interpreted left section of the upper Christina River outcrop. The basal section is dominated by thick cross-bedded sandstone facies showing stacked cross-bed sets recording tidal sand dunes. This facies is in abrupt erosional contact with the overlying sand-dominated IHS, interpreted as a within-trend normal regressive surface (WTNFS). **(B)** The interpreted right section of the upper Christina River section. Cross-bedded sandstone packages (CB 1-2) and IHS sandstone and mudstone packages (IHS 1-3) are identified in Fig. 15B. Note that the thin cross-bedded sandstone package 2 gradually pinches out within the IHS facies. Tadpole representations: blue=cross-set boundaries in CB units, yellow=cross-beds in CB units, green=lateral accretion surfaces (LASs) in IHS facies. (next page)

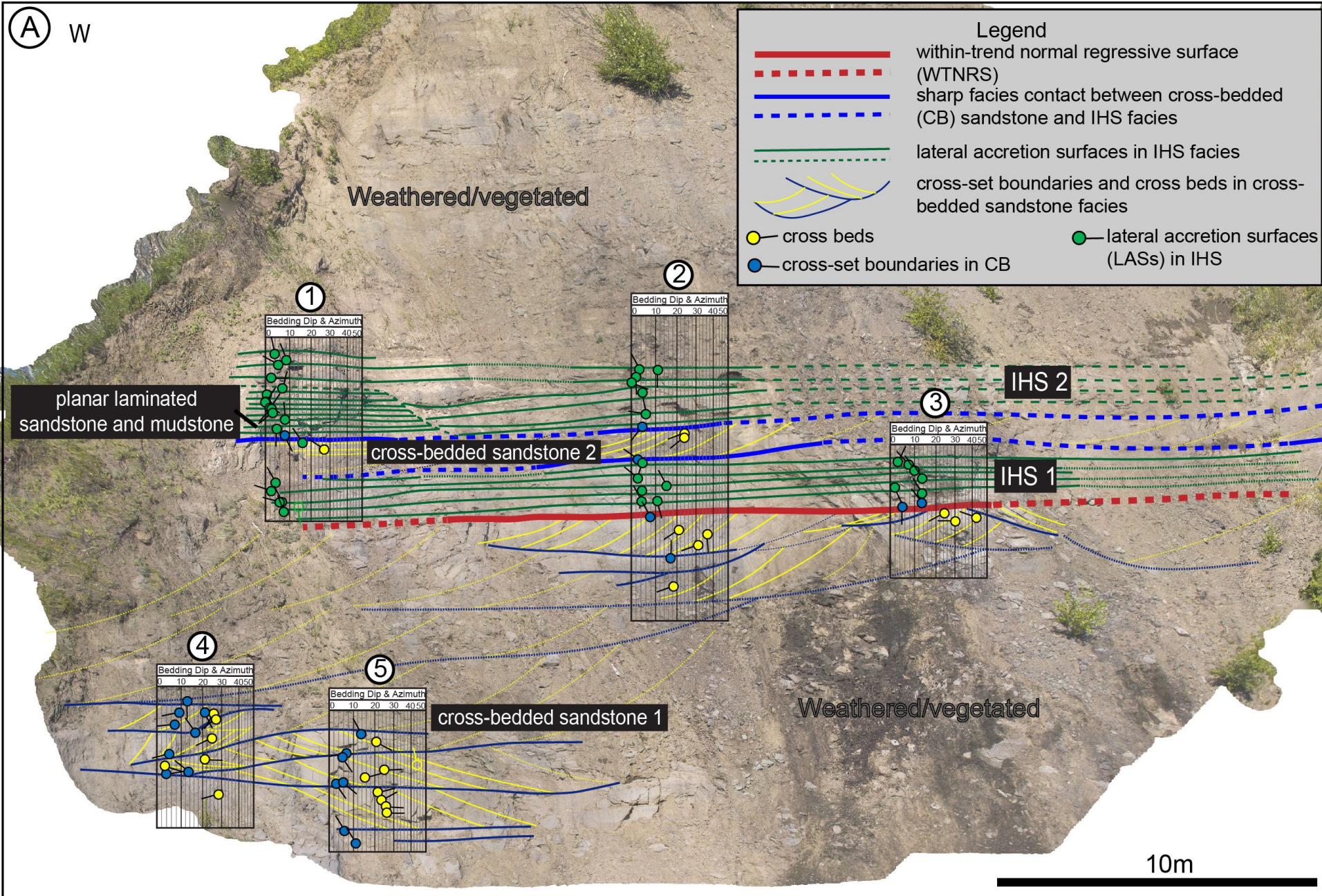
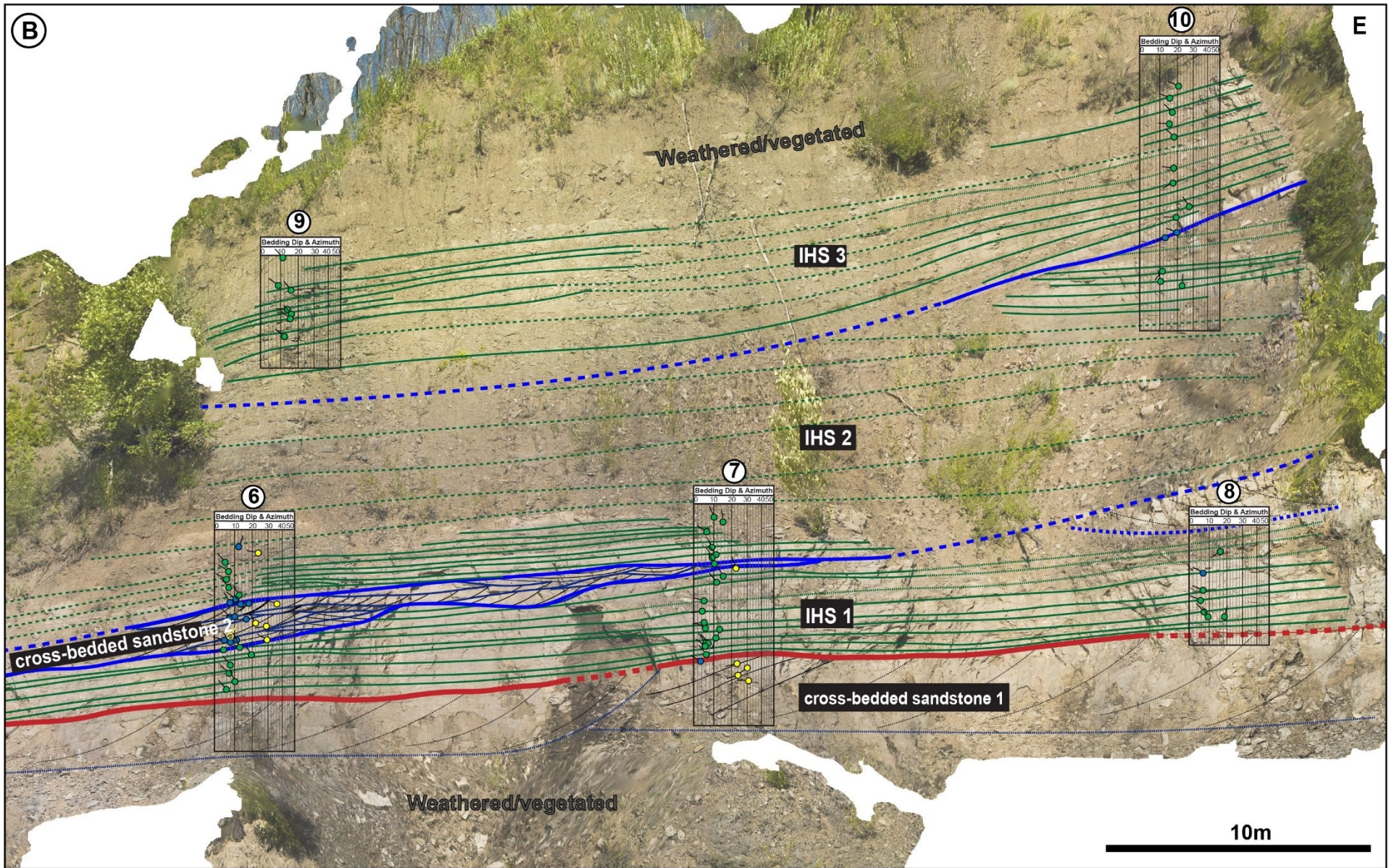


Fig. 4.15. (B) continued from the Figure.15A.



Depositional Environment Interpretation

The extensive presence of brackish-water trace fossils in both the lower and upper sections of the study area precludes a purely fluvial depositional setting. This interpretation is supported by the depositional periodicity of dune foresets at the lower Christina River section (Martinius et al., 2015). Hayes *et al.* (2017) took this a step further by using photogrammetric methods to evaluate the cross stratification. A quantitative measurement of tidal cyclicity was established. Strong periodic cycles occur at periods of approximately 56 and 33 foresets in dunes, strongly supporting an interpretation of semidiurnal synodic deposition at this locale. As such, the tidal sand dunes represented by the lower Christina River outcrop likely represent large-scale bars deposited in the middle estuary. The overlying stacked channel fills (IHS1, CB2, IHS2, IHS3) of the upper Christina River outcrop section represent point bar deposits of meander belts of tidal-fluvial channels. Similar trends of bedding thicknesses and ichnological characteristics in all IHS units also suggest a persistent depositional periods of lateral and downstream migration of channel belts.

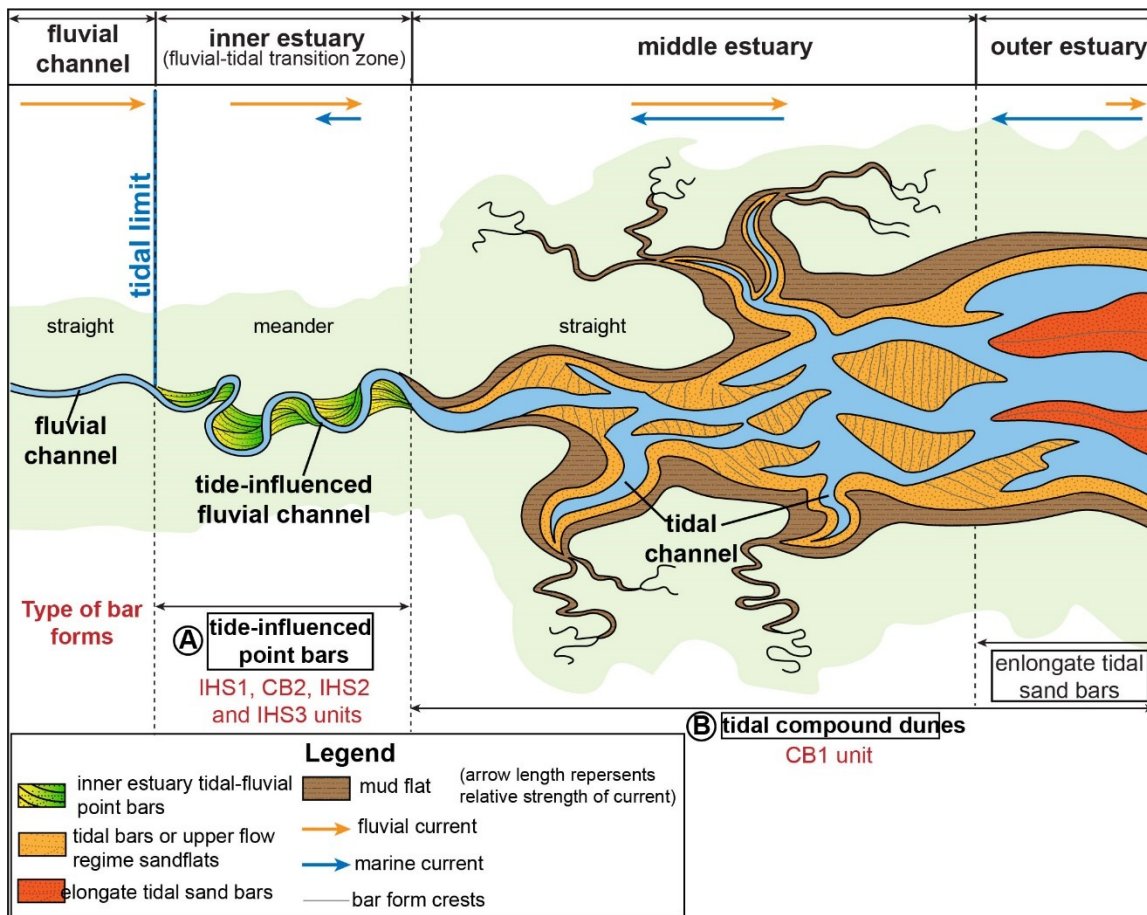
DISCUSSION

Depositional environments and processes in a tide-dominated estuary

The recognition of ancient tide-dominated estuary and deltaic deposits can be difficult. This is owing to the complicated interaction between terrestrial and marine processes in the fluvial-to-marine transition zone. The evolutionary history of the McMurray Formation can be divided into episodic 4th order sea-level fluctuation cycles during the overall 3rd order transgression of Boreal Sea (Carrigy, 1959; Flach and Mossop, 1985). Therefore, both transgressive and progradational successions are present in variable stratigraphic hierarchies based on sequential changes in the facies patterns. For simplicity, the schematic framework for a tide-dominated estuary defined by Dalrymple et al., (2007) is adopted for detailed depositional environment interpretation in this study, and a schematic diagram showing the distribution of environments is modified from their

model and shown in Fig. 16. Indeed, as is noted later in this study, progradational successions results from 4th order sea-level fluctuation also occur during the overall transgression. Using this schematic tide-dominated estuary model, the fluvial-marine transition zone can be subdivided into four sections in a seaward direction (Fig. 16): 1) a fluvial section with no recognizable tidal structures, 2) an inner estuary section (all termed fluvial-tidal transition zone) situated seaward of the tidal limit, 3) a middle estuary section expands the area that is dominated by mixed fluvial and tidal currents, and 4) a seaward most outer estuary section that is constantly reworked by strong tidal currents and waves. The observed depositional units observed at the Christina River outcrop are interpreted to represent two dominant types of bar forms in a tide-dominated estuary system: 1) tide-influenced fluvial point bars associated with relatively narrow and more sinuous channels in a fluvial-tidal transition section of tidal systems (i.e., IHS1, CB2, IHS2, and IHS3 units); and 2) simple or compound dunes associated with tidal channel thalweg deposits in the middle estuary setting (i.e., CB1 unit). The dominant processes and architectural characteristics of these bar forms are summarized below.

Figure 4.16 Schematic diagram of tide-dominated estuary setting. Tide-influenced fluvial meander belts are deposited in the inner estuary section, which correspond to stacked IHS1, CB2, IHS2 and IHS3 units. Tidal compound dunes associated with tidal channel thalweg deposits are accumulated in the middle estuary section, which correspond to CB1 unit.



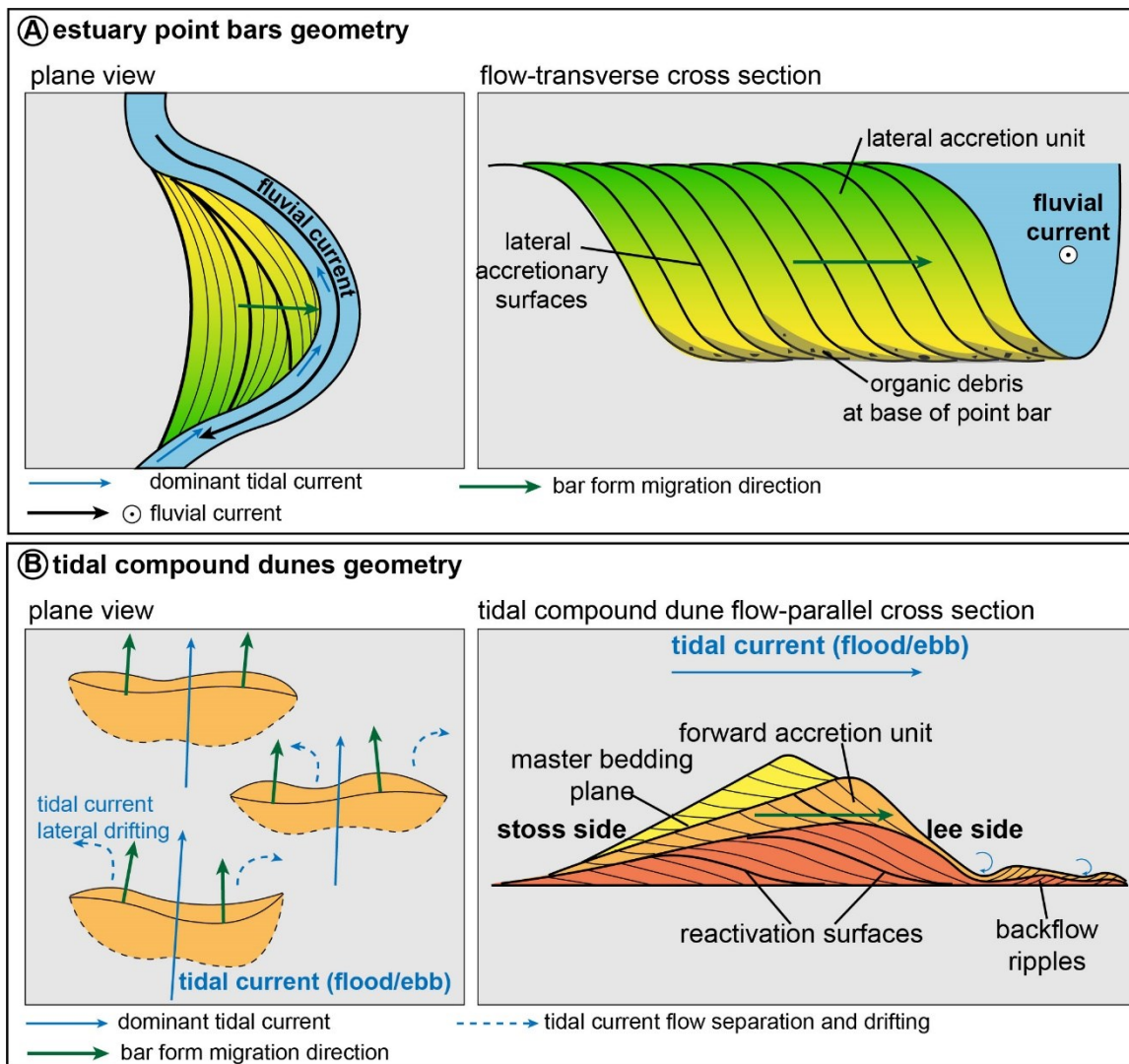
Depositional processes and architectural characteristics of tide-influenced fluvial point bars

Tide-influenced fluvial point bars are accumulated in the tightly meandering portion of the channel that coincide with the inner estuary section or fluvial-tidal transition zone (Dalrymple and Choi, 2007). This section is dominated by strong unidirectional seaward transport of sediments, which is attributed to river-dominated water flow. In general, fresh water dominates most of the section and brackish-water conditions may prevail as the channel widens in seaward direction. Tidal modulation is preserved in sediments as tidal rhythmites, mud drapes, tidal bundles, and local reverse flow structures (e.g., herringbone cross bedding) (Dalrymple and Choi, 2007).

Lateral-accretion deposits is generated by these tide-influenced fluvial point bars and their internal architecture are shown in the theoretical geometry diagram in Fig. 17A. In general, lateral accretion surfaces of the IHS units dip oblique to normal to the flow direction in the channels near the thalweg. Subaqueous sand dunes at the lower point bar tend to migrate along the bend, and sediment transport direction can be uniform or random depending on the variable degrees of influence of tidal currents. In the McMurray Formation example, previous seismic studies have successfully interpreted the complexly stacked, laterally migrated meander belts of the McMurray Formation near the town of Fort McMurray based on the morphological characteristics and abundant lateral-accretion surfaces dipping towards adjacent channel thalweg (Hubbard et al., 2011; Labrecque et al., 2011; Fustic et al., 2012; Durkin et al., 2017a; Hagstrom et al., 2019).

The stacked CB2 and IHS units observed at the Christina River outcrop are consistent with these laterally accreted point bar deposits. First of all, paleocurrent data (measured in CB2 unit) displays strong unidirectional transport direction that is commonly observed in a fluvial-dominated current region. The slight variation of paleocurrent (i.e., cross beds dip in a range from SW to NW in CB2 unit) supports the interpretation of minor tidal current influences. In cases with channels are significantly curved, the sediment transport direction can be more random than those in less curved channels due to variable migration style that can occur in such environment. Importantly, the presence of persistent bioturbation suggests a somewhat more seaward position or an overall reduction in fluvial influence.

Figure 4.17 The morphological and architectural characteristics of **(A)** tide-influenced fluvial channel point bars and **(B)** tidal compound dunes. See the occurrences of the two types of bar forms in Fig. 4.16.



Depositional processes and architectural characteristics of tidal compound dunes

Tidal compound dunes (or previously called tidal sand waves) are a common feature in most sandy inshore and continental shelf environments (Dalrymple, 2010). They are commonly associated with tidal channels in a middle estuary setting (refer to Fig. 16 for their geographic locations in a tide-dominated estuary setting). In such setting, these tidal compound dunes share similar lithological and ichnological characteristics, and have overlapping bedset thicknesses with the tide-influenced fluvial point bars in the inner estuary section. The differentiation between the

two types of depositional architectures relies on their distinct internal bedding characteristics of CB sand bodies. As shown in Fig. 17B, tidal compound dunes show cross-set boundaries that lie subparallel to paleocurrent direction, recording dunes migrating along down-dip surfaces. The occurrences of these forward accreted tidal compound dunes have been recognized in ancient and modern estuary settings (Dalrymple, 1984; Dalrymple et al., 1990; Olariu et al., 2012; Longhitano et al., 2014; Choi and Jo, 2015; Jo and Choi, 2016; Hayes et al., 2018). In a tide-dominated estuary, tidal compound dunes are subjected to seaward decrease of fluvial currents and increase of tidal currents.

The CB1 unit identified at the Christina River outcrop shows a clear bipolar paleocurrent directions (Fig. 9): a dominant SW-oriented paleocurrent and a subordinate NE-oriented paleocurrent. In a tide-dominated estuary setting that is characterized by mutually evasively evasive channels, CB1 can be interpreted as deposit of a flood-dominated channel with minor influences from ebb-oriented tidal current in adjacent channel. Given an inferred northward-facing estuary funnel, the CB1 unit represents tidal compound dunes developed on bars of a flood-dominated channel at this outcrop locale. As such, the subordinate NE-oriented paleocurrents are interpreted as deposits from ebb-oriented tidal currents.

Stratigraphic implications

Based on the previous depositional environment interpretations, the laterally extensive sharp contact between CB1 and overlying IHS units represents the erosional base of a tide-influenced fluvial channel, which correspond to an autogenic erosion surface (Château et al., 2019). The inner estuary point bar deposits were shifted seaward over top of the middle estuary tidal compound dunes, forming a within-trend normal regressive surface (WTNRS) (Catuneanu, 2006). The recognition of the WTNRS is based on the juxtaposition of inner estuary point bar deposits over middle estuary tidal sand bar deposits in the McMurray Formation. Similar sharp contact (between CB1 and overlying IHS units) has also been observed at the Amphitheatre and Steepbank outcrops by Hayes *et al.* (2018). Rose plots of CB2 (Table 1) show slightly more variable subparallel accretion and paleocurrent direction that range from 240°SW to 330°NW,

which fits one of the two following depositional settings: 1) CB2 is another smaller-scale middle estuary tidal sand dune deposit comparable to CB1; or 2) CB2 is a point bar deposit of the inner estuary meander belt, characterized by oblique to downstream accretion. The latter interpretation is favored in this study because of its much smaller scale compared to CB1, as well as its close proximity with overlying and underlying IHS point bar deposits.

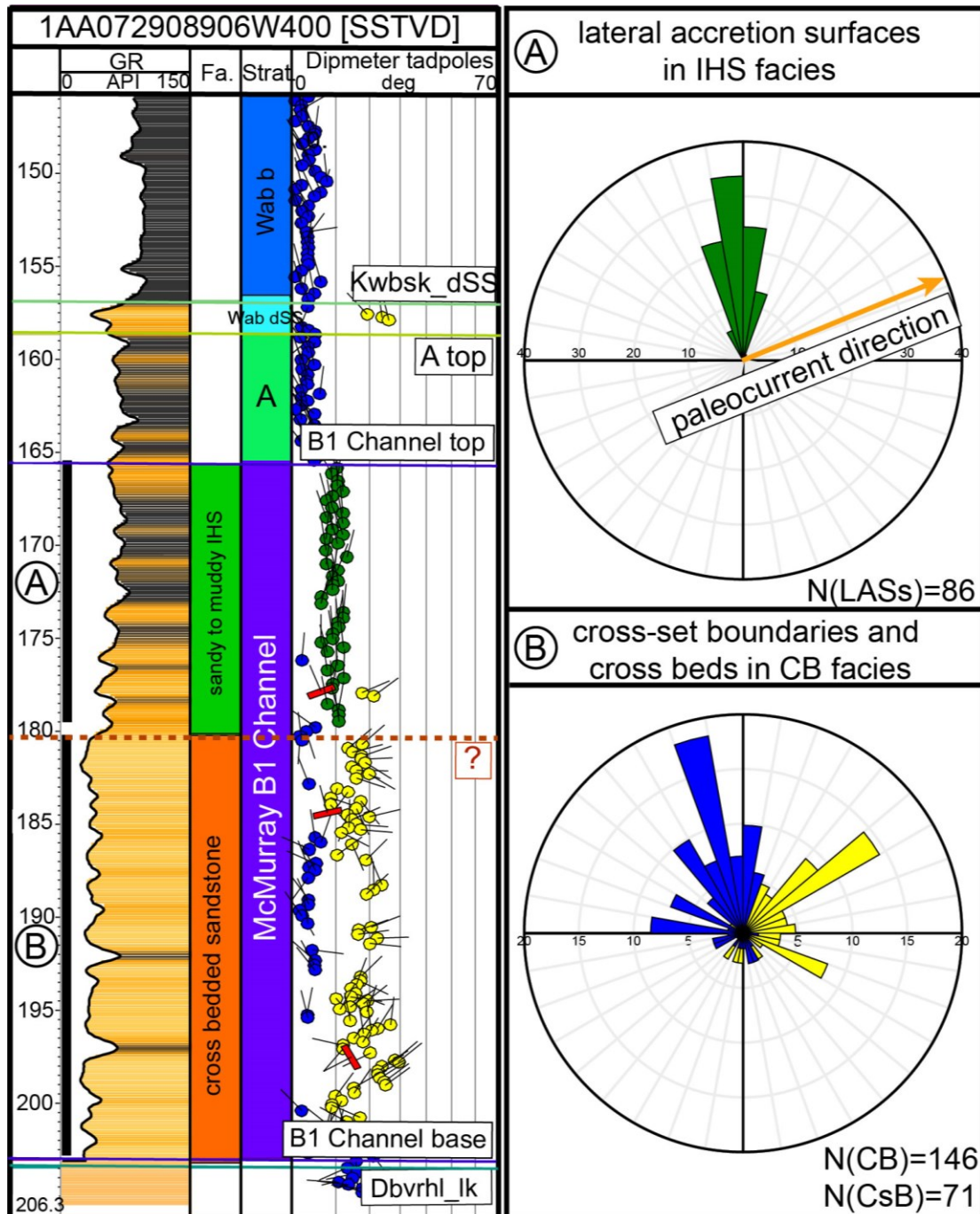
Identification of genetically related depositional packages of point bar deposit in dipmeter tadpole data

In the channel and point bar deposits of the middle McMurray Formation, three lithofacies have been widely identified: 1) thalweg-associated cross-stratified sandstone (CB); 2) bar-related inclined heterolithic stratification (IHS); and 3) gently dipping to horizontal bar-top/tidal-flat deposits. The genetic relationship between the first two lithofacies is key for identification of continuous point bar deposits, which can further assist depositional environment interpretation. In this section, dipmeter tadpole log of a well located one township (10 km) north of the Christina River outcrop are interpreted to demonstrate how bedding orientations are analyzed to indicate genetically related depositional units that represent a continuous point bar deposit. The example in Fig. 18 shows a continuous depositional package, which comprises a basal cross-bedded sandstone unit (CB) overlain by an IHS unit. The basal CB unit is characterized by NE-dipping cross beds (yellow tadpoles) and predominantly NNW-oriented cross-set boundaries (blue tadpoles), which suggest NE-oriented paleocurrent flow direction and lateral accretion of sand dunes (Fig. 18A). The overlying IHS unit is dominated by northward dipping lateral accretionary bedding (green tadpoles), and an ENE-oriented paleocurrent direction is measured at depth 178m that is represented by two yellow tadpoles (Fig. 18B). In this case, the two facies are potentially related based on the following two architectural characteristics: 1) the sediment transport directions measured in the IHS and CB units (yellow tadpoles) yield a consistently NE-oriented paleocurrent; and 2) an uniformly northward accretion directions (i.e., LASs in IHS and cross-set boundaries in CB) are present in both units. As such, the CB unit represents a

sandstone-dominated lower point-bar deposits, and the IHS unit is interpreted as the middle to upper point bar.

The consistently dipping accretion direction of a single point-bar deposit can be effectively used to differentiate genetically unrelated point-bar deposits, examples have been demonstrated in previous studies using dipmeter datasets (Nardin et al., 2010; Brekke et al., 2017; Brekke and Roenitz, 2021; Chen et al., 2021). Units with different accretion directions suggest genetically unrelated depositional packages. Cautions need to be taken when researchers encountering a succession with consistently dipping accretion surfaces or LASs, since they may represent one of the scenarios: a continuous point bar deposition, or stacked point bars that simply share a similar sediment transport direction. If a discontinuity is present within the unit (indiscernible using tadpole and core characteristics), the unit may represent unrelated stacked units. In the case of Christina River outcrop, the tide-influenced fluvial point bar succession demonstrates an example of thick, consistently dipping lateral accretion deposits. Possible depositional models are discussed in detail in later sections.

Figure 4.18 Sample dipmeter log 1 shows that the cross-bedded sandstone is potentially genetically associated with overlying IHS facies. **(A)** Rose plot showing northward-dipping lateral accretion sets (LASs) in IHS facies (green petals). Note that the sediment transport direction in this unit is oriented ENE (orange arrow), which is indicated by yellow tadpoles at depth ~178m. **(B)** Rose plot of cross-set boundaries and cross-beds measured from cross-bedded sandstone facies. Cross-set boundaries are indicated by blue petals. Yellow tadpoles represent cross-beds. Refer to Fig. 6 for tadpole legend.



ARCHITECTURAL MODEL OF POINT BARS AT CHRISTINA RIVER OUTCROP

At other McMurray Formation locations, the CB unit and overlying IHS unit have been interpreted as continuous estuary point bars (Crerar and Arnott, 2007; Hubbard et al., 2011; Fustic et al., 2012; Jablonski, 2012; Musial et al., 2013; Brekke and Roenitz, 2021). However, such an interpretation at the Christina River locale is difficult to reconcile, considering the marked erosional discontinuity (WTNRS) between the CB1 and overlying IHS and CB2 units. The IHS units at the upper Christina River section are similar to the stacked lateral accretionary sets observed at the Steepbank outcrop by Hayes *et al.* (2018) and Jablonski and Dalrymple *et al.* (2016), but they observed only one thick CB unit at the base of their measured succession. As discussed in the previous section, the paleocurrent to cross-set boundaries relationships of CB1 and CB2 are markedly different (Table. 1), which point to them being discrete genetic packages; namely CB1 recording tidal sand dunes of the middle estuary and CB2 corresponding to inner estuary fluvio-tidal point bar lateral accretion. As such, the first genetic package (Genetic Package 1) is recognized below the WTNRS, which is represented by the basal CB1 unit. Its depositional model is represented in Fig. 20.

Above the WTNRS, the bedding orientation measurements of individual units at Christina River suggest two possible depositional interpretations for the stacked IHS and CB2 units: 1) the entire succession comprises a thick, continuous channel deposit, and sharp contacts mark abrupt shifts in migration orientation or changes in the position of the point bar or laterally accreted part of the channel deposit; or 2) the outcrop comprises a cross-bedded sandstone overlain by an unrelated point bar or point bar complex. An interpreted outcrop with bedding orientation data is summarized in Fig. 19.

Previous workers have shown that multistoried lateral accretion IHS successions can be recognized in the IHS facies using sedimentological and dipmeter tadpole characteristics (Muwais and Smith, 1990; Nardin et al., 2013; Brekke et al., 2017; Hayes et al., 2018; Brekke and Roenitz, 2021). In particular, Nardin *et al.* (2013), proposed a stratigraphic hierarchy for the lateral accretion deposits of point bars in the McMurray Formation. Their study at Syncrude's Mildred Lake Mine suggests that a point bar can commonly be subdivided into lateral accretion sets. Each set can be further divided into stories, forming

multiple bedsets. According to their definition, a story includes one or more genetically related and systematically stacked bedsets bounded by surfaces of erosion or discordance. A lateral accretion set contains one or more stacked, genetically related stories bounded by erosional or discordant surfaces. Due to the intense amalgamation of the point bars and extensively weathered outcrop surfaces at Christina River, not all bedsets of the IHS facies are well preserved or exposed. Correspondingly, it is challenging to determine whether the succession represents a continuous point bar consisting of multiple lateral accretion sets or stacked multiple small-scale point bars. As such, both possible end member interpretations are discussed below, and supporting evidence is provided for each scenario. The two architectural depositional models are summarized in Fig. 21A and B.

Figure 4.19 (A) Photogrammetric 3D model of the Christina River outcrop. Dash lines represent inferred interpretations. **(B)** a representative strip log of the measured succession which consists of stacked IHS units that overlies a thick CB unit. Proposed architectural models (S1 and S2) are summarized on the right of the strip log. Abbreviation: CB – cross-bedded sandstone package, IHS – inclined heterolithic stratified sandstone and mudstone packages, LAS - lateral accretion set, PB – point bar.

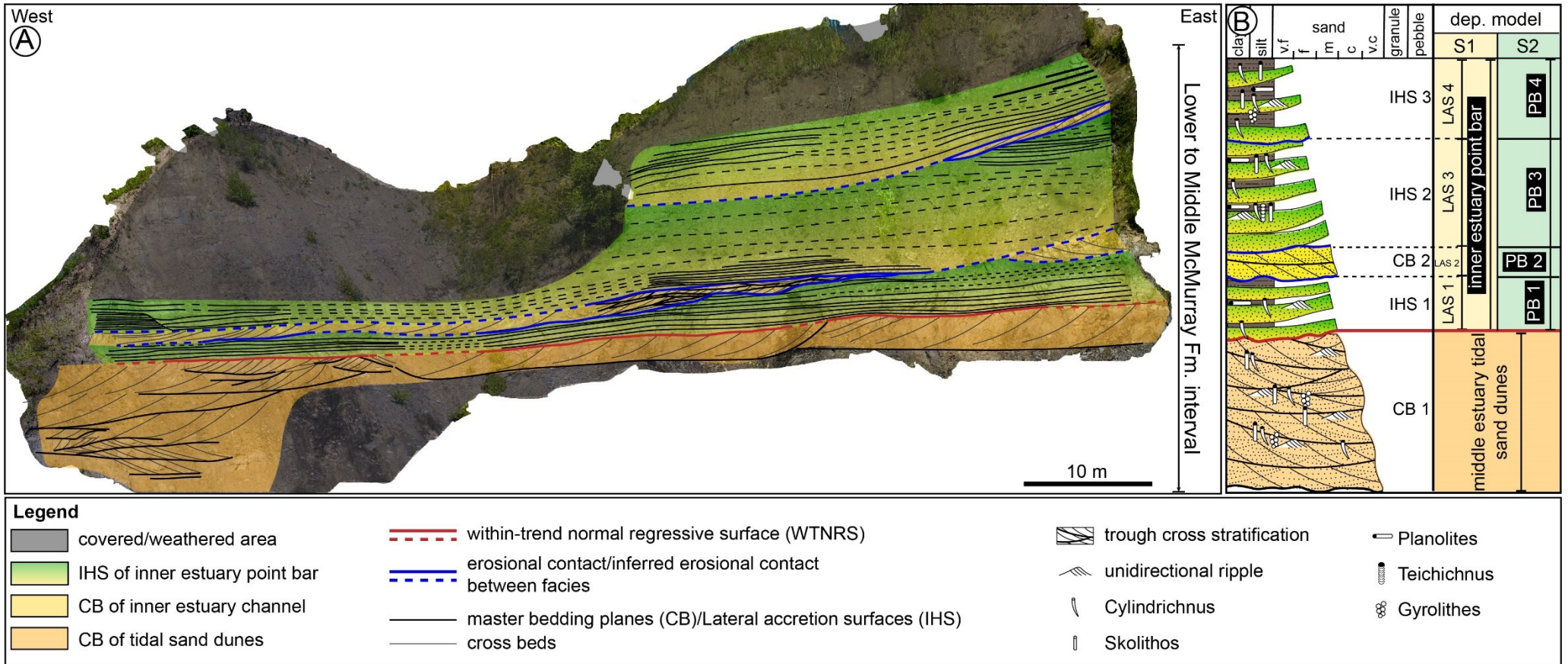
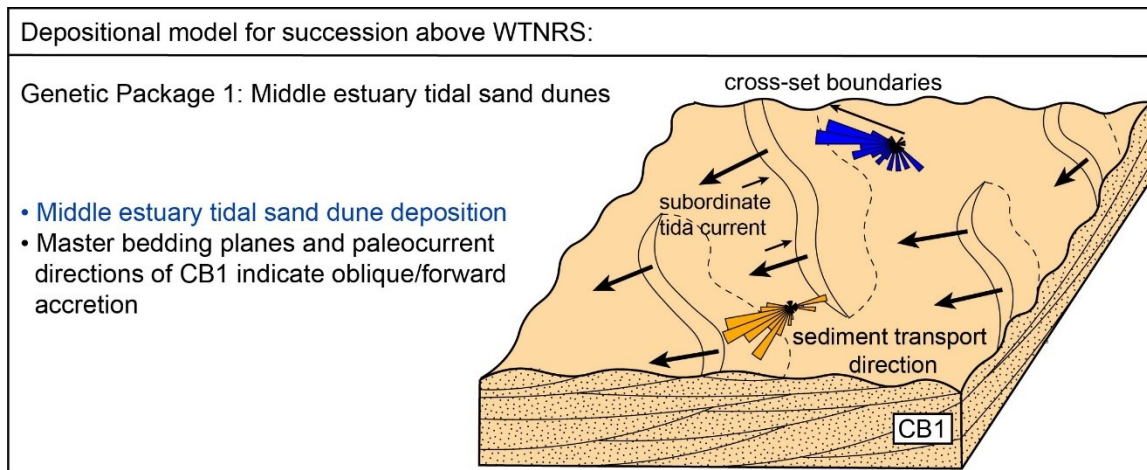


Figure 4.20 Depositional model for genetic package 1 that is below WTNRS. This package is represented by cross-bedded sandstone 1 (CB1) unit. Abbreviations: WTNRS-within-trend normal regressive surface, CB-cross-bedded sandstone.



Single point bar model

The single point bar model has been widely accepted in previous outcrop and subsurface studies (Mossop and Flach, 1983; Hubbard et al., 2011; Musial et al., 2012; Martinius et al., 2015; Jablonski and Dalrymple, 2016) and their interpretations are mainly based on a fining-upward stacking pattern (i.e., IHS overlying cross-bedded sandstone units). The evolutionary history of the single point bar model is illustrated in Fig. 21A. Genetic package 2 is characterized by rotations and shifts in a single meander belt. Based on the bedding orientation analysis, the point bar has shifted four times throughout its depositional history (T1-T4), and each shift is represented by a lateral accretion set (LAS1-4). Each of the IHS1, CB2, IHS2, and IHS3 units characterize a lateral accretion set throughout the point bar deposition as shown in Fig. 21A. This model highlights the following features: 1) lateral accretion sets are separated by internal erosional surfaces, which are interpreted as intra-point-bar erosional surfaces (Durkin et al., 2017a); and 2) the CB facies associated with the point bar is absent in LAS1, LAS3, and LAS4, similar to observations made in the McMurray Formation exposures at the Steepbank outcrop (Hayes et al., 2018). At Steepbank, the boundary separating lateral accretion sets is marked by abrupt shifts in the dipping angles of tadpole plots. As with the Christina River outcrops, each

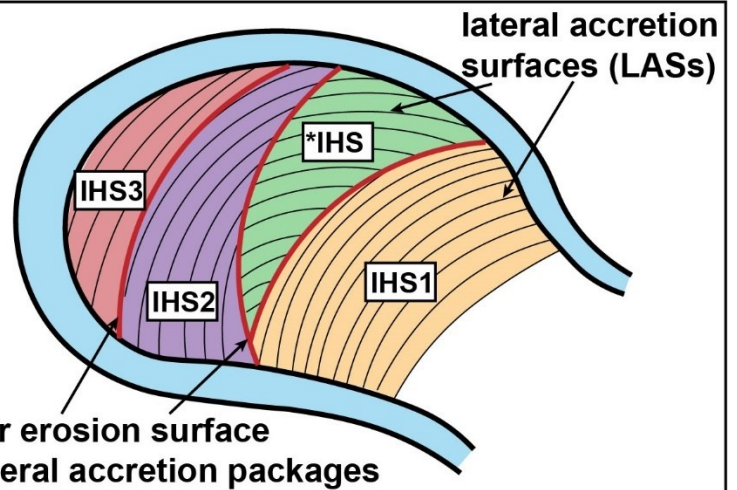
lateral accretion set consists of an overall fining- and thinning-upward succession with upward increasing bioturbation intensities. Depositional breaks between lateral accretion sets are difficult to identify using bedding orientation data. This is due to difficulties in measuring the gently dipping IHS and because many areas of the outcrop are covered. However, erosional contacts demarcating IHS sets are observed across the outcrop.

In the Christina River outcrop example, the thicknesses of these IHS units range from 4m to 13m, which have a similar scale to the lateral accretion sets observed at Syncrude's north pit (5-20m) (Nardin et al., 2013). The total thickness of the stacked IHS units is 25 to 30m, which potentially indicates a large-scale channel setting. In addition, the uniformly dipping lateral accretion beds strongly imply deposition in similar flow directions. That is to say, these packages were possibly deposited within the same channel representing a single inner estuary point bar. The benefit of this model is that it best explains the absence of thalweg-associated cross-bedded sandstones at the base of individual IHS unit. However, there are many sedimentological observations that this model cannot explain: 1) most IHS beds are pervasively bioturbated, which is difficult to explain in a large sedimentologically active fluvial point bar wherein sedimentation rates should exceed sediment colonization rates; 2) each IHS unit repeats a characteristic upward thinning in bedding thicknesses concomitant with an overall increase in bioturbation, which is again inconsistent with the expected pattern for a single, very large, laterally accreting geobody; and 3) sharp and locally scoured basal IHS contacts bracket fining upwards IHS units. Alternatives to the single point bar model are presented below.

Figure 4.21 Schematic diagram of two depositional model scenarios that can explain the succession above WTNRS (IHS1, CB2, IHS2, and IHS3). **A)** Depositional model scenario 1: Genetically related lateral accretion sets (LASs) in a single meander belt. **B)** Depositional model scenario 2: Genetically unrelated estuary point bars model. Note that the *IHS in both models are not preserved at the Christina River outcrops. Abbreviations: WTNRS-within-trend normal regressive surface, IPBES-intra-point-bar erosional surface, CB-cross-bedded sandstone, IHS-inclined heterolithic stratified sandstone and mudstone. Note the schematic diagram is meant to depict stratigraphic evolution and is not to scale. (next page)

A Depositional model Scenario 1 for succession above WTNRS:

- Inner estuary point bar deposition
- Genetically related LASs in a single inner estuary meander belt, IHS1, CB2, IHS2, and IHS3 are interpreted as LASs, and assigned to Genetic Package 2.

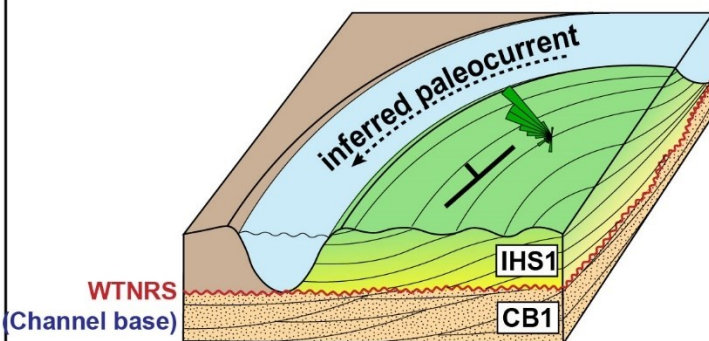


intra-point-bar erosion surface separating lateral accretion packages

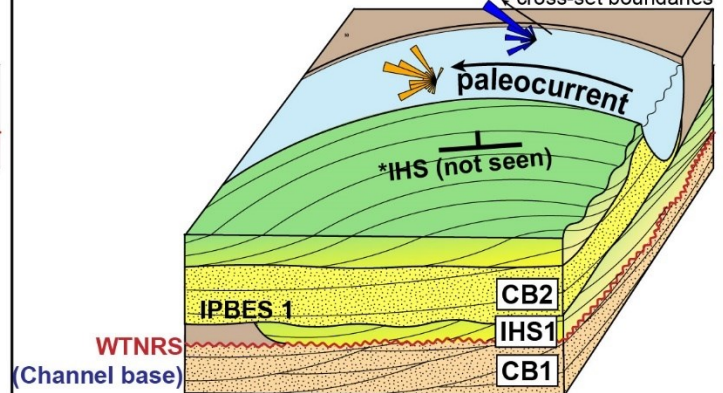
*IHS: This IHS deposit is not preserved or has been eroded by the younger IHS2, and is not seen at the Christina River outcrop.

Genetic Package 2: Inner estuary single point bar with multiple lateral accretion sets (LASs)
Same point bar rotations and shifts through time 1 to time 4 (T1-T4)

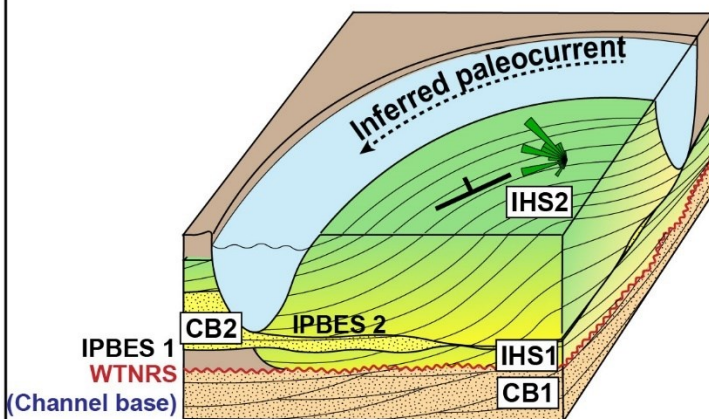
• T1: lateral accretion set 1 (IHS1) developed



• T2: CB2 and lateral accretion set 2 (*IHS) developed



• T3: lateral accretion set 3 (IHS2) developed



• T4: lateral accretion set 4 (IHS3) developed

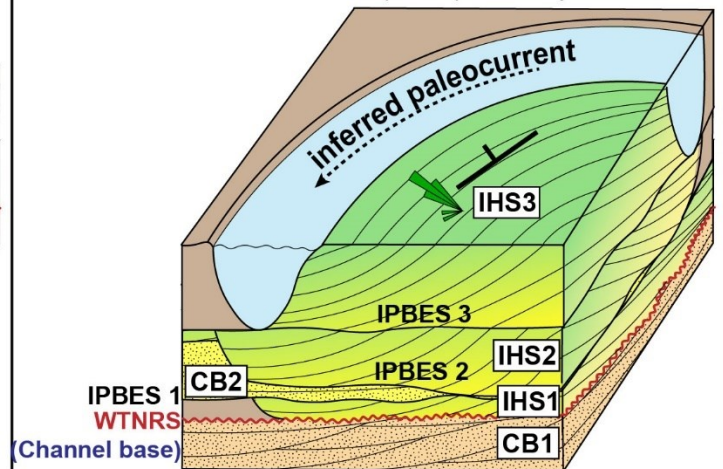
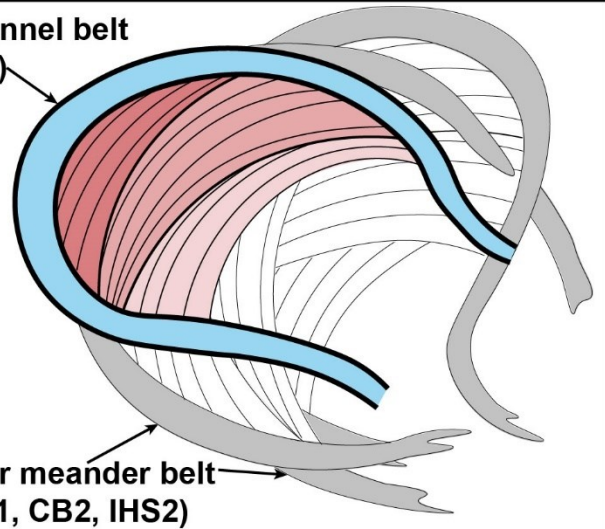


Fig. 4.20. (continued)

B Depositional model Scenario 2 for succession above WTNRS:

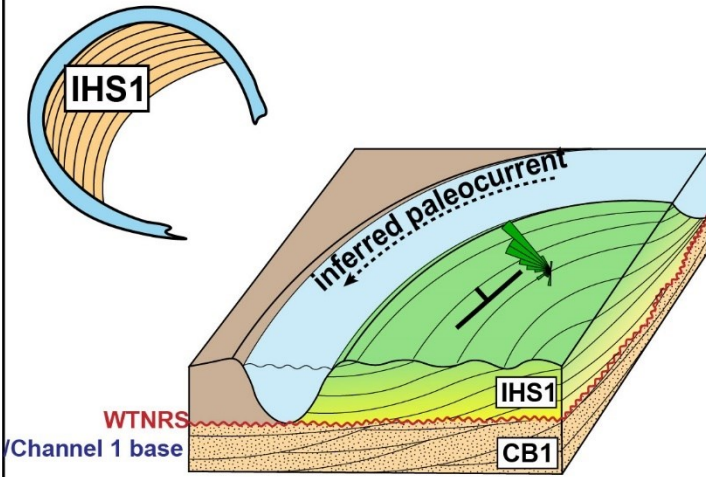
- Inner estuary point bar deposition
- Genetically unrelated, stacked inner estuary point bars, IHS1, CB2, IHS2, and IHS3 are assigned to Genetic Package 2-5.

youngest channel belt (IHS3)

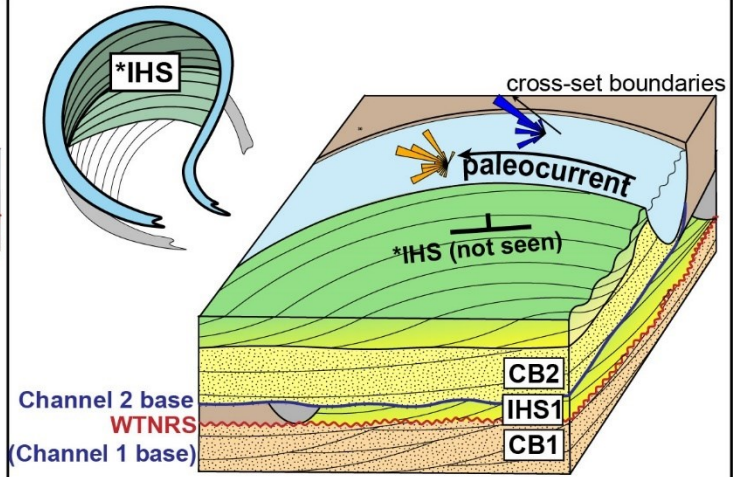


order meander belt (IHS1, CB2, IHS2)

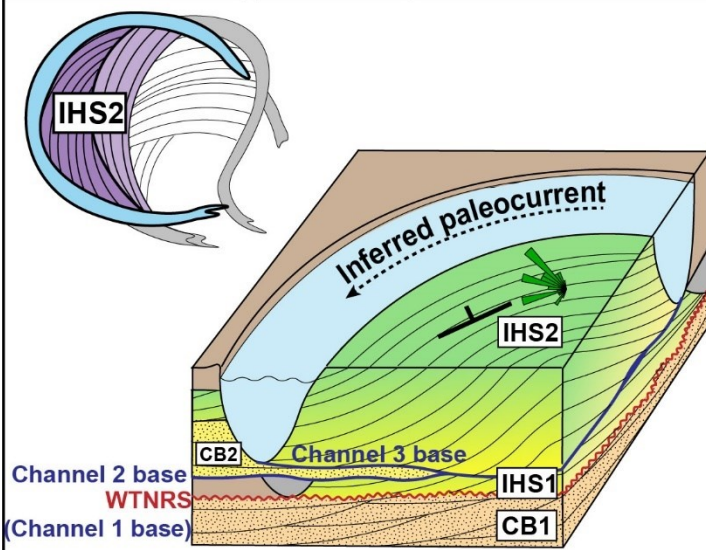
• Genetic Package 2: Estuary Channel 1



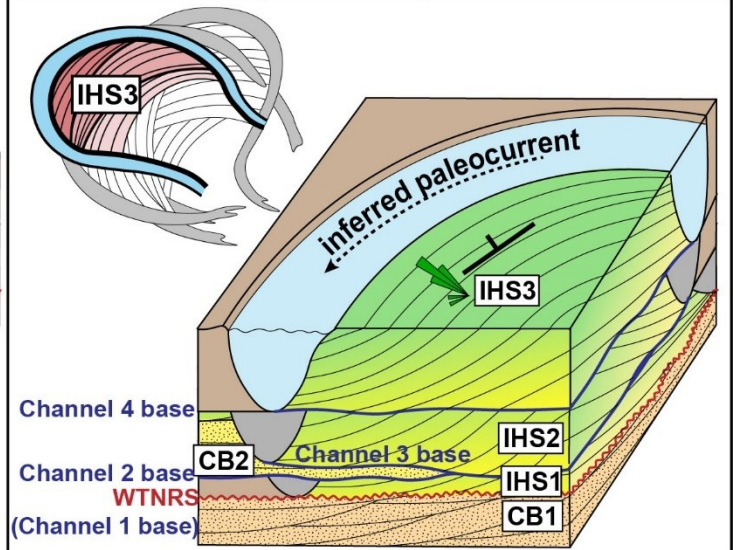
• Genetic Package 3: Estuary Channel 2



• Genetic Package 4: Estuary Channel 3



• Genetic Package 5: Estuary Channel 4



Stacked estuary point bar model

A stacked point bar interpretation was proposed for the McMurray Formation Steepbank River outcrops by Hayes *et al.* (2018). By contrast, Jablonski and Dalrymple *et al.* (2016) interpret the Steepbank succession as a single genetic unit. The evolutionary history of the stacked estuary point bar model is illustrated in Fig. 21B. The succession above the WTNRS is divided into four distinct Genetic Packages 2-5, which are interpreted to record amalgamated channel belts. Of particular note is that all four channel belts share similar lateral accretion directions. In this model, the contacts between each genetic package are marked by the erosional bases of estuary channel. In estuary channels 1, 3 and 4, CB facies associated with the point bars are absent. In particular, IHS2 infers a distinct paleocurrent direction which is not consistent with the bedding measurements of underlying CB2 unit. As such, Channel 2 associated IHS facies was possibly eroded by successive channel 3 (Fig. 21B).

The single point bar model can explain the observed uniformly dipping lateral accretion surfaces of IHS units. However, the sedimentological and ichnological trends observed in the individual IHS units are inconsistent with the single point bar model (i.e., Fig. 19B). First of all, the lithological and ichnological variations observed in a single IHS unit often occurs over a 5m- to 8m-scale (Gingras *et al.*, 2016), which is consistent with the thicknesses of IHS units observed at the Christina River outcrop (2-10m). Secondly, the persistent top truncation of parasequences indicate a low accommodation setting in the Christian River area, which may promote higher lateral accretion rates *versus* vertical aggradation. The scale of stacked small-scale point bar interpretation is similar to the multiple-stacked middle McMurray channel deposits revealed in the subsurface by Crerar and Arnott (2007) in Lewis property situated 40km northeast of the Fort McMurray. In their case, multiply stacked channel-fills were found no more than roughly 5m thick in subsurface dataset. We suggest that the stacked estuary point bar interpretation is a better fit for the Christina River outcrop because 1) it agrees with the observed lithological variations and ichnological distribution in each depositional unit; 2) sharp contacts separating depositional units are more consistent with erosive channel events, although they can occur in the same channel during peak flooding periods; and 3) the thickness of IHS units are similar in scale of multiply stacked channel-fills. In summary, considering the combined bedding orientation, as well as the sedimentological and ichnological

characteristics of the facies, the best interpretation of the McMurray interval in the Christina River outcrop is that five genetically unrelated depositional packages are present. The base consists of thick cross-bedded sandstone (CB1) recording tidal sand dunes of the middle estuary tidal bar. Amalgamated channel belts comprising four stacked channel-associated point bars (IHS1, CB2, IHS2, and IHS3) of the inner estuary complex overlie a stratigraphic discontinuity identified as a within-trend normal regressive surface (WTNRS). It is possible that genetic packages 4 and 5 (indicated in Fig. 21B) can be combined as a single genetic package, representing a continuous point bar deposition consisting of two successive lateral accretions sets. With the available dataset, this possibility cannot be entirely excluded.

CONTRIBUTION TO THE McMURRAY CONUNDRUM

The observed configuration of depositional units at Christina River outcrop suggests the architecture of lateral and downstream accretion of tide-influenced fluvial channel belts on top of tidal compound dunes. The identified WTNRS separating the two types of geobodies marks the switch to erosion owing to the progradation of inner estuary meander belts. The overprint of small-scale point bars supports the interpretation of slowly evolved meander belts in a low accommodation space setting. This is consistent with an increasing number of studies that have demonstrated that some of the tide-influenced fluvial channel systems of the middle McMurray Formation are tied to normal regression as they continue to shift in basinward direction as the shoreline prograded (Château et al., 2020; Rinke-Hardekopf et al., 2022). In terms of the sedimentological and ichnological characteristics, the IHS shows abundant evidence of brackish-water deposition. Based on the architectural, sedimentological and ichnological observations, we conclude that the observed McMurray Formation succession at the Christina River outcrop represent two types of geobodies in the inner to middle tide-dominated estuary setting (refer to Fig. 16 for their geographic locations). Tidal influences are variably subjected to the two geobodies.

CONCLUSION

This paper provides a detailed description of a tidal bar unit and at least two channel-associated units using sedimentological and ichnological facies analysis, integrated with cross-bed and bedding plane

orientation analysis. This study provides an example of how *pseudo*-tadpole plots are used to recognize genetically related packages in outcrops, and contributes to the refinement of architectural models of estuary point bar deposits. At the study locale, a lower unit consisting of cross-bedded sandstone (Genetic Package 1) is interpreted as forward/oblique accretion of sand dunes as middle estuary tidal bars. An upper unit, characterized by discrete IHS point bars and cross-bedded sandstone (Genetic Package 2 in Scenario 1, and Genetic Package 2-5 in Scenario 2) is interpreted as amalgamated fluvio-tidal meander belts of the inner estuary. In both Scenarios, the Genetic Package 1 is separated from the overlying succession by a within-trend normal regressive surface (WTNRS), marking the basinward shift of the inner estuary over the deposits of the middle estuary.

The result of this study adds to our understanding of large point-bar architectures in the sedimentary record. Our most important conclusions include: 1) the distinctive characteristics of forward-accreted tidal sand dunes and laterally accreted fluvio-tidal point bars are readily discernible using bedding orientation analysis; 2) IHS units may be underlain by erosional surfaces and in such instances may not be genetically related to the underlying cross-bedded sandstone intervals; and 3) stacked point bars or stacked lateral accretion sets may characterize an inner estuary point bar succession with complex cross cutting relationships; 4) cross-bedded sandstone that records tidal compound dunes may be under-recognized in many tidally influenced estuary deposits. Previous studies, primarily but not exclusively based on dipmeter datasets, typically interpret basal cross-bedded sandstones to represent a continuous vertical succession with overlying IHS intervals. This may be owing to difficulties in identifying subtle erosional discontinuities in many subsurface datasets and the fact that as the channel evolves, dominant drainage directions remain the same.

Chapter 5 : Variable Geobody Architecture of Fluvial to Estuary Deposits: Case Studies from the McMurray Formation

INTRODUCTION

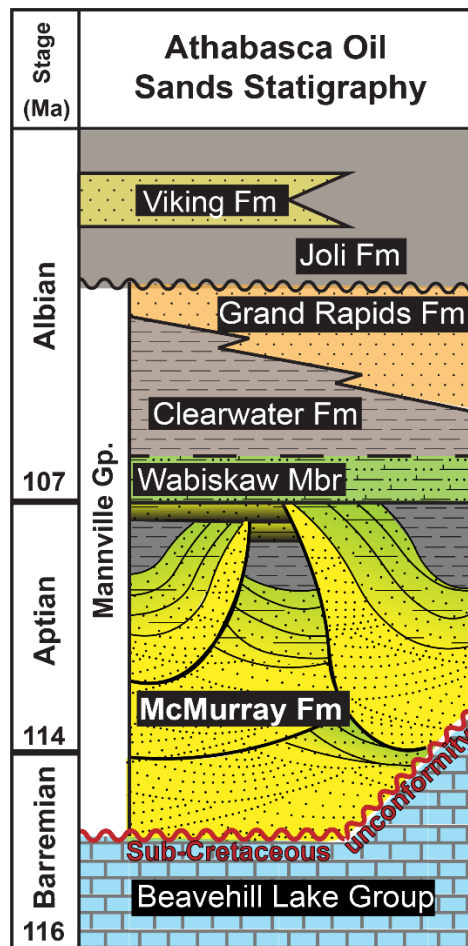
The Lower Cretaceous McMurray Formation, an important bitumen-hosting unit, has been interpreted as fluvial, fluvio-tidal, and estuary in character (e.g., Pemberton et al., 1982; Ranger and Pemberton, 1988; Wightman and Pemberton, 1997; Hein et al., 2000; Hubbard et al., 2011; Gingras et al., 2016; Durkin et al., 2017a; Hayes, 2018). Several studies have been carried out in the past twenty years using seismic, dipmeter, and outcrop datasets of the McMurray Formation. In particular, the relationship between bedding and paleocurrent orientations within McMurray strata are key to: (1) identify point-bar associated facies; (2) indicate paleocurrent and point bar migration directions; (3) recognize genetically related geobodies; and, (4) understand the bedding architecture of point bars (Muwais and Smith, 1990; Brekke and Evoy, 2004; Fustic, 2007; Nardin et al., 2013; Brekke et al., 2017; Brekke and Roenitz, 2021). Seismic modeling has been used to analyze internal morphological characterization, zone differentiation, and various types of bar forms within point bars (Fustic et al., 2008; Smith et al., 2009; Hubbard et al., 2011; Labrecque et al., 2011; Martinius et al., 2017). Finally, recent outcrop studies (Hayes, 2018; Hayes et al., 2018; Chen et al., 2022a) have demonstrated that photogrammetric 3D outcrop models can be used to recognize forward-accreting middle estuary compound dunes, which contrasts with the conventional interpretation of lateral-accreting inner estuary point bars.

Although the interpretations vary, most observers agree that three sedimentary facies are normally present in these channel-associated deposits: cross-bedded sandstones (CB); inclined heterolithic stratified sandstone and mudstone (IHS); and generally thinly bedded mudstone intervals. Importantly, a range of sedimentological expressions can be seen in McMurray Formation outcrops, including (see Fig 1): (1) clearly fluvial deposits that lack bioturbation, exhibit very abundant wood clasts, and may be unusually coarse grained, such as the Daphne Island outcrops (Harris et al., 2016) and the Crooked Rapids outcrop (Hayes, 2018); (2) tidally influenced units that are dominated by IHS, show some bedding characteristics consistent with tidally influenced sedimentary transport, but generally lack bioturbation

(e.g., Hangingstone #1 and Hangingstone #2 outcrops introduced below); and (3) estuary deposits that include pervasively bioturbated IHS (e.g., the Steepbank River outcrops; Hayes *et al.*, 2018), or sporadically burrowed compound dunes (e.g., the Amphitheater outcrops: Hayes *et al.*, 2018; the Christina River outcrop: Chen *et al.*, 2022a).

This study takes advantage of photogrammetric 3D models to establish a range of deposit characteristics that occur within the McMurray Formation, and categorically establish a fluvial versus estuarine expression of McMurray Formation geobodies. To do this, we present bedding orientation data for six representative outcrops (Fig. 5.1) of the McMurray Formation. The bedding data are interpreted in combination with their sedimentological and ichnological characteristics to propose architectural and facies differences between deposits characterized by variable fluvial and tidal influences.

Figure 5.1 Schematic stratigraphic column of the McMurray Formation as seen at measured outcrops of this study.



GEOLOGICAL BACKGROUND

The McMurray Formation was deposited on regionally truncated Devonian carbonate deposits of Woodbend Group and Beaverhill Lake group, forming the Sub-Cretaceous Unconformity in Northeast Alberta (Schneider and Grobe, 2013) (Fig. 5.2). The McMurray Formation was deposited in a broad, northward-trending paleo-valley, with several tributaries that generally flowed to the northeast (Fustic et al., 2012; Hein et al., 2013; Martinius et al., 2015). The infilling of the valley was associated with a long-term southward transgression of the Boreal Sea, suggesting that the infill was influenced by marine incursion. An informal subdivision of the McMurray Formation into the lower, middle, and upper members has found general use in McMurray research, and that tripartite stacking has been related to the evolution of McMurray depositional systems from fluvial (lower McMurray member), to estuarine and coastal plain (middle McMurray), and ultimately to energy-sheltered brackish-water embayment (upper McMurray) during the transgression (Carrigy, 1959; Flach, 1977; Flach and Mossop, 1985; Hein and Cotterill, 2006). The termination of McMurray Formation deposition is locally demarcated by a marine flooding surface at the base of the overlying Clearwater Formation shale (Crerar and Arnott, 2007), marking when the Boreal Sea topped the confines of the McMurray Valley.

McMurray strata are dominated by point bar deposits, particularly (but not limited to) in the middle part of the section. Point-bar deposits exposed near mining areas and along riverbanks have been studied extensively. In the early 1980s, many outcrop studies (e.g., Steepbank River outcrops) and examinations carried out in Suncor and Syncrude Mines identified IHS facies in the McMurray Formation as lateral accretion deposits of point bars, interpreted to represent an extensive fluvial drainage system (Mossop and Flach, 1983; Flach and Mossop, 1985). At the same outcrops, brackish- water trace fossils and tidal indicators were identified, implying that the channel bars were marine influenced and connected to the Boreal Sea shoreline to the north (Stewart and MacCallum, 1978; Pemberton et al., 1982; Smith, 1988). In the ensuing 20 years, a tide-influenced estuary depositional model was generally accepted by most McMurray researchers. However, the analysis of seismic data, integrated with dipmeter analyses, resulted in the recognition that the scale and geomorphology of the units were much more consistent with fluvial systems (Blum and Jennings, 2016; Durkin et al., 2017a; Durkin et al., 2017b). Subsequently there

has been much debated in the literature, (encapsulated by Blum, 2016 and Gingras and Leckie, 2017), and the question of estuary *versus* fluvial has become an all-or-nothing interpretation, although it is logical that both estuary and fluvial deposits comprise parts of the McMurray Formation.

Among the outcrops selected for this study, the Daphne Island and Crooked Rapids outcrops are chosen as examples of fluvial point bars. Previous work at these outcrops revealed a general lack of trace fossils or local abundance of continental traces, consistent with a continental fluvial-dominated channel interpretation (Harris et al., 2016; Hayes, 2018). Hangingstone outcrops preserve continuous point bar(s) that are largely devoid of bioturbation. They are selected to represent a transitional setting connecting fluvial and tidally influenced inner estuary channels. The Christina River outcrop also displays laterally accreted estuary point bar deposits, and is selected to show the architectural variations in point bars. Unlike the continuous point bar observed at Hangingstone outcrops, the Christina River outcrop is characterized by stacked multiple point bars, and each point bar is bounded by erosional surfaces. Additionally, a brackish-water trace fossil assemblage is present throughout the Christina River outcrop, which contrasts with the absence of trace fossils in the fluvial and tidally influenced fluvial examples. The Amphitheatre outcrop is selected to show the presence of a forward-accreted tidal compound dune complex, which has been assigned to a middle estuary setting in previous studies (Wightman and Pemberton, 1997; Hayes et al., 2018). Bioturbation is sporadically distributed but common at the Amphitheatre sections. Similar forward accreted bedforms have also been recognized at the Christina River outcrop.

STUDY AREA

The six selected outcrops of the McMurray Formation are located along the Athabasca River and its tributaries (Fig. 5.2A). The Daphne Island outcrop (57°17'56" N, 111°39'46" W) (Fig. 5.2B) is located on the east bank of the Athabasca River, approximately 100 m north of Daphne Island. This outcrop extends 206m from south to north, and consists of cross-bedded sandstone and IHS facies. The uppermost part of the outcrop is characterized by pedogenically altered deposits. The Crooked Rapids outcrop (56°35'32"

N, 111°52'04" W) (Fig. 5.2C) is also located along the Athabasca River, roughly 31 km southwest of the town of Fort McMurray. The outcrop is 1.2 km long, exposes approximately 30m of the upper McMurray and the Wabiskaw Member of the Clearwater Formation, and displays cross-bedded and IHS facies associated with channels. Two Hangingstone outcrops were selected in this study (Hangingstone #1 and Hangingstone #2; Fig. 5.2D) and are exposed along the banks of the Hangingstone River within the city of Fort McMurray. The two outcrops are 460m from each other, with Hangingstone #2 (56°42'14" N, 111°22'16" W) positioned upstream of Hangingstone #1 (56°42'26" N, 111°22'01" W). Both outcrops nicely expose complete point bar successions in the McMurray Formation, as well as the Wabiskaw Member of the Clearwater Formation and overlying Quaternary paleosols. The Christina River outcrop (56°37'21" N, 110°57'27" W) (Fig. 5.2E) is located approximately 25.8 km southwest of the city of the Fort McMurray. The McMurray Formation at this outcrop is composed of a lower and an upper section. The lower section consists of cross-bedded facies, whereas the upper section is dominated by cross-bedded and IHS facies. Finally, the Amphitheatre outcrop (57°11'35" N, 111°39'50" W) (Fig. 5.2F) is located about 1.6 km northeast of the hamlet of Fort MacKay and is exposed along the MacKay River. At this outcrop, a 10 to 20 m thick unit of cross-bedded sandstone is sharply overlain by IHS.

Figure 5.2 **A)** Location map of the measured outcrops in relation to Fort McMurray, Alberta, Canada. **B)** Satellite image of the Daphne Island outcrop, located at 57°17'56" N, 111°39'46" W. **C)** Satellite image of the Crooked Rapids outcrop, located at 56°35'32" N, 111°52'04" W. **D)** Satellite image of the Hangingstone #1 and #2 outcrops, located at 56°42'26" N, 111°22'01" W and 56°42'14" N, 111°22'16" W. **E)** Satellite image of the Christina River outcrop, located at 56°37'21" N, 110°57'27" W. **F)** Satellite image of the Amphitheatre outcrop, located at 57°11'35" N, 111°39'50" W. The measured sections are highlighted in orange. Satellite images are courtesy of Google Earth© 2022.



METHODOLOGY AND DATA ANALYSIS

This study establishes depositional environment interpretations associated with point bars in the McMurray Formation interval by interpreting sedimentological and ichnological characteristics of dominant facies within the outcrops using outcrop lithologs. In addition, photogrammetric 3D models were generated to determine the bedding orientations of major surfaces identified in the two dominant facies types (CB and IHS). The measured orientation datasets are used to characterize the geobody architectures of bar forms in the fluvial and estuarine settings.

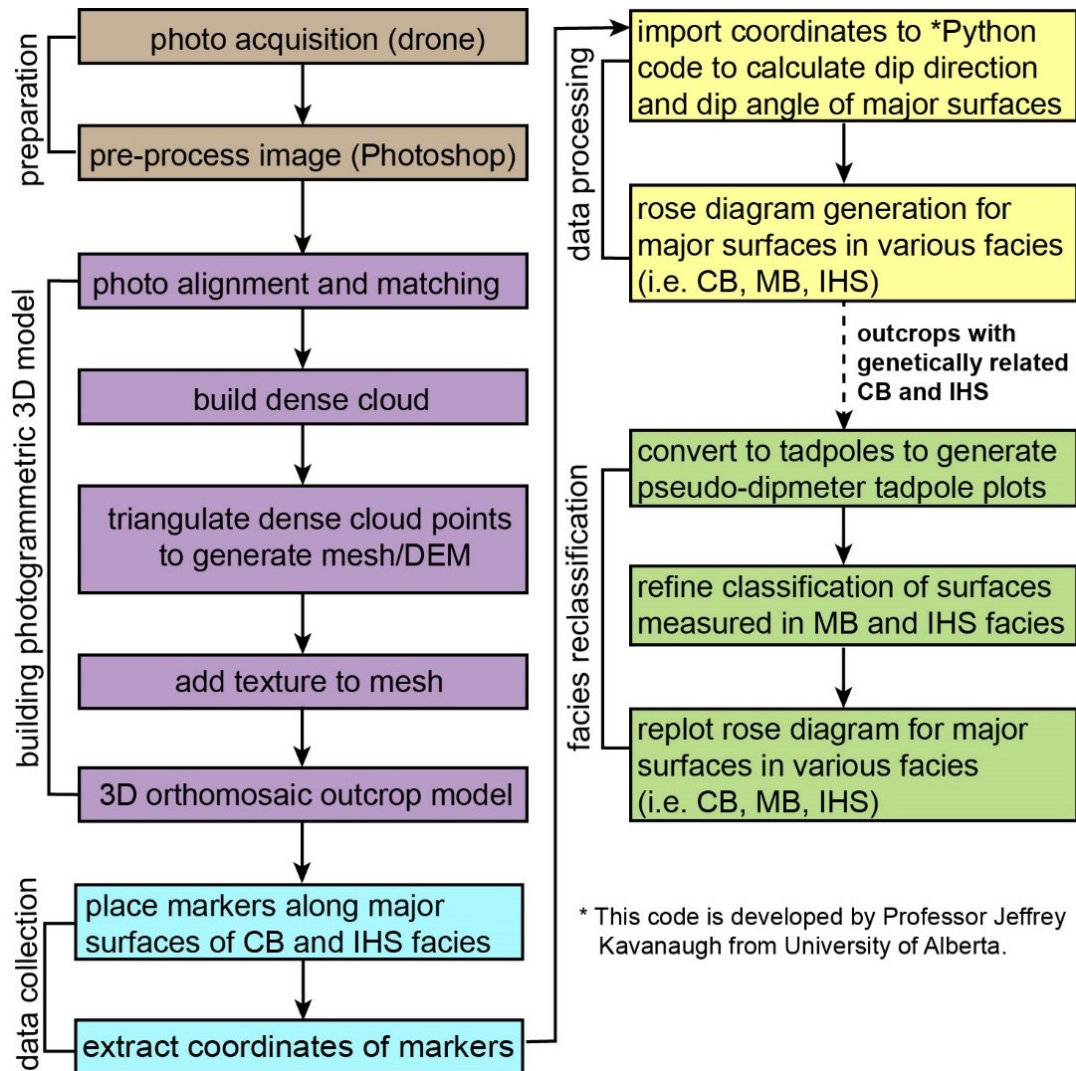
Photogrammetric 3D outcrop model

Structure-from-Motion (SfM) photogrammetry is one of the advanced outcrop study methods that can efficiently measure orientation data of surfaces from a 3D outcrop model. A few earlier studies of the McMurray Formation have demonstrated the utility of this method (Hayes et al., 2017; Hayes, 2018). A workflow employed to build a 3D outcrop model using the photogrammetric method is summarized in Fig. 5.3. The entire process can be divided into four stages (highlighted in different colors in Fig. 5.3).

Following the method introduced by Hayes *et al.*, (2018), a drone is used to take photos at each outcrop, and a minimum of 30% overlap in successive photos is required to achieve the best results. The acquired photos are processed using Adobe Photoshop to remove significant shadows, keep similar properties (i.e., contrast, color tones, brightness, greyscale, etc.), and highlight features of interest.

The processed photos are then imported to the software Metashape 1.7 (© Agisoft) to generate 3D models. These photos are aligned and matched based on their coordinates, and pixels of the 2D photos are matched by software-implemented algorithms to generate dense point clouds across the outcrop. In the subsequent step, a 3D mesh is created by generating triangular facets. Finally, textures of the photos are draped over the mesh to show spatial distributions of visual rock properties. When processing the 3D outcrop model, the software uses a series of algorithms to assign spatial information to every pixel in the model. Therefore, the entire model is georeferenced.

Figure 5.3 Schematic workflow of the 3D photogrammetry method used to characterize bar forms of the McMurray Formation at measured outcrops in this study.



Bedding orientation data collection

The completed 3D outcrop model has sufficient quality for resolving several millimetres- to decimetres-scale sedimentary features, such as sedimentary contacts, bedding, stratification, and some larger ichnofossils. Surfaces of interest can be traced out by placing markers on the models. In this study, we focus on surfaces associated with the two dominant facies comprising the middle McMurray Formation: cross-bedded sandstones (CB) and inclined heterolithic stratified sandstone and mudstone (IHS). Massive to planar laminated mudstone, representing channel abandonment, is an additional facies

commonly associated with some point bars; however, it is excluded in the bedding orientation analysis as the aim of this study is to characterize channel-associated deposits in a fluvial to estuary continuum. The surfaces measured include the traces of internal cross-stratification in the CB, the master bedding planes (MB) separating cross-bed sets, and the traces of the sandstone and mudstone beds within the IHS. The master bedding planes and cross beds in the CB facies represent sand dune accretion directions and paleocurrent directions, respectively. In the IHS facies, lateral accretion surfaces (LASs), by lithological changes between sandstone and mudstone are measured to represent the direction of point bar migration.

To measure surface orientations, marker points are placed along master bedding planes or cross-beds and a best-fit plane is projected through those points. The software extracts the coordinate information (latitude, longitude, altitude) for each marker point and the orientation of the plane is calculated. Reported measurements are actually the orientations of the best-fit planes. Since sedimentary surfaces are commonly undulatory or curved, a surface may be divided into smaller measuring segments, wherein each segment estimates a portion of the surface. At least five marker points are placed along each measuring segment. Three markers are required to generate a best-fit plane; however, the more marker points used, the more dependable is the plane estimation. In order to maximize the accuracy of bedding orientation, markers are preferred to be placed in locations where there is clear three-dimensional outcrop relief along the length of a segment.

To obtain bedding orientation information, coordinates of markers are imported to a Python algorithm. This code converts the points data into strike and dip of the measured segment of the bedding plane. This process is repeated for each segment, resulting in a group of measurements for each surface of interest. Large errors in measurement may be caused by a lack of 3D relief along outcrop surfaces and misplaced markers.

Since the McMurray Formation has undergone pre-, syn-, and post-salt tectonic events throughout the region (Broughton, 2014), corrections of bedding measurements need to be applied to remove these deformation effects. Orientation data of the upper McMurray or Wabiskaw Member interval are collected from outcrops or dipmeter logs of nearby wells to represent post-depositional bedding orientations. The restoration of bedding measurements is established by flattening the bedding planes of strata in the upper

McMurray or Wabiskaw Member. To achieve this goal, an average rotation axis is estimated at each outcrop (see Table 2), except at the Daphne Island outcrop owing to the lack of both outcrop and subsurface data.

Table 5.1 Rotation axis information used to restore orientational data to original condition at time of deposition.

Rotation axis info	Crooked Rapids	Hangingstone #1	Hangingstone #2	Christina River	Amphitheatre
plunge	4.9°	5.7°	1.95°	4.13°	5.85°
trend	220.2°WSW	173.9°SSE	51.7°NE	175.3°SSE	96.4°E

Facies and Facies Associations Classification

The relationship between CB and IHS may be genetically related and thereby represent a facies association. This relationship can be resolved, in part, by careful consideration of bedding and cross-bed orientations represented graphically. In cases where CB and IHS are obviously genetically associated (e.g., meaning this is one example of an obvious genetic association), careful analysis of bedding orientations paired with geological observations at the outcrop is crucial. This is achieved using *pseudo*-dipmeter tadpole logs generated from 3D outcrop models to classify the measured bedding data. In this study, we identified and tested bedding classifications at the Hangingstone #1 outcrop using the following steps:

1. Identify successions where low-angle dipping master bedding planes of CB are consistently dipping in the same direction as the overlying LASs within the IHS.
2. Classify these CB successions as sandier versions of IHS and representing the lowermost part of point bar deposit.
3. Plot rose diagrams for the classified major surfaces in various facies (i.e., CB, MB, IHS)

For a more detailed discussion of the bedding classification using dipmeter tadpole data, readers are directed to Brekke et al., (2017), Brekke and Roenitz (2021), and Chen et al., (2021).

RESULTS AND INTERPRETATION

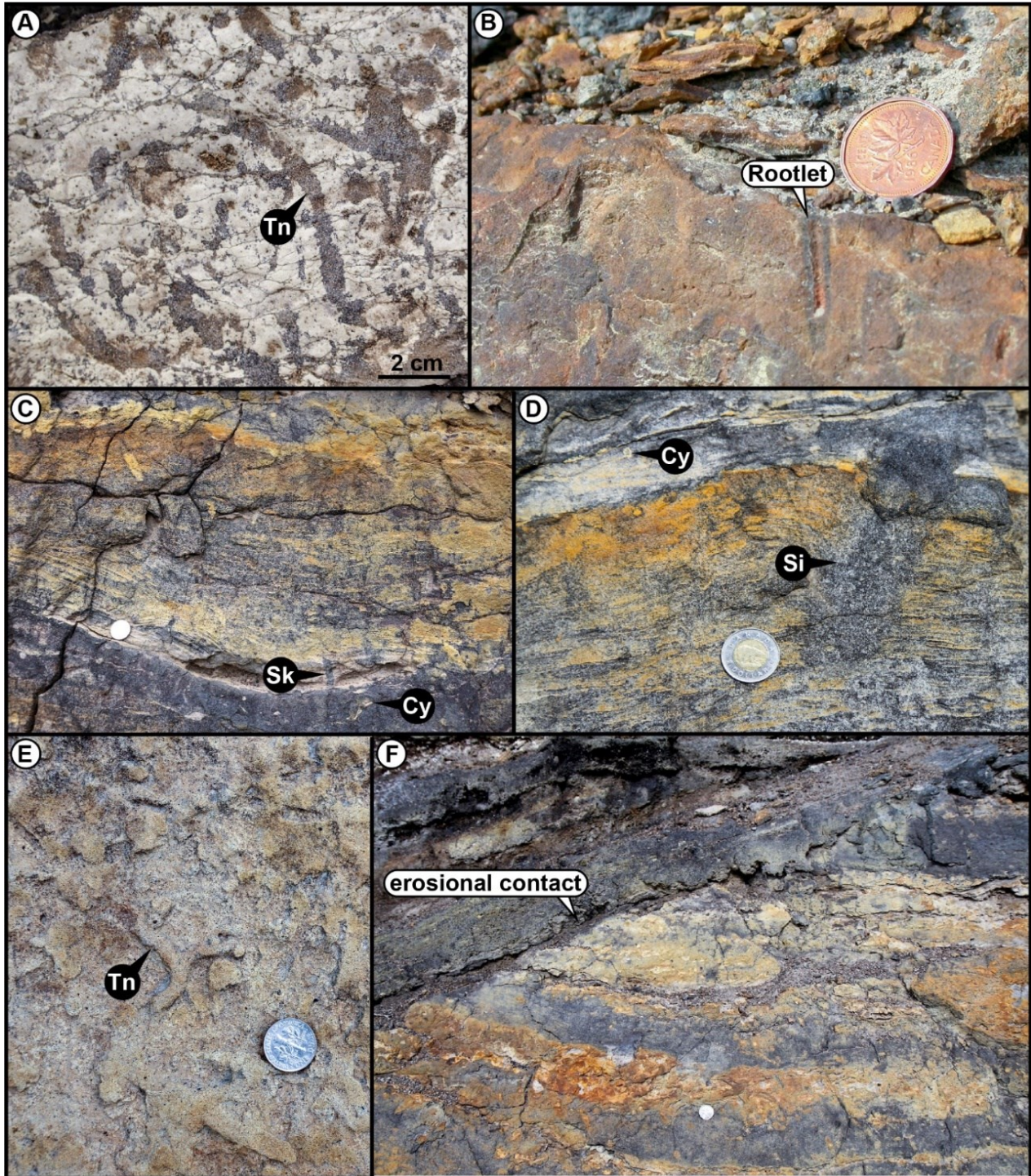
This section summarizes six outcrops that expose variable intervals of the McMurray Formation along the Athabasca River and its tributaries (e.g., the Clearwater, Christina, Hangingstone, and Mackay rivers). Together, these outcrops display a range of geobody architectures common to a fluvial to estuary setting. Below, sedimentological, ichnological and geobody architectural characteristics are summarized for each outcrop. A synthesized interpretation of these observations is provided after each outcrop description. Of particular note is that the inference of a relationship among depositional units at the different outcrops should not be assumed. For example, the CB unit at one outcrop is not correlatable to the CB units at other outcrops.

Fluvial point bars

Daphne Island Outcrop

Figure 5.4 displays close-up photos of characteristic trace fossils and sedimentary features at the Daphne Island outcrop. The 3D outcrop model and an interpreted close-up section of the outcrop are shown in Fig. 5.5. The basal succession of the Daphne Island outcrop is characterized by two stacked inclined heterolithic stratified units (IHS1 and IHS2), separated by an erosional contact. The IHS units are incised and erosionally overlain by a thick succession of trough cross-stratified to planar tabular cross-stratified sandstone (CB). The sharp contact between all three units can be traced across the outcrop. Harris *et al.* (2016) interpreted this outcrop as a regressive succession, wherein a fluvial channel (overlain by pedogenically altered sediment) is incised into the innermost estuary-associated IHS deposits. Bedding measurements associated with IHS and CB units are summarized in Table 2.

Figure 5.4 Detailed photos of common sedimentary and ichnological features identified at Daphne Island outcrop section. **A)** A bedding plane view of *Taenidium* in a mudstone bed of IHS unit. **B)** An example of rootlets in the cross-bedded sandstone unit. The rusty color is sign of oxidation. **C)** A sample section of IHS unit showing *Skolithos* and *Cylindrichnus*. **D)** A sample section of IHS unit showing *Cylindrichnus* and *Siphonichnus*. **E)** Bedding plane view of *Taenidium* in IHS unit. **F)** A sample section showing sharp contact between successive IHS units. Abbreviations: Tn-*Taenidium*, Sk-*Skolithos*, Cy-*Cylindrichnus*, Si-*Siphonichnus*. (next page)



Sedimentological and ichnological characteristics

The basal IHS1 unit is characterized by low-angle dipping lateral accretion surfaces (LASs), defined by thinly bedded mudstone and dm-scale sandstone beds (see its distribution in Fig. 5.5). In general, overall decreasing bed thicknesses and increasing proportions of mudstone to sandstone are observed from

bottom to top of the succession. Figure 5.5 shows a clear erosional contact between two IHS units, each with distinct dip angles. The sand beds of the overlying IHS2 unit are coarse grained to granule bearing whereas the underlying IHS1 unit is dominated by fine-grained sand (Fig. 5.4F). Bioturbation intensity is expressed by bioturbation index (BI) and ranges from 0 to 2 in the lower IHS1 unit, with common traces including *Taenidium*, *Siphonichnus*, *Cylindrichnus*, and *Skolithos* (Fig. 5.4A, C, D, and E). *Taenidium* is commonly found in the mudstone layers, extending downwards into underlying sandstone beds. The other trace fossils are sporadically distributed throughout the IHS1 unit. By contrast, the overlying IHS2 unit is entirely devoid of bioturbation.

Cross-bedded sandstone overlies an undulatory erosional surface cut across the IHS2 unit. The thicknesses of cross-bed sets range from 10cm to 1.3m. Sedimentary structures within the sandstone unit consist of trough to planar tabular cross-stratification, locally preserved current ripples, and oxidized rootlets (Fig. 5.4B). Some cross-bed sets locally show divergent dip directions across master bedding planes. Coal fragments are abundant (Harris *et al.*, 2016). The upper part of the CB unit has been pedogenically modified during the Quaternary (Fig. 5.5). Similar to the underlying IHS2 unit, the cross-bedded sandstone unit is also devoid of bioturbation.

Bedding orientation characteristics

Bedding and cross-bed orientation data from the channelized granular sandstone is presented in Table 2. The underlying IHS1 shows lateral accretion surfaces (LASs) dipping uniformly to the east. Flow direction inferred by the IHS unit is perpendicular to the LASs, which is oriented in northerly or southerly directions. The poles to bedding plot in the IHS unit shows less variability in dipping angles (~20°-40°) with a few outliers. IHS2 also shows predominant eastward-dipping LASs, Cross-bed foresets within the channel (CB unit) indicate a strong NE paleocurrent flow direction. Poles to bedding plot of the cross-beds suggest variable dip angles, ranging from 0° to 50°. Master bedding planes are consistently oriented ENE, which is subparallel or oblique to the paleocurrent direction.

Table 5.2 Bedding orientation characteristics of the cross-bedded sandstone and IHS facies at Daphne Island outcrop. The rose plots show dip directions of cross beds and master bedding. The pole to bedding plots show dip angle of cross beds and master beddings. The inferred paleocurrent flow direction (indicated by red arrows) is orthogonal to master beddings of IHS facies.

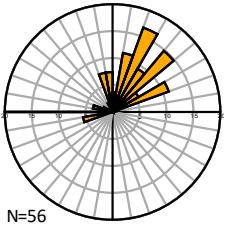
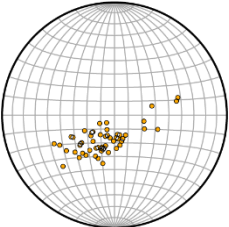
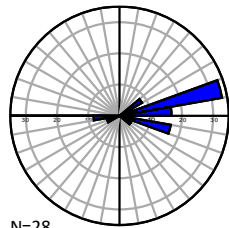
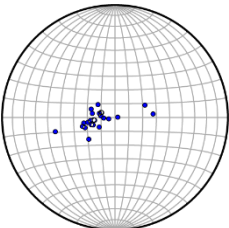
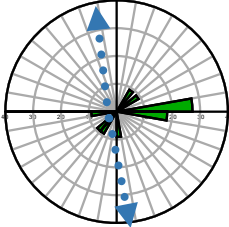
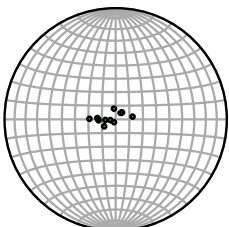
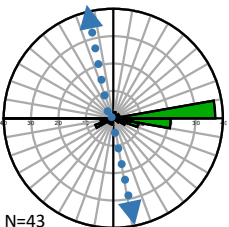
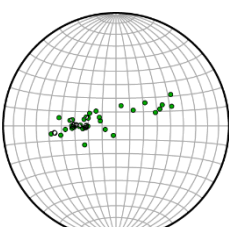
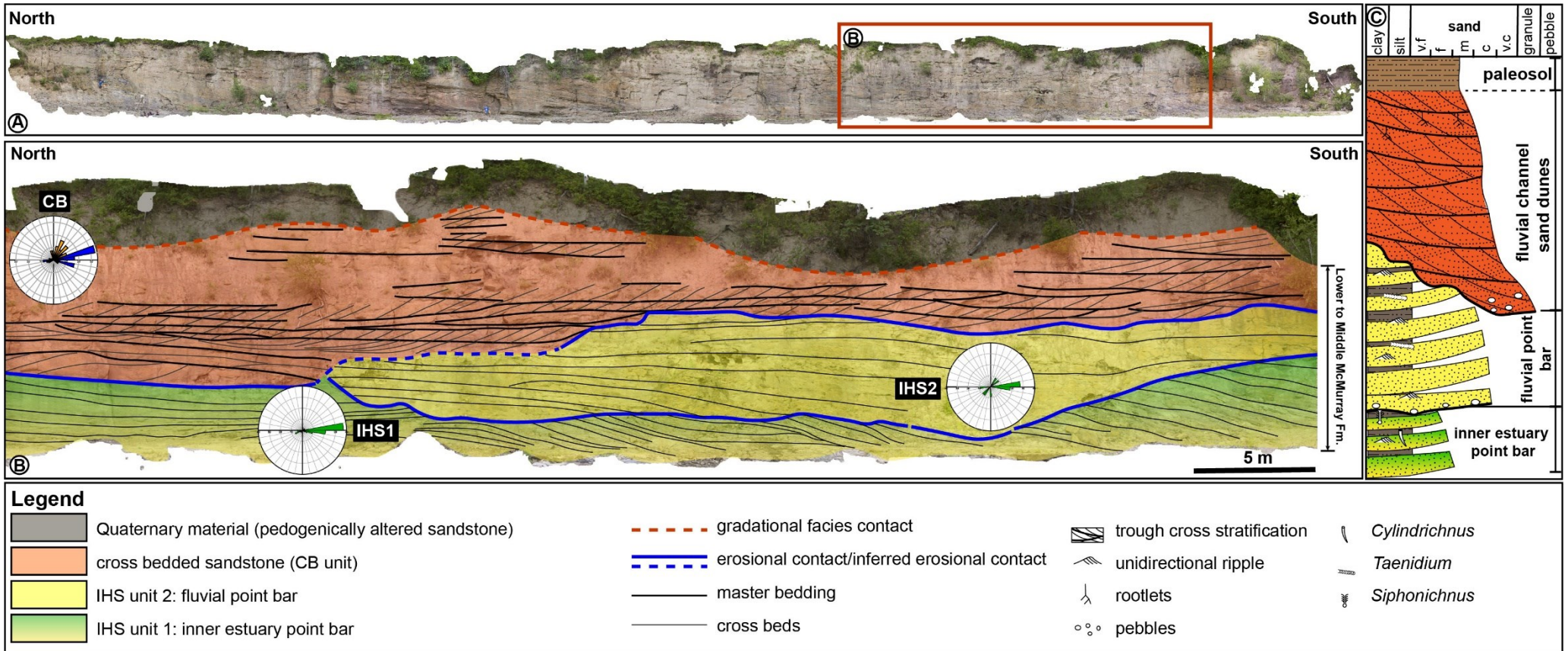
facies	bedding type	rose diagram	poles to bedding	bedding orientation	sedimentology & ichnology
Daphne Island CB	cross beds (paleocurrent)	 N=56		<ul style="list-style-type: none"> • cross beds preferentially oriented NE, indicating overall northward paleocurrent direction. 	<ul style="list-style-type: none"> • trough to planar tabular cross stratification • local current ripples • sharp contact with underlying IHS facies • bed sets thicknesses range between 0.1m-1.3m • common coal fragments (Harris et al., 2016) • Local rootlets • Trace fossils are absent
	master bedding	 N=28		<ul style="list-style-type: none"> • master beddings dip consistently towards ENE, oblique to paleocurrent direction. 	
Daphne Island IHS 2	lateral accretionary surfaces (LAS)			<ul style="list-style-type: none"> • lateral accretionary surfaces (LAS) predominantly dip towards E, indicating northward or southward paleoflow direction. • gentle dipping angle less than 15° 	<ul style="list-style-type: none"> • interbedded sandstone and mudstone defining IHS • erosionally overlain by CB unit or located by another IHS unit. • devoid of bioturbation
Daphne Island IHS 1	lateral accretionary surfaces (LAS)	 N=43		<ul style="list-style-type: none"> • lateral accretionary surfaces (LAS) consistently dip E, indicating northward or southward paleoflow direction. 	<ul style="list-style-type: none"> • interbedded sandstone and mudstone defining HIS • IHS 1 unit truncated by overlying IHS 2 unit. • continental trace fossil assemblage consists of <i>Taenidium</i>, <i>Cylindrichnus</i>, <i>Siphonichnus</i>, and minor <i>Skolithos</i>.

Figure 5.5 **A)** Photogrammetric 3D model of the Daphne Island outcrop. **B)** An interpreted zoom in section of the Daphne Island outcrop. Contact between CB sandstone unit and IHS unit can be traced across the outcrop model. Dashed lines represent gradational or inferred contacts. **C)** representative strip log of the interpreted section in B), showing fluvial channel sand dunes erosionally overlies IHS units of inner estuary point bars.



Interpretation

In the lower IHS1 unit, continental (*Taenidium*) and marine associated (*Cylindrichnus*, *Skolithos*, and *Siphonichnus*) trace fossils suggest an intercalation of freshwater and brackish-water settings. Harris *et al.* (2016) interpreted the distribution of the two types of traces as the result of seasonal changes in turbidity maxima. Given the brackish-water signatures mentioned above, this unit is best interpreted as tide-influenced inner estuary point bars in a fluviotidal setting. The consistently eastward-dipping, low-angle IHS beds are consistent with lateral accretion surfaces that dip towards the center of the channel thalweg. Sediment transport direction indicators were not observed.

Although IHS2 shows similar dipping orientations of LASs as with IHS1 unit, they are interpreted as different geobodies, owing to the marked differences in their lithological and ichnological characteristics. The granule-sized grains and absence of bioturbation in the IHS2 unit is consistent with a fluvially dominated setting, and is interpreted as a fluvial point bar deposit.

Within the CB sandstone unit, the abundant trough and planar tabular cross-stratification record the migration of large-scale subaqueous dunes. Divergently dipping cross-beds suggest variable sediment transport directions. Variable energy levels are indicated by the intercalation of cross-stratification from sand dunes and current ripples. All of the sedimentary structures suggest deposition under unidirectional flow, which is consistent with transport in a fluvial channel. This interpretation is further supported by the consistently dipping cross beds in the CB sandstone unit (Table 2). The strong unimodal cross-bed measurements suggest a preponderance of simple dunes. The oblique relationship between master bedding and cross-bedding orientations suggests that the master bedding surfaces were also accreting laterally. The absence of trace fossils and the presence of abundant coal fragments attest to freshwater conditions. Roots are associated with the pedogenically altered unit above the channel.

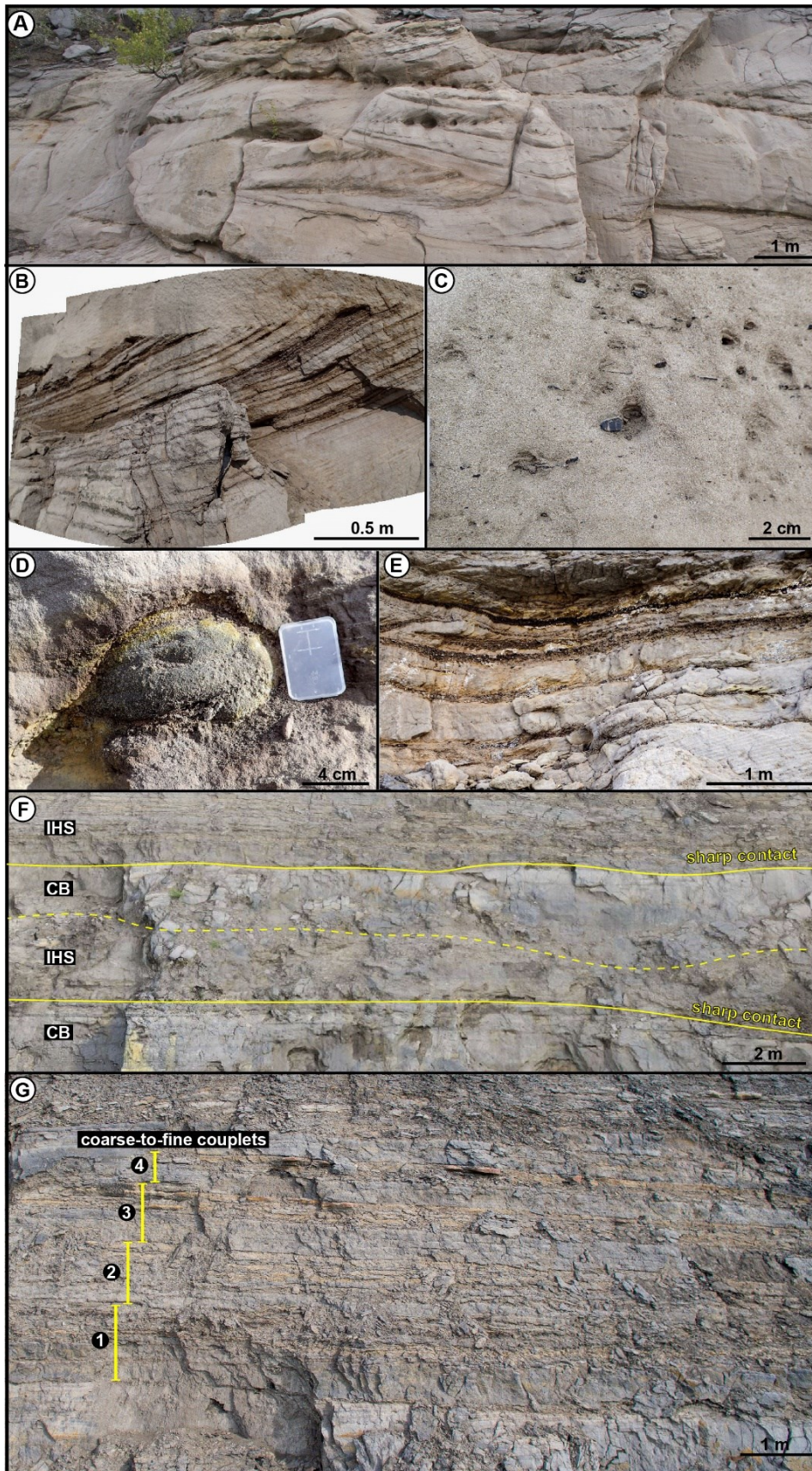
Crooked Rapids Outcrop

At Crooked Rapids, channel-associated facies sit unconformably above Devonian strata (Moberly Formation). The channel deposits comprise a basal trough cross-bedded sandstone (CB) and an upper interbedded sandstone and siltstone unit (IHS) (Fig. 5.7). Fine-grained, horizontally bedded strata (presumably upper McMurray parasequences) are present above the channel deposits. These are

stacked heterolithic, coarsening-upward mudstone and sandstone intervals, which are not interpreted in this study. The Wabiskaw Member of the Clearwater Formation is exposed in the upper part of the outcrop. This unit is differentiated from the underlying McMurray Formation by its flat-lying architecture and evenly distributed marine trace fossils, which include *Cylindrichnus*, *Siphonichnus*, *Conichnus*, and *Ophiomorpha* in sandstone layers (Hayes, 2018).

Figure 5.6 displays close-up photos of characteristic sedimentary features observed in the outcrop. Bedding measurements associated with each unit are summarized in Table 3. Hayes (2018) suggested that this outcrop conforms to a fluvial depositional model; specifically, a fluvial-channel thalweg deposit overlain by point bar or overbank deposits. An interpreted section of the northmost end of the outcrop is shown in Fig. 5.7.

Figure 5.6 Detailed photos of common sedimentary and ichnological features identified at Crooked Rapids outcrop section. **A)** Metre-scale trough cross-stratified sandstone locally showing cross bedsets dipping in opposite directions. **B)** Organic-rich debris draped in foresets of sand dunes. **C)** Coal fragments randomly distributed in CB sandstone facies. **D)** Pyrite nodule identified in CB sandstone facies. **E)** A sample section of CB sandstone facies showing planar tabular cross stratification with coal debris concentrated in the bottomsets of sand dunes. **F)** Interfingering relationship between CB and IHS facies. **G)** IHS unit at Crooked Rapids outcrop show rhythmically arranged sandstone and siltstone couplets. Note the repeated coarse-to-fine couplets and decimetre-scale sandstone beds. (next page)



Sedimentological and ichnological characteristics

The basal CB unit is characterized by approximately 20m of trough and planar tabular cross-stratified sandstone (Fig. 5.6A and Fig. 5.7). The bedding structure displays a gradual upward transition from thick-bedded, trough cross-stratification to thin-bedded, planar tabular cross-stratification. Thicknesses of cross-bed sets decrease upwards from 3m to 0.4m. An example of the metre-scale trough cross bedding is shown in Fig. 5.6A, displaying divergent dipping directions of cross beds across a master bedding plane that separates two successive cross-bed sets. Unidirectional ripples are more common in thinly bedded, planar tabular cross-stratified sandstone intervals near the top of this unit. Abundant organic detritus occurs as carbon-rich drapes on cross-bed foresets (Fig. 5.6B and E), and centimetre-scale coal fragments are randomly distributed in the sandstone facies (Fig. 5.6C). Centimetre-scale pyrite nodules are locally present (Fig. 5.6D). Of particular note is the absence of bioturbation throughout the unit.

Above the CB unit, an IHS interval consisting of alternating sandstone and siltstone is present. An interfingering relationship between the CB and IHS units is apparent at the south end of the outcrop (Fig. 5.6F and Fig. 5.7B). The IHS unit is characterized by vertically stacked, regularly laminated coarse / fine couplets (Fig. 5.6G). Each couplet is characterized by decimetre-scale sandstone at the bottom and centimetre-scale mudstone on the top. The bedding thicknesses of couplets decrease upward. The IHS consists of laminated sandstone interbedded with siltstone that is very organic rich (coal fragments) locally. In the IHS unit, the gently dipping lateral accretion surfaces are traceable over tens of metres at the outcrop. Unidirectional current ripple lamination is the most common sedimentary structure, and trace fossils are completely absent in this unit.

Bedding orientation characteristics

In the basal CB unit, cross beds consistently dip in a W-NW direction. Dip angles of these cross beds range from 0 to 30°. Master bedding planes in this unit show more variability, but predominantly dip towards the W and NNW directions. An oblique relationship between cross beds and master bedding planes is observed. The overlying IHS unit is characterized by gently dipping (mainly less than 20°) lateral accretion surfaces (LASs) that are consistently oriented SW. A subset of the data is oriented NE (Table 3).

Table 5.3 Bedding orientation characteristics of the cross-bedded sandstone and IHS facies at Crooked Rapids outcrop. The rose plots show dip directions of cross beds and master bedding. The pole to bedding plots show dip angle of cross beds and master beddings. The inferred paleocurrent flow direction (indicated by red arrows) is orthogonal to master beddings of IHS facies.

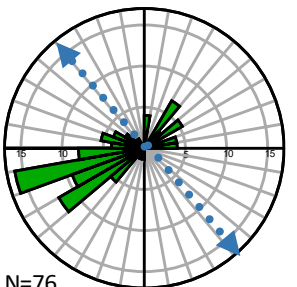
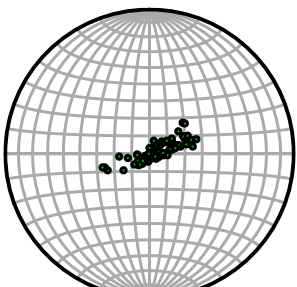
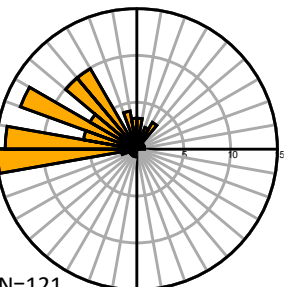
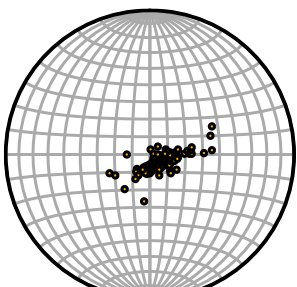
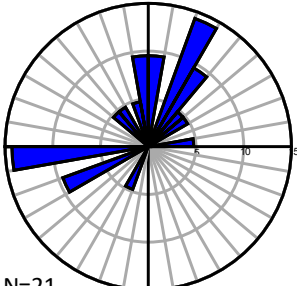
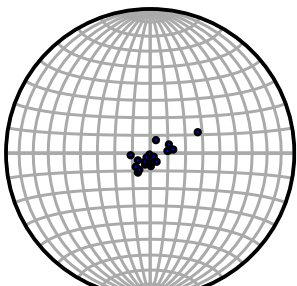
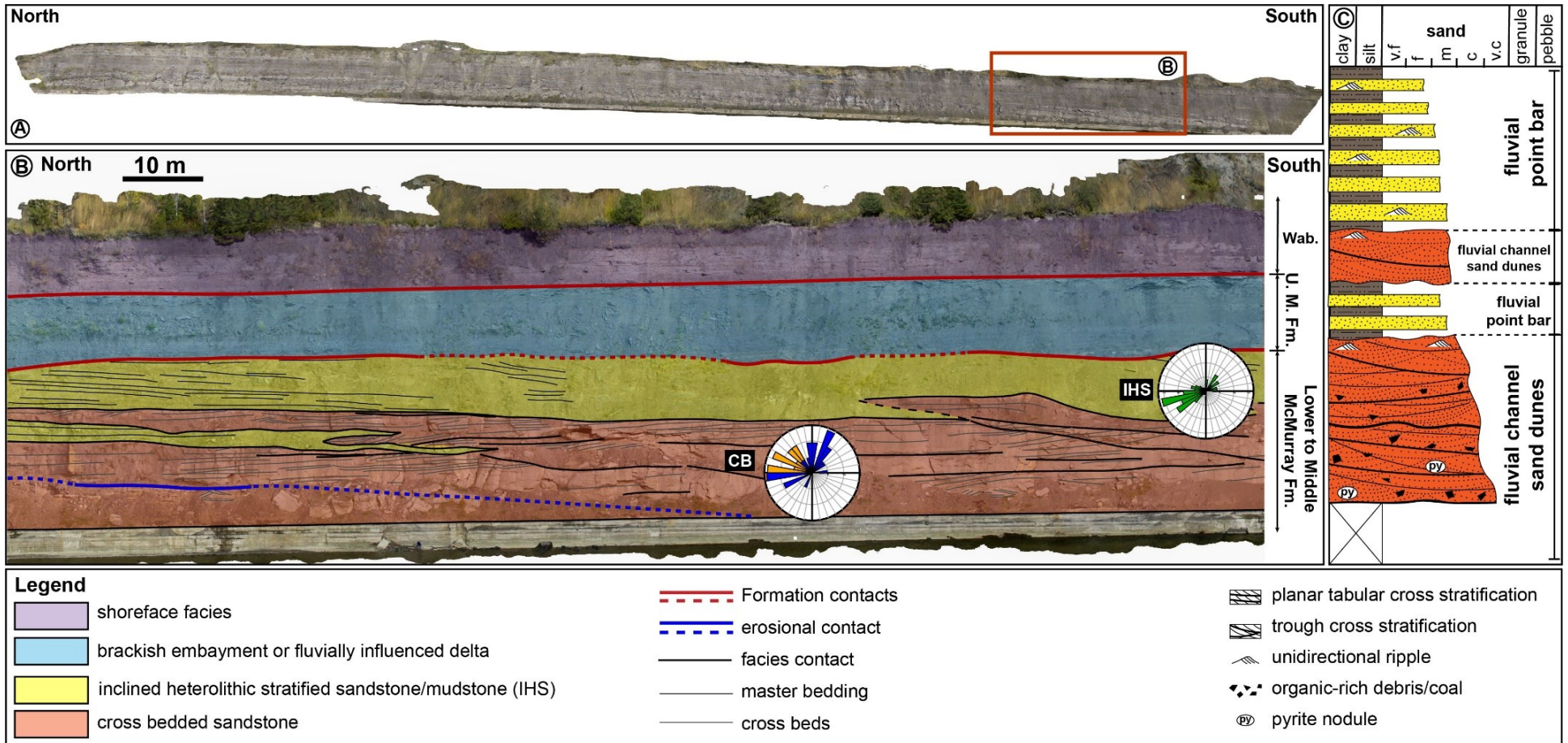
facies	bedding type	rose diagram	poles to bedding	bedding orientation	sedimentology & ichnology
Crooked Rapids IHS	lateral accretionary surfaces (LAS)	 N=76		<ul style="list-style-type: none"> lateral accretionary surfaces (LAS) consistently dip SW, and subordinate dataset is oriented NE. The LAS orientation indicates NW- or SE-oriented paleoflow direction. 	<ul style="list-style-type: none"> IHS beds are defined by alternating siltstone and coal local unidirectional flow ripples or climbing ripples IHS facies truncated by overlying CB facies, or by another IHS unit. trace fossils are absent
	cross beds (paleocurrent)	 N=121		<ul style="list-style-type: none"> cross beds preferentially oriented W-NW, indicating overall westward paleocurrent direction. 	<ul style="list-style-type: none"> dominated by trough cross stratification, gradually transit to planar tabular cross stratification towards top sharp contact with overlying IHS facies bed sets thicknesses range between 0.4m-1.3m minor centimetre scale pyrite nodules common coal fragments draped along foresets of cross beds current ripples common in planar tabular cross stratified sandstone interval. Trace fossils are absent
master bedding	 N=21		<ul style="list-style-type: none"> master beddings dip predominantly towards NE or WSW MB is oblique/orthogonal to paleocurrent direction. 		

Figure 5.7 A) Photogrammetric 3D model of the south end of Crooked Rapids outcrop. **B)** An interpreted zoom in section of the Crooked Rapids outcrop. Contact between CB sandstone unit and IHS unit can be traced across the outcrop model. Dashed lines represent gradational or inferred contacts. **C)** representative strip log of the north end of the interpreted section in B), showing fluvial point bar deposit overlies fluvial channel sand dunes.



Interpretation

In the CB unit, moderately high current energies are indicated by abundant dune-scale cross-stratification, which are capable of transporting centimetre-scale pyrite nodules and coal fragments. A general decrease in energy level is apparent from the progressive transition from trough and planar tabular cross-stratification to current ripple lamination towards the upper part of the section. This unit represents deposition under unidirectional flow. The bimodal master bedding orientations and their oblique relationship with sediment transport direction are consistent with migrating three-dimensional subaqueous sand dunes associated with lateral accretion. Master bedding planes commonly show lateral accretion characteristics in a fluvial channel. The general absence of trace fossils supports a freshwater-dominated, energetic depositional environment, wherein organisms did not colonize the substrate.

The overlying IHS unit is characterized by rhythmically arranged sandstone and siltstone couplets, indicating repetitive occurrence of autocyclic depositional mechanism (Thomas et al., 1987). The origin of IHS deposits in the McMurray Formation has been interpreted to reflect 1) shifting of the turbidity maximum due to fluctuation of fluvial discharge in tidally influenced marginal marine settings (e.g., Smith, 1988; Ranger and Pemberton, 1992); 2) differential sedimentation of high-stage and waning-stage of fluvial system (e.g., Hubbard et al., 2011; Jablonski and Dalrymple, 2016). However, the IHS at Crooked rapids is largely defined by beds that are sand versus organic-detritus rich. Flocculation does not seem to have been involved in the formation of these beds. The sedimentological and ichnological observations made at the Crooked Rapids Outcrop supports the later fluvial interpretation for the following reasons. Ichnologically, the IHS unit is completely devoid of bioturbation at Crooked Rapids, which is attributed to stressed colonization condition in point bars developed below the water line, with the exceptions of limited infaunal trace makers occurred from the top of mud-beds (Gingras *et al.*, 2016). Sedimentologically, each coarse-to-fine couplet is results largely from rapid 2-stage event sedimentation (Thomas et al., 1987; Gingras et al., 2016; Russell et al., 2018): 1) the thick, basal sandstone bed is deposited during high-stage fluvial discharge with rapid “dumping” of sediment; and 2) the relatively thinner mudstone bed is produced by short-lived waning flood-stage, which produce laminated, siltstone-dominated, organic-rich deposit from the remaining suspended load. Given its interfingering relationship with the underlying CB unit, the IHS is interpreted as the middle to the upper part of a fluvial point bar. Correspondingly, the CB

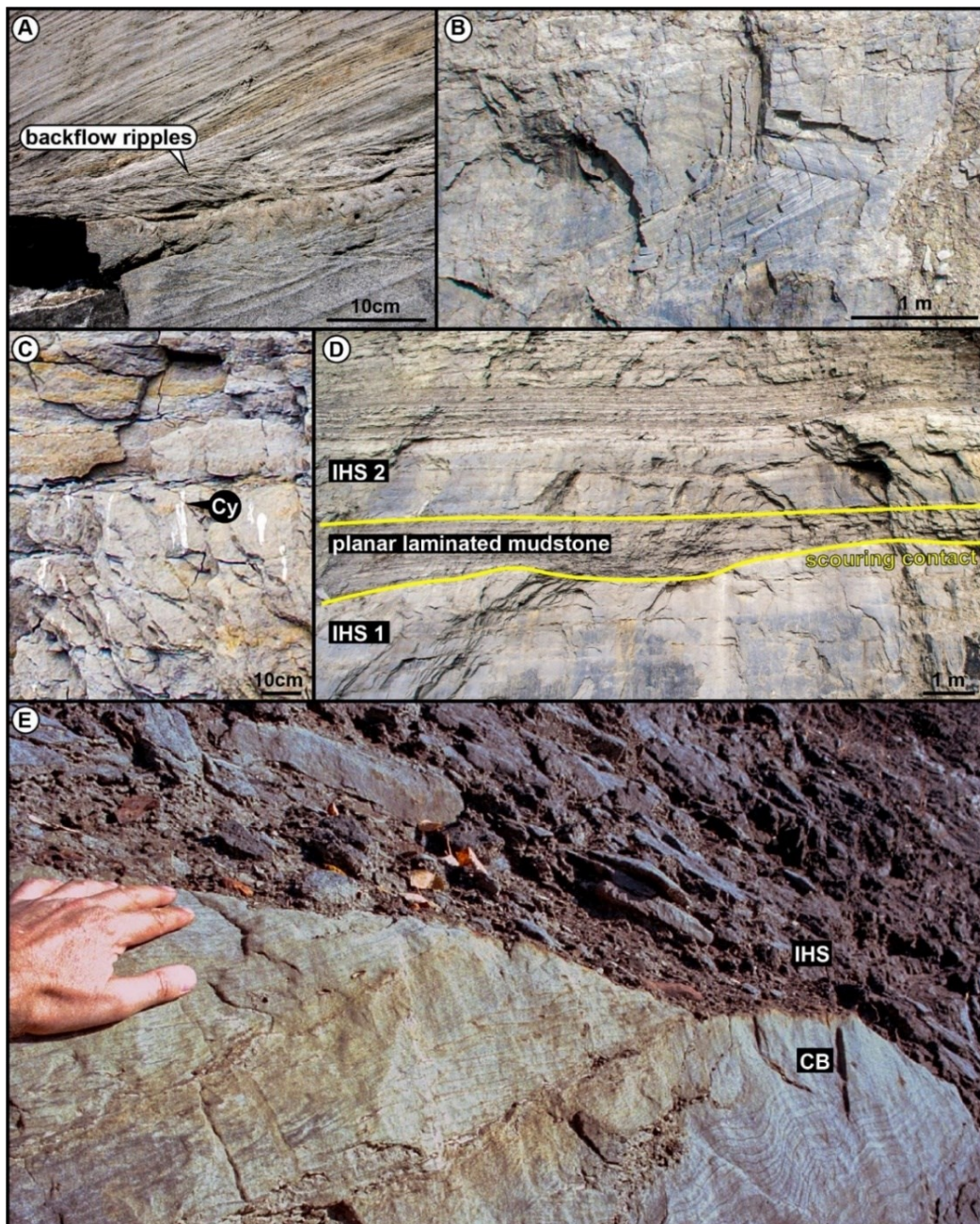
unit is interpreted as a fluvial lower point bar deposit. This interpretation is supported by bedding measurements as well. The consistently dipping LASs in the IHS unit show that the point bar is migrated in the SW direction, inferring NW- or SE-oriented paleocurrent direction in the channel. This inferred paleocurrent orientation is more or less consistent with what is measured in the underlying CB unit, indicating that the two units are genetically related. In addition, the consistently SW-dipping LAS in the IHS unit is the same as the W-oriented component of the master bedding planes in the CB, which also support the contention that the CB and IHS units belong to the same point bar succession. Alternatively, the bimodal characteristics of the CB unit (W and NNE oriented) suggest that at least part of the CB unit (with W-oriented master bedding planes) is actually part of the IHS. The IHS unit becomes sandier with depth, until it is entirely sand, presumably in the channel thalweg. The interfingering relationship between CB and IHS makes the actual contact between them very difficult to discern. Based on the above evidence, the CB and IHS are best interpreted as a genetically related fluvial channel deposit.

Tidally influenced fluvial deposits

Hangingstone #1 Outcrop

Hangingstone #1 exposes 30m of McMurray Formation, which is overlain by a 7m thick, heavily weathered undefined unit, glauconitic sandstone of the Wabiskaw C Member, and Quaternary deposits. The 3D outcrop model and an interpreted section of the outcrop are shown in Fig. 5.9. This outcrop displays four different facies: a basal cross-bedded sandstone (CB unit), two inclined heterolithic stratified sandstone/siltstone units (IHS1 and IHS2), and a planar laminated mudstone unit separating IHS1 and IHS2. The basal CB unit gradually transitions into the overlying IHS1 unit. Pseudo tadpole plots have been used to assist differentiation between the adjacent CB and IHS1 units. In the middle of the succession, a thin layer of planar laminated mudstone occurs, which is bound by sharp contacts with overlying and underlying IHS units. Figure 5.8 displays close-up photos of characteristic trace fossils and sedimentary observations at the outcrop. Bedding measurements associated with IHS and CB facies are summarized in Table 4. Rose plots of individual IHS units are also indicated in Fig. 5.9.

Figure 5.8 Detailed photos of common sedimentary and ichnological features identified at Hangingstone #1 and #2 outcrops. **A)** backflow ripples developed on top of a cross bed set at Hangingstone #1 outcrop. **B)** A sample section of CB sandstone unit showing successive bed sets with opposite dipping directions at Hangingstone #2 outcrop. **C)** A sample section of CB sandstone facies showing vertical tubular burrows of *Cylindrichnus* at Hangingstone #1 outcrop, observed in the lowermost IHS units that was buried by small scale slumping sediments at the time of photo acquisition. **D)** A zoom in section showing erosional contact within IHS facies at Hangingstone #1 outcrop. **E)** A zoom in section showing sharp contact between CB and IHS facies at Hangingstone #2 outcrop. Abbreviation: Cy-*Cylindrichnus*



Sedimentological and ichnological characteristics

The bottom part of the outcrop is characterized by trough and planar tabular cross stratified sandstone (CB sandstone unit). Its basal contact and underlying IHS facies unit are significantly obscured by covered section. The exposed 3m thick CB sandstone unit commonly shows divergent dip directions (Fig. 5.8B), and backflow ripples are locally preserved at the bases of cross-bed sets (Fig. 5.8A). Trace fossils are not observed, except in the lowermost IHS unit, below the interpreted CB unit at the Northeast end of the outcrop, where *Cylindrichnus* is locally present (Fig. 5.8C). At the time of photo dataset collection, the basal bioturbated units were buried by small-scale slumping of the outcrop.

The CB sandstone grades upward into IHS facies (IHS1 unit) and shows an overall decrease in bedding thicknesses coupled with slight increases in mudstone contents. IHS1 is capped by the planar-laminated mudstone, which is dominantly horizontally bedded. A second IHS succession (IHS2 unit) overlies the planar laminated mudstone unit. In comparing the two IHS units, it is apparent that the one above the mudstone unit shows a higher mudstone content and more gently dipping master bedding planes.

Bedding orientation characteristics

As shown in Table 4, bedding measurements of the basal CB unit preferentially show NE-dipping cross-beds, suggesting a NE-flowing channel. Master bedding planes within this unit are gently dipping and dominantly oriented NW, which is perpendicular to the cross-bed orientations. Both IHS units show predominantly SW-NW dipping lateral accretion surfaces. The dip angles of the LASs range from 0° to 20°. Comparing the two individual IHS units, IHS1 is dominated by WNW-dipping LAS orientations whereas those of the IHS2 unit are oriented slightly more WSW (see rose plots in Fig. 5.9). Paleocurrent directions inferred by the LAS surfaces are oriented NNW-NNE, which is consistent with measurements from the CB unit.

Table 5.4 Bedding orientation characteristics of the cross-bedded sandstone and IHS facies at Hangingstone #1 outcrop. The rose plots show dip directions of cross beds and master bedding. The pole to bedding plots show dip angle of cross beds and master beddings. The inferred paleocurrent flow direction (indicated by red arrows) is orthogonal to master beddings of IHS facies.

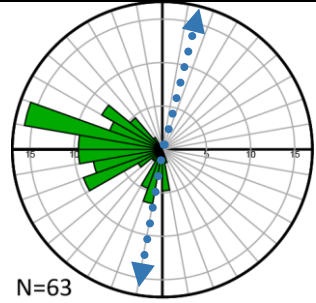
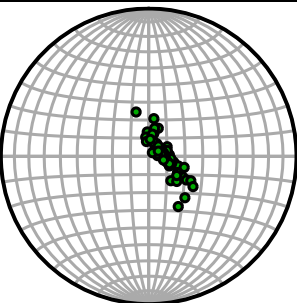
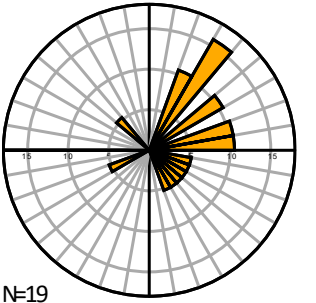
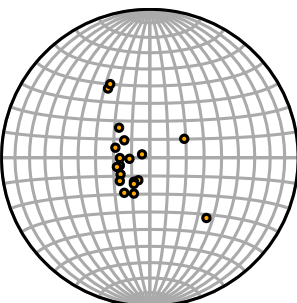
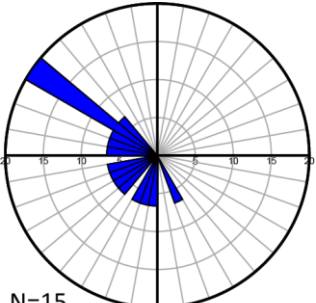
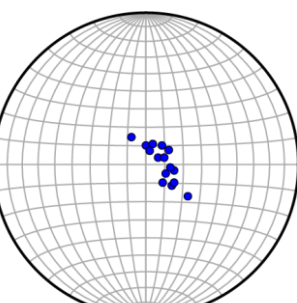
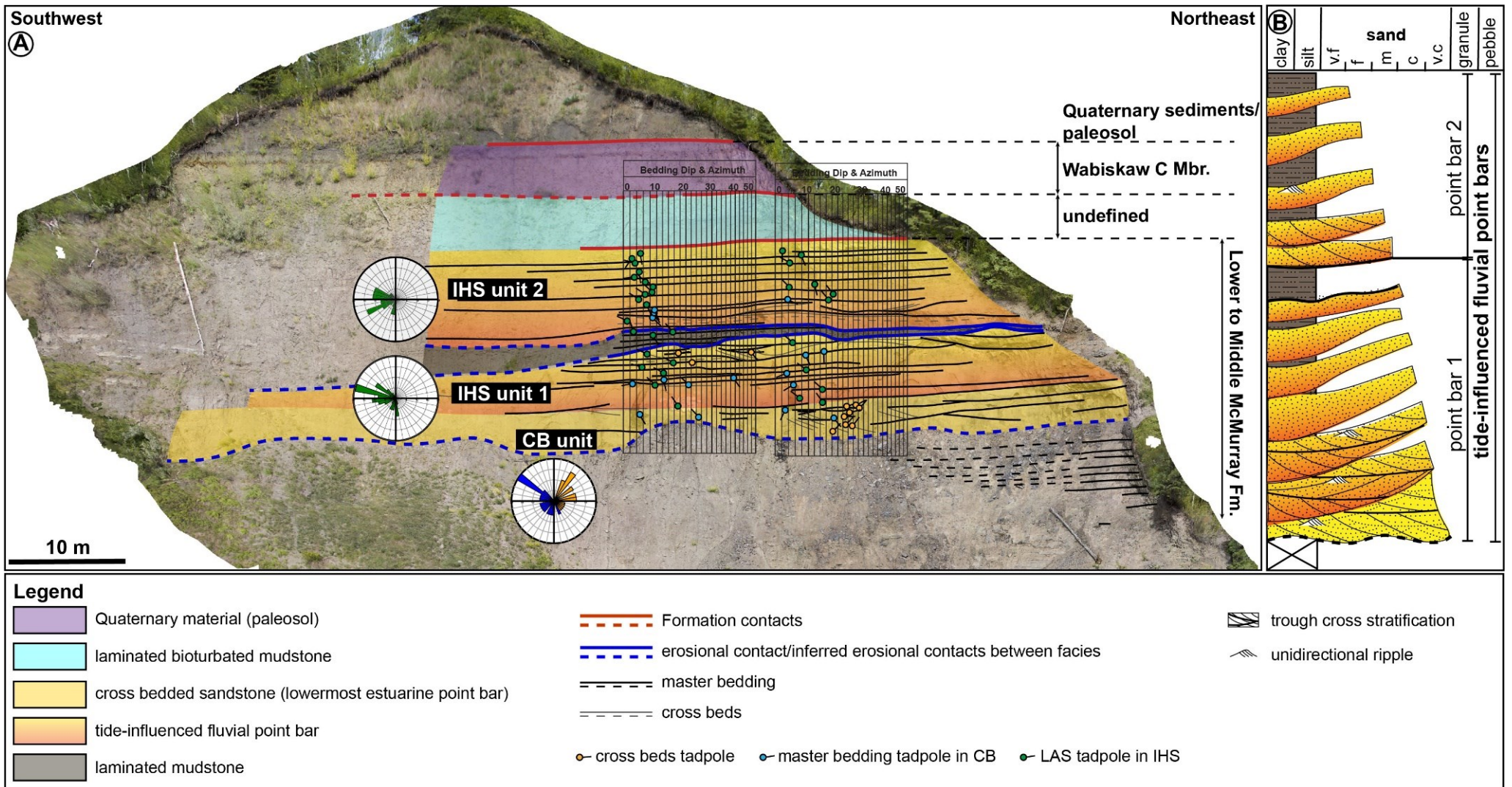
facies	bedding type	rose diagram	poles to bedding	bedding orientation	sedimentology & ichnology
Hangingstone #1 IHS 1&2	lateral accretionary surfaces (LAS)	 N=63		<ul style="list-style-type: none"> lateral accretionary surfaces (LAS) consistently dip NW, and subordinate dataset is oriented SSE. The LAS orientation indicates NNE- or SSW-oriented paleoflow direction which is consistent with paleocurrent measurement from CB facies. 	<ul style="list-style-type: none"> interbedded siltstone and mudstone defining IHS differentiation between LAS in sand-rich IHS and master beddings in CB is difficult. trace fossils are absent
	cross beds (paleocurrent)	 N=19		<ul style="list-style-type: none"> cross beds preferentially oriented NE, indicating overall northeastward paleocurrent direction. 	<ul style="list-style-type: none"> trough to planar tabular cross stratification gradational contact between CB and overlying IHS facies bed sets thicknesses range between 0.2m-1.1m common backflow ripples near the top of sand dunes trace fossils are absent
master bedding	 N=15		<ul style="list-style-type: none"> master beddings dip in variable direction ranges from 160°SE to 320°NW. 		

Figure 5.9 A) Photogrammetric 3D model of the Hangingstone #1 outcrop. Pseudo-tadpole plots in the diagram are used for reclassification of CB and IHS units. **B)** representative strip log of the interpreted section showing deposition of stacked two point bars in inner estuary setting.



Interpretation

The CB sandstone unit is interpreted as amalgamated 2D and 3D subaqueous sand dunes, based on the abundant planar tabular and trough cross-stratification. The divergently dipping cross-beds indicate that the sand dunes were accumulated within a channel. The gradational contact between the CB and IHS1 units implies that the two units are genetically related and represent a point bar deposit. The thinly alternating sandstone and siltstone intervals of the IHS signify deposition associated with two modes of sedimentation: a freshet-driven flow interval and a normal (non-flood) flow interval. Although we recognize that IHS can be associated with fluvial intervals (e.g., Crooked Rapids, above), the characteristics displayed at Hangingstone 1 (e.g., thinly bedded, regular in thickness, silt-dominated with rare organic detritus) signal a reduction of overall fluvial inflow. As such, we consider the IHS here to be indicative of a tidal back-water effect in spite of the absence of bioturbation in IHS1 and IHS2. This suggests that overall, the IHS were mainly deposited in freshwater condition.

The paleocurrent direction inferred by the IHS1 agrees with the measurements from the underlying CB unit, implying the CB and IHS1 were deposited within the same channel. Given its gradational relationship with the CB unit, IHS1 is interpreted as a middle point bar deposit. The CB unit, with similarly oriented master bedding planes, represents the lowermost point bar deposit in a tide-influenced fluvial channel lying landward of salt water incursion but within the tidal backwater zone. Master bedding planes of the IHS1 and IHS2 share similar dip orientations, which can be interpreted as one of the following scenarios: 1) the two IHS units represents two different successive point bar deposits that share similar lateral accretion directions; or 2) the two IHS units belong to the same point bar of a meander belt.

The planar laminated mudstone in the middle of the outcrop has an erosional basal contact, and is predominantly horizontally bedded. The mudstone unit is up to 1.9m thick at the outcrop. It is, in turn erosively truncated by IHS2. Given the sharp boundaries of the mudstone unit, it is best interpreted as a switch to fine-grained sedimentation following channel abandonment of IHS1. If so, two point bars (IHS1 and IHS2) share very similar lateral accretion directions, but are associated with different channels. However, the single point bar scenario cannot be entirely excluded based on current data. In particular, the dip angles of the LASs in the two IHS units decrease upward, which is a common characteristic of

continuous point bar deposition (Brekke et al., 2017; Chen et al., 2021). In this scenario, the mudstone unit would represent a fluvial freshet period that preserves a thicker mud bed in the IHS couplet.

Hangingstone #2 Outcrop

Hangingstone #2 outcrop is located 460m SW of the Hangingstone #1 outcrop. It exposes a 20m thick McMurray Formation section that is overlain by a 4m thick glauconitic sandstone interval of the Wabiskaw C Member. Quaternary-aged sediments occur near the top of the outcrop. The 3D outcrop model and an interpreted section of the outcrop are shown in Fig 5.10. The McMurray Formation interval displays a continuous depositional package, characterized by gradational transitions from a cross-bedded sandstone unit (CB) to an inclined heterolithic sandstone and siltstone unit (IHS). Sedimentary structures and bioturbation characteristics at the outcrop are very similar to those of the Hangingstone #1 outcrop (refer to Fig. 5.8 as examples). Bedding measurements associated with IHS and CB facies are summarized in Table 5 and Figure 5.10.

Sedimentological and ichnological characteristics

The basal CB succession is a 4-6m thick, trough and planar tabular cross stratified sandstone with locally observed divergently dipping cross beds. Backflow ripples commonly occur in the bottomsets of the cross beds. The basal contact of this unit is entirely covered by slumped sediments, and a sharp upper contact marks the abrupt transition from the CB to the overlying IHS unit (Fig. 5.8E). Trace fossils are absent in this unit.

The overlying IHS unit is approximately 5-7m thick and composed of alternating sandstone and siltstone beds. The proportion of sandstone *versus* siltstone beds decreases upward, which is commonly accompanied by declining bedding thicknesses. Current ripples are locally present in sandstone intervals. Similar to the IHS facies at Hangingstone #1, trace fossils are absent in the IHS unit here.

Bedding orientation characteristic

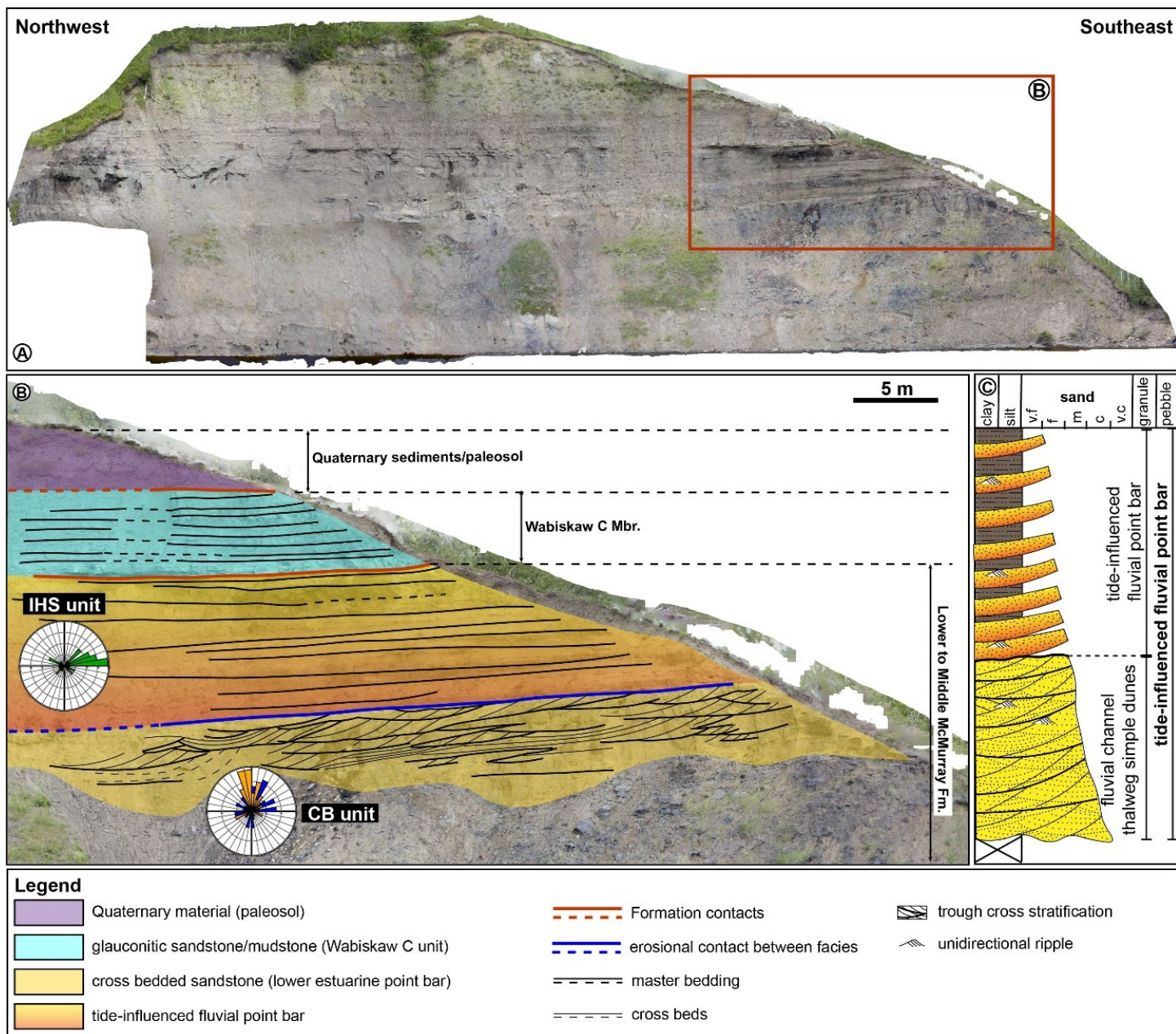
The cross beds in the sandstone unit show low- to high-angle dips that are consistently oriented in the NNW direction. Master bedding planes within this unit are variably oriented, and dip directions are strongest in the NNE-SSW and ENE-WSW directions. The overlying lateral accretion surfaces (LASs) are gently dipping (dominantly 0°-10°) and consistently dip towards the ENE with minor NW and SE

components of the dataset. The LASs of the IHS infer a NNW- or SSE-oriented sediment transport direction, which is consistent with measurements in the CB sandstone unit.

Table 5.5 Bedding orientation characteristics of the cross-bedded sandstone and IHS facies at Hangingstone #2 outcrop. The rose plots show dip directions of cross beds and master bedding. The pole to bedding plots show dip angle of cross beds and master beddings. The inferred paleocurrent flow direction (indicated by red arrows) is orthogonal to master beddings of IHS facies.

facies	bedding type	rose diagram	poles to bedding	bedding orientation	sedimentology & ichnology
Hangingstone #2 IHS	lateral accretionary surfaces (LAS)	<p>N=47</p>		<ul style="list-style-type: none"> lateral accretionary surfaces (LAS) consistently dip ENE, and subordinate dataset is oriented NW or SE. The LAS orientation indicates NNW- or SSE-oriented paleoflow direction which is consistent with paleocurrent measurement from CB facies. 	<ul style="list-style-type: none"> interbedded siltstone and mudstone defining IHS differentiation between LAS in sand rich IHS and master beddings in CB is difficult. trace fossils are absent
	cross beds (paleocurrent)	<p>N=47</p>		<ul style="list-style-type: none"> cross beds preferentially oriented NNW, indicating overall northward paleocurrent direction. 	<ul style="list-style-type: none"> trough to planar tabular cross stratification gradational contact between CB and overlying IHS facies bed sets thicknesses range between 0.2m-1.1m common backflow ripples near the top of sand dunes trace fossils are absent
Hangingstone #2 CB	master bedding	<p>N=35</p>		<ul style="list-style-type: none"> master beddings show random dipping orientations but show a preferred WSW-ENE and NNE-SSW trends. MB is perpendicular/oblique to paleocurrent direction 	

Figure 5.10 **A)** Photogrammetric 3D model of the Hangingstone #2 outcrop. **B)** An interpreted zoom in section of the Hangingstone #2 outcrop. **C)** representative strip log of the interpreted section in B), showing lateral accretionary deposit of point bar overlies inner estuary channel sand dunes. The exposed succession represents a single point bar deposit.



Interpretation

The interpretation of the CB and IHS units at Hangingstone #2 is similar to CB and IHS1 units at Hangingstone #1 outcrop. The McMurray Formation interval represents a continuous point bar of a tide-influenced fluvial channel. The key difference between the CB units observed at Hangingstone #1 and #2 is the orientation of master bedding planes. The master bedding planes of the CB at Hangingstone #2 show substantially more variability than do those at Hangingstone #1. The relationship between cross beds and master bedding planes at this outcrop shows both oblique and orthogonal components, and can be interpreted as migrating subaqueous sand dunes within the channel. Given the variable master-bedding dips in this example, the CB sandstone is not considered to be part of the lower point bar.

Along with the absence of bioturbation in the IHS unit, the sedimentary characteristics of this outcrop are very similar to that observed at Hangingstone #1 (e.g., thinly bedded sandstone/siltstone beds that lack coarse grain sizes, and the general absence of trace fossils). This indicates reduced fluvial influence and likely reflects a tidal back-water effect within the lower fluvial setting, representing a transitional setting between fluvial and estuarine environments. Although the two Hangingstone outcrops are only 460m apart from one other, the LASs of IHS units dip in opposite directions (westward at Hangingstone #1 and eastward at Hangingstone #2). This observation suggests that similar facies units at the two outcrops cannot be simply correlated in spite of their close geographic locations.

Inner estuary point bars and compound dune complex

Christina River Outcrop

At Christina River, five depositional units are recognized at the outcrop: two cross-bedded sandstone units (CB1 and CB2 units) and three IHS units (IHS1, IHS2, and IHS 3 units). The interpreted 3D outcrop model is shown in Fig. 5.12. All depositional units are characterized by sharp basal and upper contacts. The basal succession of the Christina River outcrop is dominated by a thick, cross-bedded sandstone (CB1), which can be continuously traced over 300m along the river bank. The upper succession of the outcrop is composed of stacked IHS units. A thin CB2 unit present in this succession separates IHS1 and IHS2 in the west, and gradually pinches out towards the east end of the outcrop. Sedimentary structures

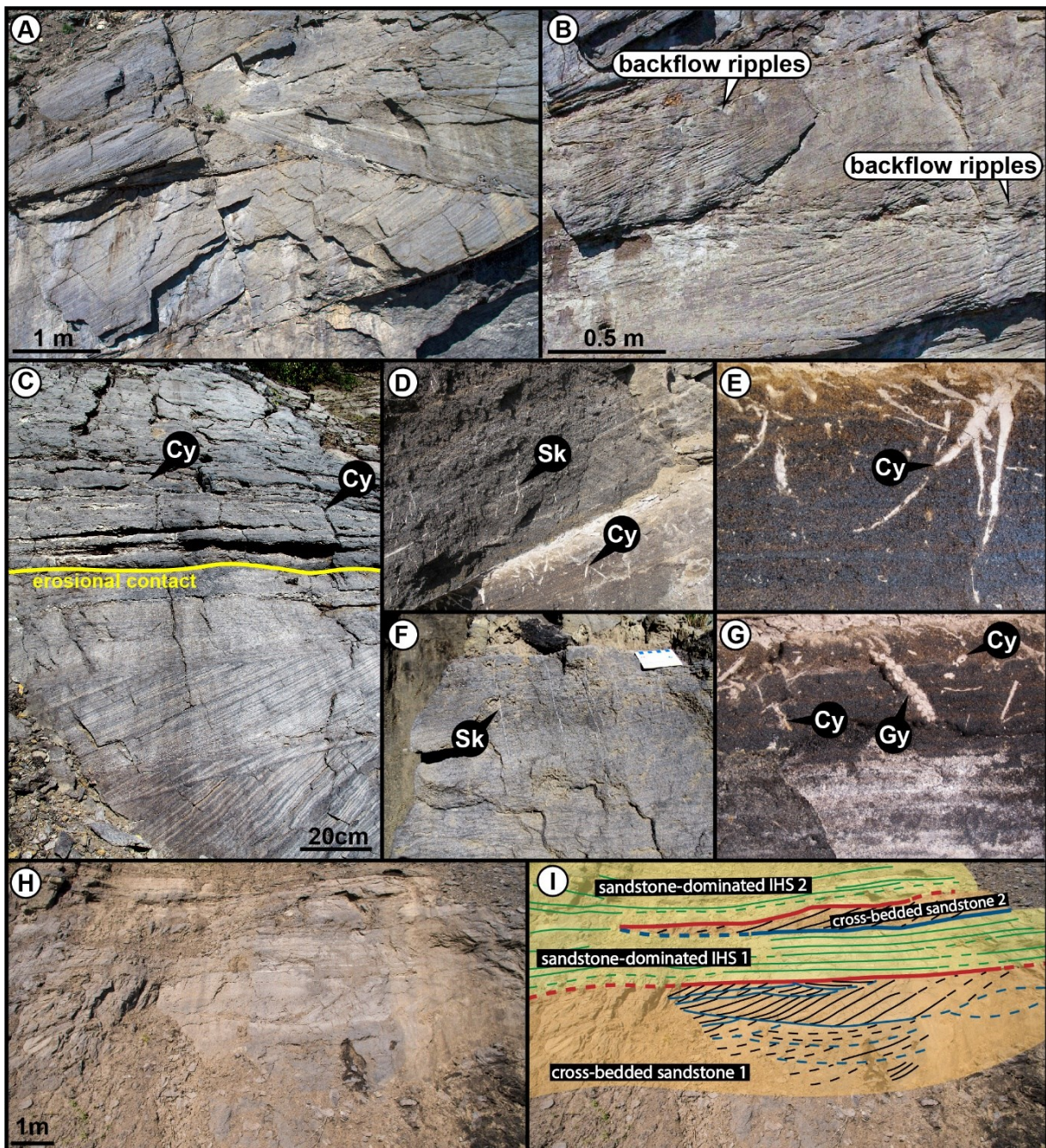
and trace fossils examples are displayed in Fig. 5.11, and bedding measurements associated with IHS and CB facies are summarized in Table 6. Rose plots of individual depositional units are labeled on the outcrop model in Fig. 5.12.

Sedimentological and ichnological characteristics

The lowermost CB1 unit is best exposed at the west end of the outcrop. CB1 unit is composed of an approximately 15m thick, trough and planar tabular cross-stratified sandstone. CB1 is correlatable across the outcrop, but its basal contact is entirely covered by weathered sediments. The facies is dominated by decimetre- to metre-scale trough and planar tabular cross-stratification. The topsets of cross beds are commonly truncated by successive cross-bed sets, and adjacent cross-beds locally show divergent dip directions (Fig. 5.11A). Centimetre-scale unidirectional backflow ripples are confined to the bottomsets of cross beds (Fig. 5.11B), and organic-rich debris is preferentially concentrated along the tangential bases of these bottomsets. Bioturbation is absent to rare in the CB facies. *Cylindrichnus*, *Skolithos*, and *Gyrolithes* locally subtend from mudstone beds near truncated surfaces of cross-bed sets (Fig. 5.11D, E, F, and G). The *Skolithos* are present as vertical burrows up to 30cm long. The CB2 unit shares similar sedimentary and ichnological characteristics as CB1, but shows much thinner bed thicknesses that are dominated by decimetre-scale planar tabular cross-stratification.

The CB units (CB1 and CB2) are abruptly overlain by inclined heterolithic sandstone and siltstone units (IHS1, IHS2, and IHS 3). These IHS units contain common, diminutive *Cylindrichnus*, *Skolithos*, and *Planolites*. Minor *Teichichnus* and monospecific *Gyrolithes* have also been reported from this interval by previous workers (Gingras et al., 2016). Bioturbation is significantly more common in mudstone (BI 3) than in sandstone intervals (BI 0-1). In sandstone intervals of IHS units, unidirectional ripples are common. Each IHS unit is characterized by an upward decrease in bioturbation intensity and an increase in mudstone content. Bedding thicknesses also decrease towards the top of each IHS unit. The sharp contact between CB1 and IHS1 can be traced across the outcrop (Fig. 5.12), and close-up photos are shown in Fig. 5.11C, H, and I. Distinct IHS units are identified at the outcrop based on: 1) sharp basal contacts of IHS units; 2) erosional contacts separating IHS units with distinct dipping orientations.

Figure 5.11 Detailed photos of common sedimentary and ichnological features identified at Christina River outcrop. **A)** A sample section of CB sandstone unit showing successive bed sets with opposite dipping directions. **B)** Backflow ripples developed on top of a cross bed set in the CB sandstone facies. **C)** Metre-scale trough cross-bedded sandstone is erosionally overlaid by IHS facies. **D)** Skolithos and Cylindrichnus identified in CB sandstone facies. Note Cylindrichnus traces originate from mudstone layer and descend into underlying sandstone. **E)** zoom in photo of Cylindrichnus in CB sandstone facies. **F)** zoom in photo of Skolithos in CB sandstone facies. **G)** zoom-in photo of Gyrolithes and Cylindrichnus in IHS facies. **H)** Uninterpreted section showing CB and IHS units. **I)** Interpretation of H) showing stacked cross-bedded sandstone and IHS units separated by sharp contacts. Abbreviations: *Cy*-*Cylindrichnus*, *Sk*-*Skolithos*, *Gy*-*Gyrolithes*.



Bedding orientation characteristics

The CB1 unit extends 200m to the west. To maximize the number of bedding measurements in this unit, this extended section is also included in the bedding orientation analysis. Cross beds of the CB1 unit consistently dip in the SW direction, with a subordinate NE-dipping subset of the data (Table 6). The poles to cross-beds show low- to high-angle dips that range from 0° to 40°. Master bed planes occur as boundaries between cross-bed sets and display strong unimodal characteristics oriented in the WNW direction. Dip angles of these master bedding planes are generally <30°. The measured master bedding planes show an oblique to subparallel relation to the cross-bed orientations. The CB2 unit shows slightly more variable dip orientations, which range between the WSW to NW directions. The master bedding planes of CB2 are also variable, but show a dominant NW-oriented dip. The master bedding planes of CB2 are oblique or orthogonal to its cross-bed orientations.

The master bedding planes of the IHS units represent lateral accretion surfaces (LASs), which clearly show a unimodal NW-oriented direction. These LASs are horizontal to gently dipping (0°-15°) and infer a SW- or NE-oriented paleocurrent direction, which is parallel to the strike of the LASs.

Table 5.6 Bedding orientation characteristics of the cross-bedded sandstone and IHS facies at Christina River outcrop. The rose plots show dip directions of cross beds and master bedding. The pole to bedding plots show dip angle of cross beds and master beddings. The inferred paleocurrent flow direction (indicated by red arrows) is orthogonal to master beddings of IHS facies.

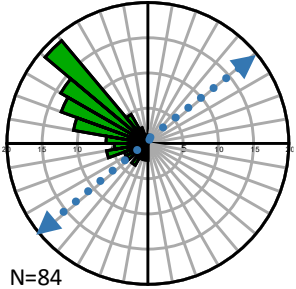
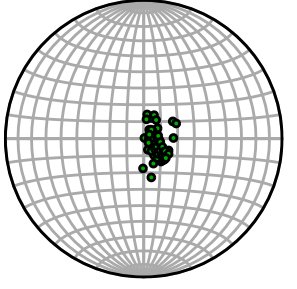
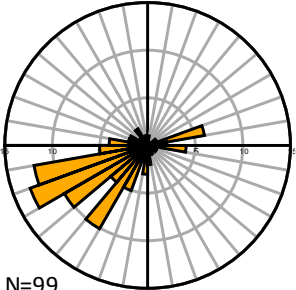
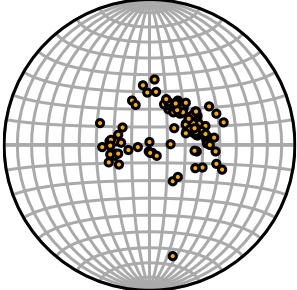
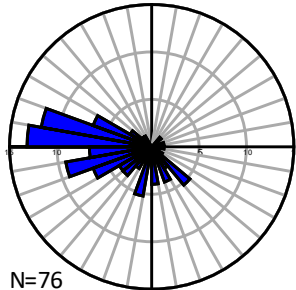
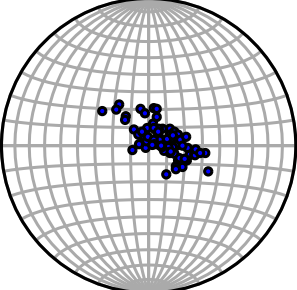
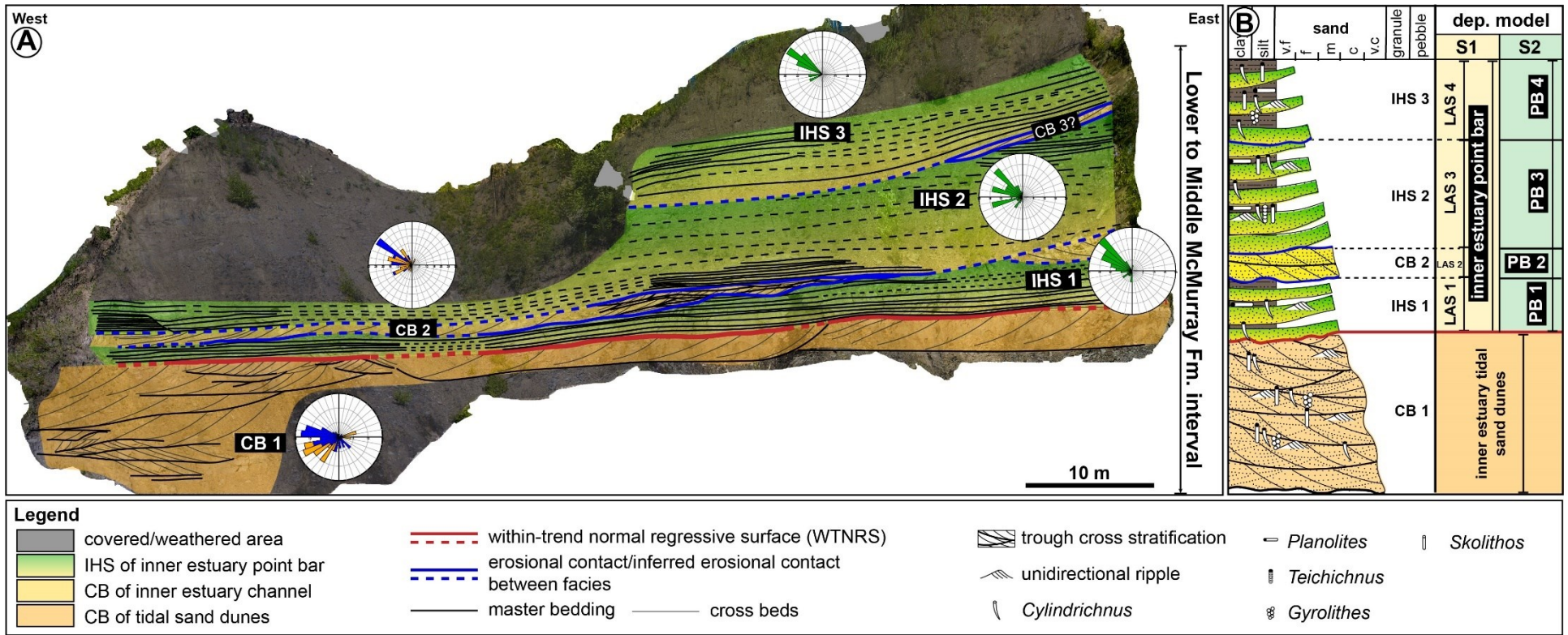
facies	bedding type	rose diagram	poles to bedding	bedding orientation	sedimentology & ichnology
Christina River IHS	lateral accretionary surfaces (LAS)	 <p>N=84</p>		<ul style="list-style-type: none"> lateral accretionary surfaces (LAS) consistently dip NW, and minor subordinate dataset is oriented W-NW. LAS orientation indicates NE or SW paleoflow direction 	<ul style="list-style-type: none"> interbedded sandstone and mudstone defining IHS common unidirectional ripples in sandstone intervals. IHS facies truncated by overlying CB facies or by another IHS unit. brackish-water trace fossils include: <i>Planolites</i>, <i>Teichichnus</i>, <i>Cylindrichnus</i>, <i>Skolithos</i> and monospecific <i>Gyrolithes</i> (Gingras et al., 2016).
	cross beds (paleocurrent)	 <p>N=99</p>		<ul style="list-style-type: none"> cross beds preferentially dip SW, indicating sediments transported by NNW oriented paleocurrent. 	
Christina River CB	master bedding	 <p>N=76</p>		<ul style="list-style-type: none"> master beddings dip consistently towards NW and SE, oblique to paleocurrent direction. 	<ul style="list-style-type: none"> trough to planar tabular cross stratification common flow reversals indicated by oppositely dipping cross beds common back/reverse flow ripples sharp contact with overlying IHS facies bed sets thicknesses range between 0.2m-1.5m brackish-water trace fossil assemblage characterized by <i>Cylindrichnus</i>, <i>Skolithos</i>, and <i>Gyrolithes</i>.

Figure 5.12 A) Photogrammetric 3D model of the Christina River outcrop. Dash lines represent inferred interpretations. Note rose plots of individual units are indicated in the diagram. **B)** representative strip log of the interpreted section with proposed depositional models. Abbreviations: EM-end member, LAS-lateral accretionary set, CB-cross bedded sandstone, IHS-inclined heterolithic stratified sandstone/mudstone.



Interpretation

The cross-bedded sandstone consisting of metre-scale trough and planar tabular cross-stratification are interpreted as subaqueous sand dunes. A nearly unidirectional paleocurrent direction is indicated by the consistent dip to the cross beds. Backflow ripples near the bottom of cross bedsets are the result of vortex flow in the trough of sand dunes, wherein the near-bed backflow direction is opposite to the dominant current flow (Martinius et al., 2015). The dominance of trough cross stratification and the general paucity of bioturbation result from rapid depositional rates and shifting sediments. The upward thinning of cross-bed sets, and increasing abundance of current ripples suggest a gradual decrease of flow energy, which is consistent with the expected characteristics of fluvial- and tidal-channel deposition. *Cylindrichnus*, *Skolithos*, *Gyrolithes*, and *Planolites* constitute common dwelling burrows, and are indicative of brackish-water conditions (e.g., Pemberton et al., 1982; Wightman et al., 1987; MacEachern and Gingras, 2007; Gingras et al., 2016). The brackish-water trace fossil assemblage also supports a depositional environment characterized by tidal transport, such that marine larvae were advected to the sedimentary locale. In addition, such a tidal-influenced interpretation also agrees with the quantitative measurement of tidal cyclicity at the same outcrop by Hayes et al. (2017). Their study measured strong periodic cycles that occurred at periods of approximately 33 and 56 foresets in dunes, which strongly supports an interpretation of semi-diurnal synodic deposition at this locale. Overall, the sedimentology and ichnology of the CB facies suggest that the cross-bedded sandstone either represents thalweg-associated compound dunes or subaqueous sand dunes of tidal bars. These two settings share very similar sedimentological and ichnological characteristics; therefore, distinguishing between them depends on their internal bedding architectures. Thalweg-associated compound dunes in tidally influenced meander belts are expected to have cross beds oriented almost parallel to the strike of the lateral-accretion master bedding planes. By contrast, subaqueous sand dunes of middle estuary tidal bars are characterized by somewhat oblique relationships between master bedding planes and cross-bed orientations, since oblique or forward accretion is predominant (Olariu et al., 2012). The bedding configuration of the CB1 unit shows clear oblique- to forward-accretion characteristics, and so is more consistent with a subaqueous tidal dune interpretation. The CB2 unit shows a similar oblique relationship between the master bedding planes and the cross beds; however, the more variable master bedding

plane orientations are more consistent with a channelized setting. CB2, therefore, is interpreted to record thalweg-associated compound dune deposits.

The IHS facies is characterized by gently dipping, alternating sandstone and siltstone intervals. The heterolithic lithology signifies an episodic or seasonal depositional style: alternating freshet- and base flow periods of a river. The distribution of the trace fossils indicates regular variations in fluvial outflow. The increased abundance of trace fossils in the mudstone beds symbolizes the base flow conditions of the river. The diminutive size of the ichnogenera and low diversity of the suite are characteristic of brackish-water conditions. Based on the sedimentary and ichnological characteristics, the gently dipping, IHS facies is interpreted as an inner estuary point-bar deposit. In such depositional setting, the sand beds of the IHS represent the freshet discharge of the river, and the mud beds correspond to base flow conditions when brackish water was able to penetrate the system and tidal flux are able to affect the overall deposition. Such an interpretation sets the underlying CB1 unit as a distinct depositional package that is not genetically related to the overlying IHS units. The contact between the two unit is erosional, separating the underlying middle estuary sand dunes of tidal bars from the overlying inner estuary point-bar deposit. It has been defined as a within-trend normal regressive surface (WTNRS; Catuneanu, 2006) that occurs as an internal discontinuity within a system tract. Master bedding planes of all IHS units show a strong consistency (uniformly dipping to the NW), which suggest one of the following architectural interpretations (depositional models are also summarized in Fig. 5.12B): 1) these units are associated with the same point bar; or 2) multiple channel events shared similar flow directions over time. In the former scenario, the IHS units can be interpreted as stacked lateral accretion sets of a single point bar, separated by intra-point bar erosional surfaces. This interpretation best explains their common dip orientation. The latter scenario suggests that they record four distinct packages, which better explains the erosional contacts, bioturbation pattern, and bedding thickness variations observed in each unit. Both scenarios are reasonable interpretations, based on the available data at the outcrop. Their consistent dip orientations would, therefore, be coincidence. More details about the *pseudo* dipmeter logs and two depositional models are discussed in Chen et al., (2022a).

Amphitheatre Outcrop

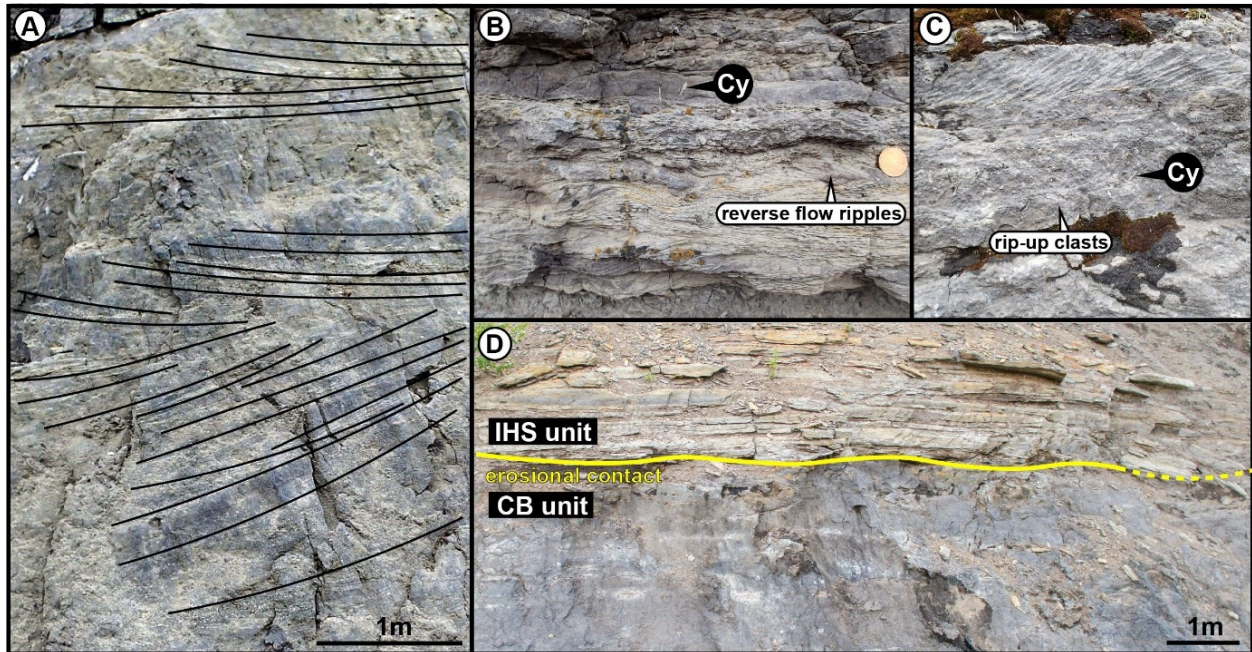
Figure 5.14 shows an interpreted section of the Amphitheatre outcrop. The McMurray Formation exposed at this location is composed of three depositional units: 1) a basal cross-bedded sandstone unit (CB) sharply overlain by 2) an inclined heterolithic unit (IHS1) comprising interbedded siltstone and sandstone, which grades into 3) a flat-lying, thinly bedded, siltstone-dominated horizontally stratified unit (HS 2). HS 2 is erosionally truncated and overlain by Quaternary-aged sediment. Examples of sedimentary and ichnological characteristics at the outcrop are presented in Figure 5.13, and orientation measurements associated with IHS and CB facies are summarized in Table 7.

Sedimentological and ichnological characteristics

The CB unit is characterized by 10m-15m thick, thinly to thickly bedded trough and planar tabular cross-stratified sandstone. Bedding thicknesses range from 0.1-1.0m and gradually thin upwards. Locally, the cross-bed sets are oriented in divergent directions (Fig. 5.13A). Other common sedimentary structures include backflow current ripples (Fig. 5.13B) near the bottomsets of large-scale cross beds, and sporadically distributed mudstone rip-up clasts (Fig. 5.13C). Bioturbation in this unit is dominated by *Cylindrichnus* (Fig. 5.13B and C). Rare *Siphonichnus* has been reported by previous workers (Hayes *et al.*, 2018). In general, the bioturbation index of this unit ranges between BI 1 to 3.

The CB sandstone unit is abruptly overlain by the IHS sandstone and siltstone unit. This contact is characterized by an undulatory surface that can be traced across the outcrop (Fig. 5.13D). This unit exhibits low to moderate but highly variable intensities of bioturbation (BI 1-4), with occurrences of sporadically distributed *Cylindrichnus* and *Planolites* (Hayes *et al.*, 2018). The overlying thinly bedded siltstone-dominated IHS2 unit is characterized by a uniform distribution of trace fossils and moderate levels of bioturbation intensity (BI 4). The suite comprises *Gyrolithes*, *Planolites*, and *Cylindrichnus*. The contact between IHS1 and HS1 appears to be gradational; however, the transition between the two is commonly covered by scree.

Figure 5.13 Detailed photos of common sedimentary and ichnological features identified at Amphitheatre outcrops. **A)** A sample section of CB sandstone unit showing successive bed sets with reversed dipping directions at Amphitheatre outcrop. **B)** A sample section of CB sandstone facies showing reverse flow ripples and *Cylindrichnus* burrows. **C)** A sample section of CB sandstone facies showing rip-up clasts and *Cylindrichnus*. **D)** A zoom in section showing concavo-convex erosional contact between basal CB sandstone unit and overlying IHS unit. Abbreviation: Cy-*Cylindrichnus*.



Bedding orientation characteristics

The basal CB unit is characterized by gently to steeply dipping (0° - 40°), randomly oriented cross-beds with a preferred northward direction that primarily ranges between NW and NE. Master bedding planes show bimodal characteristics in both the SW and SE directions. The orientation relationships between master bedding planes and cross beds include both subparallel and orthogonal components (Table. 7). Lateral accretion surfaces (LASSs) in IHS1 are near horizontal (dominantly 0 - 10°) and dip toward the SSW and the SSE. The paleoflow direction inferred by the LASSs indicates an east or west paleoflow direction.

Table 5.7 Bedding orientation characteristics of the cross-bedded sandstone and IHS facies at Amphitheatre outcrop. The rose plots show dip directions of cross beds and master bedding. The pole to bedding plots show dip angle of cross beds and master beddings. The inferred paleocurrent flow direction (indicated by red arrows) is orthogonal to master beddings of IHS facies.

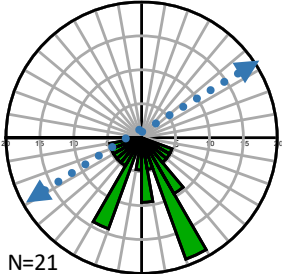
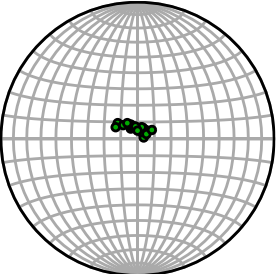
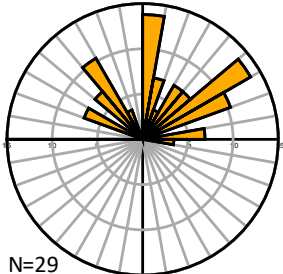
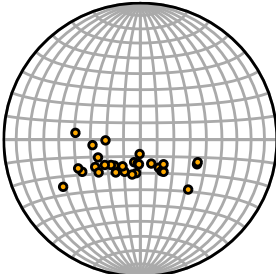
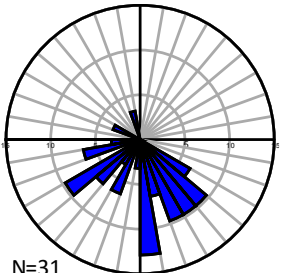
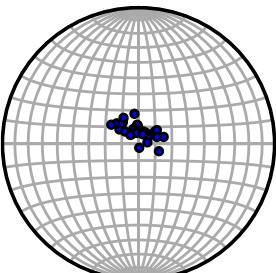
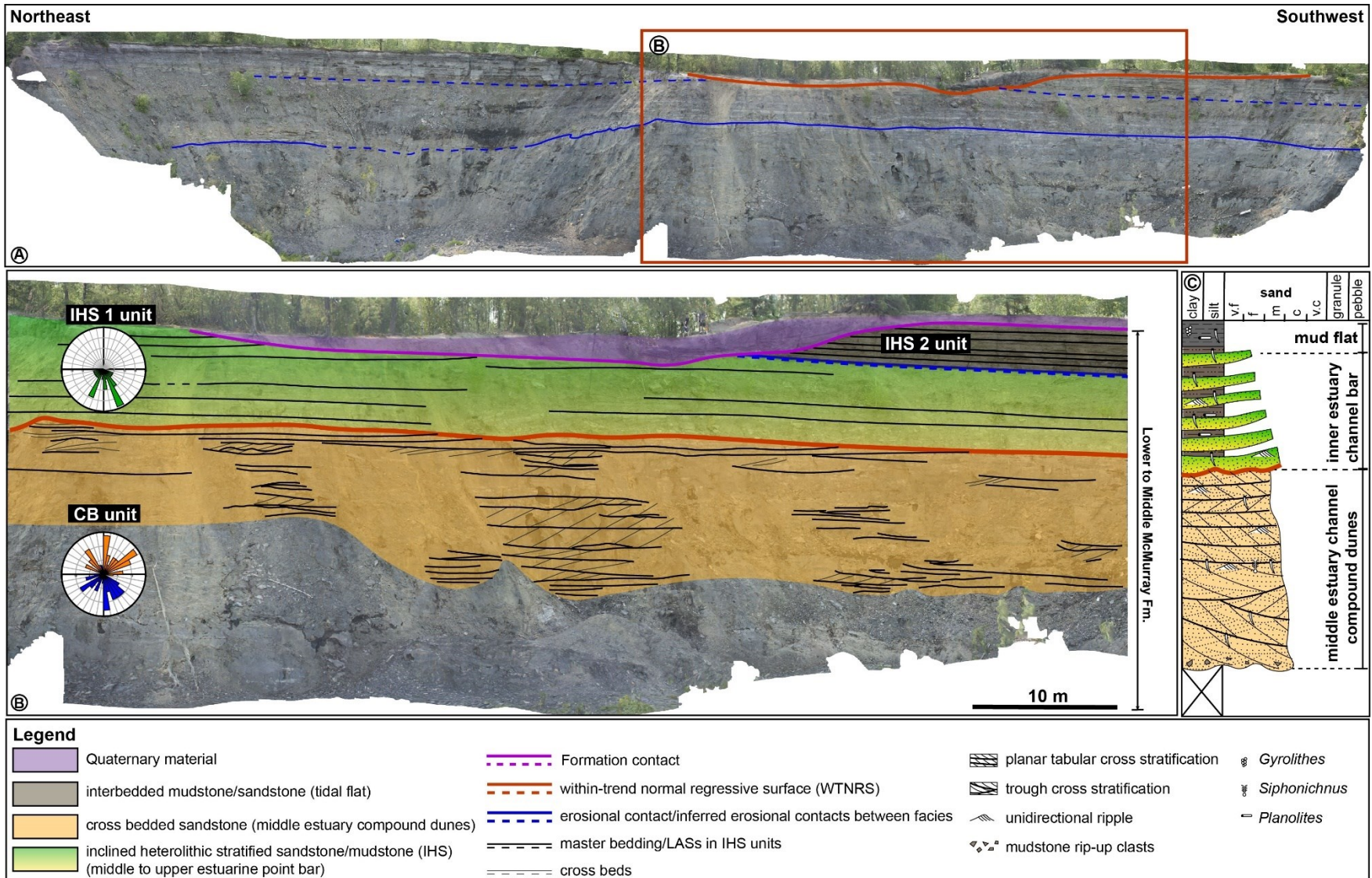
facies	bedding type	rose diagram	poles to bedding	bedding orientation	sedimentology & ichnology
Amphitheatre IHS 1	lateral accretionary surfaces (LAS)	 N=21		<ul style="list-style-type: none"> • lateral accretionary surfaces (LAS) consistently dip SE-SW. • The LAS orientation indicates NE- or SW-oriented paleoflow directions, which is partially consistent with paleocurrent measurement from CB facies. 	<ul style="list-style-type: none"> • interbedded sandstone and mudstone defining IHS • common brackish-water trace fossils include: <i>Cylindrichnus</i>, <i>Skolithos</i>, <i>Planolites</i> and <i>Gyrolithes</i> are also documented in Hayes et al., (2018) at the same outcrop.
Amphitheatre CB	cross beds (paleocurrent)	 N=29		<ul style="list-style-type: none"> • cross beds dips randomly between NW to NE orientation, NE direction is slightly more dominant. • indicating overall northward paleocurrent direction. 	<ul style="list-style-type: none"> • trough to planar tabular cross stratification • common flow reversals indicated by oppositely dipping cross beds • common back/reverse flow ripples • local rip-up breccia • sharp contact with overlying IHS facies • bed sets thicknesses range between 0.1m-0.8m • brackish-water trace fossil assemblage characterized by <i>Cylindrichnus</i> and rare <i>Siphonichnus</i> (Hayes et al., 2018).
	master bedding	 N=31		<ul style="list-style-type: none"> • master beddings show no preferred orientation, two datasets show dominance of W and SE directions. 	

Figure 5.14 **A)** Photogrammetric 3D model of the Amphitheatre outcrop. **B)** An interpreted zoom in section of the Amphitheatre outcrop. **C)** representative strip log of the interpreted section in B), showing lateral accretionary deposit of point bar overlies middle/outer estuary channel compound dunes. The contact between the two units represents a regressive surface of erosion.



Interpretation

The dominance of trough and planar tabular cross-stratification, localized rip-up clasts, and the uniformly northward dipping cross beds in the CB unit are consistent with a subaqueous sand dune architecture. The measured cross-bed thicknesses range from 0.1m-1m. The low-diversity trace fossil assemblage comprising of *Cylindrichnus* and rare *Siphonichnus* is indicative of brackish-water conditions. Compared with CB facies observed at other McMurray outcrops, master bedding plane and cross-bed orientations at the Amphitheatre outcrop show more variability, which is consistent with the expected characteristics of 3D dunes rather than 2D dunes (Dalrymple, 1984; Longhitano *et al.*, 2014). Importantly, based on cross-bed orientations, the sediment transport direction is subparallel to the master bedding planes, which excludes the possibility of a laterally accreted point bar interpretation. The sand dunes appear to have migrated up the master bedding surfaces, which is best interpreted as the upcurrent side of a forward-accreted compound dune deposit (Olariu *et al.*, 2012; Hayes *et al.*, 2018). The oblique arrangement of the master bedding planes with respect to the cross bedding is a common result of flow separation and lateral drifting of currents in the troughs of large-scale sand dunes (Longhitano *et al.*, 2014). Given the above bedding architectures and sedimentary observations, the CB unit at the Amphitheatre outcrop is interpreted to represent a forward-accreted, large-scale compound dune deposit in a middle estuary environment.

The overlying IHS units (IHS1 and IHS2) show similar characteristics to the tide-influenced point bars observed in previous outcrop examples. The LASs of IHS1 consistently dip southward, which suggests an east- or west-oriented paleocurrent. This inferred paleocurrent orientation is not consistent with the sediment transport direction identified in the CB unit. This suggests that the CB and IHS units are not genetically related depositional packages. The overall increase in bioturbation intensity from IHS1 to IHS2 suggests a continuous estuary point bar deposit that ultimately grades into horizontally stratified and pervasively bioturbated intertidal flat deposits (Gingras *et al.*, 2016). As such, the best interpretation of the Amphitheatre outcrop is a basal northward-migrating middle estuary compound dune unit, which was truncated by an inner estuary channel that migrated into the locale and shoaled to intertidal levels. The contact between CB and IHS1 is interpreted as a within-trend normal regressive surface (WTNRS; Catuneanu, 2006), which has also been identified previously at Christina River Outcrop.

DISCUSSION

The outcrops described above display sedimentary and architectural characteristics of four important McMurray Formation depositional environments: 1) fluvial environments (e.g., Daphne Island and Crooked Rapids); 2) tide-influenced fluvial environments (e.g., Daphne Island, Hangingstone #1 and #2); 3) inner estuary channel-point bar environments (e.g., IHS of Christina River and Amphitheatre); and 4) middle estuary tidal compound dune environments (e.g., CB of Christina River and Amphitheatre). Schematic diagrams showing the internal architectural differences among the four types of deposits are shown in Figure 5.15. The identification of each type of deposit requires both facies (sedimentological and ichnological characteristics) and architectural analyses of the dominant facies (CB and IHS facies units) at each outcrop locale. In the following section, synthesized sedimentological and architectural characteristics are provided for each type of deposit in the fluvial to estuary settings. A schematic diagram showing the distribution of subenvironments in a macrotidal estuary is shown in Figure 5.16. Estimated locations of deposits observed at studied outcrops are also indicated. Representative lithologs of studied outcrops are shown in Figure 5.17A and rose plots of CB and IHS facies at each outcrop are presented in Figure 5.17B. In addition, the Steepbank # 3 is another well-known McMurray Formation outcrop that has been studied in detail by Hayes et al. (2017). The physiographic location of its CB and IHS geobodies are also indicated in Figure 5.17B. Readers are directed to their paper for detailed sedimentological, ichnological, and bedding orientational analysis of the McMurray Formation at the Steepbank #3 outcrop.

Figure 5.15 The internal architectural difference between bar forms. **A)** Plan-view morphology of a fluvial point bar indicating major surfaces dipping orientation relative to the fluvial current; **B)** Plan-view morphology of an inner estuary point bar indicating major surfaces dipping orientation relative to fluvial and minor tidal currents; **C)** Plan-view morphology of a middle estuary longitudinal tidal dunes indicating migration direction of sand dunes relative to tidal currents; **D)** Flow-transvers view of a fluvial or estuary point bar; **E)** Flow-parallel cross sectional view of large-scale tidal sand dunes.

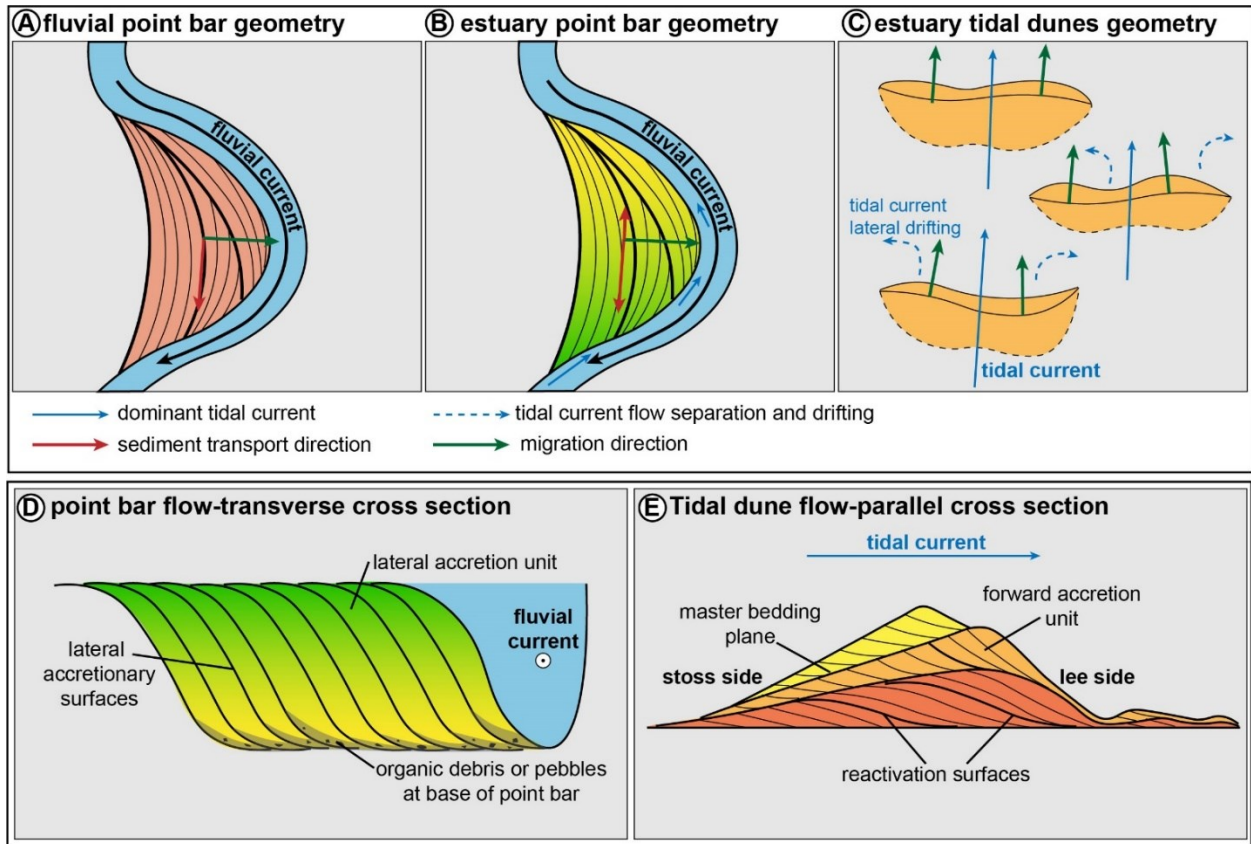


Figure 5.16 A schematic diagram showing subenvironments of an estuary. Estimated locations of geobodies observed at each outcrop is indicated in the diagram.

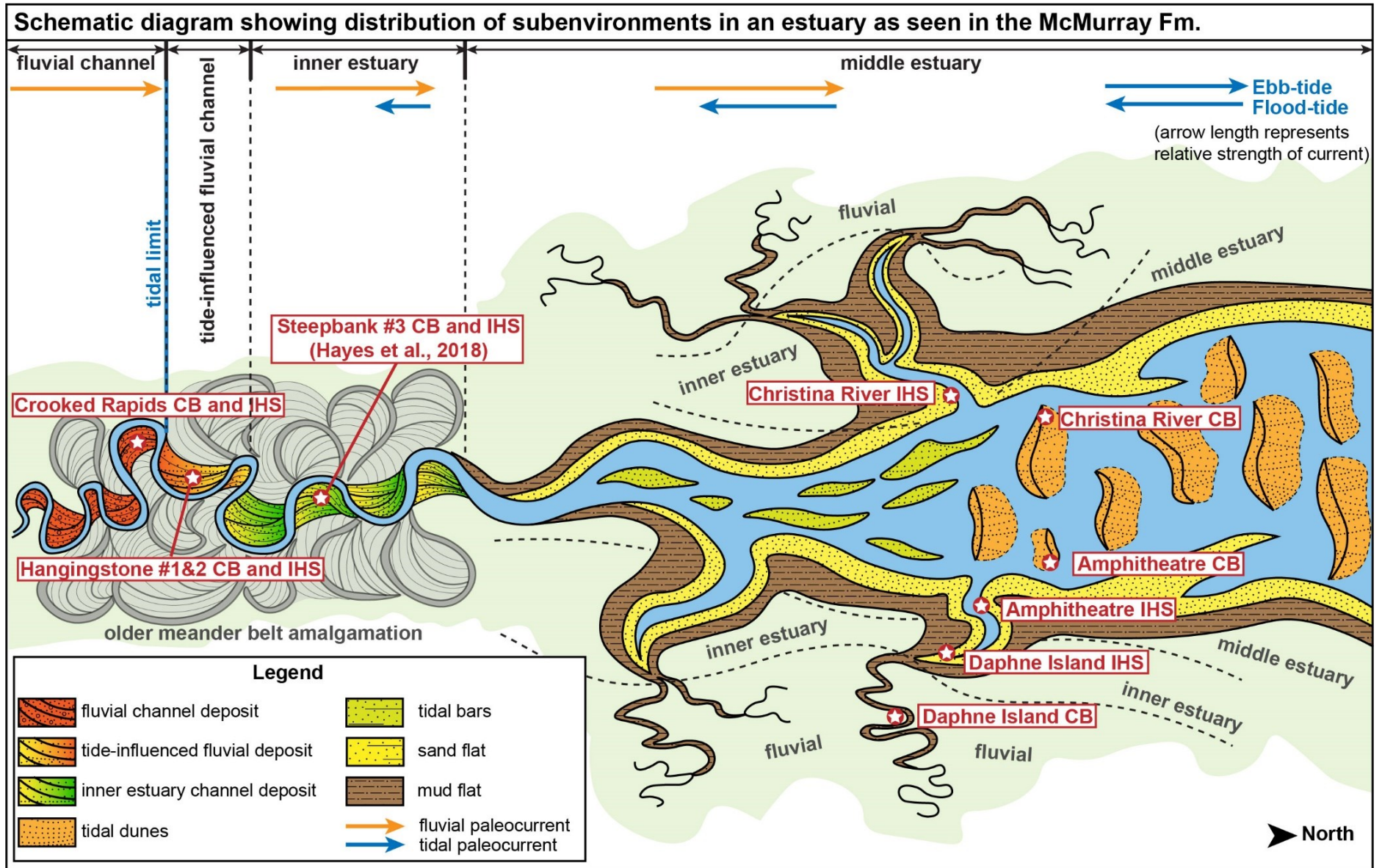
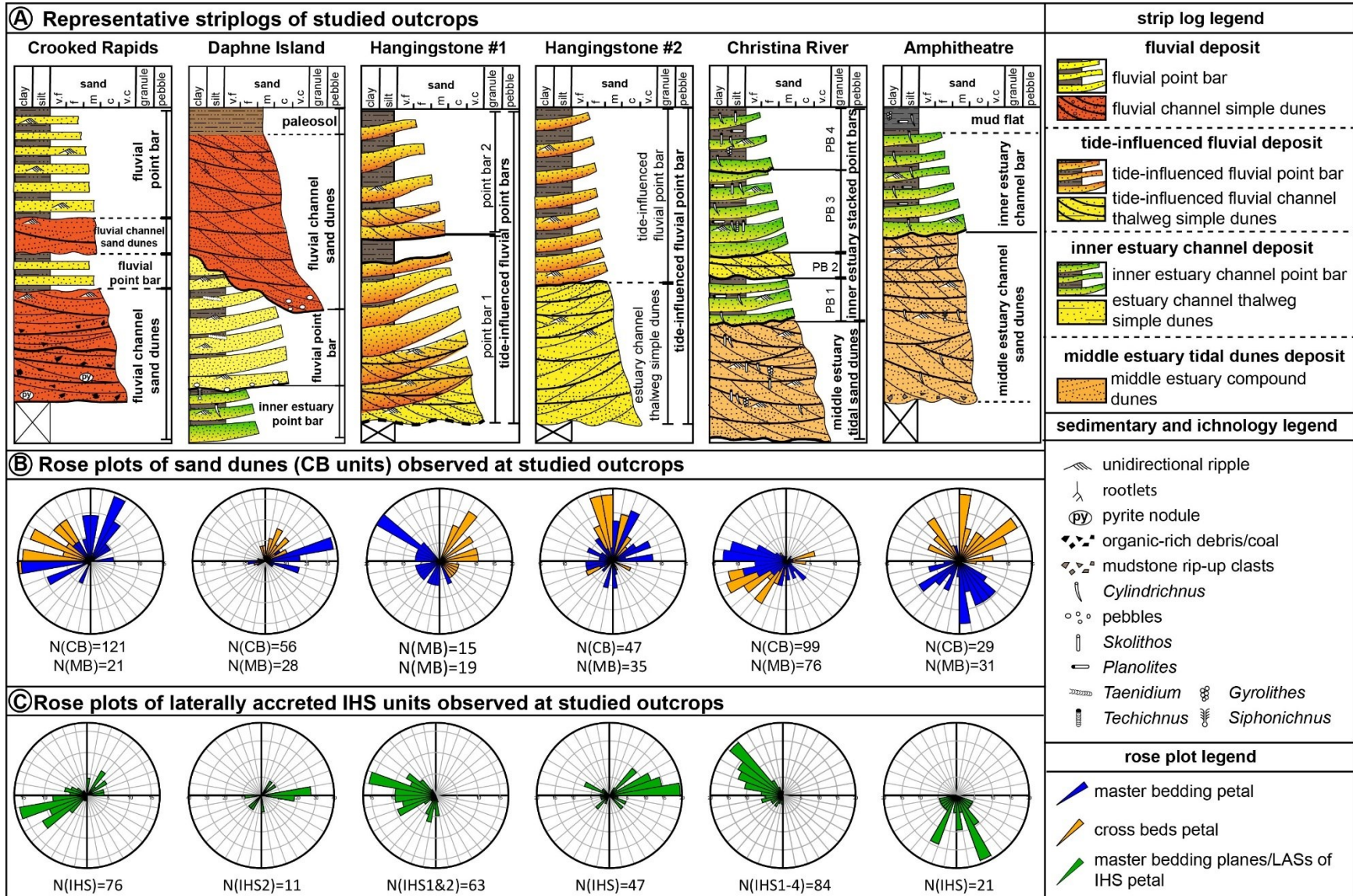


Figure 5.17 Geobody architectural interpretation of each outcrop in this study. **A)** Representative strip logs of studied outcrops. **B)** Rose plots of master bedding planes and cross beds in CB sandstone units of studied outcrops. **C)** Rose plots of master bedding planes of IHS units of studied outcrops.



Fluvial deposits Sedimentology and Architectural Synthesis

Fluvial point bars in the McMurray Formation can be distinguished from tidally influenced deposits by the following sedimentary characteristics: 1) abundant organic debris in cross-beds, foresets, and LASs, with sparsely to abundantly distributed centimetre-scale coal fragments; 2) the presence of rootlets near bar tops; 3) a general absence of bioturbation and those that occur corresponding to low numbers of traces common to continental facies (e.g., *Taenidium*), indicating persistent freshwater conditions; and 4) and interfingering relationship between CB and IHS facies.

The architectural characteristics of these fluvial deposits are two-fold. The channel thalweg environment is dominated by uniformly dipping master bedding planes (MB) and cross beds (CB). The cross beds and master bedding orientations of the cross-bedded sandstone facies vary from oblique to perpendicular to one another (Fig. 5.15A), which suggests a laterally accreted, simple dune deposit. The LASs within the IHS at both Crooked Rapids and Daphne Island outcrops (Fig. 5.17B) are nearly perpendicular to the sediment transport directions indicated by the dunes.

The point bar deposit in the fluvial setting is characterized by IHS containing low-diversity suites consisting of ichnogenera common to freshwater deposits. The IHS displays variable expressions in these fluvial deposits. It is not developed at all in the coarse-grained fill at the Daphne Island outcrop. At Crooked Rapids, the IHS is thickly bedded, with a typical range of thickness of 10-50cm, which contrasts with 5-15cm thick beds observed in its tidally influenced counterparts. The normally graded, coarse-to-fine couplets in fluvial IHS units are indicative of fluvial depositional processes that are characterized by alternating high-stage (sand beds deposition) and low-stage flooding events (silt/mud beds deposition). The deposition and preservation of the silty/muddy waning flow deposition is highly variable in fluvial deposit, because seasonal flooding events in such settings are more destructive than in estuarine settings (Hayes, 2018). This is supported by the complete paucity of trace fossils in IHS units of fluvial outcrops, since the limited traces from the top of mud-beds (Gingras et al., 2016) are often removed by succeeding freshet phase of a flooding event. The fluvial IHS of Crooked Rapids contains abundant carbonaceous detritus, which is normally absent in the tidally influenced IHS at Hangingstone #1 and Hangingstone #2 outcrops. Finally, the interfingering relationship between CB and IHS is a unique characteristic that has

only been observed in the intervals at Daphne Island and Crooked Rapids. This can be attributed a fluvial environment, which lacks the tidal backwater erosion effects that yield an erosional contact between the two facies.

Tidally influenced fluvial deposits Sedimentology and Architectural Synthesis

Tidally influenced fluvial deposits represent a transitional setting between fluvial and inner estuary environments (Fig. 5.16A). The key differences between tidally influenced fluvial deposits and IHS of the inner estuary are: 1) general absence of ichnogenera; 2) generally good preservation of point bar deposits; and 3) common erosional contacts between CB and IHS facies, suggesting stacked point bar deposition.

The architectural characteristics of a tidally influenced fluvial deposit are very similar to fluvial point bars in that they exhibit: unidirectional sediment transport directions with an oblique to perpendicular relationship between master bedding plane and cross bed orientations. As such, lateral accretion of channel fills is indicated. Of particular note, there is a slight increase in the variability of master bedding plane orientations observed in the CB of Hangingstone #1 and #2 outcrops, which contrast with the nearly unimodal orientations of purely fluvial sand dunes. Since the bedform morphology of sand dunes is a function of bed shear stress, accommodation space, and paleocurrent conditions (Reading, 1996; Longhitano et al., 2014), the transformation between two dimensional and three dimensional simple dunes is a result of greater variability in flow conditions, which can be attributed to: 1) dynamic flow velocities in channels, 2) changes of cross-sectional area of the seaway, and 3) tidal backwater dampening fluvial flow on a diurnal to semidiurnal cycle. In addition, the more complete preservation of point bars in the tidally influenced fluvial setting suggests a lower degree of channel belt amalgamation and the presence of accommodation space, both of which are more likely to occur within the proximal coastal plain.

Inner estuary IHS Sedimentology and Architectural Synthesis

Tide-influenced point bars of inner estuary channels share some similarities with fluvial point bars in terms of their dominant sedimentary and internal architectural characteristics. This is because both

systems are dominated by unidirectional currents and characterized by an upward decrease in hydrodynamic energy. In the case of the Christina River and Amphitheatre outcrops, the tide-influenced point bar is represented by the IHS units. They have the following defining characteristics, which set them apart from the fluvial or tidally influenced fluvial point bars described above: 1) widespread presence of brackish-water trace fossil suites (Pemberton et al., 1982; Musial et al., 2012; Hein, 2015; Gingras et al., 2016; Shchepetkina et al., 2016; Hagstrom et al., 2019); and 2) commonly stacked point bar architecture.

The bedding characteristics of the inner estuary IHS are also similar to the tidally influenced fluvial point bars, which also are dominated by laterally accreted point bar deposits. However, their stacking pattern is distinctively different. In the Christina River outcrop example, the IHS succession is composed of stacked IHS units with variable thicknesses that range from 4m to 13m. The complete preservation of point bar (CB of channel thalweg into the sandy/muddy his deposits, and ultimately capped by channel abandonment mudstone) is not generally observed in each genetic package. The IHS facies is preferentially preserved as the relict deposit of point bars, with the CB facies associated with the lower point-bar strata rarely preserved (e.g., CB2 unit at Christina River outcrop). Similar architectural characteristics in the IHS facies are also observed at Steepbank #3 outcrops by Hayes et al. (2018). In both the Christina River and Steepbank #3 (Hayes et al., 2018) examples, each IHS unit displays an upward increase of mudstone beds, bioturbation intensity, and decrease of bed thicknesses. Despite the consistent bed orientations of the stacked IHS units, we consider the interpretation of stacked point-bar deposits at both outcrops to best explain the sedimentological character of the LASs.

Estuary Compound Dunes Sedimentology and Architectural Synthesis

Tidal bars and tidal dunes constitute the two dominant types of bedforms observed in the middle to outer estuary setting (Olariu *et al.*, 2012). The configuration of bedforms (represented by the CB unit) at the Christina River and Amphitheatre outcrops indicates forward accretion of bedforms, which is consistent with a tidal dune interpretation. These compound tidal dunes are interpreted as composite tabular sand bodies with their crests oriented approximately perpendicular to the tidal currents (Fig. 5.15C and E, Fig. 5.16, and Fig. 5.17). Modern analogs of these longitudinal compound dunes have been observed at San Francisco Bay and Cobequid Bay (Olariu *et al.*, 2012; Hayes *et al.*, 2018). From a

sedimentological perspective, the tidal dunes observed at Christina River and Amphitheatre outcrops share many similarities with fluvial channel sandstone except for the following diagnostic features: 1) The upper boundary of cross-bed sets show moderate to abundant bioturbation with ichnogenera of a brackish-water suite; and 2) tidal cyclicity apparent in the foresets of sand dunes, suggesting semidiurnal synodic deposition (Hayes *et al.*, 2017; Chen *et al.*, 2022a).

In addition to the subparallel paleocurrent and dune accretion directions, there is a difference between the bedding configurations observed at the Christina River and the Amphitheatre examples: sand dunes of Christina River migrate in the same direction as the dip of the master-bedding planes, whereas dunes at Amphitheatre suggest an upslope accretion direction. We interpret this as evidence for large-scale compound dunes within the McMurray deposits that display stoss and lee positions at a very large-scale (e.g., 100's of metres to kilometres) compound sand dune complex. Also, the different paleocurrent directions (with approximately 180° difference as shown in Fig. 5.17) indicated by CB units at the two outcrops may record a flood- or ebb-dominated location of deposition in the estuary. Finally, the estuary compound dunes are often eroded by the overlying inner estuary point bar deposit, forming within-trend normal regressive surfaces (WTNRS) (Catuneanu, 2006) during regression.

CONCLUSION

This study reviews the sedimentological and ichnological characteristics of six outcrops of the McMurray Formation, and analyzes the internal architecture of cross-bedded sand dunes and IHS using bedding orientation data measured from their photogrammetric 3D models. This research provides insights into differentiating deposits of four depositional environments in a tide-dominated estuary. This paper provides detailed descriptions of fluvial deposits, tidally influenced fluvial deposits, inner estuary IHS deposits, and middle estuary tidal compound dunes through the integration of physical sedimentological, ichnological, and bed orientation analyses. The results provide ancient analogs of lithofacies in fluvial to estuary settings, which adds to the understanding of point bars and sand dunes in the sedimentary record.

The key findings of this study are: 1) the accurate interpretation of a particular deposit requires the combined analyses from sedimentary, ichnological, and bedding orientation characteristics; 2) fluvial deposits are distinctively enriched in organic debris, are typically devoid of trace fossils (except low numbers of continental traces), and contain very thick IHS beds in the larger channels (e.g., Crooked Rapids); 3) tidally influenced fluvial deposits are characterized by near complete preservation of unburrowed point bars that display very regular cm-dm bed-thickness distributions; 4) estuary point bar deposits are bioturbated with ichnological suites positively correlated to brackish-water environments, and characterized by stacked, partially preserved point bars (IHS units) with predictable cm-dm bed thickness distributions; and 5) the identification of forward-accreted tidal compound dunes relies on the identification of subparallel accretion and paleocurrent directions. The differentiation of these distinct deposits is crucial for establishing stratigraphic models, and for paleogeographic reconstructions in sedimentologically complex fluvial to marginal marine settings.

Chapter 6 : Summary and Conclusion

THESIS SUMMARY

The studies in this dissertation investigate the sedimentological, ichnological, and stratigraphic characteristics within fluvial and tidally influenced fluvial meander-belt and point-bar deposits of the McMurray Formation in the north of the Christina River area, Alberta, Canada. In particular, architectural characteristics of variable geobodies in these environments are investigated using bedding orientational data derived from dipmeter tadpole logs and photogrammetric outcrops. This dissertation includes four chapters: 1) a core-based facies analysis that describes the sedimentological, ichnological and stratigraphic characteristics of the formation and interpreting paleodepositional environments associated with the interval; 2) an integrated facies characteristics and dipmeter tadpole study of point bar deposit that reveals stacking patterns and internal architecture of meander belts of fluvio-estuarine channels; 3) a photogrammetric outcrop modelling case study that recognizes genetically related depositional packages of the formation using their facies and bedding architectural characteristics; and 4) a synthesized (digital) outcrop study that explores variable configuration of depositional units in the McMurray Formation. Key findings of this project are summarized below.

STRATIGRAPHIC FRAMEWORK

Nineteen lithofacies and six facies associations were identified in the McMurray Formation through logging of 67 drill cores across the project area. Chapter 2 presents a stratigraphic framework which is characterized by four allostratigraphic units. Each unit is characterized by estuary channel fill that is overlain by a shallow marine allomember and bounded by allogenic and autogenic flooding surfaces. We proposed that the stratigraphic model that best fits our dataset is the normal regression-dominated fluvio-estuarine channel belt model. Applying the concept of this model, the identified allostratigraphic units (containing allomembers and their associated channel belts) are likely result from 4th order regressive cycles that were developed during the overall rise of Boreal Sea (3rd order). This normal regression-

dominated stratigraphic model has been increasingly acknowledged in shallow marine environment (Pattison, 2019; Weleschuk and Dashtgard, 2019; Pattison, 2020; Château et al., 2020; Rinke-Hardekopf et al., 2022), and is considered as a best-fit for this study because: 1) it better explains the indiscernible sedimentological and ichnological characteristics among various channel belts; 2) it indicates the channel belts observed in the formation are mainly regressive channel fills, but it does not entirely exclude the presence of transgressive deposit in the McMurray Formation; 3) it better interprets the erosional contacts observed between CB and IHS facies at outcrop studies (e.g., Ranger and Gingras, 2010, Hayes et al., 2018, and Chen et al., 2022) as 'within-trend normal regressive surface' (WTNRS) (Catuneanu, 2006), which implies that the CB and IHS are not genetically related; 4) it does not require significant base-level fluctuation to produce the stacked channel belt configuration observed in the McMurray Formation. Since it is challenging to differentiate allogenic and autogenic deposits due to the intense amalgamation and migration of channel belts in the study area, we conclude that the McMurray Formation in the Christina River region mainly consists of deposits of a basinward prograded fluvio-estuarine channel system. Transgressive channel fills may also be present as relict deposits that were preserved below the regressive deposits.

INTEGRATION OF FACIES AND DIPMETER TADPOLE DATA

The facies description and dipmeter tadpole patterns are commonly conducted independently. A few studies have incorporated dipmeter tadpole logs and microresistivity image logs to reconstruct paleoenvironments and stratal architectures of point-bar deposits in the McMurray Formation (Brekke et al., 2017; Brekke and Roenitz, 2021). In Chapter 3, a dataset consists of 52 dipmeter logs are analyzed in combination with 47 drilled cores to establish an integrated facies-dipmeter framework. Point bars deposited as a single, continuous geobody are associated with the migration of solitary channel, which can be recognized by consistently dipping lateral-accretion bedsets (Brekke and Roenitz, 2021). The sedimentological and dipmeter tadpole characteristics of a point bar include: 1) a lower point-bar section characterized by planar and trough cross-bedded sandstone with local mud clasts with disorganized, low- to high-angle dip angles; 2) a middle section represented by inclined heterolithic stratified lateral accretion

deposits that exhibit consistent low-angle dips (5° - 18°); and 3) an upper section of point bar or in some cases abandoned channel strata comprising laminated and lenticular mudstone or bioturbated heterolithic intertidal strata, each showing low-angle ($<4^{\circ}$) dipmeter measurements. Facies classification is specific to the McMurray Formation in the study area, but the principles are applicable to other subsurface studies in similar depositional settings.

LARGE POINT-BAR ARCHITECTURE

In Chapter 4, depositional packages were recognized and interpreted at the Christina River Outcrops to explore depositional models that can result in the observed point bar architecture. Photogrammetric 3D outcrop model was generated at the outcrops, and important surfaces (e.g., cross beds, cross-set boundary (i.e., master bedding planes), and lateral accretion surfaces) are picked and their dips and dip azimuths are calculated for interpretation. Five genetic depositional packages are recognized. The lowermost cross bedded sandstone unit (Genetic Package 1) represents a forward/oblique accreted tidal sand dune unit, which is in erosional contact with the overlying laterally accreted estuary point bar succession (represented by Genetic Package 2-5). Similar discontinuity between the cross bedded sandstone and overlying IHS unit in outcrops have been previously recognized by many researchers (Ranger and Gingras, 2008; Ranger and Gingras, 2010; Hayes et al., 2018). This observation suggests that the cross bedded sandstone is not always genetically associated with the IHS deposit. Forward-accreted bedding configuration of master bedding planes and cross beds within cross bedded sandstone units further supports this idea, which is consistent with tidal compound dunes in middle estuary (Olariu et al., 2012). Therefore, the interpreted IHS of inner estuary point bars incises into middle estuary tidal dunes, forming within-trend normal regressive surface (WTNRS). The consistent dip direction of stacked IHS successions lead to nonunique interpretation of the point bar internal architectural characteristics: 1) a thick point bar deposit with sharp contacts marking abrupt shifts in migration orientation; or 2) stacked unrelated point bar or point bar complex. The forward accreted tidal dunes identified at the Christina River Outcrop is similar to what was observed at the Amphitheatre outcrops by Hayes et al. (2018), which strongly suggest the cross-bedded sandstone that records tidal sand dunes. This facies may be

significantly under-recognized in many tidally influenced estuary deposits. Bedding orientation analysis is crucial in differentiating forward-accreted tidal dunes *versus* lateral-accreted point bars. This analytical method helps to differentiate regressive and transgressive channel fills in the McMurray Formation.

VARIABLE GEOBODY ARCHITECTURE ALONG FLUVIAL TO ESTUARY SETTINGS

The photogrammetric 3D outcrop models provide different insights into the subsurface data based paleoenvironment interpretations. In Chapter 5, this method is applied to six McMurray outcrops to further investigate paleoenvironments of the depositional units. The outcrops display sedimentary and architectural characteristics of four important McMurray depositional environments: 1) fluvial environment (e.g., Daphne Island and Crooked Rapids), 2) tide-influenced fluvial environment (e.g., Daphne Island, Hangingstone #1 and #2), 3) inner estuary channel-point bars environments (e.g., IHS of Christina River and Amphitheatre); and 4) middle estuary tidal compound dune environments (e.g., CB of Christina River and Amphitheatre). The differentiation between the deposits of the first three depositional environments rely on their distinct sedimentological and ichnological characteristics. Fluvial deposits are characterized by rhythmically arranged, decimetre-scale coarse-to-fine couplets, enriched organic debris and are devoid of brackish water trace fossils that are commonly identified in estuarine channel fill, and importantly, show an interfingering contact between thalweg-associated sand dunes and the overlying laterally accreted point bar facies. Tide-influenced fluvial deposits are characterized by unburrowed point bars, with very regular centimetre- to decimetre-scale bed thickness distributions. Estuary point bar deposits share many similarities in sedimentological characteristics with the tide-influenced fluvial deposits, estuary point bar deposits can be differentiated from their extensive, diminutive brackish-water trace fossils, and stacked, partially preserved point bars. The identification of forward-accreted middle estuary tidal compound dunes, by contrast, relies on the subparallel accretion and paleocurrent direction indicated by master bedding planes and cross beds. The application of 3D photogrammetry technique in multiple outcrops has been proven useful for fast acquisition of large quantity of bedding orientation data, which also ensure sufficient precision for depositional environment interpretation.

RECOMMENDATION FOR FUTURE WORK

This dissertation makes contributions to the paleoenvironment interpretation of lithofacies associated with large point bar deposits in meander belts of fluvial and fluvio-tidal settings. There are many extensions to this work that would help expand and strengthen the results, including, but not limited to, petrography (e.g., variations in mineralogical composition within and between different point bars), reservoir properties (e.g., porosity, permeability, and hydrocarbon distribution in different parts of a reservoir unit), and stratigraphic correlation of the same formation in nearby area. From the outcrop analysis point of view, validation of the suggested depositional models, in particular the Christina River outcrop (Chapter 4) requires calibration to a modern point-bar analog.

The identification of the variable geobody architectures has been proven useful in outcrops, however, the recognition of these geobodies in subsurface data remains challenging. A major limitation of this type of research in the project area is the quality of vintage dipmeter data that are collected by three armed dipmeter tools in the 1960s. The black and white dipmeter tadpoles only record numeric values of dip and dip azimuth without specifying types of measured surfaces, which makes it difficult to analyze relationship between different types of bedding orientations. Dipmeter data collected by more advanced tools (e.g., microresistivity image logs) produces image log in the cylindrical wellbore, and displays vertical colored bands that correspond to resistivity values of six pads. The resulting image allows precise identification of types of measured surfaces, which can be utilized to investigate internal bedding architectures. If a high quality dipmeter dataset is available, the cross bedded sandstone facies can be reclassified using bedding orientational analytical method described in this dissertation.

CONCLUSIONS

The conclusions of this thesis enhance awareness of variable geobody architectures in a fluvial to estuary settings. The results highlight that the estuary point bar is not the one-and-only interpretation for all cross bedded sandstone and inclined heterolithic stratified sandstone and mudstone facies. The importance of integrated studies that combine multiple analytical methods provide new insights to the characterization and interpretation of complex fluvial and fluvio-tidal meander-belts successions in a

fluviotidal estuary. The stratigraphic framework, facies and dipmeter tadpole characteristics of point bars, and internal architecture of variable geobodies described in this project will undoubtedly guide future geological investigations in sedimentologically complex fluvial to marginal marine depositional settings.

References

- AER, 2015, Alberta's energy reserves 2014 and supply/demand outlook 2014–2023: Alberta Energy Regulator, ST98-2015, 299p.
- AER, 2022, Athabasca-In Situ Thermal, Alberta Energy Regulator, August 9th, 2022, <https://www.aer.ca/providing-information/data-and-reports/statistical-reports/st98/reserves/oil-sands-area-assessment/athabasca>.
- AEUB, 2003, Athabasca Wabiskaw-McMurray Regional Geological Study: Alberta Energy and Utilities Board, Report 2003-A, 195p.
- Allen, J. R., 1963, The classification of cross-stratified units. With notes on their origin: *Sedimentology*, v. 2, no. 2, p. 93-114.
- Armenio, E., De Serio, F., and Mossa, M., 2017, Analysis of data characterizing tide and current fluxes in coastal basins: *Hydrology and Earth System Sciences*, v. 21, no. 7, p. 3441-3454.
- Baniak, G. M., and Kingsmith, K. G., 2018, Sedimentological and stratigraphic characterization of Cretaceous upper McMurray deposits in the southern Athabasca oil sands, Alberta, Canada: *AAPG Bulletin*, v. 102, no. 2, p. 309-332.
- Barton, M., Porter, I., and Mahood, R., 2014, Impact of the Prairie Evaporite dissolution collapse on McMurray stratigraphy and depositional patterns, Shell Albian Sands Lease 13, northeast Alberta: *Bulletin of Canadian Petroleum Geology*, v. 1, p. 175-199.
- Barton, M., Porter, I., O'Byrne, C., and Mahood, R., 2017, Impact of the Prairie Evaporite dissolution collapse on McMurray stratigraphy and depositional patterns, Shell Albian Sands Lease 13, northeast Alberta: *Bulletin of Canadian Petroleum Geology*, v. 65, no. 1, p. 175-199.
- Barton, M. D., 2016, The architecture and variability of valley-fill deposits within the Cretaceous McMurray Formation, Shell Albian Sands Lease, northeast Alberta: *Bulletin of Canadian Petroleum Geology*, v. 64, no. 2, p. 166-198.
- Bhattacharya, J. P., and MacEachern, J. A., 2009, Hyperpycnal rivers and prodeltaic shelves in the Cretaceous seaway of North America: *Journal of Sedimentary Research*, v. 79, no. 4, p. 184-209.
- Blum, M., and Jennings, D., 2016, The McMurray conundrum: Conflicting interpretations of environment of deposition and paleogeography, AAPG annual convention & exhibition, Calgary, Canada, June 19-22, 2016, v. Search and Discovery: Tulsa, OK, United States, American Association of Petroleum Geologists and Society for Sedimentary Geology, p. 51338.
- Brekke, H., and Couch, A., Use of image logs in differentiating point bar and tidal bar deposits in the Leismer area: implications for SAGD reservoir definition in the Athabasca oilsands, Canadian Society of Petroleum Geologists Annual Meeting, Calgary, Alberta, 2011.
- Brekke, H., and Evoy, R. W., 2004, Implications of dipmeter data for the definition of the internal architecture in point-bar deposits from the Athabasca oil sands, Canadian Society of Petroleum Geologists (CSPG) Annual Meeting, Calgary, Alberta, May 31-June 4, 2004, AAPG Datapages/Search and Discovery Article, p. 90213.

- Brekke, H., MacEachern, J. A., Roenitz, T., and Dashtgard, S. E., 2017, The use of microresistivity image logs for facies interpretations: An example in point-bar deposits of the McMurray Formation, Alberta, Canada: AAPG Bulletin, v. 101, no. 5, p. 655-682.
- Brekke, H., and Roenitz, T., 2021, Using high-resolution microresistivity image logs to reconstruct paleoenvironments and stratal architectures: An example from the McMurray Formation, Leismer area, northeastern Alberta, Canada: AAPG Bulletin, v. 105, no. 8, p. 1563-1593.
- Broughton, P. L., 2013, Depositional setting and oil sands reservoir characterization of giant longitudinal sandbars at Ells River: Marginal marine facies of the McMurray formation, northern Alberta Basin, Canada: AAPG Studies in Geology, v. 64, p. 313-357.
- Broughton, P. L., 2014, Syndepositional architecture of the northern Athabasca Oil Sands Deposit, northeastern Alberta: Canadian Journal of Earth Sciences, v. 52, no. 1, p. 21-50.
- Broughton, P. L., 2016a, Alignment of fluvio-tidal point bars in the middle McMurray Formation: implications for structural architecture of the Lower Cretaceous Athabasca Oil Sands Deposit, northern Alberta: Canadian Journal of Earth Sciences, v. 53, no. 9, p. 896-930.
- Broughton, P. L., 2016b, Collapse-induced fluidization structures in the Lower Cretaceous Athabasca Oil Sands Deposit, Western Canada: Basin Research, v. 28, no. 4, p. 507-535.
- Broughton, P. L., 2018a, Mudstone clast breccia in the Cretaceous Athabasca Oil Sands, Western Canada: fluvial debris-flow transitions into traction carpets: The Journal of Geology, v. 126, no. 1, p. 63-97.
- Broughton, P. L., 2018b, Salt tectonism and distribution of brackish-water trace fossils in the Cretaceous McMurray Formation, Athabasca Oil Sands, Alberta Foreland Basin: Canadian Journal of Earth Sciences, v. 55, no. 12, p. 1354-1383.
- Broughton, P. L., 2019, Corrigendum: Salt tectonism and distribution of brackish-water trace fossils in the Cretaceous McMurray Formation, Athabasca Oil Sands, Alberta Foreland Basin!(CORRIGENDUM)(Correction notice): Canadian Journal of Earth Sciences, v. 56, no. 4, p. 431.
- Buatois, L. A., and Mángano, M. G., 2011, Ichnology : organism-substrate interactions in space and time, Cambridge, United Kingdom, Cambridge University Press, 366 p.
- Caplan, M. L., and Ranger, M. J., 2001, Description and interpretation of coarsening-upward cycles in the McMurray Formation, northeastern Alberta: preliminary results, Canadian Society of Petroleum Geologists, Rock the Foundation Convention, Calgary, Alberta, Canada, June 18-22, 2001, v. Rock The Foundation Convention, Canadian Society of Petroleum Geologists Core Conference, p. 30-38.
- Carling, P. A., Chateau, C. C., Leckie, D. A., Langdon, C. T., Scaife, R. G., and Parsons, D. R., 2015, Sedimentology of a tidal point-bar within the fluvial-tidal transition: River Severn Estuary, UK, *in* Ashworth, P. J., Best, J. L., and Parsons, D. R., eds., Developments in Sedimentology, Volume 68, Elsevier, p. 149-189.

- Carrigy, M., and Kramers, J., 1973, Guide to the Athabasca Oil Sands area. [electronic resource], Edmonton, Alberta, Alberta Research, Information series / Alberta Research: 65, 211 p.
- Carrigy, M. A., 1959, Geology of the Fort McMurray Formation. Part III, General geology of the Fort McMurray area, Edmonton, Research Council of Alberta, Geological Division, 141 p.
- Carrigy, M. A., 1963a, Criteria for differentiating the McMurray and Clearwater formations in the Athabasca oil sands, Edmonton, Research Council of Alberta, 39 p.
- Carrigy, M. A., 1963b, Paleocurrent directions from the McMurray Formation: Bulletin of Canadian Petroleum Geology, v. 11, no. 4, p. 389-395.
- Carrigy, M. A., 1971, Deltaic sedimentation in Athabasca tar sands: AAPG Bulletin, v. 55, no. 8, p. 1155-1169.
- Catuneanu, O., 2006, Principles of sequence stratigraphy, Amsterdam, Boston, Elsevier, Developments in sedimentology; 58, 375 p.
- Château, C. C., Dashtgard, S. E., and MacEachern, J. A., 2020, Refinement of the stratigraphic framework for the Regional C depositional unit of the McMurray Formation and implications for the early transgression of the Alberta Foreland Basin, Canada: Journal of Sedimentary Research, v. 90, no. 10, p. 1322-1345.
- Château, C. C., Dashtgard, S. E., and MacEachern, J. A., 2021, Acceleration in the rate of the Boreal Sea transgression recorded in the Lower Cretaceous McMurray Formation, Canada: Marine and Petroleum Geology, v. 133, p. 105221.
- Château, C. C., Dashtgard, S. E., MacEachern, J. A., and Hauck, T. E., 2019, Parasequence architecture in a low-accommodation setting, impact of syndepositional carbonate epikarstification, McMurray Formation, Alberta, Canada: Marine and Petroleum Geology, v. 104, p. 168-179.
- Chen, Q., Kavanaugh, J., Gingras, M. K., Ranger, M. J., and MacEachern, J. A., 2022a, Recognizing genetically related depositional packages using 3D photogrammetric outcrop models in a fluvially dominated, tidally influenced meander-belt succession: Sedimentary Geology, v. 442, p. 106288.
- Chen, Q., Shchepetkina, A., Melnyk, S., and Gingras, M. K., 2022b, Integrating facies analysis with dipmeter data to characterize point bars of the Lower Cretaceous McMurray Formation, Christina River, AB, Canada: Marine and Petroleum Geology, v. 136, p. 105449.
- Chen, Q., Shchepetkina, A., Melnyk, S., Gingras, M. K. J. M., and Geology, P., 2021, Integrating facies analysis with dipmeter data to characterize point bars of the Lower Cretaceous McMurray Formation, Christina River, AB, Canada, p. 105449.
- Choi, K., and Jo, J., 2015, Morphodynamics and stratigraphic architecture of compound dunes on the open-coast macrotidal flat in the northern Gyeonggi Bay, west coast of Korea: Marine Geology, v. 366, p. 34-48.
- Choi, K. S., Dalrymple, R. W., Chun, S. S., and Kim, S.-P., 2004, Sedimentology of Modern, Inclined Heterolithic Stratification (IHS) in the Macrotidal Han River Delta, Korea: Journal of Sedimentary Research, v. 74, no. 5, p. 677-689.

- Christopher, J. E., 1974, The Upper Jurassic Vanguard and Lower Cretaceous Mannville Groups of Southwestern Saskatchewan: Saskatchewan Department of Mineral Resources, no. 151, 349p.
- Collins, D. S., Johnson, H. D., Allison, P. A., Guilpain, P., and Damit, A. R., 2017, Coupled 'storm-flood' depositional model: Application to the Miocene–Modern Baram Delta Province, north-west Borneo: *Sedimentology*, v. 64, no. 5, p. 1203-1235.
- Crerar, E. E., and Arnott, R., 2007, Facies distribution and stratigraphic architecture of the lower Cretaceous McMurray Formation, Lewis property, northeastern Alberta: *Bulletin of Canadian Petroleum Geology*, v. 55, no. 2, p. 99-124.
- Dai, F., Feng, Y., and Hough, R., 2014, Photogrammetric error sources and impacts on modeling and surveying in construction engineering applications: *Visualization in Engineering*, v. 2, no. 1, p. 1-14.
- Dalrymple, R. W., 2010, Tidal depositional systems, in James, N. P., and Dalrymple, R. W., eds., *Facies Models 4: St. John's, Newfoundland & Labrador, Canada*, Geological Association of Canada, p. 201-231.
- Dalrymple, R. W., and Choi, K., 2007a, Morphologic and facies trends through the fluvial-marine transition in tide-dominated depositional systems; a schematic framework for environmental and sequence stratigraphic interpretation: *Earth-Science Reviews*, v. 81, no. 3-4, p. 135-174.
- Dalrymple, R. W., and Choi, K., 2007b, Morphologic and facies trends through the fluvial–marine transition in tide-dominated depositional systems: a schematic framework for environmental and sequence-stratigraphic interpretation: *Earth-Science Reviews*, v. 81, no. 3, p. 135-174.
- Dalrymple, R. W., Knight, R. J., Zaitlin, B. A., and Middleton, G. V., 1990, Dynamics and facies model of a macrotidal sand-bar complex, Cobequid Bay–Salmon River estuary (Bay of Fundy): *Sedimentology*, v. 37, no. 4, p. 577-612.
- Dalrymple, R. W. J. S., 1984, Morphology and internal structure of sandwaves in the Bay of Fundy: *Sedimentology*, v. 31, no. 3, p. 365-382.
- Dashtgard, S. E., and MacEachern, J. A., 2016, Unburrowed mudstones may record only slightly lowered oxygen conditions in warm, shallow basins: *Geology*, v. 44, no. 5, p. 371-374.
- Deschamps, R., Kohler, E., Gasparrini, M., Durand, O., Euzen, T., and Nader, F., 2012, Impact of mineralogy and diagenesis on reservoir quality of the Lower Cretaceous Upper Mannville Formation (Alberta, Canada): *Oil & Gas Science and Technology*, v. 67, no. 1, p. 31-58.
- Dronkers, J., 1986, Tidal asymmetry and estuarine morphology: *Netherlands Journal of Sea Research*, v. 20, no. 2-3, p. 117-131.
- Durkin, P. R., Boyd, R. L., Hubbard, S. M., Shultz, A. W., and Blum, M. D., 2017a, Three-dimensional reconstruction of meander-belt evolution, Cretaceous McMurray Formation, Alberta foreland basin, Canada: *Journal of Sedimentary Research*, v. 87, no. 10, p. 1075-1099.
- Durkin, P. R., Horner, S. C., and Hagstrom, C. A., 2020, Comment on “Using a modern analogue to interpret depositional position in ancient fluvial-tidal channels: Example from the McMurray

- Formation, Canada” by Andrew D. La Croix, Shahin E. Dashtgard, James A. MacEachern, *Geoscience Frontiers*, Volume 10, Issue 6, Pages 2219-2238: *Geoscience Frontiers*, v. 11, no. 3, p. 1081-1086.
- Durkin, P. R., Hubbard, S. M., Holbrook, J., and Boyd, R., 2017b, Evolution of fluvial meander-belt deposits and implications for the completeness of the stratigraphic record: *Geological Society of America Bulletin*, v. 130, no. 5-6, p. 721-739.
- Fernández, O., 2005, Obtaining a best fitting plane through 3D georeferenced data: *Journal of Structural Geology*, v. 27, no. 5, p. 855-858.
- Flach, P. D., 1977, A lithofacies analysis of the McMurray Formation, lower Steepbank River, Alberta [MSc unpublished MSc Thesis]: University of Alberta, 139 p.
- Flach, P. D., and Mossop, G. D., 1985, Depositional environments of Lower Cretaceous McMurray Formation, Athabasca Oil Sands, Alberta: *AAPG Bulletin*, v. 69, no. 8, p. 1195-1207.
- Flemming, B. W., 2012, Siliciclastic back-barrier tidal flats, *in* Davis Jr., R. A., and Dalrymple, R. W., eds., *Principles of Tidal Sedimentology*: Dordrecht, Springer, p. 231-267.
- Fustic, M., 2007, Stratigraphic dip analysis—A novel application for detailed geological modeling of point bars, and predicting bitumen grade, McMurray Formation, Muskeg River Mine, northeast Alberta: *Natural Resources Research*, v. 16, no. 1, p. 31-43.
- Fustic, M., Hubbard, S. M., Spencer, R., Smith, D. G., Leckie, D. A., Bennett, B., and Larter, S., 2012, Recognition of down-valley translation in tidally influenced meandering fluvial deposits, Athabasca Oil Sands (Cretaceous), Alberta, Canada: *Marine and Petroleum Geology*, v. 29, no. 1, p. 219-232.
- Fustic, M., Skulski, L., Hanson, W., Vanhooren, D., Bessette, P., Hinks, D., Bellman, L., and Leckie, D., Geological mapping and reservoir characterization of oil sands reservoir by integrating 3D seismic, dipmeter, core descriptions, and analogs in the McMurray Formation, NE Alberta, AAPG Hedberg Conference, Banff, Alberta, Canada, 2008, v. Search and Discovery Article, American Association of Petroleum Geologists, p. 40281.
- Gingras, M., 2014, The nature of TR cycles in the McMurray Formation, *in* Oil Sands & Heavy Oil Symposium: A local to global multidisciplinary collaboration Canadian Society of Petroleum Geoscientists (CSPG) and AAPG Joint Symposium, Calgary, Alberta, October 14-16, 2014: Calgary, Alberta.
- Gingras, M., and Leckie, D., 2017, The argument for tidal and brackish water influence in the McMurray Formation reservoirs: *Canadian Society of Petroleum Geologists Reservoir*, v. 44, p. 21-24.
- Gingras, M. K., Bann, K. L., Maceachern, J. A., Waldron, J., and Pemberton, S. G., 2007, A conceptual framework for the application of trace fossils, *in* MacEachern, J. A., Bann, K. L., Gingras, M., and Pemberton, S. G., eds., *Applied Ichnology*, Volume 52, SEPM Society for Sedimentary Geology, p. 1-26.

- Gingras, M. K., Dashtgard, S. E., MacEachern, J. A., and Pemberton, S. G., 2008, Biology of shallow marine ichnology: a modern perspective: *Aquatic Biology*, v. 2, no. 3, p. 255-268.
- Gingras, M. K., and MacEachern, J. A., 2012, Tidal ichnology of shallow-water clastic settings, *in* Davis Jr., R. A., and Dalrymple, R. W., eds., *Principles of Tidal Sedimentology*: Dordrecht, Springer, p. 57-77.
- Gingras, M. K., MacEachern, J. A., and Dashtgard, S. E., 2011, Process ichnology and the elucidation of physico-chemical stress: *Sedimentary Geology*, v. 237, no. 3-4, p. 115-134.
- Gingras, M. K., MacEachern, J. A., Dashtgard, S. E., Ranger, M. J., and Pemberton, S. G., 2016, The significance of trace fossils in the McMurray Formation, Alberta, Canada: *Bulletin of Canadian Petroleum Geology*, v. 64, no. 2, p. 233-250.
- Gingras, M. K., Pemberton, S. G., Saunders, T., and Clifton, H. E., 1999, The ichnology of modern and Pleistocene brackish-water deposits at Willapa Bay, Washington: variability in estuarine settings: *Palaos*, v. 14, no. 4, p. 352-374.
- Gingras, M. K., Ranger, M. J., and Caplan, M., The Incised Valley Fill of the McMurray Formation, Northeastern Alberta, Comprises Estuarine and Deltaic Deposits, AAPG Annual Meeting, Salt Lake City, Utah, May11-14, 2003, 2003, AAPG Search and Discovery Article.
- Hagstrom, C. A., 2019, Stratigraphic Architecture and Lithofacies Distribution in Meander-Belt Deposits, South Saskatchewan River and Cretaceous McMurray Formation, Alberta [Doctor of Philosophy unpublished Ph.D thesis]: University of Calgary, 281 p.
- Hagstrom, C. A., Hubbard, S. M., Leckie, D. A., and Durkin, P. R., 2019, The effects of accretion-package geometry on lithofacies distribution in point-bar deposits: *Journal of Sedimentary Research*, v. 89, no. 5, p. 381-398.
- Harris, B., Timmer, E., Ranger, M., Gingras, M., and Leckie, D., 2016, Continental ichnology of the Lower McMurray Formation inclined heterolithic strata at Daphne Island, Athabasca River, north-eastern Alberta, Canada: *Bulletin of Canadian Petroleum Geology*, v. 64, no. 2, p. 218-232.
- Hayes, B., Christopher, J., Rosenthal, L., Los, G., McKercher, B., Minken, D., Tremblay, Y., Fennell, J., and Smith, D., 1994, Cretaceous Mannville Group of the western Canada sedimentary basin, *Geological Atlas of the Western Canada sedimentary basin, Volume 4*: Edmonton, AB, Canada, Canadian Society of Petroleum Geologists and Alberta Research Council, p. 317-334.
- Hayes, D. A., 2018, Three-dimensional Outcrop Modelling of Fluvial and Estuarine Outcrops in the Lower Cretaceous McMurray Formation, Northeast Alberta, Canada [MSc unpublished MSc Thesis]: University of Alberta, 151 p.
- Hayes, D. A., Timmer, E. R., Deutsch, J. L., Ranger, M. J., and Gingras, M. K., 2017, Analyzing dune foreset cyclicity in outcrop with photogrammetry: *Journal of Sedimentary Research*, v. 87, no. 1, p. 66-74.
- Hayes, D. A., Timmer, E. R., Ranger, M. J., Kavanaugh, J. L., and Gingras, M. K., 2018, Using structure-from-motion photogrammetry to recognize lateral versus forward accretion bedforms in the Lower

- Cretaceous McMurray Formation, NE Alberta, Canada: *Bulletin of Canadian Petroleum Geology*, v. 66, no. 4, p. 725-751.
- Hayes, M. O., 1975, Morphology of sand accumulation in estuaries: an introduction to the symposium, *in* Cronin, L. E., ed., *Geology and Engineering*, Volume 20, Acad. Press, Inc. : New York, N.Y., United States, p. 3-22.
- Hein, F., 2015, The Cretaceous McMurray oil sands, Alberta, Canada: A world-class, tidally influenced fluvial–estuarine system—an Alberta government perspective, *in* Ashworth, P. J., Best, J. L., and Parsons, D. R., eds., *Developments in Sedimentology*, Volume 68, Elsevier, p. 561-621.
- Hein, F., Cotterill, D., and Rice, R., 2006, Subsurface geology of the Athabasca Wabiskaw-McMurray succession: Lewis–Fort McMurray area, northeastern Alberta: Alberta Energy and Utilities Board, EUB/AGS Earth Sciences Report 2006-06, 67p.
- Hein, F., Langenberg, C., Kidston, C., Berhane, H., Berezniuk, T., and Cotterill, D., 2001, A comprehensive field guide for facies characterization of the Athabasca Oil Sands, Northeast Alberta: Alberta Energy and Utilities Board Special Report, v. 13, p. 415.
- Hein, F. J., Berhane, H., and Cotterill, D. K., 2000, An atlas of lithofacies of the McMurray Formation Athabasca oil sands deposit, northeastern Alberta: surface and subsurface: Alberta Energy and Utilities Board, 2000-07, 216p.
- Hein, F. J., and Cotterill, D. K., 2006, The Athabasca oil sands—a regional geological perspective, Fort McMurray area, Alberta, Canada: *Natural Resources Research*, v. 15, no. 2, p. 85-102.
- Hein, F. J., Dolby, G., and Fairgrieve, B., 2013, A regional geologic framework for the Athabasca oil sands, northeastern Alberta, Canada: *AAPG Studies in Geology*, v. 64, p. 207-250.
- Hein, F. J., and Langenberg, C. W., 2003, Reply to discussion of seismic modeling of fluvial-estuarine deposits in the Athabasca oil sands using ray-tracing techniques, Steepbank River area, northeastern Alberta: *Bulletin of Canadian Petroleum Geology*, v. 51, no. 3, p. 354-366.
- Hubbard, S., Pemberton, S., and Howard, E., 1999, Regional geology and sedimentology of the basal Cretaceous Peace River Oil Sands deposit, north-central Alberta: *Bulletin of Canadian Petroleum Geology*, v. 47, no. 3, p. 270-297.
- Hubbard, S. M., Smith, D. G., Nielsen, H., Leckie, D. A., Fustic, M., Spencer, R. J., and Bloom, L., 2011, Seismic geomorphology and sedimentology of a tidally influenced river deposit, Lower Cretaceous Athabasca oil sands, Alberta, Canada: *AAPG Bulletin*, v. 95, no. 7, p. 1123-1145.
- Jablonski, B. V., 2012, Process sedimentology and three-dimensional facies architecture of a fluvially dominated, tidally influenced point bar: middle McMurray Formation, lower Steepbank River area, northeastern Alberta, Canada [Master of Science unpublished MSc Thesis]: Queen's University (Canada), 372 p.
- Jablonski, B. V., and Dalrymple, R. W., 2016, Recognition of strong seasonality and climatic cyclicity in an ancient, fluvially dominated, tidally influenced point bar: Middle McMurray Formation, Lower Steepbank River, north-eastern Alberta, Canada: *Sedimentology*, v. 63, no. 3, p. 552-585.

- James, D., and Oliver, T., 1977, The sedimentology of the McMurray Formation, east Athabasca: The oil sands of Canada: Canadian Institute of Mining and Metallurgy, Special, p. 17-26.
- James, D. P., 1978, The sedimentology of the McMurray Formation, east Athabasca [MSc unpublished MSc Thesis]: University of Calgary, 198 p.
- Jo, J., and Choi, K., 2016, Morphodynamic and Hydrodynamic Controls On the Stratigraphic Architecture of Intertidal Compound Dunes On the Open-Coast Macrotidal Flat In the Northern Gyeonggi Bay, West Coast Of Korea: *Journal of Sedimentary Research*, v. 86, no. 10, p. 1103-1122.
- Johnson, S. M., and Dashtgard, S. E., 2014, Inclined heterolithic stratification in a mixed tidal–fluvial channel: differentiating tidal versus fluvial controls on sedimentation: *Sedimentary Geology*, v. 301, p. 41-53.
- Keith, D., MacGillivray, J., Wightman, D., Bell, D., Berezniuk, T., and Berhane, H., 1990, Resource characterization of the McMurray/Wabiskaw deposit in the Athabasca central region of northeastern Alberta: Alberta Oil Sands Technical and Research Authority, 63p.
- Keith, D., Wightman, D., Pemberton, S., MacGillivray, J., Berezniuk, T., and Berhane, H., 1988, Sedimentology of the McMurray Formation and Wabiskaw Member (Clearwater Formation), Lower Cretaceous, in the central region of the Athabasca oil sands area, northeastern Alberta: *Canadian Society of Petroleum Geologists*, v. Memoir 15, p. 309-324.
- La Croix, A. D., Dashtgard, S. E., and MacEachern, J. A., 2019, Using a modern analogue to interpret depositional position in ancient fluvial-tidal channels: Example from the McMurray Formation, Canada: *Geoscience Frontiers*, v. 10, no. 6, p. 2219-2238.
- La Croix, A. D., Dashtgard, S. E., and MacEachern, J. A., 2020, Reply to comment by Durkin et al. on “Using a modern analogue to interpret depositional position in ancient fluvial-tidal channels: Example from the McMurray Formation, Canada” by A.D. La Croix, S.E. Dashtgard, and J.A. MacEachern: *Geoscience Frontiers*, v. 11, no. 3, p. 1087-1092.
- Labrecque, P. A., Hubbard, S. M., Jensen, J. L., and Nielsen, H., 2011, Sedimentology and stratigraphic architecture of a point bar deposit, Lower Cretaceous McMurray Formation, Alberta, Canada: *Bulletin of Canadian Petroleum Geology*, v. 59, no. 2, p. 147-171.
- Langenberg, C., Hein, F., Lawton, D., and Cunningham, J., 2002, Seismic modeling of fluvial-estuarine deposits in the Athabasca oil sands using ray-tracing techniques, Steepbank River area, northeastern Alberta: *Bulletin of Canadian Petroleum Geology*, v. 50, no. 1, p. 178-204.
- Lin, W., and Bhattacharya, J. P., 2021, Storm-flood-dominated delta: A new type of delta in stormy oceans: *Sedimentology*, v. 68, no. 3, p. 1109-1136.
- Longhitano, S. G., Chiarella, D., and Muto, F., 2014, Three-dimensional to two-dimensional cross-strata transition in the lower Pleistocene Catanzaro tidal strait transgressive succession (southern Italy): *Sedimentology*, v. 61, no. 7, p. 2136-2171.
- MacEachern, J., and Bann, K., 2008, The role of ichnology in refining shallow marine facies models, *in* Hampson, G. J., Steel, R. J., Burgess, P. M., and Dalrymple, R. W., eds., *Recent Advances in*

- Models of siliciclastic shallow-marine stratigraphy: SEPM, Special Publication, Volume 90: Tulsa, Oklahoma, U.S.A, SEPM Society for Sedimentary Geology, p. 73-116.
- MacEachern, J., Bann, K., Hampson, G., Steel, R., Burgess, P., and Dalrymple, R., 2008, The role of ichnology in refining shallow marine facies models, Recent advances in models of siliciclastic shallow-marine stratigraphy, Volume 90, Society for Sedimentary Geology (SEPM) Tulsa, USA, p. 73-116.
- MacEachern, J. A., and Bann, K. L., 2020, The Phycosiphon Ichnofacies and the Rosselia Ichnofacies: Two new ichnofacies for marine deltaic environments: *Journal of Sedimentary Research*, v. 90, no. 8, p. 855-886.
- MacEachern, J. A., and Bann, K. L., 2023, Departures from the archetypal deltaic ichnofacies: Geological Society, London, Special Publications, v. 522, no. 1, p. SP522-2022-2056.
- MacEachern, J. A., Bann, K. L., Bhattacharya, J. P., and Howell, C. D., 2005, Ichnology of deltas: organism responses to the dynamic interplay of rivers, waves, storms, and tides: *Society for Sedimentary Geology*, v. 83, p. 49-85.
- MacEachern, J. A., and Gingras, M. K., 2007, Recognition of brackish-water trace-fossil suites in the Cretaceous Western Interior Seaway of Alberta, Canada, *in* Bromley, R., Buatois, L., Mangano, G., Genise, J., and Melchor, R. N., eds., *Sediment–Organism Interactions: A Multifaceted Ichnology*, Volume 88: Tulsa, Oklahoma, U.S.A., SEPM Society for Sedimentary Geology, p. 149-193.
- MacEachern, J. A., and Pemberton, S. G., 1994, Ichnological aspects of incised-valley fill systems from the Viking Formation of the Western Canada sedimentary basin, Alberta, Canada, *in* Dalrymple, R. W., Boyd, R., and Zaitlin, B. A., eds., *Incised-Valley Systems: Origin and Sedimentary Sequences*, Volume SEPM Special Publication No. 51: Tulsa, Oklahoma, USA, SEPM Society for Sedimentary Geology, p. 129-157.
- Martinius, A., Fustic, M., Garner, D., Jablonski, B., Strobl, R., MacEachern, J., and Dashtgard, S., 2017, Reservoir characterization and multiscale heterogeneity modeling of inclined heterolithic strata for bitumen-production forecasting, McMurray Formation, Corner, Alberta, Canada: *Marine and Petroleum Geology*, v. 82, p. 336-361.
- Martinius, A., Jablonski, B. V., Fustic, M., Strobl, R., and Van den Berg, J., 2015, Fluvial to tidal transition zone facies in the McMurray Formation (Christina River, Alberta, Canada), with emphasis on the reflection of flow intensity in bottomset architecture: *Developments in Sedimentology*, v. 68, p. 445-480.
- Mathison, J., 2004, Sequence-stratigraphic architecture of the McMurray Formation, Canadian Society of Petroleum Geologists/Canadian Society of Exploration Geophysicists Convention, Calgary, June 2-6, 2004, v. *Partners in a New Environment*, p. 29-37.
- McLean, J., 1977, The Cadomin Formation: stratigraphy, sedimentology, and tectonic implications: *Bulletin of Canadian Petroleum Geology*, v. 25, no. 4, p. 792-827.

- Melnyk, S., and Gingras, M. K., 2020, Using ichnological relationships to interpret heterolithic fabrics in fluvio-tidal settings: *Sedimentology*, v. 67, no. 2, p. 1069-1083.
- Mossop, G. D., 1980, Geology of the Athabasca oil sands: *Science*, v. 207, no. 4427, p. 145-152.
- Mossop, G. D., and Flach, P. D., 1983, Deep channel sedimentation in the Lower Cretaceous McMurray Formation, Athabasca Oil Sands, Alberta: *Sedimentology*, v. 30, no. 4, p. 493-509.
- Musial, G., Labourdette, R., Franco, J., and Reynaud, J.-Y., 2013, Modeling of a tide-influenced point-bar heterogeneity distribution and Impacts on steam-assisted gravity drainage production: Example from Steepbank River, McMurray Formation, Canada: *AAPG Studies in Geology*, v. 64, p. 545-564.
- Musial, G., Reynaud, J.-Y., Gingras, M. K., Féliès, H., Labourdette, R., and Parize, O., 2012, Subsurface and outcrop characterization of large tidally influenced point bars of the Cretaceous McMurray Formation (Alberta, Canada): *Sedimentary Geology*, v. 279, p. 156-172.
- Muwais, W., and Smith, D., 1990, Types of channel-fills interpreted from dipmeter logs in the McMurray Formation, northeast Alberta: *Bulletin of Canadian Petroleum Geology*, v. 38, no. 1, p. 53-63.
- Nardin, T., Carter, B., and Bassey, N., 2010, Braided river and avulsive depositional systems in the McMurray Formation-LIDAR and subsurface data integration at Syncrude's Aurora North mine, AAPG Conference and Exhibition, Volume Search and Discovery Article: Calgary, Alberta, Canada, American Association of Petroleum Geologists, p. 30143.
- Nardin, T. R., Feldman, H. R., and Carter, B. J., 2013, Stratigraphic architecture of a large-scale point-bar complex in the McMurray Formation: Syncrude's Mildred Lake Mine, Alberta, Canada: *AAPG Studies in Geology*, v. 64, p. 273-311.
- Nelson, H., and Glaister, R., 1978, Subsurface environmental facies and reservoir relationships of the McMurray oil sands, northeastern Alberta: *Bulletin of Canadian Petroleum Geology*, v. 26, no. 2, p. 177-207.
- Olariu, C., Steel, R. J., Dalrymple, R. W., and Gingras, M. K., 2012, Tidal dunes versus tidal bars: The sedimentological and architectural characteristics of compound dunes in a tidal seaway, the lower Baronia Sandstone (Lower Eocene), Ager Basin, Spain: *Sedimentary Geology*, v. 279, p. 134-155.
- Pattison, S. A. J., 2019, Re-evaluating the sedimentology and sequence stratigraphy of classic Book Cliffs outcrops at Tusher and Thompson canyons, eastern Utah, USA: Applications to correlation, modelling, and prediction in similar nearshore terrestrial to shallow marine subsurface settings worldwide: *Marine and Petroleum Geology*, v. 102, p. 202-230.
- Pattison, S. A. J., 2020, Sediment-supply-dominated stratal architectures in a regressively stacked succession of shoreline sand bodies, Campanian Desert Member to Lower Castlegate Sandstone interval, Book Cliffs, Utah–Colorado, USA: *Sedimentology*, v. 67, no. 1, p. 390-430.
- Pearson, N. J., and Gingras, M. K., 2006, An Ichnological and Sedimentological Facies Model for Muddy Point-Bar Deposits: *Journal of Sedimentary Research*, v. 76, no. 5, p. 771-782.

- Pemberton, S. G., Flach, P. D., and Mossop, G. D., 1982, Trace fossils from the Athabasca oil sands, Alberta, Canada: *Science*, v. 217, no. 4562, p. 825-827.
- Pemberton, S. G., and Wightman, D. M., 1992, Ichnological Characteristics of Brackish Water Deposits, *in* Pemberton, S. G., ed., *Applications of Ichnology to Petroleum Exploration: A Core Workshop: SEPM Core Workshop, Volume 17, SEPM Society for Sedimentary Geology*, p. 141-167.
- Ranger, M., 2006, The northeastern sector of the Lower Cretaceous Athabasca oil-sands basin: Facies and fluids, *in* Gilboy, C. F., and Whittaker, S. G., eds., *Saskatchewan and Northern Plains Oil & Gas Symposium, Volume Saskatchewan Geological Society Special Publication 19, Saskatchewan Geological Society*, p. 249-256.
- Ranger, M. J., 1994, A basin study of the southern Athabasca Oil Sands Deposit [Doctor of philosophy unpublished PhD Thesis]: University of Alberta, 310 p.
- Ranger, M. J., and Gingras, M., Stratigraphy and sequence stratigraphic surfaces of the McMurray Formation, 2008 Hedberg Conference, Banff, Alta. American Association of Petroleum Geologists, Search and Discovery Article 90075.[Abstr.], 2008a.
- Ranger, M. J., and Gingras, M., 2010, Geology of the Athabasca oil sands: field guide & overview, Canadian Society of Petroleum Geologists, 137 p.
- Ranger, M. J., and Gingras, M. K., 2008b, Stratigraphy and sequence stratigraphic surfaces of the McMurray Formation, Hedberg Conference, Volume Search and Discovery Article: Banff, Alberta, American Association of Petroleum Geologists, p. 90075.
- Ranger, M. J., and Pemberton, S. G., 1988, Marine influence on the McMurray Formation in the Primrose area, Alberta: Canadian Society of Petroleum Geologists, v. Memoir 15, p. 439-450.
- Ranger, M. J., and Pemberton, S. G., 1992, The sedimentology and ichnology of estuarine point bars in the McMurray Formation of the Athabasca Oil Sands deposit, north-eastern Alberta, Canada, *Applications of Ichnology to Petroleum Exploration: A Core Workshop, Volume 17, SEPM Society for Sedimentary Geology*, p. 401-421.
- Ranger, M. J., and Pemberton, S. G., 1997, Elements of a stratigraphic framework for the McMurray Formation in south Athabasca area, Alberta: Canadian Society of Petroleum Geologists, v. Memoir 18, p. 263-291.
- Reading, H. G., 1996, *Sedimentary Environments: Processes, Facies and Stratigraphy*, 3rd edition, Blackwell Science, 688 p.
- Reineck, H.-E., and Singh, I. B., 1980, *Depositional sedimentary environments: with reference to terrigenous clastics*, New York, Springer-Verlag Berlin Heidelberg, 551 p.
- Rinke-Hardekopf, L., Dashtgard, S. E., MacEachern, J. A., and Gingras, M. K., 2022, Resolving stratigraphic architecture and constraining ages of paralic strata in a low-accommodation setting, Firebag Tributary, McMurray Formation, Canada: *The Depositional Record*, v. 8, p. 754-785.
- Russell, C. E., Mountney, N. P., Hodgson, D. M., and Colombera, L., 2018, A novel approach for prediction of lithological heterogeneity in fluvial point-bar deposits from analysis of meander

- morphology and scroll-bar pattern, *in* Ghinassi, M., Colombera, L., Mountney, N. P., Reesink, A. J. H., and Bateman, M., eds., *Fluvial Meanders and Their Sedimentary Products in the Rock Record*, p. 385-417.
- Savrda, C. E., and Bottjer, D. J., 1986, Trace-fossil model for reconstruction of paleo-oxygenation in bottom waters: *Geology*, v. 14, no. 1, p. 3-6.
- Schneider, C., and Grobe, M., 2013, Regional cross-sections of Devonian stratigraphy in northeastern Alberta (NTS 74D, E): Alberta Energy Regulator, 2013-05, 25p.
- Shchepetkina, A., Gingras, M., Pemberton, S., MacEachern, J., and Plint, G., 2016a, What does the ichnological content of the Middle McMurray Formation tell us?: *Bulletin of Canadian Petroleum Geology*, v. 64, no. 1, p. 24-46.
- Shchepetkina, A., Gingras, M. K., Zonneveld, J.-P., and Pemberton, S. G., 2016b, Sedimentary fabrics of the macrotidal, mud-dominated, inner estuary to fluvio-tidal transition zone, Petitcodiac River estuary, New Brunswick, Canada: *Sedimentary Geology*, v. 333, p. 147-163.
- Sisulak, C. F., and Dashtgard, S. E., 2012, Seasonal controls on the development and character of inclined heterolithic stratification in a tide-influenced, fluvially dominated channel: Fraser River, Canada: *Journal of Sedimentary Research*, v. 82, no. 4, p. 244-257.
- Smith, D. G., 1988, Tidal bundles and mud couplets in the McMurray Formation, northeastern Alberta, Canada: *Bulletin of Canadian Petroleum Geology*, v. 36, no. 2, p. 216-219.
- Smith, D. G., Hubbard, S. M., Leckie, D. A., and Fustic, M., 2009, Counter point bar deposits: Lithofacies and reservoir significance in the meandering modern Peace River and ancient McMurray Formation, Alberta, Canada: *Sedimentology*, v. 56, no. 6, p. 1655-1669.
- Smith, N. D., 1972, Some sedimentological aspects of planar cross-stratification in a sandy braided river: *Journal of Sedimentary Research*, v. 42, no. 3, p. 624-634.
- Stewart, G., and MacCallum, G., 1978, Athabasca oil sands guide book, Canadian Society of Petroleum Geologists, 33 p.
- Strobl, R. S., Wightman, D. M., Muwais, W. K., Cotterill, D. K., and Yuan, L., 1997, Geological modelling of McMurray Formation reservoirs based on outcrop and subsurface analogues: *Canadian Society of Petroleum Geologists*, v. Memoir 18, p. 292-311.
- Thomas, R. G., Smith, D. G., Wood, J. M., Visser, J., Calverley-Range, E. A., and Koster, E. H., 1987, Inclined heterolithic stratification—terminology, description, interpretation and significance: *Sedimentary Geology*, v. 53, no. 1-2, p. 123-179.
- Tonkin, N. S., 2012, Deltas, *in* Kanust, D., and Bromley, R. G., eds., *Trace Fossils as Indicators of Sedimentary Environments*, Volume 64, Elsevier, p. 507-528.
- Weleschuk, Z. P., and Dashtgard, S. E., 2019a, Evolution of an ancient (Lower Cretaceous) marginal-marine system from tide-dominated to wave-dominated deposition, McMurray Formation: *Sedimentology*, v. 66, no. 6, p. 2354-2391.


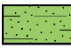





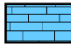




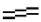
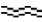

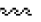


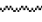
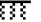


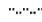
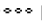
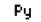

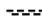

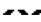
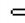




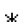
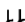
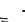

















- Weleschuk, Z. P., and Dashtgard, S. E. J. S., 2019b, Evolution of an ancient (Lower Cretaceous) marginal-marine system from tide-dominated to wave-dominated deposition, McMurray Formation: *Sedimentology*, v. 66, no. 6, p. 2354-2391.
- Wightman, D. M., Attalla, M. N., Wynne, D. A., Strobl, R. S., Berhane, H., Cotterill, D. K., and Berezniuk, T., 1995, Resource characterization of the McMurray/Wabiskaw deposit in the Athabasca oil sands area: a synthesis, Edmonton, Alberta, Canada, Alberta Oil Sands Technology and Research Authority, v. Technical Publication Series #10, 220 p.
- Wightman, D. M., and Pemberton, S. G., 1997, The Lower Cretaceous (Aptian) McMurray Formation: an overview of the Fort McMurray area, northeastern, Alberta: *Canadian society of Petroleum Geologists*, v. Memoir 18, p. 312-344.
- Wightman, D. M., Pemberton, S. G., and Singh, C., 1987, Depositional modelling of the upper Mannville Lower Cretaceous east central Alberta: Implications for the recognition of brackish water deposits: *The society of Economic Paleontologists and Mineralogists, Special Publication*, v. 32, p. 189-220.
- Wignall, P. B., and Myers, K. J., 1988, Interpreting benthic oxygen levels in mudrocks: A new approach: *Geology*, v. 16, no. 5, p. 452-455.
- Williams, G. D., 1963, The Mannville Group (Lower Cretaceous) of central Alberta: *Bulletin of Canadian Petroleum Geology*, v. 11, no. 4, p. 350-368.

Appendix A.

CORE LOGS FROM THE CHRISTINA RIVER REGION

Digital strip logs for logged cores within area that extends between Townships 89-90 and Ranges 5-8W4M. Cores were logged at the Core Research Center (CRC), Calgary, Canada, using AppleCORE software (donated by Dr. Mike Ranger). For each logged core, a digital strip log (.bmp) and an AppleCORE files (.acr) are included in the file below. Note there is no available cores in Township 89 Ranges 5 at the time when cores were logged.

Filename: strip logs files T89-90R5-8.7z

Core Strip Log Legend			
Lithology			
 sand/sandstone	 silty shale	 shale/mudstone	 organic shale
 siltstone	 muddy siltstone	 coal	 limestone
 lost core			
Physical Structures			
 oscillatory ripples	 current ripples	 planar tabular bedding	 low angle tabular bedding
 wavy parallel bedding	 lenticular bedding	 convolute bedding	 high angle tabular bedding
 chaotic bedding	 scour	 synaeresis cracks	 slump/SSD
 climbing-ripple lamination			
Accessories			
 silt lamina	 pebbles/granules	 pyrite	 coal fragments
 shale lamina	 coal lamina	 rip up clasts	
Ichnofossils			
 Planolites	 Cylindrichnus	 Teichichnus	 Palaeophycus
 Gyrolithes	 Asterosoma	 Rootlets	 Thalassinoides
 Arenicolites	 Chondrites	 Skolithos	 Lockeia
Fractures			
/ fracture (general) ⇔ collapse			
Staining			
 excellent	 very good	 good	 fair
 poor	 nil		
Bioturbation			
 barren	 sparse	 low	 moderate
 abundant	 intense	 complete	